

## Stress Provinces of India– Contribution to World Stress Map

D.S. Subrahmanyam

National Institute of Rock Mechanics, Bangalore, Karnataka, India

Correspondence should be addressed to D.S. Subrahmanyam, subbu3268@gmail.com

Publication Date: 21 January 2014

Article Link: <http://scientific.cloud-journals.com/index.php/IJAESE/article/view/Sci-158>



Copyright © 2014 D.S. Subrahmanyam. This is an open access article distributed under the **Creative Commons Attribution License**, which permits unrestricted use, distribution, and reproduction in any medium, provided the original work is properly cited.

**Abstract** In the Geological studies there are several field maps that are available to know the ground features and various geological parameters, but if the tectonic stress directions are measured at various available places and marked globally on a world map then it is called World Stress Map (WSM). These stress directions are helpful not only for academic research but also for compiling the vast data on a global scale to know the geodynamics and plate movement. The world stress map shows the orientations of Maximum Principal Horizontal Stress Direction measured at various places in different countries. There are two types of stresses available based on the regional and local scales. Regional stresses are also called first order estimates which are based on the measurements of earth quake focal mechanism studies at the particular site globally or regionally. But the second order stresses are completely local parameters generally carried out for specific engineering purpose. To prepare the world stress map the first order stresses are very important and generally incorporated in the world stress map and the less importance is given for second order stress, since these measurements are most of the times determined at shallow depths and are not reliable indicators to include in the stress map. However the first and second order stress directions are mapped on the world stress map to know the possible global phenomenon like plate dynamics. The world stress map is being prepared and updated periodically by WSM project. The 1992 version of the World Stress Map was derived mainly from geological observations on earthquake focal mechanisms, volcanic alignments and fault slip interpretations. Less than 5% of the data was based upon hydraulic fracturing or overcoring measurements of the type commonly used in mining and civil engineering projects. The 2005 version of world stress map shows the huge number of data collected from hydrofracturing, overcoring, borehole breakout etc.

**Keywords** *First Order Stress; Focal Mechanism; Horizontal Compressive Stress; National Institute of Rock Mechanics; Second Order Stress; World Stress Map*

### 1. Introduction

The stress map of an area gives the possible indication of Maximum Principal Stress orientation which is regional in nature. This orientation data can't be considered for design purpose in any major underground mining or civil engineering project. Hence it clearly indicates that the stress

measurements should be conducted for a required orientation for any specific engineering purpose. The stress directions under consideration will be influenced by regional tectonic features such as faults, shear zones, presence of dykes etc. These stresses may be considerably varied in magnitude and directions from the trends described in first order stress maps. The insitu stress measurements play a vital role in overall design process during the construction of major underground structures.

It is therefore worth considering the first and second order stresses with reference to the study of present day plate dynamics. The Stress Map of India is being prepared by National Institute of Rock Mechanics (NIRM), mainly focusing on second order stress data that is available from various parts of the country. The data has been collected from various underground openings where in-situ stress measurements have been conducted by hydrofracture method. Many of these measurements have been made for specific engineering applications (e.g. dam site evaluation, mining work), places where topography, fracturing or nearby excavations could strongly perturb the regional stress field.

Nearly 300 reliable indicators of the orientation of horizontal stress in the Indian crust have been collected in-order to explain the regional trends of stress orientations across India. Stress provinces were demarcated based on the trajectories throughout the country. This data has been correlated with reference to the motion of Indian plate. The possible regional pattern of stress in Indian sub-continent with reference to the first order stress, and also a number of locally anomalous stress orientations influenced by second-order sources of stress such as structure and topography with reference to the present day plate dynamics, have been correlated.

## 2. World Stress Map

The latest and updated World Stress Map (WSM) is to be prepared in the year 2014 by incorporating the available data from different countries. Due to the structure of the database the data can be selected according to a number of criteria such as type, location, regime, depth, and so on.

This updated world stress map is expected to provide not only the possible information of Maximum Principal Stress direction of various places, but also information about the depth of the measurement, the magnitude of the maximum horizontal compression and also available lithology of the particular area. The data will be generated from different types of stress measurements like focal mechanism, borehole breakouts, hydrofracturing, overcoring etc.

The reliability and compatibility of the data are indicated by a quality ranking from A to E, with A being the highest quality and E the lowest (for further investigations only the most reliable data with a quality of A, B or C should be used). An overview about the quality ranking scheme is given by Zoback (1992) as well as on the World Stress Map (WSM) website (<http://www.world-stressmap.org>). The new release of the WSM (Muller et al., 2000) encompasses 10 920 data records, each with up to 56 detail entries.

In the previous stress maps prepared by Zoback in the year 1992 and Muller in the year 1997 (Figure 1) most of the data has been generated by taking into consideration of 63% from earthquakes, 22% from borehole breakouts. Second order stress data has not been considered in the preparation of the map. However new data mainly which is coming from Europe, Australia and America additionally included data from mid-ocean ridges which may be directly related to plate boundary processes and which had so far been excluded from the WSM database are now included.

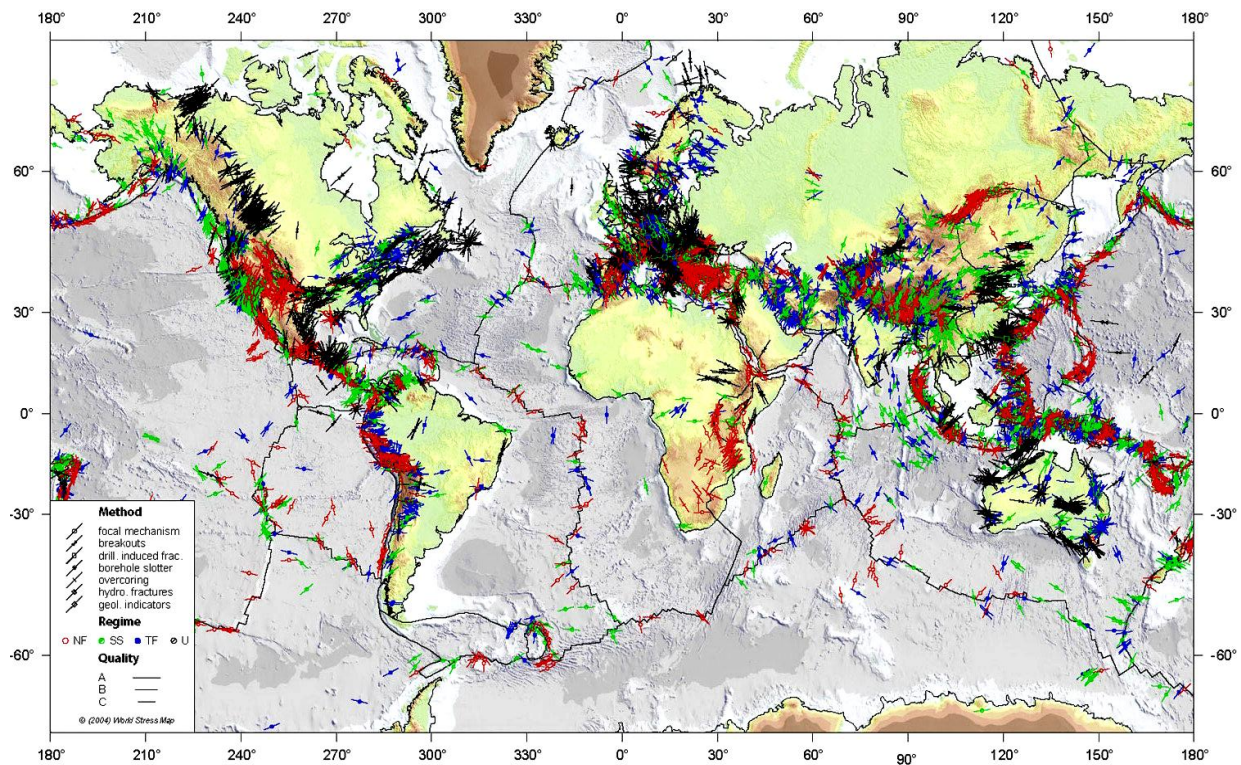


**Figure 1:** World Stress Map Giving Orientations of the Maximum Horizontal Compressive Stress, Courtesy from [www.world-stress-map.org](http://www.world-stress-map.org)

## 2.1. Benefits of World Stress Map

The World Stress Map project offers not only free access to this global database via the Internet, but also continue in its effort to expand and improve the database, to develop new quality criteria.

The database that is available from World stress map will not only be helpful in both academic researches but also for commercial and economical investigations. In academic research these data will contribute to know the possible movement of plates. In commercial way these data will be helpful in providing information about the stability of underground structures, to locate the suitable sites for nuclear repositories. In underground constructions the long axis of the cavern should be parallel to maximum compression; hence the tunnels and big caverns will be oriented in suitable areas as per the data available in the world stress map. In the hydrocarbon reservoirs, the possible direction of fluid flow will be based on the direction of maximum principal stress direction, hence the knowledge about the direction will be helpful in monitoring the production of oil wells. In the hydrocarbon industry, hydraulic fracturing studies are conducted to create the fractures for enhancing the yielding of the reservoirs; these fractures will be extended parallel to the Maximum principal stress direction. If the data is readily available in the maximum possible areas globally it becomes an easier task and dilinates many hydrocarbon reservoirs.

## 3. Stress Provinces in India

So far the data has been generated by other organisations to contribute in preparation of world stress map, based on the studies of Focal Mechanism i.e. first order stress. A little contribution was made towards the second order stress because of the lack of data. National Institute of Rock Mechanics (NIRM) has conducted in-situ stress measurements at various places like central India, southern shield and east and west Himalayas.

In-situ stress measurements were conducted at various places by hydro fracturing method at the depth ranging from 30 to 350m for various specific engineering design purposes. These orientations are quite homogeneous in broad regions except in few places where the geological anomalies occurred. Over other regions the horizontal stress directions seem to be completely incoherent from site to site.

Figure 2, Index map of India showing the physiographic/tectonic provinces referred in this paper. The arrows indicate the maximum compressive horizontal stress ( $\sigma_H$  max) orientation as generated from hydrofracturing stress measurements. The blue lines indicate different stress provinces as revealed by stress analysis. NIRM has proposed three broad regions based on regionally consistent Maximum Principal Horizontal stress  $\sigma_H$  orientations as given below

- The Himalayas
- Mid-continent Stress Province
- Southern Shield

The Himalayas are further divided into North Western Himalayas, Central Himalayas and Eastern Himalayas.



**Figure 2:** Index Map of India Showing Stress Provinces (to be updated), Courtesy from NIRM

#### 4. NIRM's Contribution to World Stress Map

NIRM has collected nearly 300 reference points and their orientations along with magnitude have been indicated on Indian map. The orientations are derived from the data generated from different

states of India i.e., Himachal Pradesh, Jammu & Kashmir, Uttaranchal, Sikkim, Arunachal Pradesh and also from the neighbouring countries i.e. Bhutan and Nepal. Whatever data collected at NIRM, Stress orientations are intrinsically much more amenable to analysis than magnitudes because measurements of stress directions at all depths can be meaningfully compared. Besides that, measured stress orientations can be compared to directions from earthquake fault plane solutions and directions inferred from geologic indicator of stress. **The final stress map will be prepared by incorporating the First and second order stress data by collecting data from various other organisations in India. The updated map will be sent to World stress map to incorporate in the same.**

**The project authorities of World stress map urged that there is little information in the WSM apart from data from focal mechanism solutions. They would like to collect intensively new data from Indian sub-continent.**

**Dr. Oliver Heidbach** who is Head of the World stress Map project coordinated with National Institute of Rock Mechanics and asked to contribute for a new WSM database which is going to be published in 2014.

## 5. Conclusions

Nearly 300 stress indicators along with their magnitude, depth of the investigations conducted, and the direction of Maximum principal stress are available with NIRM. Some of the data has been plotted in the given map and remaining data is under review. The data is being compiled to prepare the latest map and periodical updating is required on timely basis once the new data is acquired from the projects. The regional pattern of Maximum Principal Horizontal stress ( $\sigma_H$ ) direction can be delineated from the given data. The average orientation of  $\sigma_H$  shows the more or less in correlation with the direction of movement of Indian plate.

On the basis of regionally consistent orientations three stress provinces are recognized in a broader term: The Himalayas, the mid-continent stress province and southern shield. The Himalayas are further divided into Northwestern Himalayas, Central Himalayas and Eastern Himalayas.

In general the  $\sigma_H$  orientation is NNE-NE throughout the central and Northern India with a mean direction of about N23°E. This orientation is sub parallel to the direction of compression expected from the forces present along the Himalayan collision, which resist the northward movement of the IAP. There is however a large amount of scatter in  $\sigma_H$  orientations throughout the Indian subcontinent suggesting that some of the stress indicators reflect local sources of stress rather than the collisional tectonics.

The Himalayas where we are having maximum data (Around 150) is having orientation varying from N20°- 30°E. In the central part of India the average orientation N10°-20°W is derived from the data generated from the measurements around Aaravali region, Hyderabad and also some parts of Eastern Ghats. In the shield area, the average orientation- N20°E, is the result of data compiled from KGF (Karnataka), Mumbai and Mangalore (Karnataka). The thick lithosphere in India is associated with far field tectonic forces allow the stress field to be more easily perturbed by local effects of geological discontinuities like great thrusts of Himalayas and topography.

## Acknowledgements

The author is thankful to Dr. V. Venkateswarlu, Director, National Institute of Rock Mechanics (NIRM), for his encouragement and necessary corrections in the manuscript. Also thankful to Dr. S. Sengupta

for sharing the important technical information and inputs in the preparation of the stress provinces of India.

## References

Zoback M.D. and Haimson B.C., 1983: *Hydraulic Fracturing Stress Measurements*. U.S. National Committee for Rock Mechanics, National Academy Press, Washington, D.C. 270.

Zoback M.D. and Healy J.H. *Friction, Faulting and in situ Stress*. Annual Geophysics. 1984. 2, 689-698,

Zoback M.D. and Zoback M.L. *State of Stress and Intraplate Earthquakes in the Central and Eastern United States*. Science. 1981. 213; 96-104.

Zoback M.D. and Zoback M.L., 1991: *Tectonic Stress Field of North America and Relative Plate Motions*. The Geology of North America, Decade Map Vol. 1, Neotectonics of North America, edited by B. Slemmons et al. Boulder, Colo. 339-366.

Zoback M.D., Moos D. Mastin L., and Anderson R.N. *Wellbore Breakouts and in situ Stress*. Journal of Geophysics Research. 1985. 90; 5523-5530.

Zoback M.D., et al. First- And Second-Order Lithospheric Stress Patterns.

Zoback M.L. *State of Stress and Modern Deformation of the Northern Basin and Range Province*. Journal of Geophysics Research. 1989. 94; 7105-7128.

Zoback M.L. and Magee M. *Stress Magnitudes in the Crust: Constraints from Stress Orientation and Relative Magnitude Data*, Philos. Trans. Royal Soc. London, Set. A. 1991. 337; 181-194.

Zoback M.L. and Zoback M.D. *State of Stress of the Conterminous United States*. Journal of Geophysics Research. 1980. 85, 6113-6156.

Gowd T.N., Srirama Rao S.V., and Gaur V.K. *Tectonic Stress Field in Indian Subcontinent*. Journal of Geophysical Research. 1992. 97; 11879-11888.

Sengupta S., Joseph D., and Nagraj C. *Stress Perturbation near Two Fault Zones in Himalayas-Field Measurements and Numerical Simulation*. Proceedings of Third International Conference on Mechanics of Jointed and Faulted Rock- MJFR-3. 1997. 83-88.

## Search for Generic Provenance and Petrographic Evolution of Sandstones, Bhadasar Formation (Middle Jurassic), Jaisalmer Basin, Rajasthan, India

Shyam N. Mude<sup>1</sup>, Suyog A. Jagtap<sup>2</sup>, and P. Kundal<sup>3</sup>

<sup>1</sup>Department of Geology, Fergusson College, Pune, Maharashtra, India

<sup>2</sup>Department of Civil Engineering, JSPM Narhe Technical Campus (University of Pune), Pune, Maharashtra, India

<sup>3</sup>Postgraduate Department of Geology, RTM Nagpur University, Nagpur, Maharashtra, India

Correspondence should be addressed to Suyog A. Jagtap, [suyog.jagtap@gmail.com](mailto:suyog.jagtap@gmail.com)

Publication Date: 24 January 2014

Article Link: <http://scientific.cloud-journals.com/index.php/IJAESE/article/view/Sci-164>



Copyright © 2014 Shyam N. Mude, Suyog A. Jagtap, and P. Kundal. This is an open access article distributed under the **Creative Commons Attribution License**, which permits unrestricted use, distribution, and reproduction in any medium, provided the original work is properly cited.

**Abstract** Provenance and petrographic studies of sandstones of the Bhadasar Formation have been ascertained by means of heavy mineral and petrographic analysis. Petrography reveals an abundance of angular to sub-round mono-crystalline, at places poly-crystalline quartz followed by orthoclase, microcline and plagioclase feldspar. The overall composition of sandstone matches with those of calc-arenites. The heavy mineral crop of sandstones of the Bhadasar Formation shows Euhedral to sub-hedral as well as rounded to sub-rounded grains of tourmaline, zircon, garnet, rutile, apatite, epidote, staurolite, kyanite and hornblende with decreasing order of abundance. Heavy mineral suite coupled with petrography indicates a mixed provenance dominated by a sedimentary source which is derived from intra-cratonic basins.

**Keywords** *Heavy Minerals; Petrography; Provenance; Bhadasar Formation; Jaisalmer Basin*

### 1. Introduction

The heavy mineral analysis is one of the most important and widely used techniques in determination of the provenance studies in today's world; it has been more than 10 decades since the study of heavy minerals was established. Heavy minerals are extremely sensitive indicators of basinal processes and source area lithology (Morton, 1985; Stattegger, 1987) because it provides wider spectrum of silicates, oxides, sulphates and phosphates than lighter minerals (Mansoor, 2002). The heavy mineral data is used conjunction with microprobe analysis; it provides sensitive information on the mineralogical composition of sediments source rocks (Morton, 1991; Morton and Hallsworth, 1999). The heavy mineral studies on modern basins have provided actuality analogues which leads to a better understanding of the geological history of their ancient counterpart (Mange and Maurer, 1992).

The recent past has witnessed growing interest in interpreting the tectonic provenance using detrital grains, as these helps to interpreting the provenance and tectonic settings (Dickinson, 1970; Uddin and Lundberg, 1998). Sometime interpretations based on modified compositions i.e. after recycling or post depositional changes may result distorted provenance setting (Mack, 1984; Dickinson, 1988). Nevertheless, there are certain mineral species can be used directly as provenance indicators (Blatt et al., 1980)

In recent years (Mansoor, 2002) have successfully used heavy minerals and petrofacies analysis to deciphering the provenance and tectonic settings of the sedimentary deposits from the some Jurassic formations of the Jaisalmer basin. The present paper attempts to study of provenance based on heavy minerals assemblage as well as petrography which obtained from sandstone of the Bhadasar formation of the Jaisalmer basin, Rajasthan.

## 2. Methodology

Samples were systematically collected from two members of the Bhadasar formation of Middle Jurassic age exposed in and around Jaisalmer district. Total six sample were considered for heavy mineral (Gravity – settling in bromoform) and petro graphic analysis from different localities of respective members of the Bhadasar formation. The samples were disaggregated by using agate mortar, later disaggregate material is subjected to sieving by using 230 mesh. After sieving acid treatment is given to the sample by using 10% dilute hydrochloric acid to removing mineral stain and calcium carbonate and then unnecessary material is decanted and sample is kept in the oven for drying. After that sample is performed for actual heavy mineral separation by means of high-density liquid i.e. bromoform (Sp.gr. 2.89), then obtained heavy mineral suites were mounted on the glass slide by using Canada balsam and the heavy mineral slides were prepared.

## 3. Geology of the Area

The Jaisalmer Basin characterized by the eastern shelf part of large Indus Basin, Jaisalmer Basin is a Pericratonic shelf extended towards west, dipping eastern flank of Indus Basin, bounded by Divikote-Nachna uplifts towards east and south east, while Fatehgarh fault marked by its southern limit. The Malani igneous Suite of Pre-Cambrian age and metamorphic rocks constitutes the basement for the Jaisalmer Basin.

Geologically, the Mesozoic rocks of Jaisalmer area is represented by limestone, shale, siltstone and sandstone and have been subdivided into six formation as shown in the Figure 1 of geological map of the study area, namely Lathi Formation, Jaisalmer Formation, Baisakhi Formation, Bhadasar Formation, Pariwar Formation and Habur Formation respectively (Das Gupta, 1975; Swami Nath et. al., 1959).

The rocks of Bhadasar Formation consists of ferruginous sandstone with intercalations of thin beds of clay, siltstone, shale and these are well exposed in and around the Bhadasar, Kolar Dungar, Mokal villages and also along the Jaisalmer-Ramgarh road. (Das Gupta, 1975) subdivided the Bhadasar Formation into two member viz., Kolar Dungar Member and Mokal Member. The Kolar Dungar Member forms the base of the Bhadasar Formation and it is best exposed in Bhadasar village and Kolar Dungar hill where it attains maximum thickness. The Mokal Member is well exposed at Bhadasar to Mokal village and conformably overlies the rocks of the Kolar Dungar Member.

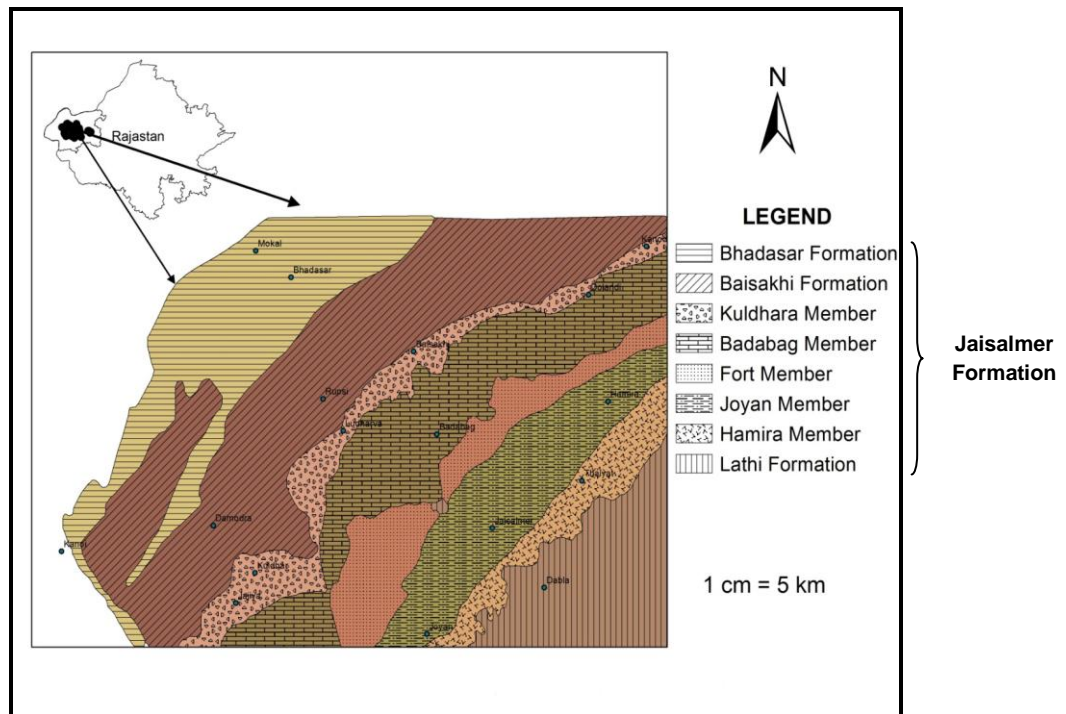


**Figure 1:** Geological Map of the Study Area  
(After Dave and Chatterjee, 1996; Roy and Jakhar, 2002)

### 3. Results

#### 3.1. Petrography

The Bhadasar Formation is divided into two members lower Kolar Dungan Member and Mokai Member which consists of calcareous sandstone and typically displays reddish brown (Figure 2, 2, 3 & 4), light yellow (Figure 2, 5 & 6) and grayish white colors (Figure 2, 1). In general based on the (Folk, 1980) classification, the microscopic analysis indicates that the rocks belong to calc-arenite category. The overall nature of the grains is fine to coarse grained, moderately sorted and exhibits angular, sub-rounded to well rounded forms. Within detrital components quartz can be observed dominantly as monocrystalline in form, at places polycrystalline variety can be readily observed (Figure 2, 1 & 2). Feldspar can be found as an orthoclase, microcline and plagioclase varieties but in general orthoclase feldspar predominates over microcline and the plagioclase feldspar (Figure 2, 3 & 4). The grains exhibits point, straight as well as concave-convex contacts. Detrital components are found to be embedded in coarse grained calcite and calcareous cement, within cementing matter the development of euhedral zoned dolomite crystals (Figure 2, 3) are also observed. At places within clay rich micritic matter the development of muscovite flakes can be seen (Figure 2, 2, 4 & 5).

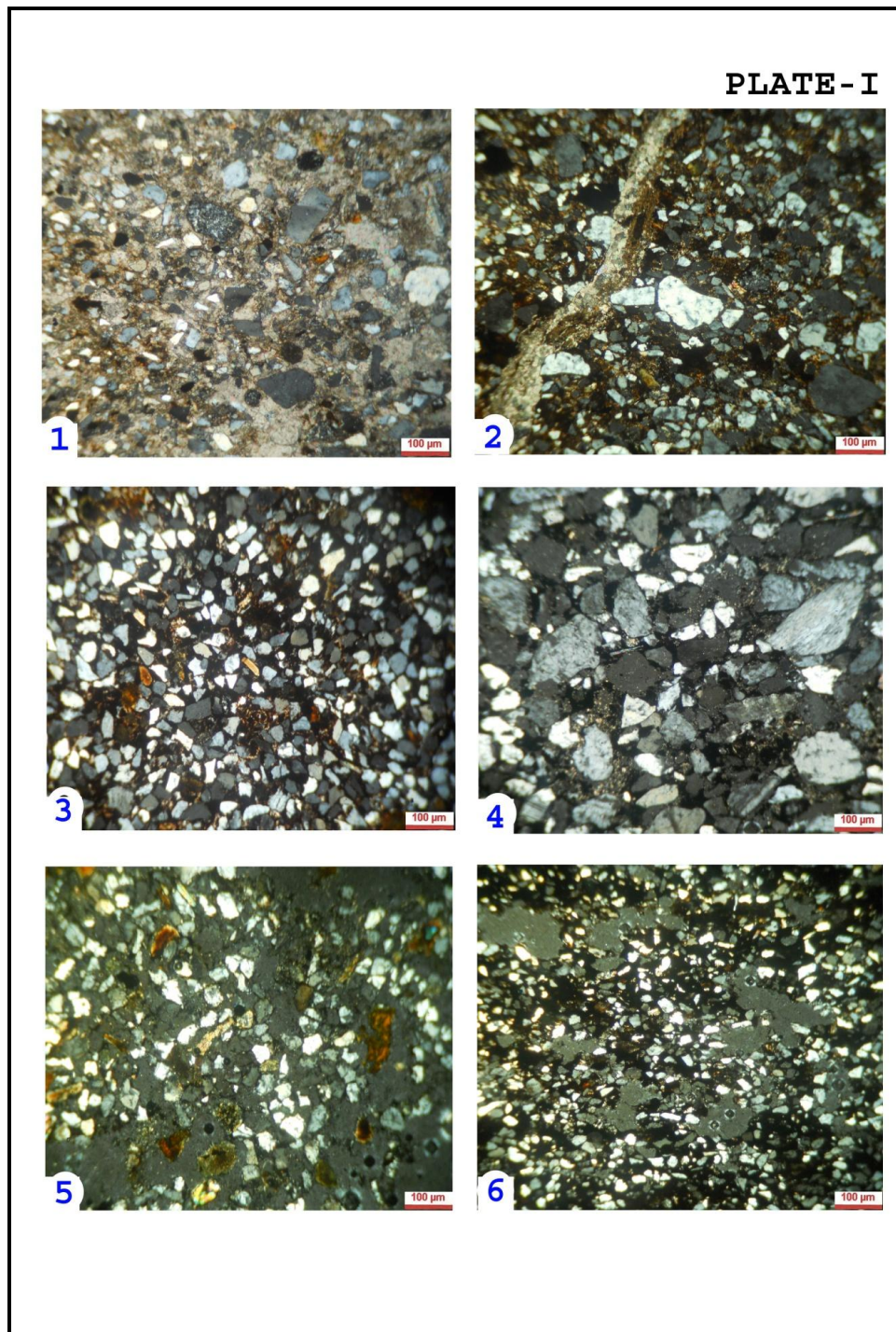


**Figure 2:** Photomicrograph Showing (1) Fine to Medium Grained Calc-Arenite (2) Fine to Coarse Grained & Intruded Calcite Vein (3) Medium to Fine Grained, Well Sorted, Angular To Sub-Rounded Calc-Arenite (4) Fine To Coarse Grained, Ill Sorted Calc-Arenite (5 & 6) Fine Grained Calc-Arenite

### 3.2. Heavy Minerals

The heavy mineral comprises dominantly of non-opaque variety and includes tourmaline, zircon, rutile, garnet, staurolite, epidote, monazite, apatite, kyanite and hornblende. In general heavy mineral crops are chiefly found to be sub-hedral to sub-round in variety.

### 3.3. Tourmaline

Tourmaline is the most dominant heavy mineral amongst the all non-opaque and exhibits variety colors like greenish, greenish brown, pinkish brown. Within few grains inclusions of non-opaque minerals were observed. Sub-rounded to sub-hedral as well as prismatic grains is not uncommon (Figure 3, 1 - 4).

### 3.4. Zircon

Zircon is the second most abundant heavy mineral is found within the non-opaque and it occurs as colorless to pink in color and shape vary from euhedral to sub-hedral in forms. Within zircon few grains exhibits zoning and some of the grains show randomly distributed inclusions of opaque and non-opaque minerals. The common microscopic properties like straight extinction, high order polarization color, zoning and high refractive index are quite distinct (Figure 3, 5 - 8).

### 3.5. Rutile

The rounded to sub-rounded grains of rutile can be identified by its typical characteristic blood red color. All most all the grain shows high refractive index as well as week pleochroism (Figure 3, 9 & 10).

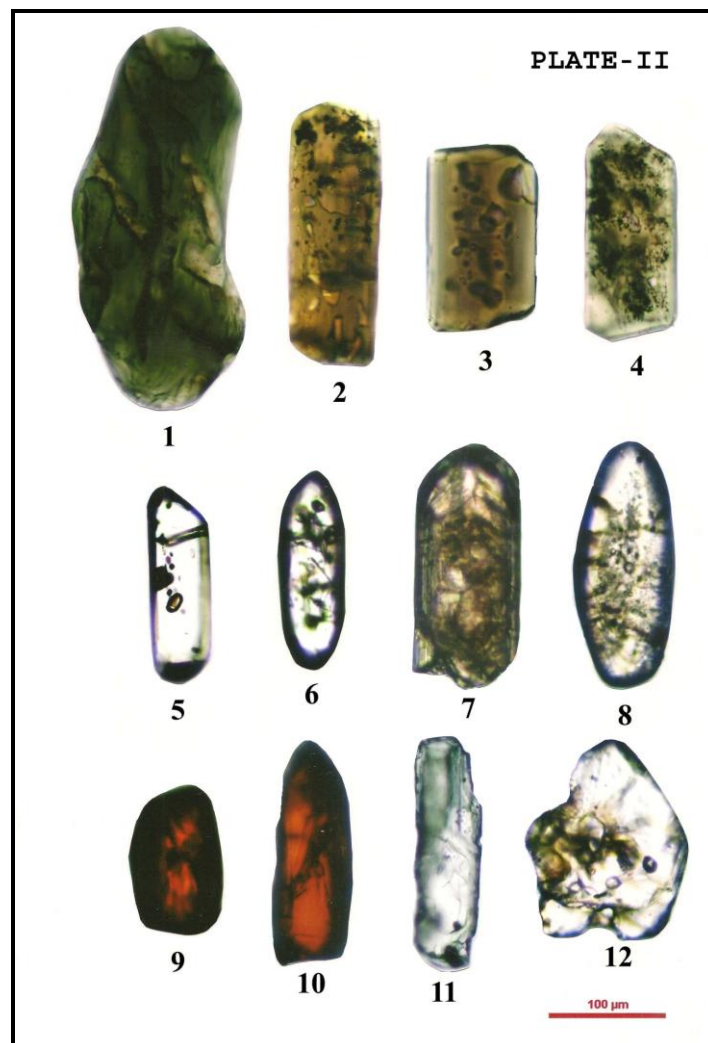


**Figure 3:** (1- 4) Tourmaline, (5 - 8) Zircon, (9 & 10) Rutile, (11) Kyanite, (12) Apatite

### 3.6. Garnet

It can be observed as colorless and typical pink in color, most of the grains are found to be rounded to sub-round in form with inclusions of opaque and non-opaque minerals. The typical microscopic properties like isotropism and high relief are quite distinct (Figure 4, 1 & 2).

### 3.7. Epidote, Apatite, Staurolite, Monazite and Kyanite

Epidote occurs as greenish brown in color and subhedral in form (Figure 4, 4). The colorless variety of apatite is also not uncommon (Figure 3, 12). The golden yellow colored staurolite is occurs in small amount and shows low birefringence as well as high relief (Figure 4, 5). Very few grains of honey yellow colored monazite can be observed as rounded to sub-round in form (Figure 4, 3). Colorless, typical bladed variety of kyanite grains are identified by its diagnostic characteristic of inclined extinction and step like variations in the interference color (Figure 3, 11).

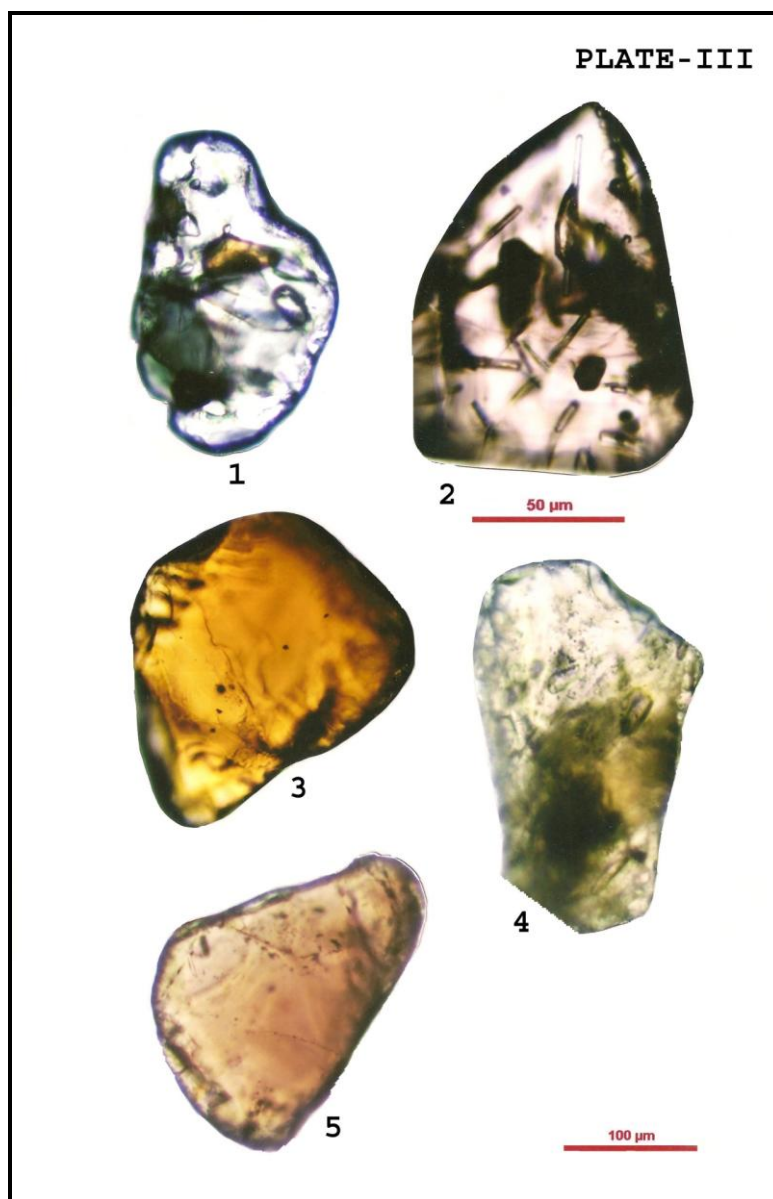


**Figure 4:** (1 & 2) Garnet, (3) Monazite, (4) Epidote, (5) Staurolite

#### 4. Conclusions

Petrographic study of sandstones of the Bhadasar Formation indicates dominance of angular, sub-rounded to well round mono-crystalline non-undulatory quartz in association with poly-crystalline quartz and by presence of orthoclase, microcline and plagioclase feldspar. The overall composition of sandstone matches with those of calc-arenitic framework (Figure 2, 1-6). The observed overall mono-crystalline and poly-crystalline quartz grain depicts gneissic provenance as well as massive plutonic rocks like granites and brecciated quartzites as a source area whereas the presence of feldspars specify that these sandstones have been originated from plutonic, volcanic and metamorphic rocks (Blatt et. al., 1980; Friedman and Sanders, 1978).

The heavy mineral analysis depicts (Figure 3 and 4), sub-rounded grain of greenish tourmaline is indicative of their source from granites. Sub-hedral yellowish brown tourmaline suggests a metamorphic source. The colourless, sub-hedral zircon indicates a felsic igneous source rock with inclusions of opaque mineral and zircon. Garnet is pink in color indicating their source from marble. Rounded grains of wine red coloured rutile suggest their source from metamorphic rocks, probably amphibolites or other mafic igneous rocks. The minor amount of other heavy minerals like, epidote, staurolite, apatite, kyanite, hornblende and monazite are typically indicative of their derivation from felsic and mafic igneous rocks to high grade metamorphic rocks. The study indicates that these minerals are derived from rocks of magmatic origin particularly granite and its derivatives, felsic and mafic igneous rocks to high-grade metamorphic rocks (Morton, 1985; Stattegger, 1987 and Mansoor, 2002). Most of the quartz and heavy mineral grains can be observed as polycyclic in nature.

The assemblages of heavy minerals and petrographic composition of sandstone of the Bhadasar Formation is indicative of intracratonic basin setup receiving sediments from metasedimentary rocks of a recycled orogenic provenance. On the other hand the contributions from igneous source terrain as well as high grade metamorphic rocks cannot be ruled out.

#### Acknowledgement

The authors are greatly thankful to the Head, Postgraduate Department of Geology; RTM Nagpur University and Head, Department of Geology, Fergusson College, Pune for providing facilities in present work and constant encouragement during the preparation of manuscript.

#### References

- Blatt H., Middleton G.V. and Murray R.C., 1980: *Origin of Sedimentary Rocks*. Prentice Hall. 782.
- Das Gupta S.K. *Revision of the Mesozoic-Tertiary Stratigraphy of the Jaisalmer Basin, Rajasthan*. Indian Jour. Earth Sci. 1975. 2 (10) 77-94.
- Dave A. and Chatterjee T.K. *Integrated Foraminiferal and Ammonoid Biostratigraphy of Jurassic Sediments in Jaisalmer Basin, Rajasthan*. Jour. Geol. Soc. India. 1996. 47; 477-490.
- Dickinson W.R. *Interpreting Detrital Modes of Graywackes and Arkoses*. Jour. Sed. Petrol., 1970. 59; 239-264.
- Dickinson W.R., 1970: *Provenance and Sediments Dispersal in Relation to Palaeo-Tectonics and Palaeogeography of Sedimentary Basin*. In: K.L. Kleinspehn and C. Paola (Eds.), *New Perspective in Basin Analysis*. Springer-Verlag, New York. 3-25.
- Folk R.L., 1980: *Petrology of Sedimentary Rocks*. Hamphill's, Austin, Texas, 182.

Mack G.H. *Exceptions to the Relationship between the Plate Tectonics and Sandstone Composition*. Jour. Sediment. Petrol. 1984. 54; 212-220.

Mange M.A. and Maurer H.F.W., 1992: *Heavy Minerals in Color*. Chapman and Hall, London. 147.

Mansoor Alam M. *Generic Provenance, Tectonics and Petrofacies Evolution of the Sandstones, Jaisalmer Formation (Middle Jurassic), Rajasthan*. Jour. Geol. Soc. India. 2002. 59; 47-57.

Morton A.C. *A New Approach to Provenance Studies: Electron Microprobe Analysis of the Detrital Garnet from Middle Jurassic Sandstone of the Northern North Sea*. Sedimentology. 1985. 32; 553-566.

Morton A.C. *Geochemical Studies of Detrital Heavy Minerals and Their Application to Provenance Studies*. In: Morton A.C., Todd S.P., and Haughton P.D.W. (Eds.), *Developments in Sedimentary Provenance Studies*. Spl. Publ. Geol. Soc. London. 1991. 57; 31-45.

Morton A.C. and Hallsworth C.R. *Processes Controlling the Composition of Heavy Mineral Assemblages in Sandstones*. Sedim. Geol. 1999. 124; 03-29.

Roy A.B. and Jakhar S.R., 2002: *Geology of Rajasthan (Northwest India): Precambrian to Recent*. Scientific Publishers (India), Jodhapur, 421.

Statterger K. *Heavy Minerals and Provenance of Sands: Modelling of Lithological End Members from River Sands of Northern Austria and from Sandstone of the Austroalpine Gosau Formation (Late Cretaceous)*. J. Sedim. Petrol. 1987. 57; 301-310.

Swami Nath J., Krishnamurthy J.G., Verma K.K. and Chandak G.J. *General Geology of Jaisalmer, Rajasthan*. ECAFE Symposium, Min. Res. and Dev. Ser. 1959. 10; 154-155.

Uddin A. and Lundberg N. *Unroofing History of the Eastern Himalaya and the Indo-Burman Ranges: Heavy Minerals Study of the Cenozoic Sediments from the Bengal Basin, Bangladesh*. Jour. Sediment. Res. 1998. 68 (3) 465-472.

## Rate of Sedimentation in Veeranam Lake, South India, Using $^{137}\text{Cs}$ and $^{210}\text{Pb}$

T. Pruthviraj<sup>1</sup>, S. Vasudevan<sup>1</sup>, Bhishm Kumar<sup>2</sup>, R.K. Singhal<sup>3</sup> and V. Vijayakumar<sup>4</sup>

<sup>1</sup>Department of Earth Sciences, Annamalai University, Tamilnadu, India

<sup>2</sup>Isotope Hydrology Section, International Atomic Energy Agency, Vienna, Austria

<sup>3</sup>Analytical Chemistry Section, Bhabha Atomic Research Centre, Mumbai, Maharashtra, India

<sup>4</sup>Department of Civil Engineering, Roever College of Engineering and Technology, Tamilnadu, India

Correspondence should be addressed to T. Pruthviraj, iniyavan4geo@gmail.com; devansiva@gmail.com

Publication Date: 19 August 2014

Article Link: <http://scientific.cloud-journals.com/index.php/IJAESE/article/view/Sci-183>



Copyright © 2014 T. Pruthviraj, S. Vasudevan, Bhishm Kumar, R.K. Singhal and V. Vijayakumar. This is an open access article distributed under the **Creative Commons Attribution License**, which permits unrestricted use, distribution, and reproduction in any medium, provided the original work is properly cited.

**Abstract** In recent years there has been an increased interest in the dating of recent lake sediments, since its importance for the reconstruction of pollution history and other activities of man has been well demonstrated. This is imperative as there has not been any record on this aspect of research in Lake Veeranam. Hence, in the present study it is proposed to establish the rate of sedimentation and determination of sediment age. The present study gives special emphasize on understanding the rate of sedimentation in Veeranam Lake. The core sediment of 46cm has been collected from the lake using gravity corer were sliced to 2cm and subjected to the analysis of  $^{137}\text{Cs}$  and  $^{210}\text{Pb}$  trends. The radio isotopic ( $^{137}\text{Cs}$  and  $^{210}\text{Pb}$ ) study reveals that the rate of sedimentation is 0.32 cm/year ( $^{210}\text{Pb}$ ) and 0.35 cm/year ( $^{137}\text{Cs}$ ) and the useful life of the lake may be of 965.71 years ( $^{137}\text{Cs}$ ) or 1056.25 years ( $^{210}\text{Pb}$ ) under normal environmental conditions.

**Keywords** *Dating; Environmental Conditions; Lake Life; Sediment Age*

### 1. Introduction

The usefulness of a particular isotope will depend on its half-life, and the accuracy of the associated model. For example, radiocarbon dating based on the decay of  $^{14}\text{C}$  (half-life 5730 years) may provide accurate dates over a period spanning thousands of years, but will be inaccurate when used conventionally for dating sediments younger than approximately 1800AD as a result of anthropogenic inputs of  $^{14}\text{C}$  into the environment (Seuss, 1965). Radionuclides, such as lead-210 ( $^{210}\text{Pb}$ ,  $t_{1/2} = 22.3\text{Y}$ ) and cesium-137 ( $^{137}\text{Cs}$ ,  $t_{1/2} = 30.2\text{Y}$ ), are the most common and reliable method employed to calculate short term (year to decades) sediment deposition and accumulation rates in the estuarine, fluvial and lacustrine environment (Kim, 2003).

Estimation of sedimentation rates in lakes and reservoir are vital in many schemes involving the formulation and impoundments of water storage, and pragmatic measurements can contribute both

directly through their role in developing and testing models. The computation of Lake sedimentation is in the present study considered as a tool of scientific prediction in the planning, management, and operational phases of conservation of Veeranam Lake. The present study is the first of its kind on the detailed investigation about the rate of sedimentation in Veeranam Lake, a typical major lacustrine system of the tropics enjoying moderate rain fall and climate, located essentially in the Northern Tamil Nadu. As the Veeranam lake is the major wetland system supplies water to the agriculture activity in the Cuddalore district and is known for its New Veeranam water scheme, through which water has been transported to Chennai to meet out the metro water demand.

## 2. Study Area

The area chosen for this study is Veeranam Lake, which was created during Chola period in the tenth century, built from 1011 to 1037AD and is 16-kilometre (9.9 mi) long dam in northern Tamil Nadu. Veeranam Lake is located 14 km (8.7 mi) SSW of Chidambaram in Cuddalore district, Tamil Nadu, India. The lake falls between north latitudes 11°15' to 11°25' N and east longitudes 79°30' to 79°35' E (Figure 1). It falls in the geological survey of India toposheet no. 58 M/11. The lake is bounded by Vellar River in the north and Coleroon River in the south. It has good network of roads and railways.

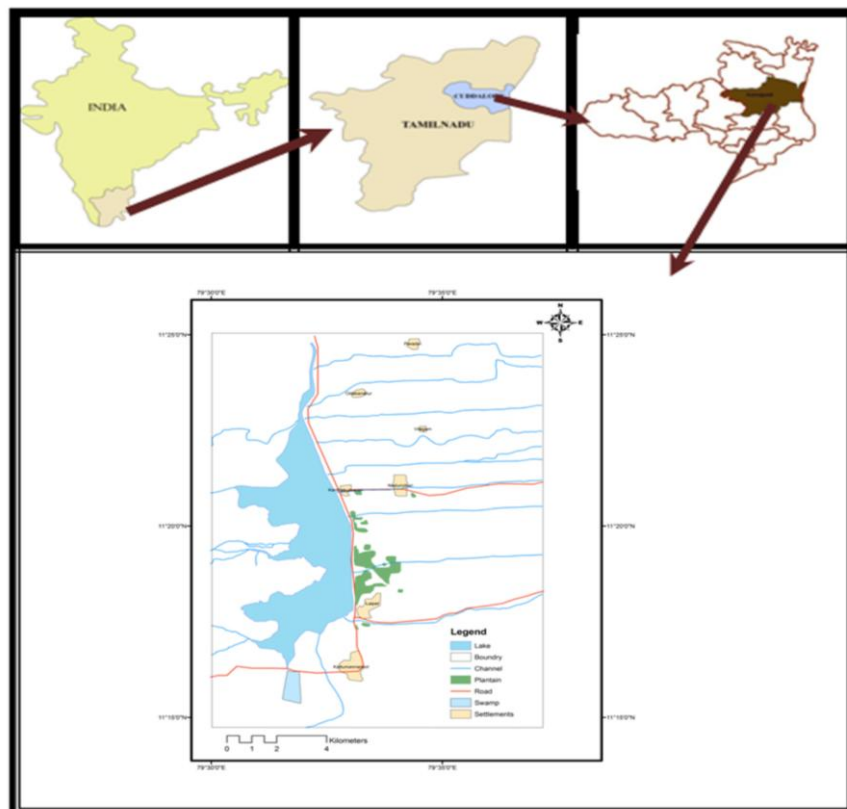


**Figure 1:** Geographic Location of Veeranam Lake

## 3. Methodology

$^{137}\text{Cs}$  is produced in the atmosphere due to cosmic ray interactions. However, its concentration increased many folds in the atmosphere due to the test of nuclear weapons and since 1954, it has been globally detectable.  $^{137}\text{Cs}$  is strongly absorbed on tiny particles like clay materials, silts and humic materials. Surface soils with an adsorptive capacity will have a  $^{137}\text{Cs}$  content and therefore be able to act as a self-tracer.

The sediment core was recovered from deepest part of the Veeranam Lake and the location is shown in Figure 2. Samples were ground and placed in a polyethylene tube (4.5 OD x 3 cm heights) and inserted into the well of an intrinsic high pure Germanium (HPGE) gamma detector. For measurement of  $^{137}\text{Cs}$  activity the multichannel gamma ray spectrometer (MCA) was used. The Priston Gamma Tech., USA (PGT) converts the radioactivity incident on the Germanium crystal into analogue signal that is received by the MCA system. The core sample from Veeranam Lake was counted for four hours to determine the activity of  $^{137}\text{Cs}$  at 662 keV. The analysis was performed at National Institute of Hydrology (NIH), Roorkee, India, in Canberra – Gamma ray spectroscopy GC –3520.

The applications of  $^{210}\text{Pb}$  dating are many and varied; this method is very popular and has been applied in several lake studies, the world over. A sediment core records a detailed history of the environment in its vicinity and the  $^{210}\text{Pb}$  dating technique provides a chronology covering a time scale of 100 to 150 years, uniquely suited to the period of man's greatest impact.

The  $^{210}\text{Pb}$  activity is measured through the  $\alpha$ - counting of its grand-daughter, namely  $^{210}\text{Po}$ , which is assumed to be in secular equilibrium with its parent. The  $\alpha$ -counting of the grand-daughter product ( $^{210}\text{Po}$ ) is more widely used. In this case, the basic radiochemical procedure involves adding of  $^{208}\text{Pb}$  as a yield tracer, leaching the sediment samples with aquaregia, filtering off the residual solids and converting to chloride with concentrated HCl. The final solution is taken in 0.5 M HCL. Polonium nuclides are then spontaneously deposited on silver planchette by adding ascorbic acid in the HCl solution. The alpha counting was performed using silicon surface barrier detector connected to a multi-channel analyzer. The entire operation is controlled through the Genie -2000 Software v 3.2. The counts were carried out for six hours to determine the activity of Veeranam Lake core sediment sample. The analysis was carried out in Canberra – Alpha Analyst – Alpha spectrometer – 7200-04.

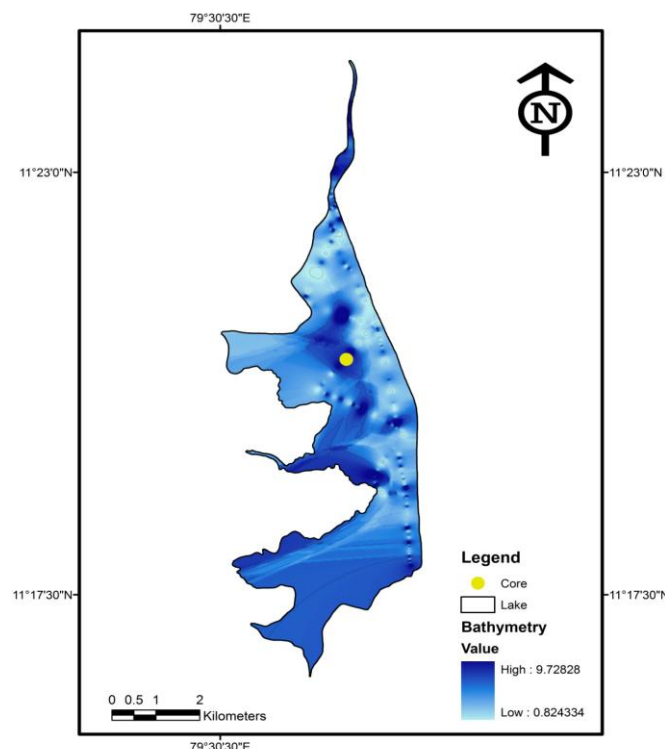


**Figure 2:** Core Location in the Bathymetry Map of the Veeranam Lake

## 4. Results and Discussion

### 4.1. Sedimentation Rate

#### A) Cesium – 137 ( $^{137}\text{CS}$ ) Dating

Over the last 25 years there have been many convincing demonstrations of the chronological value of  $^{137}\text{Cs}$  measurements especially in relatively rapidly accumulating sediments (Livingstone and Cambray, 1978; Heit et al., 1984). Counting the gamma emissions of  $^{137}\text{Cs}$  at 662 KeV is relatively simple, non-destructive procedure. The 30.17 years of half-life ensures the continuing use of the method for chronological purposes some way into the next 50 to 75 years. Moreover, in areas affected by deposition from the 1986 Chernobyl accident an additional “Spike” is now emerging as a possible future aid to sediment dating.

The technique is based on the following characteristics of  $^{137}\text{Cs}$ ; Relatively short residence time in the atmosphere, Absolutely of anthropogenic origin with no natural production, Significant variation in production levels during different time periods, Half Life is 30.17 years, Reliable records of global distribution, Characteristic to adhere with organic, silt and clayey material accompany by negligible mobility in the environment.

The first occurrence of  $^{137}\text{Cs}$  in core sediment of Veeranam Lake is observed at 38 cm (Figure 3). However, samples below 38cm were not available for present study and we cannot therefore assign a date to the first appearance of  $^{137}\text{Cs}$  in core sediments of Veeranam Lake. The 16cm peak in  $^{137}\text{Cs}$ , however, is interpreted to represent 1963 the peak year of nuclear testing (Chillrud et al., 1999). Based on this, it is assigned that the date of 1963 to the 16cm depth in core of Veeranam Lake (Figure 3). At the sampling location, the  $^{137}\text{Cs}$  profile closely paralleled its weapon fallout record pattern reported by earlier investigators (Eakins and Cambay, 1985; Engstrom et al., 1985; Farmer, 1978) i.e., an initial appearance in 1952-53; a subsidiary peak in 1957-58; and major peak in 1963-64. With the depth corresponding to 1963-64 as time marker, the average sedimentation rate (both linear and mass unit) of Veeranam Lake was computed. The close similarity in the deposition and fallout pattern of  $^{137}\text{Cs}$  probably indicates that the residence time of  $^{137}\text{Cs}$  in the lake water is small and post-depositional mobility of the radionuclide in the sediment core, if any, is insignificant. However, the  $^{137}\text{Cs}$  profile of Veeranam Lake may be viewed as an ideal case.

#### B) Lead – 210 ( $^{210}\text{Pb}$ ) Dating

Lead-210 geochronology is an isotopic method of age estimation based on the radioactive decay of  $^{222}\text{Rn}$  and  $^{210}\text{Pb}$ . Since its inception, the  $^{210}\text{Pb}$  method has been practiced using the basic techniques, models and assumptions of its originator (Goldberg, 1963). The strong community confidence in this method is demonstrated by numerous successful results and the increased number of studies using it. Because of the relatively short half-life of  $^{210}\text{Pb}$  (22.26 years), this method is chiefly applied in palynological, limnological, marine, and glaciological studies to estimate sedimentation rates for the past century or more. The  $^{210}\text{Pb}$  method is widely used in the determination of sedimentation rates in lacustrine and marine depositional records.

Disintegration of the intermediate isotope  $^{226}\text{Ra}$  (half-life 1622 years) yields the inert gas  $^{226}\text{Rn}$ , this in turn decays (half-life 3.83 days) through a series of short-lived isotopes to  $^{210}\text{Pb}$ . Radium-226 is supplied to the lake sediments as part of the particulate erosive input. The  $^{210}\text{Pb}$  formed by the in situ decay of this radium is termed as the “supported  $^{210}\text{Pb}$ ” and is normally assumed to be in radioactive equilibrium with the radium. In general, however, this equilibrium will be disturbed by a supply of  $^{210}\text{Pb}$  from other sources. Lead-210 activity in excess of the supported activity is called the “excess” or “unsupported”  $^{210}\text{Pb}$ .

The principal source of unsupported  $^{210}\text{Pb}$  is generally taken to be direct atmospheric fallout, although the importance of the other sources has not been extensively evaluated. In this context three components have been identified (Oldfield and Appleby, 1984):

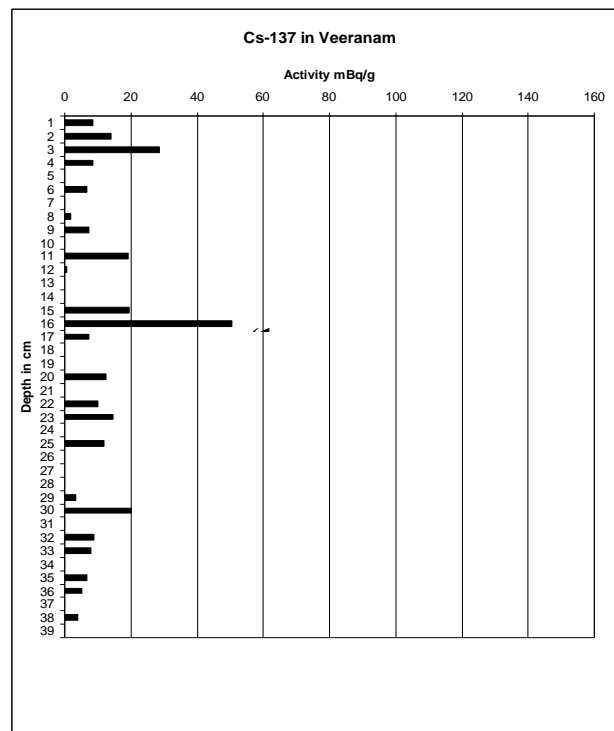


**Figure 3:** Sediment dating of  $^{137}\text{Cs}$  deposition Profile in Veeranam Lake.

The  $^{210}\text{Pb}$  dating techniques have been used to cross check and authenticate the results obtained using  $^{137}\text{Cs}$  dating technique in the present study. The estimation of sedimentation rate using  $^{137}\text{Cs}$  dating technique is easier in comparison with  $^{210}\text{Pb}$  dating technique as later requires complicated chemical process for the separation of  $^{210}\text{Pb}$  from sediments. The sedimentation rates estimated by  $^{210}\text{Pb}$  dating technique are found close to the sedimentation rates determined by  $^{137}\text{Cs}$  dating technique. The  $^{210}\text{Pb}$  activities determined in the sediment cores are shown in Figure 4. The total  $^{210}\text{Pb}$  activities are depicted by an almost linear decline in relation to depth. The  $^{210}\text{Pb}_{\text{excess}}$  is assumed to come from the atmosphere (or) fluxes not explained by the  $^{238}\text{U}$  series equilibrium. The  $^{210}\text{Pb}_{\text{excess}}$  was fitted to the least square procedure ( $r^2 = 0.202$ ) and slope ( $r^2 = 0.202$ ;  $n = 4.40$ ;  $P < 0.05$ ) and slope of the long linear curve ( $Y = -12.3x + 54.59$ ) allowed the calculation of the sedimentation rate (6.2 mm/year) (Apple by and Oldfield, 1992). Thus, the bottom of the sediment core (46cm) was estimated to be near 1935 year old. As the atmospheric deposition flux of  $^{210}\text{Pb}$  at the lake site is unknown, the available mean atmospheric flux of  $^{210}\text{Pb}$  at Mumbai station, India, ( $0.025 \text{ Bq/cm}^2/\text{yr}$ ; Edington et al., 1976) has been considered. As seen in Figure 4, at core location, the (total)  $^{210}\text{Pb}$  profile shows a more or less exponential decrease in concentration with depth to a constant value maintained by in-situ decay of  $^{226}\text{Ra}$ . In lakes, the inflow velocity and other forces such as gravitational force and the secondary forces of flow turbulence control the spatial distribution of incoming sediments.

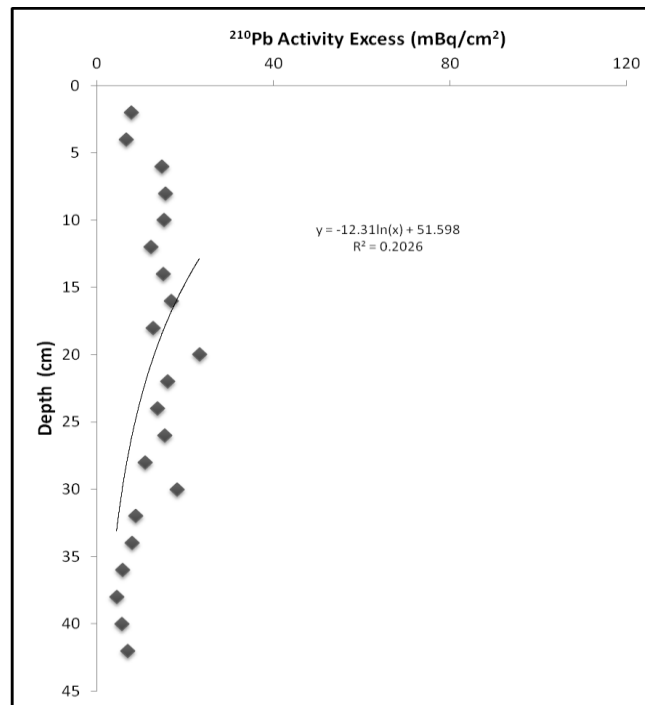


**Figure 4:** Sediment dating of  $^{210}\text{Pb}$  Concentration Profile in Veeranam Lake Core

## 5. Computation of Lake Life

The lake may be in filled with deposited sediment and gradually become a wetland such as a swamp or marsh. Large water plants accelerate this closing process significantly because they partially decompose to form peat soils that fill the shallows. Conversely, peat soils in a marsh can naturally burn and reverse this process to recreate a shallow lake. Turbid lakes and lakes with many plant-eating fish tend to disappear more slowly. A "disappearing" lake (barely noticeable on a human timescale) typically has extensive plant mats at the water's edge. These become a new habitat for other plants, like peat moss when conditions are right, and animals, many of which are very rare.

The lake life has been estimated taking into account the estimated sediment accumulation rates in the single zone and the present volume of the lake. The useful life of the Veeranam Lake is calculated as;

$$\text{Useful Life of the Lake } (L_U) = D_m \times 100 / R_s$$

$$\begin{aligned} \text{i) } \quad ^{137}\text{Cs} &= 3.38 \times 100 / 0.35 \\ &= 965.71 \text{ Years} \end{aligned}$$

$$\begin{aligned} \text{ii) } \quad ^{210}\text{Pb} &= 3.38 \times 100 / 0.32 \\ &= 1056.25 \text{ Years} \end{aligned}$$

The total sedimentation in Veeranam Lake, taking into account mean accumulation rate is 0.32cm/yr ( $^{210}\text{Pb}$ ) and 0.35 cm/yr ( $^{137}\text{Cs}$ ). If the sediment deposition continues at the same rate, the lake may completely be filled up in 965.71 years ( $^{137}\text{Cs}$ ) or 1056.25 years ( $^{210}\text{Pb}$ ) under normal environmental conditions.

## 6. Conclusion

The first occurrence of  $^{137}\text{Cs}$  in Veeranam core is at 38cm. The maximum peak value of  $^{137}\text{Cs}$  at 16cm was interpreted to represent 1963 the peak year of nuclear testing (Chillrud et al., 1999). With the depth corresponding to 1963-64 as time marker, the average sedimentation rate in Veeranam Lake computed as 6.1mm/year. The total  $^{210}\text{Pb}$  activities determined in the sediment cores depicted by an almost linear decline in relation to depth. The  $^{210}\text{Pb}$  excess is assumed to come from the atmosphere (or) fluxes not explained by the  $^{238}\text{U}$  series equilibrium. The  $^{210}\text{Pb}_{\text{excess}}$  allowed the calculation of sedimentation rate as 3.2mm/ year. Veeranam Lake, taking into account means accumulation rate ranges between 0.32 cm/year ( $^{210}\text{Pb}$ ) and 0.35 cm/year ( $^{137}\text{Cs}$ ). The rate of sedimentation calculated based on  $^{137}\text{Cs}$  and  $^{210}\text{Pb}$  reveals that the life span of the Veeranam Lake is around 965.71 years and 1056.25 years respectively. The computations of the lake life were estimated with the condition, which prevails during sampling.

## Acknowledgements

The authors are thankful to the authorities of University Grants Commission (UGC), New Delhi, Government of India, for their financial assistance to carry out this study in the form of major research project (200-F-135) and National Institute of Hydrology, Isotope hydrology division, Roorkee, India, for  $^{137}\text{Cs}$  and  $^{210}\text{Pb}$  analysis.

## References

- Appleby and Oldfield. 1992: *Application of Lead-210 to Sedimentation Studies*. In: Uranium Series Disequilibrium: Application to Earth, Marine & Environmental Sciences. Ivanovich, M., and R.S., Harmon (Eds.). Oxford University Press, Oxford. 731-778.
- Chillrud, S.N., Bopp, R.F., Simpson, H.J., Ross, J.M., Shuster, E.L., Chaky, D.A., Walsh, D.C., Choy, C.C., Tolley, L.R., Yarme, A. *Twentieth Century Atmospheric Metal Fluxes into Central Park Lake, New York City*. Environmental Science and Technology. 1999. 33 (5) 658-662.
- Eakins, J.D., and Cambray, R.S., 1985: *Studies of Environmental Radioactivity in Cumbria*. Report AERE-R-11182, UK AERE, Harwell.
- Edington, N., Plowright, W., and Watt, R.G. *Generalised Porcine Cytomegalic Inclusion Disease: Distribution of Cytomegalic Cells and Virus*. Journal of Comparative Pathology. 1976. 86; 191-202.
- Engstrom, D.R., Swain, E.B., and Kingston, J.C. *A Palaeolimnological Record of Human Disturbance from Harvey's Lake, Vermont: Geochemistry, Pigments and Diatoms*. Freshwater Biol. 1985. 15; 261-288.
- Farmer, J.G. *The Determination of Sedimentation Rates in Lake Ontario using the  $^{210}\text{Pb}$  dating Method*. Canadian Journal of Earth Science. 1978. 15; 431-437.
- Goldberg, E.D. *Geochronology with  $\text{Pb-210}$ , in Radioactive Dating*. International Atomic Energy Agency Contribution. 1963. 1510; 121-131.
- Heit, M., Miller, K.M., Krey, P., Bogen, D., and Freely H., 1984: *Other Radionuclides: Plutonium with Some Comments about  $^{137}\text{Cs}$  Chronologies in Freshwater Sediments*. Workshop on Paleolimnological Studies of the History and Effects of Acidic Precipitation, Rockland, ME. 34-77.

Kim, Y.S., Peacock, D.C.P., and Sanderson, D.J. *Mesoscale Strike-Slip Faults and Damage Zones at Marsalforn, Gozo Island, Malta*. Journal of Structural Geology. 2003. 25; 793-812.

Livingstone, H.D., and Cambray, R.S. *Confirmation of <sup>137</sup>CS dating by Algal Stratigraphy in Rostherne Mere*. Nature (London). 1978. 276; 259-261.

Oldfield, F., and Appleby, P.G. *A Combined Radiometric and Mineral Magnetic Approach to Recent Geochronology in Lake Affected by Catchment Disturbance and Sediment Redistribution*. Chem. Geol. 1984. 44; 67-83.

Suess, H.E. *Secular Variations of the Cosmic-Ray- Produced Carbon 14 in the Atmosphere and their Interpretations*. Journal of Geophysical Research. 1965. 70 (23) 5937-52.

## Study of Snow Cover Dynamics of Pinder Watershed in Central Himalaya using Remote Sensing and GIS Techniques

N.C. Pant, Manish Kumar, J.S. Rawat and Neha Rani

Centre of Excellence for NRDMS in Uttarakhand, Department of Geography, Kumaun University, SSJ Campus, Almora, Uttarakhand, India

Correspondence should be addressed to J.S. Rawat, jsrawat1955@gmail.com

Publication Date: 12 July 2014

Article Link: <http://scientific.cloud-journals.com/index.php/IJAESE/article/view/Sci-194>



Copyright © 2014 N.C. Pant, Manish Kumar, J.S. Rawat and Neha Rani. This is an open access article distributed under the **Creative Commons Attribution License**, which permits unrestricted use, distribution, and reproduction in any medium, provided the original work is properly cited.

**Abstract** This paper is an attempt to examine the dynamics of snow cover using Normalized Difference Snow Index (NDSI) in Pinder Watershed, Central Himalaya, India. Landsat satellite imageries of three different time periods, i.e., Landsat TM of 1990, Landsat TM of 1999 and Landsat TM 2011 were used to quantify snow cover. The geographical distribution of snow cover reveals that in 1990 and 1999 about 9.40% (176.20 km<sup>2</sup>) and 8.60% (161.08 km<sup>2</sup>) area of the Pinder Watershed was under snow cover while in 2011 the snow cover was found 7.80% (147.50 km<sup>2</sup>). These data suggest that due to global warming about 28.7 km<sup>2</sup> snow cover of Pinder Watershed has been converted into non-snow cover area at an average rate of 1.36 km<sup>2</sup>/year during the last two decades, i.e., in between 1990 to 2011.

**Keywords** NDVI; Snow Cover Dynamics; Pinder Watershed; Central Himalaya; RS/GIS Application

### 1. Introduction

Snow cover plays an important role in the climate system by changing the energy and mass transfer between the atmosphere and the surface. Atmospheric and man-made activities have great impact on snow. Snow melt dynamics generate a complex set of interactions, which dictates a need for long-term monitoring of snow cover in conjunction with other climatological variables.

Snow-cover information is important for a wide variety of scientific studies, water supply and management applications. The distribution of snow in space and time is an important parameter for a wide variety of reasons. Knowledge of the extent of the snow is valuable information because it provides insight to the amount of water to be expected from snowmelt available for runoff and water supply. In addition, the snow cover itself is a surface condition that affects radiation and water balance determinations that are inputs to hydrological cycle and climate studies (Cess et al., 1991; Cohen, 1994; Cohen & Entekhabi, 2001; Douville & Royer, 1996; Foster et al., 1996; Stieglitz et al., 2001; Yang et al., 1999). In Indian context, many perennial rivers are fed by snow and ice cover where people rely on snowmelt for irrigation of croplands and drinking water. Area and spatial

distribution of snow and ice cover in alpine regions varies significantly over time, due to seasonal and interannual variations in climate (Zhen and Li, 1998). Small Alpine glaciers are disappearing rapidly (Farge, 2003). According to Farge (2003), historic data on recession have been captured and analyzed in geographic information system and chronosequences have been produced that show over 72% of the largest glaciers have disappeared over the past century. Canon (2003) has advocated that since the end the small Ice Age (1850), the glacier regions of Colombia have lost 80% of their area. Considering current climate change trends an analysis of this process suggests that the glacier will disappear completely within the next century (Canon, 2003). Therefore, there is a need for monitoring the area and spatial distribution of snow and ice cover from local to global scales. Thus, snow cover area monitoring is currently an important tool in studies of global climate change, particularly because satellite remote sensing data provide timely and efficient snow cover information for large areas.

Satellite remote sensing offers the opportunity to monitor and evaluate various snow parameters and processes at regional and global scale (Hall and Martinec, 1985; Hall et al., 2005) and the remote sensing technique has been used extensively for snow-cover monitoring in the Himalayan region with the help of numerous satellite sensors (Kulkarni and Rathore, 2003). Geographical Information System (GIS) along with remote sensing technology facilitate fast and efficient ways to analyse, visualise and report the seasonal snow-cover changes. A number of earlier remote sensing studies have used Landsat Thematic Mapper (TM) data and explored various TM spectral bands to identify and map snow and ice cover (Hall et al., 1995, 1998; Bronge and Bronge, 1999; Sidjak and Wheate, 1999). Snow and ice cover have very high spectral reflectance values in the visible bands (TM1, 2, 3), but low reflectance values in the mid-infrared band (TM5). Hall et al., (1995, 1998) has proposed the NDSI technique for identifying and mapping snow and ice cover. The fundamental objective of the present paper is to study snow cover dynamics of a Central Himalayas watershed viz., the Pinder watershed using NDVI technique.

## 2. Study Area

The study area, viz., the Pinder Watershed (Figure 1) which extends between 29°59'41"N to 30°18'57"N latitudes and 79°05'43"E to 80°04'38"E longitudes, encompasses an area of 1872.98 km<sup>2</sup> in the Central Himalaya, India. The altitude of the watershed varies between 757 m and 6746 m. The Pinder River originates from the Pinder glacier. Studies reveals that Pinder glacier has been retreated at the rate of 26.22 m/year during 1845 to 1906 (Stracrchey, 1945; Holland et al., 1906 and Cotter, 1906), 20 m/year during 1906 to 1958 and 25 m/year during 1958 to 1966 (Tiwari and Jangpangi, 1962 and Tewari, 1972).

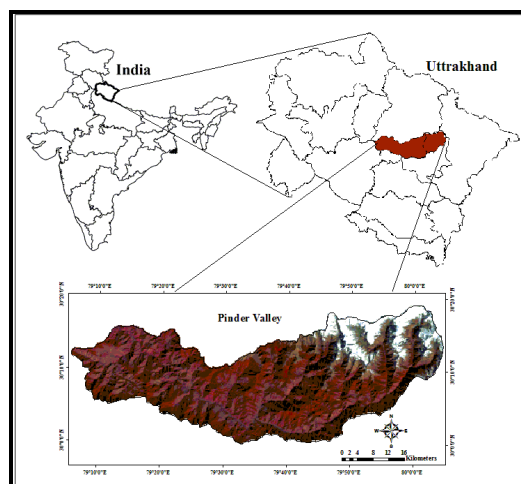


**Figure 1:** Location Map of the Study Area

### 3. Methodology

To work out with snow cover area, remotely sensed data are extremely valuable. To examine the snow cover area in the Pinder watershed, Landsat satellite imageries of three different dates and years were acquired by Global Land Cover Facility site and GLOVIS. The first imagery used in the present study was Landsat TM of 15<sup>th</sup> November 1990 at 30 m resolution. The second and third imageries were of Landsat TM data of 15<sup>th</sup> October 1999 and 2011 at a resolution of 30 m. These imageries helped in understanding the extent of snow cover area in the watershed over the last 21 years (i.e. 1990 to 2011). ERDAS Imagine software was used for processing the satellite imageries. The Area of Interest (AOI) was calculated and finally the required image was extracted by sub-setting of the image. The subset image was then reprojected. The upper limit of snow area was delineated using NDSI (Hall et al., 1998):

$$\text{NDSI} = \frac{\text{TM2}-\text{TM5}}{\text{TM2}+\text{TM5}}$$

Hall et al., (1998) suggested that a NDSI threshold of >0.40 be used to map snow cover. After displaying the NDSI imagery on the screen of Arc map, the lower limit of snow cover in the watershed area was digitized for different years. By superimposing the lower limit of snow cover of different years, the area of change from snow cover area to non-snow cover area was worked out.

### 4. Results and Discussion

The results obtained through the analysis of NDSI imagery are diagrammatically illustrated in Figure 2 and 3 and data are registered in Table 1 and 2. Figure 2 depicts distribution of NDSI variation while Figure 3 depicts spatial distribution of snow cover area in 1990, 1999 and 2011 in the study area. A brief account of these results is discussed in the following paragraphs.

#### 4.1. Status of Snow Cover

From the Figure 3 which is based on NDSI values of Figure 2, area under snow cover during different years was worked out which is presented in Table 1. The Table 1 reveals that the snow cover area in Pinder watershed was about 9.40% (176.20 km<sup>2</sup>) in 1990, about 8.60% (161.08 km<sup>2</sup>) in 1999 and about 7.80% (147.50 km<sup>2</sup>) in 2011.

**Table 1:** Snow Covers Area in Different Years in the Pinder Watershed, Central Himalaya, India

Years	Snow Area (km <sup>2</sup> )	Percentage
1990	176.20	9.40
1999	161.08	8.60
2011	147.50	7.80

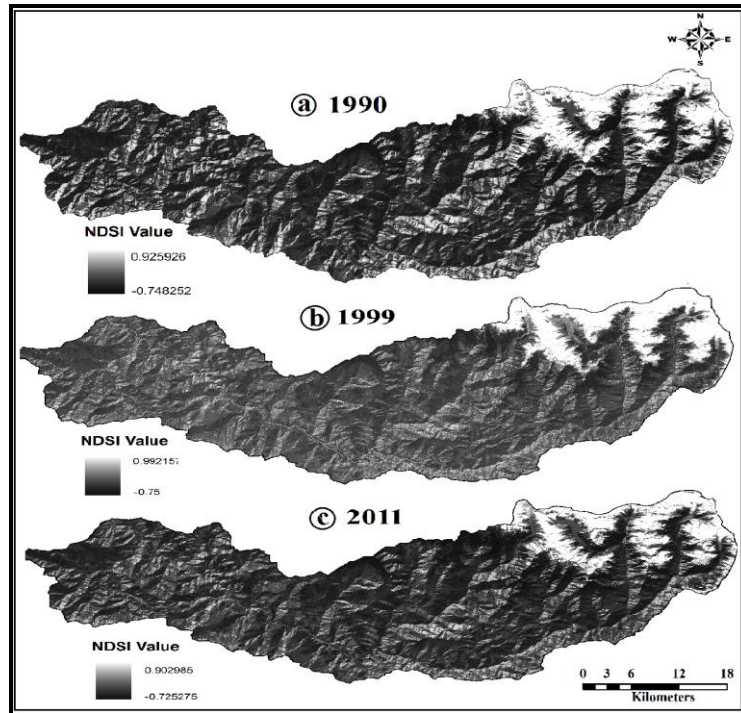


**Figure 2:** Geographical Distribution of NDSI Value in Different Years in the Pinder Watershed; (a) 1990, (b) 1999 and (c) 2011

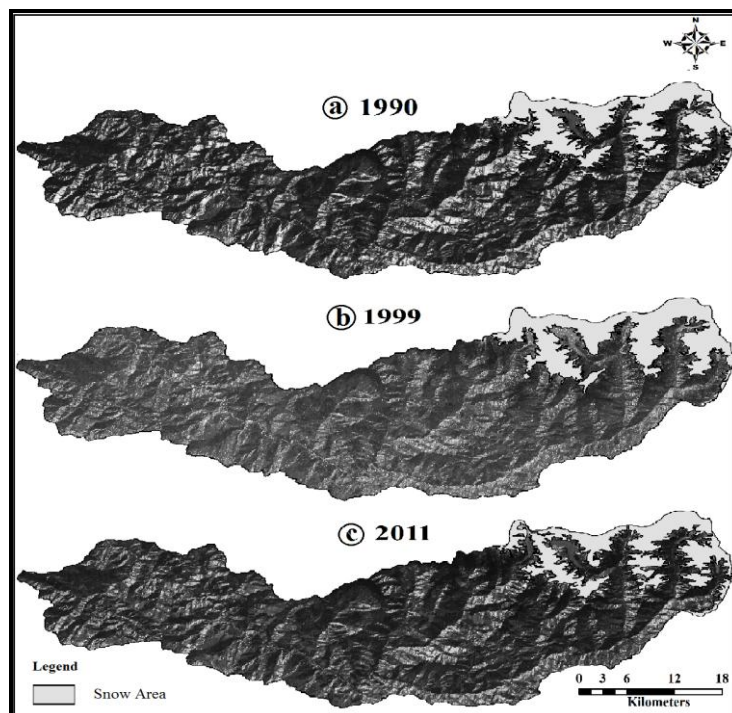


**Figure 3:** Geographical Distribution of Snow Cover Area Based on NDSI Values (>0.4) in Different Years in the Pinder Watershed; (a) 1990, (b) 1999 and (c) 2011

#### 4.2. Change in Snow Cover

The data presented in Table 2 suggest that due to global warming the snow cover area in the Pinder watershed has been shifted towards higher elevation and has been depleted considerably during the

last two decades. Results reveal that during 1990 to 2011, about 28.70 km<sup>2</sup> snow cover of the Pinder watershed has been converted into non-snow cover area from the snow cover area at an average rate of 1.36 km<sup>2</sup>/year (Table 2). The change from snow cover area to non-snow cover area during 1990 to 1999 and 1999 to 2011 was found about 15.12 km<sup>2</sup> (at the rate of 1.68 km<sup>2</sup>/year) and 13.58 km<sup>2</sup> (at the rate of 1.13 km<sup>2</sup>/year), respectively (Table 2).

**Table 2:** Amount and Rate of Snow Cover Change during Different Periods in the Pinder Watershed, Central Himalaya, India

Years	Period	Change from Snow Cover to Non-Snow Cover	
		Area	Rate
1990-1999	9 years	15.12 km <sup>2</sup>	1.68 km <sup>2</sup> /year
1999-2011	12 years	13.58 km <sup>2</sup>	1.13 km <sup>2</sup> /year
<b>1990-2011</b>	<b>21 years</b>	<b>28.70 km<sup>2</sup></b>	<b>1.36 km<sup>2</sup>/year</b>

## 5. Conclusions

The present study carried out in a Central Himalayan watershed, viz., the Pinder reveals that during the last two decades about 28.70 km<sup>2</sup> area of the Pinder watershed has been converted into non-snow cover area from snow cover area. With the help of these data, it can be extrapolated that the snow cover area in Pinder watershed is depleting at the average rate of 1.36 km<sup>2</sup>/year. It is evident from this study that the snow cover area is depleting steadily in the Central Himalaya due to global warming. If the trend of snow cover depletion continues, the water resources of the region will be in danger which may result in severe environmental degradation, social disruption and ecological damages in the Central Himalayan region.

## Acknowledgement

This paper constitutes a part of the Uttarakhand State Council for Science and Technology, Government of Uttarakhand and NRDMS Division, DST, New Delhi research projects NRDMS/11/1817/011.

## References

- Bronge, B.O., and Bronge, C. *Ice and Snow-Type Classification in the Vestfold Canon, M.A., Colombian Case, Cinturon Andino Biosphere Reserve*. Proceedings of the International Launching Workshop, Entlebuch Biosphere Reserve. 2003. 17-31.
- Canon, M.A. *Colombian Case, Cinturon Andino Biosphere Reserve, Proceedings of the International Launching Workshop*. Entlebuch Biosphere Reserve. 2003. 17-31.
- Cess, R.D., Potter, G.L., Zhang, M.H., Blanchet, J.P., Chalita, S., Colman, R., Dazlich, D.A., Del Genio, A.D., Dymnikov, V., Galin, V., Jerrett, D., Keup, E., Lacis, A.A., Le Treut, H., Liang, X.Z., Mahfouf, J.F., Mcavanev, B.J., Melshko, V.P., Mitchell, J.F.B., Morcrett, J.J., Norris, P.M., Randall, D.A., Rikus, L., Roeckner, E., Royer, J.F., Schlese, U., Sheinin, D.A., Slingo, J.M., Sokolov, A.P., Taylor, K.E., Washington, W.M., Wetherald, R.T. and Yagai, I. *Interpretation of Snow-Climate Feedback as Produced by 17 General Circulation Models*. Science. 1991. 253; 888-892.
- Cohen, J. *Snow and Climate*. Weather. 1994. 49; 150-155.
- Cohen, J., and Entekhabi, D. *The Influence of Snow Cover on Northern Hemisphere Climate Variability*. Atmosphere–Ocean. 2001. 39 (1) 35-53.

- Cotter, G. de P. *Notes on Certain Glacier in Kumaun*. Geological Survey India. 1906. 35; 148-152.
- Douville, H., and Royer, J.F. *Sensitivity of the Asian Summer Monsoon to an Anomalous Eurasian Snow Cover within the Meteo France GCM*. Climate Dynamics. 1996. 12 (7) 449-466.
- Farge, D.B. *Glacier National Park, Biosphere Reserve and GLORIA Site*. Proceedings International Launching Workshop, USA, Entlebuch Biosphere Reserve. 2003. 99-108.
- Foster, J., Liston, G., Koster, R., Essery, R., Behr, H., Dumenil, L., Verseghy, D., Thompson, S., Pollard, D. and Cohen, J. *Snow Cover and Snow Mass Intercomparison of General Circulation Models and Remotely Sensed Data Sets*. Journal of Climate. 1996. 9; 409-426.
- Hall, D.K., and Martinec, J. *Remote Sensing of Ice and Snow*. Chapman and Hall, NY. 1985.
- Hall, D.K., Foster, J.L., Verbyla, D.L., and Klein, A.G. *Assessment of Snow Cover Mapping Accuracy in a Variety of Vegetation-Cover Densities in Central Alaska*. Remote Sensing of Environment. 1985. 66; 129-137.
- Hall, D.K., Riggs, G.A., and Salomonson, V.V. *Development of Methods for Mapping Global Snow Cover using Moderate Resolution Imaging Spectroradiometer Data*. Remote Sensing of Environment. 1995. 54; 27-140.
- Hall, D.K., Foster, J.L., Verbyla, D.L., and Klein, A.G. *Assessment of Snow Cover Mapping Accuracy in a Variety of Vegetation-Cover Densities in Central Alaska*. Remote Sensing of Environment. 1998. 66; 129-137.
- Hall, D.K., Kelly, R.E.J., Foster, J.L. and Chang, A.T.C., 2005: *Hydrological Applications of Remote Sensing: Surface States: Snow*. In Encyclopedia of Hydrological Sciences. Anderson, M.G., (Ed.) John Wiley, Chichester. 3456.
- Holland, T.H. *A Preliminary Survey of Certain Glacier in Northwest Himalaya*. Geological Survey India. 1906. 35; 124-126.
- Kulkarni, A.V., and Rathore, B.P. *Snow Cover Monitoring in Baspa Basin using IRS WiFS Data*. Mausam. 2003. 54; 335-340.
- Sidjak, R.W., and Wheate, R.D. *Glacier Mapping of the Illecillewaet IceĀ Eld, British Columbia, Canada, using Landsat TM and Digital Elevation Data*. International Journal of Remote Sensing. 1999. 2; 273-284.
- Stieglitz, M., Ducharne, A., Koster, R., and Suarez, M. *The Impact of Detailed Snow Physics on the Simulation of Snow Cover and Subsurface Thermodynamics at Continental Scales*. Journal of Hydrometeorology. 2001. 2 (3) 228-242.
- Strachey, R. *A Description of Glacier of Pindari and Kaphnee River in the Kumaun Himalaya*. Journal Asiatic Society Bengal. 1845. 16; 794-812.
- Tewari, A.P. *Recent Change in the Position of the Pinder Glacier Kumaun Himalaya, Almora District U.P. India*. Proceeding Symposium of Role of Snow and Ice in Hydrology, UNESCO-WMO-IAIS. 1972. 15; 1144-1149.

Tewari, A.P., and Jangpangi, B.C. *The Retreat of the Snout of the Pindari Glacier Proceeding Symposium of Obsegurgle Intern.* Association Science Hydrology. 1962. 58; 245-248.

Yang, Z.L., Dickinson, R.E., Hahmann, A.N., Niu, G.K., Shaikh, M., Gao, X.G., Bales, R.C., Sorooshian, S., and Jin, J.M. *Simulation of Snow Mass and Extent in General Circulation Models.* Hydrological Processes. 1999. 13 (12-13) 2097-2113.

Zhen, Q., and Li, Z., 1998: *Remote Sensing Monitoring of Glaciers, Snow and Lake Ice in Qinghai–Xizang (Tibetan) Plateau.* In Contemporary Climatic Variations over Qinghai Xizang (Tibetan) Plateau and their Influences on Environments. Edited by M., Tang, G., Cheng and Z., Lin. Guangzhou, China: Guangdong Science and Technology Press. In Chinese. 279-308.

## Presence of Miocene Oysters: Rise and Fall of a Paleo-Estuary in the East Coast of India

Riffin T. Sajeev

Department of Geology, AWH Special College, Calicut, Kerala, India

Correspondence should be addressed to Riffin T. Sajeev, riffin@rediffmail.com

Publication Date: 24 July 2014

Article Link: <http://scientific.cloud-journals.com/index.php/IJAESE/article/view/Sci-198>



Copyright © 2014 Riffin T. Sajeev. This is an open access article distributed under the **Creative Commons Attribution License**, which permits unrestricted use, distribution, and reproduction in any medium, provided the original work is properly cited.

**Abstract** Living oysters of *Crassostrea Sp.* are abundantly found on the east coast of peninsular India. Most of the living *Crassostrea Sp.* is reported from Athinkarai estuary near Mandapam. The primary object of this study is to report the occurrence of fossils of *Crassostrea sp.* belonging to Mio-Pliocene outcrops from an ephemeral stream channel of Thoppuvila River up to Attankarai Pallivasal, Tirunelveli dist., Tamil Nadu, India. The present study focuses on revealing the nature of a vast paleo estuary that existed on the foothills of the southern end of the Western Ghats during the Mio-Pliocene age. The authors had studied the taphonomical features of *Crassostrea Gigantissima Sp.* Focusing on the adaptation features like heaviness and foliated nature of shell and orientation of oyster colonies for survival. The predatory signatures on the fossil specimens indicate traces of a well flourished marine environment that resembled an estuary subjected to high energy disturbances. The chalky calcareous deposits found throughout the study area could have acted as an accelerating agent for the thick, foliated and heavy calcite shells of *C. Gigantissima Sp.*

**Keywords** *Adaptation; Crassostrea Sp.; Ichnotaxa; Mahendragiri Hills; Mio-Pliocene; Taphonomy*

### 1. Introduction

Oysters are a highly influential group of creatures whose actions determine the features of biodiversity of an ecosystem, Marine food cycle, nutrient distribution and the quality of sea water (Alexandra et al., 2010). The Indian coast is home to a wide variety of Oyster species, most of which dwells along the intertidal biota. *Crassostrea Rivularis*, *Crassostrea Madrasensis*, *Crassostrea Gryphoides* and *Saccostrea Cucullata* are the most commonly available oysters in the Indian coastal zones (Rao, 1974). Oysters are highly sensitive to the environmental conditions and specifically adapted to estuarial ecosystems. The reconstruction of certain estuarial conditions can be made possible by recording its shell remains (Surge, D.M., et al., 2003). A detailed study of Oligocene bivalves from the western coasts of India is available (R.P., Kachhara et al., 2012) and large concentrations of Oligocene oysters from Argentina is also reported (Ana Parras et al., 2005; E., Farinati et al., 2002; G.S., Bressan et al., 2010).

Tuticorin and Tirunelveli coastal stretches are composed of beds of Panamparai sandstone, with wedged deposits of fine grained limestone, and pebbles. The fossil lineage found across this area shows a relative age of mio-pliocene. These beds of Panamparai sandstone, thus state influence from both marine and terrestrial/continental agents (Narayanaswamy, 1947). These deposits resemble that of the Cuddalore formation and are usually classified under the Warkhali beds of mio-pliocene origin. Molluscan studies in the area nearby Kanyakumari are mostly based on living species of oysters. Beds of living *Crassostrea Madrasensis* have been reported in the Vaigai estuary at Athankarai near mandapam (Rao et al., MS). An enormous number of studies about the physiological, habitual and the culturing of living oysters in crassostrea species are available (Carriker M.R., et al., 1980; D., Timothy J., et al., 1988; Melissa Southworth, 2010; Nagappan Nayar K., et al., 1987). There is no record of fossils of *Crassostrea Gigantissima* sp. in between Tuticorin and Kanyakumari. The authors had found a vast area of calcareous bed/Fossil assemblage in the channels of an ephemeral stream which leads to Thoppuvila River nearby Koodamkulam. Most of the fossil specimens of crassostrea species were subjected for predatory ambush by Ichnotaxa. Hence, the author is hereby analyzing the possibility of existence of a large estuary during Mio-Pliocene age in this area.

## 2. Materials and Methods

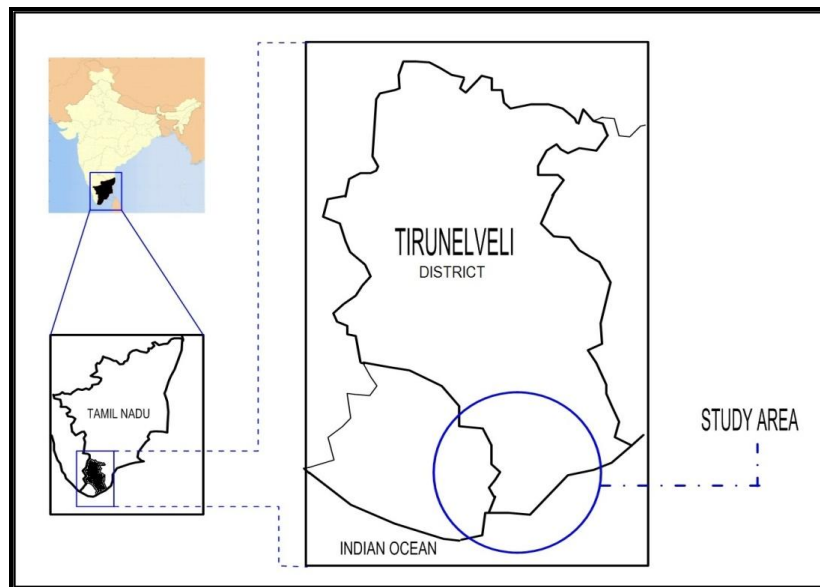


**Figure 1:** Map Showing Study Area at the Foothill of Southern End of the Western Ghats

The study area is situated at a geo code of latitude  $8^{\circ}19'12''\text{N}$  and longitude  $77^{\circ}39'24''\text{E}$ . The paleo estuarial outcrop is estimated to cover a wide area of around  $450\text{ km}^2$ . The satellite view of this area show that it is a valley of the southern end of the Western Ghats and is flourished with ephemeral stream channels originating from the Mahendragiri and Thekumalai from about 1.5 km elevation.

Figure 2 shows a Panoramic view of Thoppuvila River. The calcareous samples were collected from the marked outcrops. The elevation of the sampled outcrops ranges from 7 m to 39 m along a distance of 12 km from the sea.



Figure 3 shows the outcrops where the specimens were collected. All these areas comprise of calcareous, chalky material bedding which has been proved through chemical analysis. The specimens specifically come under two categories-one with color of sea sand sediment and another in black/gray in color. This may have happened due to the nature of sedimentation that occurred in its habitat during the Mio-Pliocene age. More than 10 samples were collected from each marked area to further understand the extent of the calcareous bed/chalky deposits in this geographical area.

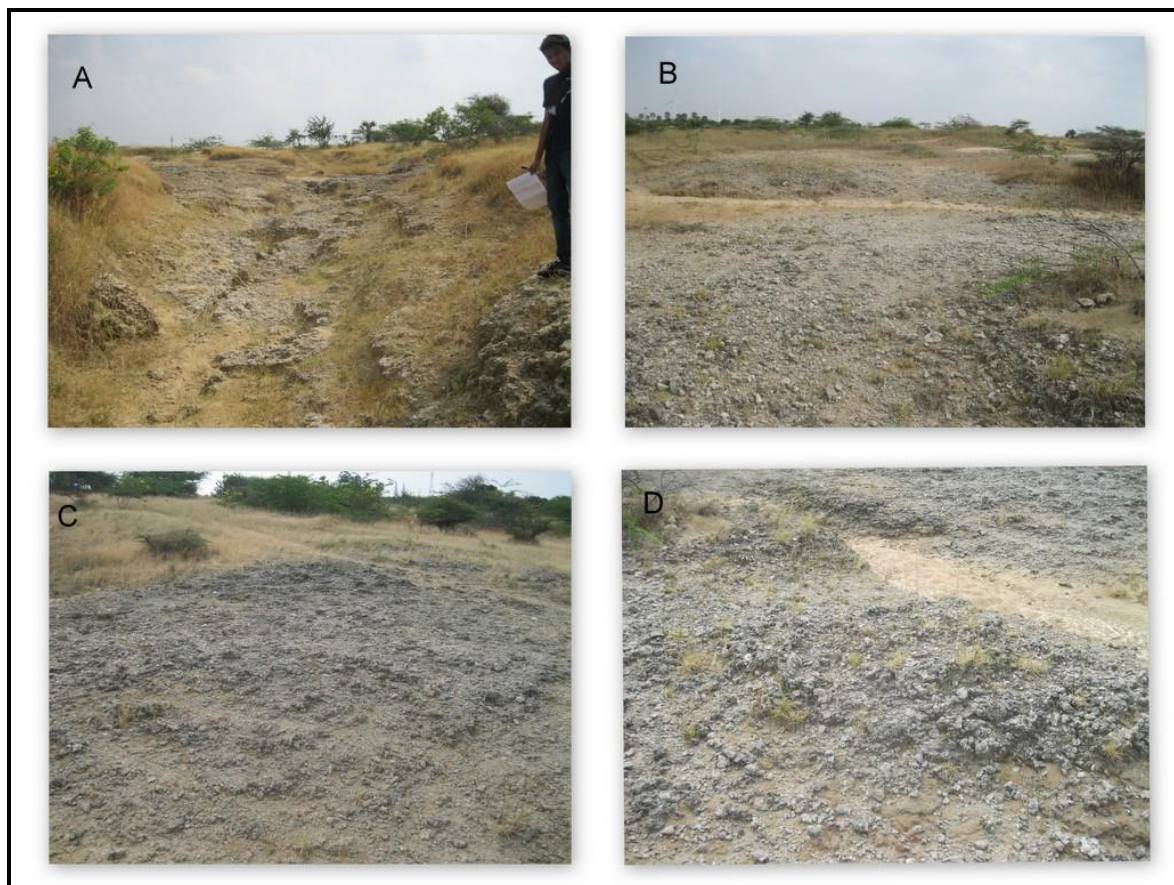


**Figure 3:** Outcrops Containing Calcareous/Chalky Deposits

Specimens of *Crassostrea Sp.* are of various sizes. The Species were identified as *Crassostrea Gigantissima* due to its morphological features. Fossil oysters were collected on the banks and Dry flow channel of Thoppuvila River around 15 kms away from the sea. Individual species of *crassostrea* cluster together with chalky deposits to form Oyster beds around 2m thick. Sediments consisting of dark grey sandy mudstone surround the oysters. In the middle parts of the bed, the oysters are found in a standing position with their umbones pointing downwards. At other parts of the bed, the oysters are found in a parallel position. Such parallel disorientations may be caused by the scouring forces of

tides and waves during the mio-pliocene age. Most of the shells are disarticulated, and for that reason, the accurate orientation of the oysters cannot be determined. The outcrops from which shells were collected consisted primarily of cemented clay with sand component. Two types of shell orientation were noted during sample collection: 1) life position, 2) random orientation. Shells in life position were recognized in outcrop as being both upright (dorsal beak pointing down section and ventral margin facing upward) and articulated (both valves together) as shown in Figure 4.



**Figure 4:** Articulated Fossil Specimen of *C. Gigantissima Sp.*

It was important to collect shells in life position as it is likely they were not transported and are accurate representatives of the environment in which they lived. All specimens were collected from within the outcrop by prying several inches into the outcrop. Articulated shells were observed at a height of 8 meters on the banks of Thoppuvila river channel. Many of the shells obtained from the nearby area of sea were evidently subjected for the predatory actions of *Ichnotaxa*. A major portion of the surface of the outcrop shows broken fragments of oysters or 'is subjected to disarticulation'. Figure 5 shows the scattered oyster fragments of same species of *Crassostrea Sp.* in various sampling sites along the banks and the dry flow channel of Thoppuvila River.

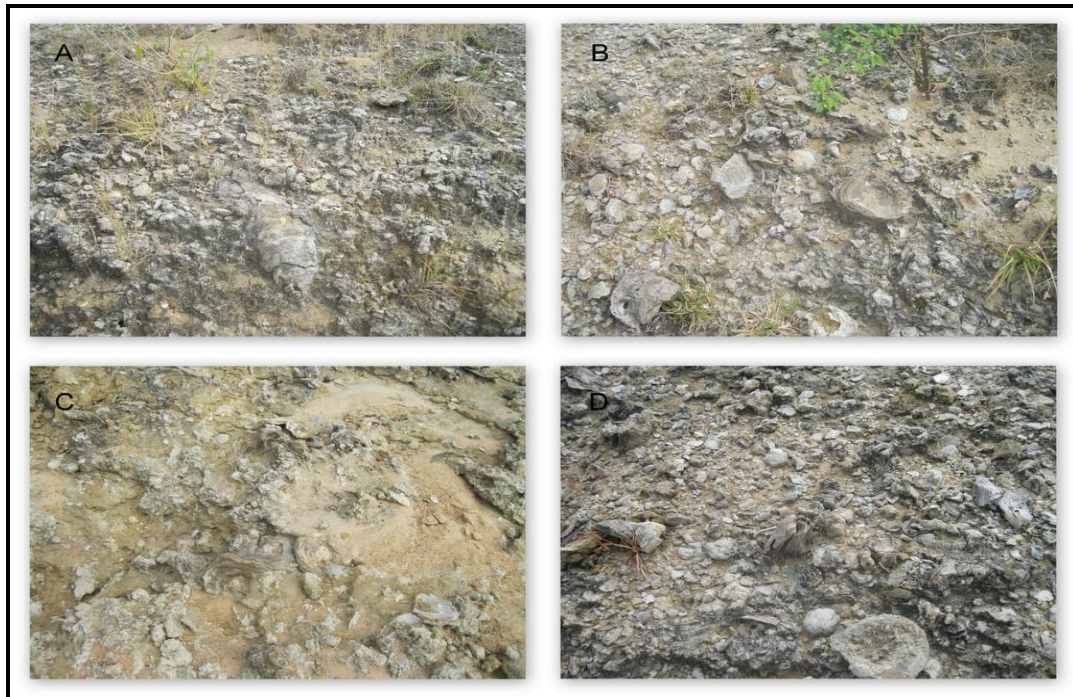


**Figure 5:** Oyster Fragments on Various Parts of the Study Area

### 2.1. Shell Morphology

The studied specimens consist of 30 disarticulate valves. The major morphological features of the specimens are observed as; both valves are large, heavy and thick with an outline of dorsoventrally elongated structure. All specimens have a height/ length ratio largely greater than 1.3 (from 1.5 to 3.2). Most of the specimens are of a straight, slender and spatulate form, which gradually broadens toward the ventral margin. A shallow body cavity is located in the ventral area of the shell valves. The left valve is longer, thicker and higher than the right valve for all specimens. Most of the specimens are moderately curved towards the centre and their marginal extensions overweigh those of the right valve. The right valve is either curved inwards or is flat shaped and the absence of chomata on the marginal layers of these shells is a noticeable characteristic feature. The dimensional characteristics of specimens exhibit an elongated or moderately curved conical shaped ligament area with a height: length ratio greater than 1 ( $H/L > 1$ ). The left valve shows a shallow umbonal cavity just below the hinge plate. Crescent shaped adductor muscle scar is clearly visible on most specimens. The outer surfaces of all specimens show a moderately rough shell structure with growth lines and exhibit an undulating nature. The calcite shell plates are arranged in inter-wedged patterns with varying thickness, ranging from a few micrometers to a millimeter. These layers are arranged in such a way that the thickness of calcite layers decrease towards the inner part of each valve.

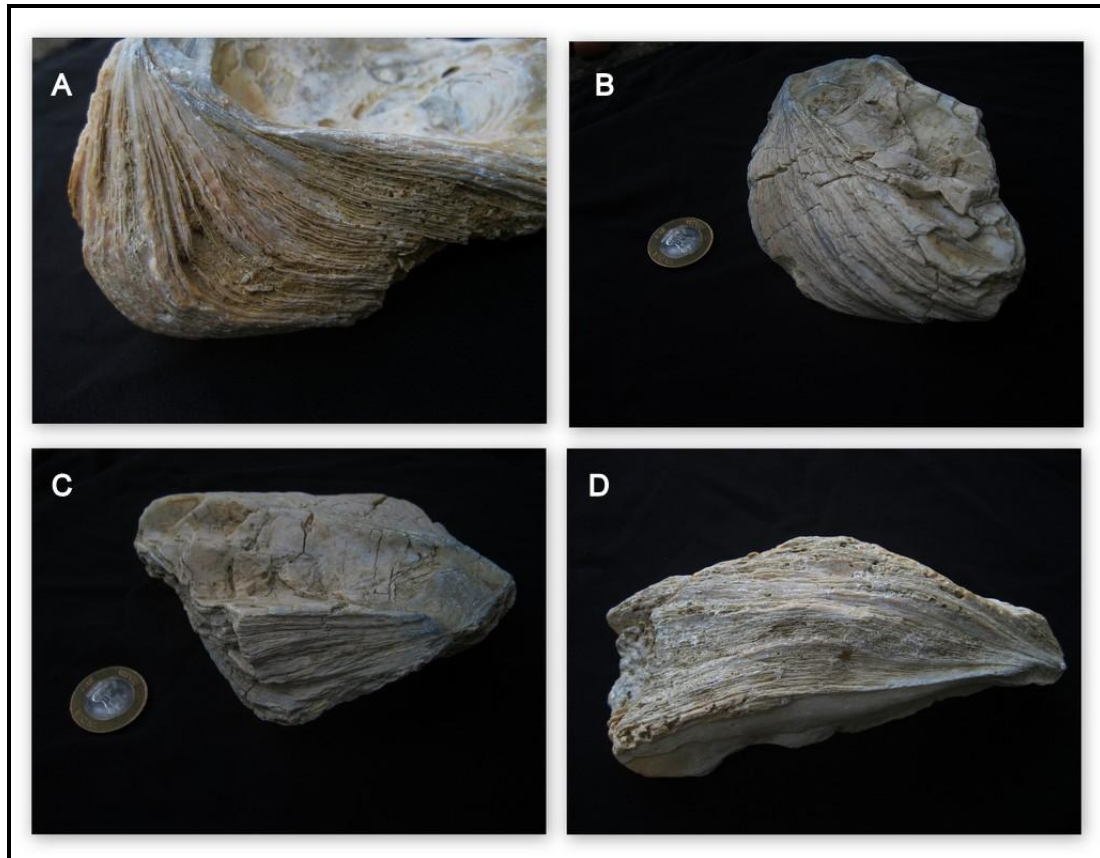


**Figure 6:** Foliated Shell Structure of *C. Gigantissima*

Carter and Clark (1985) construed these features of oyster shell as 'regularly foliated'. The Specimens of *Crassostrea Gigantissima* Sp. clearly show such a foliated character (Figure 6). In many areas, single sheets are inclined slightly to the inner surface of the valve and arranged successively and regularly overlap in parallel in a pattern like tiles of a roof. Even though the foliated sheets of calcite is locally compact, the sheets generally show varying degrees of porosity such as fenestrate look, lace structure or regularly spaced small pores. The regularly foliated structures alternate with thicker layers arranged as elongated lenses and reaching 2-3 mm in thickness with a mean value of about 1 mm.

### 3. Discussion

The satellite map given as Figure 7A shows that the major channel of Thoppuvila River originates from the Mahendragiri hills, which is the southern end of the Western Ghats with a maximum elevation of average 1350 meters. At present this river is being flourished by a vast number of narrow ephemeral stream channels originating from nearby areas of Mahendragiri R F and Thekumalai R F. Figure 7D graphically narrates the mainstream of Thoppuvila River and some narrow water channels flowing towards the sea. This in turn gives rise to a braided landscape forming deltas in between the stream channels nearby Thoppuvila river around an estimated area of 460 km<sup>2</sup> ( Figure 7B ).

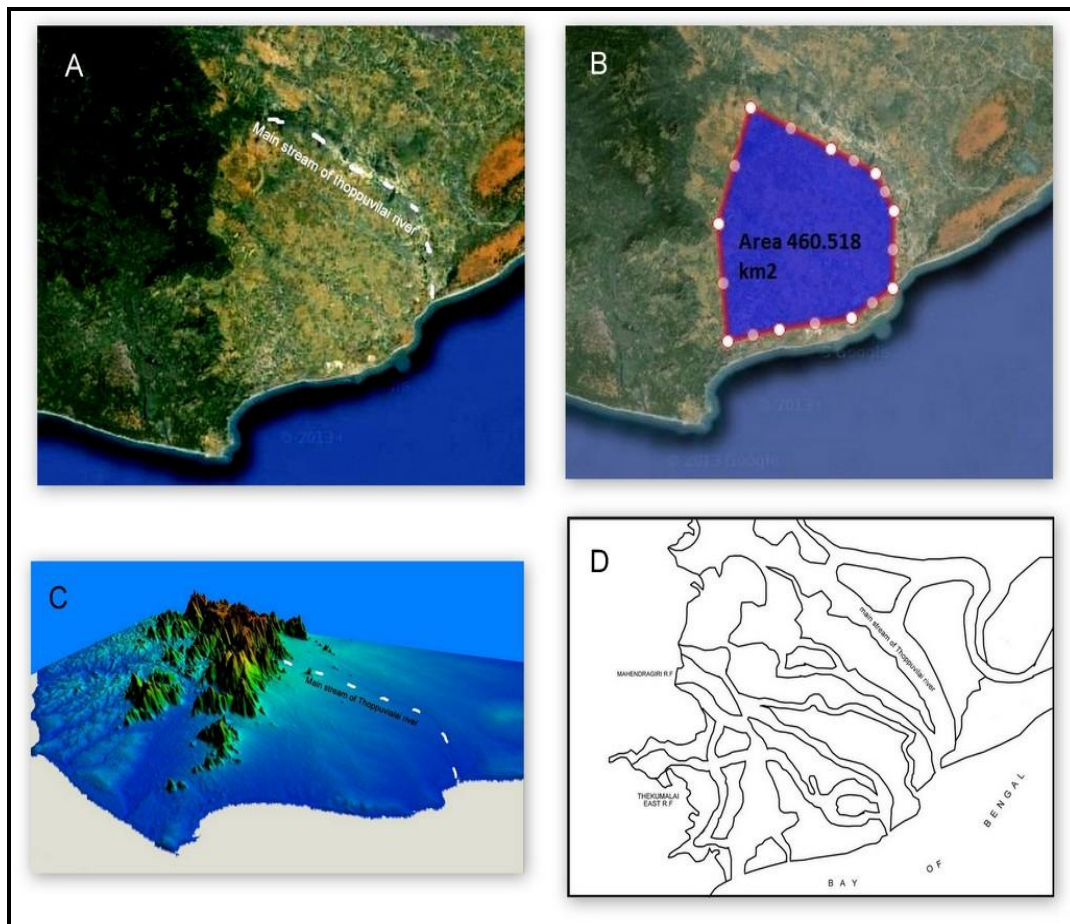


**Figure 7:** (A) Nambiyar/Thoppuvila River Main Channel (B) Extent of Proposed Paleo-Estuary (C) SRTM Geospatial Representation of Study Area (D) Possible Water Channels in Study Area

Considering the thickness of sedimentation built up of alluvium and fluvial deposits, the author infers that for a long period of time during the tertiary-quaternary period, the whole area was open to sea with a mouth of length around 15 kms with successive sand bars. The possibility of formation of sandbars forming due to the action of high energy tides from the sea accompanied by strong winds cannot be ruled out. Under such a situation, a relatively waterlogged landscape can generate along a vast area on the foothills of Mahendragiri. The over deposition of sediments in the waterlogged space can give rise to deltas. The subsequent deposition of sediments by the downstream freshwater from Mahendragiri hills and sea sand deposition can eventually create a landscape resembling an ideal estuary, where the salinity fluctuation is suitable for the survival of larvae of oysters during the tertiary period. The present slope system of this area shows a saturated level of sedimentation near the sea and exposed pediment landscapes in areas farther away from the sea. A Three dimensional projection of the study area is represented in Figure 7C. This proposed Paleo-Estuary shows a linear mount obliquely from Mahendragiri hills towards the sea with an average elevation of 20 m. This may be the area of uplift during the mio-pliocene age and the possible cause for an abrupt marine regression which in turn leaves behind the remnants of its dwellers. The pediment landforms at some places in the channel of Thoppuvila River near Urumankulam are shown in Figure 8. Here, the bed rocks are exposed with traces of fluvial weathering.



**Figure 8:** Exposed Rock Beds at Study Area

The authors surveyed through the Thoppuvila River during summer, when the whole landscape was dry enough to undergo the topographic and stratigraphic analysis. This proved worthwhile. The observed geological setting along the banks of the surveyed area includes a layer of light brown alluvial deposits followed by alternating layer composed of sand grain, clay and silt fragments. A remarkable layer of calcareous bedding is present just above the stream channels. Calcareous chalky deposits include vast beds of fossilized oyster shells, most of which are subjected to disarticulation.

Most of the water channel and the elevated banks of Thoppuvila River contain calcareous columns and fossils of *C. Gigantissima Sp.* and *C. Gryphoides Sp.* The exposed part of oyster colony shows a degraded nature due to weathering. Most of the fossils are found as broken fragments. The authors found that the color and relative thickness of *Crassostrea Sp.* shells differ with respect to distance from the sea. This may be due to the variation in the nature of sediments and the relative depth of the paleo-estuary which existed during the tertiary/quaternary period in that area.

Living species of *Crassostrea* are being cultured and studied by marine researchers nearby mandapam, Tamil Nadu. The commercially exploited oyster species in Indian waters are *Crassostrea gryphoides*, *C. madrasensis*, *C. rivularis* and *Saccostrea cucullata* (Rao, 1974). *Crassostrea madrasensis* and *Saccostrea cucullata* occur throughout the Indian coast whereas *C. gryphoides* and *C. rivularis* are restricted to the north-west coastal regions (Mahadevan and Nagappan Nayar, 1987). In Karnataka, Nethravati, Sharavati, Kali, Mulky river estuary and estuaries at Uppunda, Bhatkal, Venkatpur and Kundapur possess oyster beds ranging from 1 ha to 5 ha (Mahadevan, 1987). The morphological features of the living species differ remarkably from their fossil ancestors on the basis of shell thickness, size and calcite density. The authors are trying to reveal the reasons behind such characteristic features. According to Halina Pugaczewska (1971), the lineage of *Crassostrea* species start from *Alectryonia* to a new evolutionary species called *ostrea* during the upper cretaceous period.

Crassostrea Species has evolved in Neogene period, and is still continuing (Figure 9). In Indian subcontinent, the evolution of *Alectryonia Sp.* to *Rastellum Sp.* with evolutionary a characteristic of well-defined commissure was also recorded (Riffin, 2013).

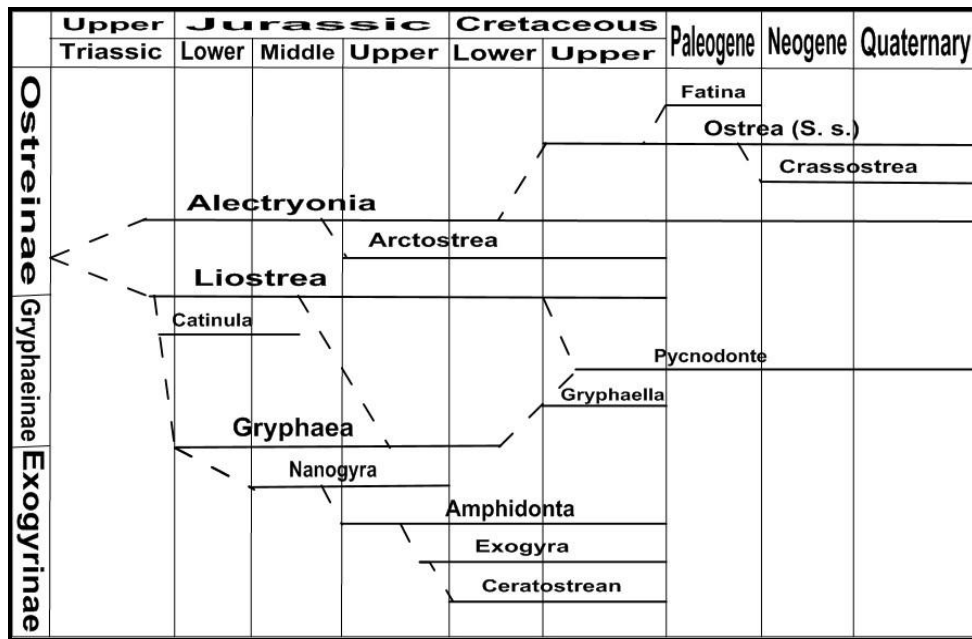
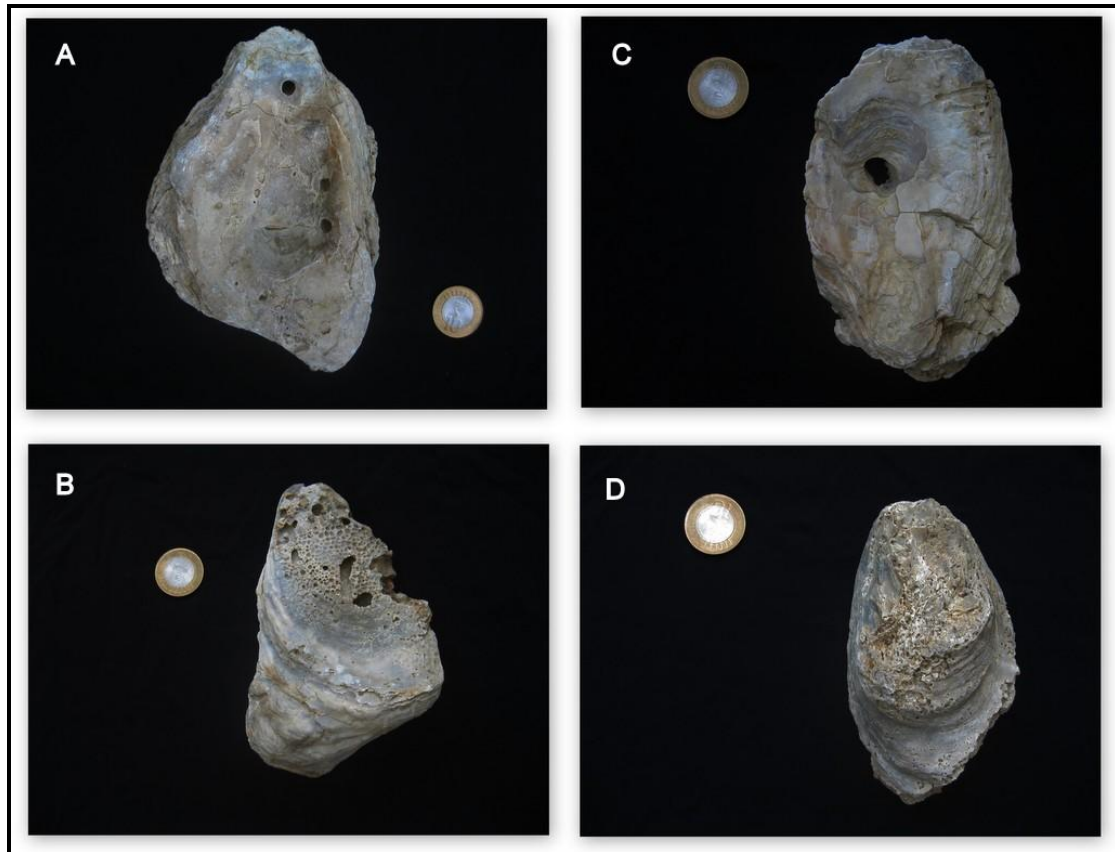


Figure 9: Evolution Tree of Oysters after Halina Pugaczewska (1971)

The presence of *Crassostrea* even 15 kms away from the sea and the Presence of calcareous beds/chalky deposits towards the hillside unambiguously exposes the fact that, there was an existence of a vast paleo estuary in that area. The living habits of *Crassostrea* require the geomorphological features of an estuary, where the highly energized tides from the sea push up salt water toward the mouth of the estuary. At the same time, the fresh water streams from the Mahendragiri hills normalize the salinity conditions of the estuary. These conditions may not cross the maximum or minimum salinity level which may be harmful to the oyster *Crassostrea Sp.* Generally, the estuaries are shallow in nature. So we assume the proposed paleo-estuary was also shallow. The physical analysis in the area shows the presence of fossils of *Crassostrea Gigantissima* in the water channels and the presence of oyster colonies on the elevated banks of Thoppuvila River. The relative thickness of sediments between the river bed and the elevated calcareous deposits vary from a range of 8 m to 10 m. Such a thick sedimentation with calcareous/chalky deposits can lead to the fact that the whole survey area was, in fact submerged underwater in the form of a massive paleo-estuary during the mio-pliocene age.

Almost all of the specimens collected by the author are found to be subjected for bioerosion and predatory action by *ichnospecies*. *Caulostrepsis* borings are seen along the growth laminae of some specimens. U shaped galleries, also formed due to the boring action of *Caulostrepsis* are also found on both the internal and external part of the fossil oyster specimens. The boring action of *clinoid sponges* or simply 'entobia' is widely seen in some specimens. *Entobia* consists of rounded chambers which are interconnected by cylindrical cavities bored within the surface of the shell. The presence of *entobia* and the evidence of the action by *ichnospecies*. *Caulostrepsis* also contribute to the fact that there was indeed a fluvial source resembling an estuary present along the eastern coast of India during the mio-pliocene age. Figure 10 shows the predatory signatures created by *ichnospecies* on fossil specimens of *C. Gigantissima Sp.*



**Figure 10:** Ichnotaxa Signatures on *C. Gigantissima Sp.*

This paleo estuary would have provided a perfectly balanced atmosphere where the fresh water from the elevated terrain would equalize the upstream movement of saline water from the sea. Such a perfectly balanced estuarial condition would be suitable for the existence of *Crassostrea Sp* along the length of the estuary. As we move further away from the sea, the degree of salinity and the intensity of water flow would differ considerably. Therefore, the *Crassostrea* specimens found further offshore would differ in shell thickness and density. The thick shell laminar growth layers of calcite found in the *Crassostrea Sp* could be an adaptive measure undertaken by the oysters in order to avoid burial in rapidly accumulating sand and mud through the downstream flow from Mahendragiri hills and fluvial deposit from the sea side. Shell secretion by mollusks is accomplished by an organ called the mantle which produces shell carbonate from the extrapallial fluid (EPF) which is a mixture of biological and ambient fluids (Ponder and Lindberg, 2008). Due to biological fluid exchange that takes place during respiration and feeding, the percentage of various constituents, including Dissolved Inorganic Carbon (DIC), in EPF can vary temporally (McConnaughey and Gillikin, 2008). When considering the sessile and suspension feeding habitat of *crassostrea sp.*, The shell thickness, lamellar foliated nature of calcite and the heaviness of the shell can be inferred as a unique adaptation accepted by the oyster community to survive the heavy tidal energy and sedimentation from the sea and rapid flow of fresh water and debris from the Mahendragiri hills in Thoppuvila river during the Mio-pliocene age.

The Paleoclimatic analysis of the study area is possible with the help of the life history of *Crassostrea Sp*. The annual growth patterns present on the chondrophore of the left valve of *Crassostrea Sp* provide vital evidence relating to the climate in which it lives. The chondrophore consists primarily of foliated calcite and in some specimens, annual growth patterns are expressed within the chondrophore as small morphological ridges and valleys that give this area of the shell a 'washboard' appearance (Kent, 1988; Lawrence, 1988). Figure 11 shows appearance of chondrophore on various specimens.

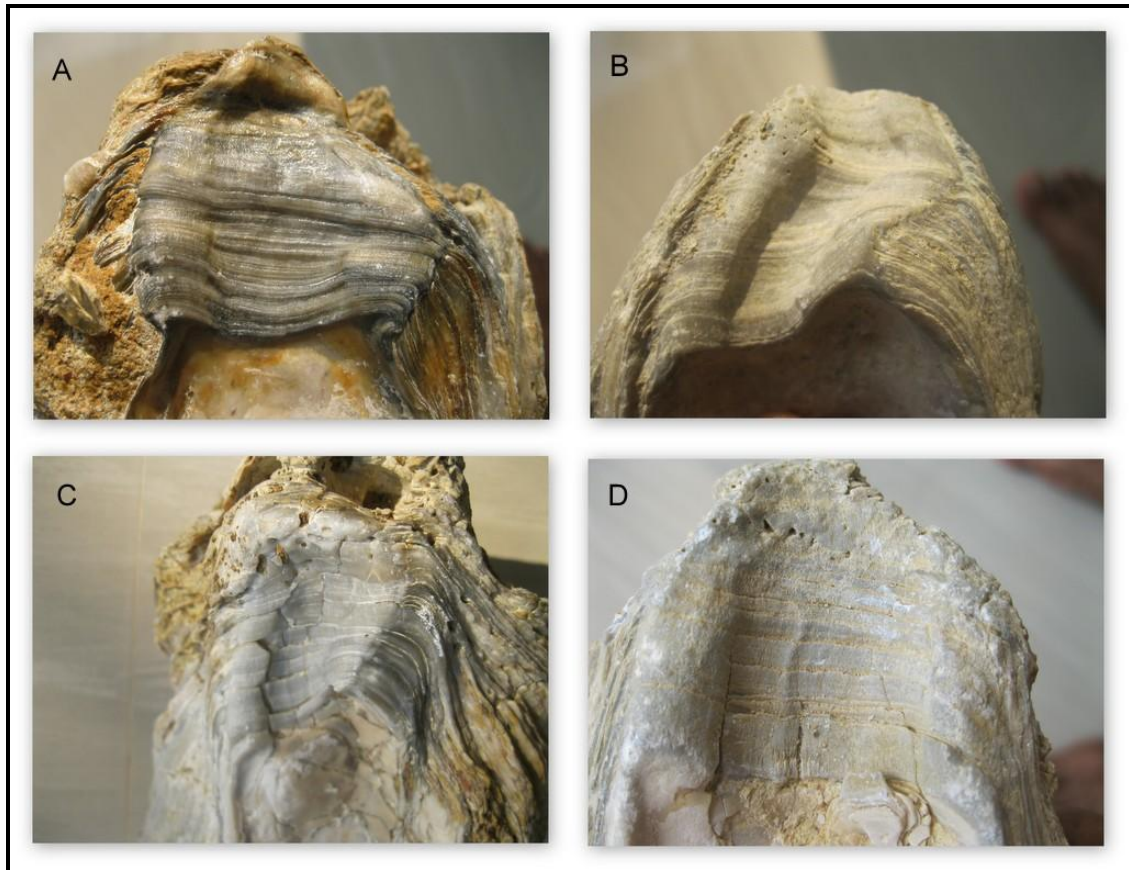


**Figure 11:** Chondrophore Features on Fossil Specimens

Prior studies have interpreted these patterns to represent annual growth in the sense that the small morphological ridges represent warmer months of the year while the valleys represent cooler months (Kent, 1988; Lawrence, 1988). This hypothesis has been supported through the use of oxygen isotopes in both recent and fossil *Crassostrea* (Andrus and Crowe, 2000; Kirby, 2000). In the present study, almost all samples show chondrophore ridges which infers to the fact that these oysters were subjected to warm and cool climatic conditions during their lifespan. The straight, elongated and spatulate shape of the specimens can be an accurate indicator of the mud sticking habit of these oysters, and the variation in size and thickness may be due to difference in sedimentation. The specimens seem to have developed an elongated, triangular shaped ligament area to acquire a mechanically stable shell structure in which the dorsal part of the specimen anchors itself to the marine bed. Upon further taphonomical investigation, it becomes clear that the oysters grow in a vertical position. Such a position is structurally unstable. So, in order to counter this defect, the oysters grow very close to each other, forming a colony. Figure 12 shows some specimens are cemented together their left valves, such a situation is another adaptation by the oysters to get a stabilized position in the sediment deposit of proposed paleo-estuary on the foothills of Mahendragiri hills.

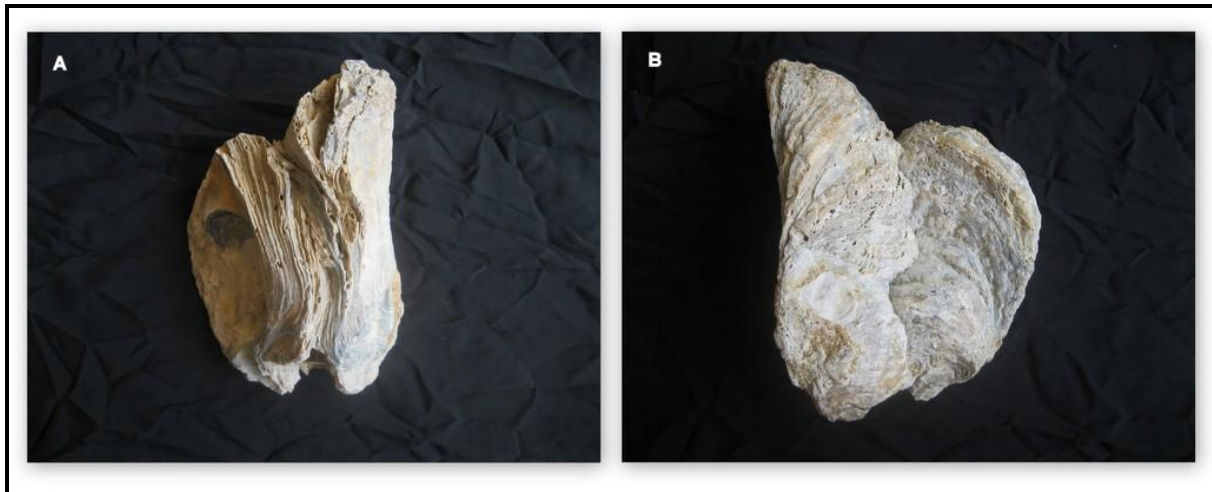


**Figure 12:** Cemented Fossils of *C. Gigantissima Sp.*

The chalky deposits seen in the whole outcrops can be construed as an efficient adaptation to make a defensive shield against the predatory action of *Ichnotaxa*. Chalky deposits can fuel the shell thickness in oysters as well as restrict predatory ambush to an extent (Kirby, 2000, 2001). The presence of thick bed of chalky deposits in the water channel of Thoppuvila River and on its banks is a clear evidence for this postulate. In physical measurements, the authors found the thickness of chalky deposits became thin due to heavy weathering process near sea side. Living Oysters of *Crassostrea sp.* such as *C. columbiensis* and *C. angulata* exhibit thin shell thickness and are commonly located in marine environments including estuaries, lagoons and intertidal marshes. Such habitats undergo sudden salinity fluctuations which are not tolerable by most marine predators (Taylor & Bushek, 2008). Most oysters found at the proposed estuary seem to deviate from its vertical growth position. Such disorientation in position can be due to the flow of heavy fine grained sediments through this area while undergoing marine regression during Mio-Pliocene age. Breaking waves and storms can result in high energy events which can eventually remove and disarticulate individual, thick shelled oysters from the colony.

#### 4. Conclusion

The presence fossils of *Crassostrea Sp.* including *C. Gigantissima* and calcareous/chalky deposits in surrounding areas and flow channels of the Nambiyar/Thoppuvila river from the foothill of Mahendragiri hills to the Bay of Bengal near Attankarai Pallivasal supports the existence of a vast paleo estuary which covered an area estimated around 460 km<sup>2</sup>. The mode of disarticulation of oyster shells due to the action of physical forces as well as bio erosional aspects including effects of *Ichnotaxa* also corroborates the existence of a paleo estuary in the geo code latitude 8°19'12"N and longitude 77°39'24"E. The nature of paleo estuary and the relation between foliated calcite shells and chalky deposits are analyzed. This Non-reported paleo-estuary shows a linear mount obliquely from Mahendragiri hills towards the sea with an average elevation of 20 m. This may be the area of uplift during the mio-pliocene age and requires further studies for revealing the geomorphologic features through isotopic studies for accurate dating of its stratigraphy.

#### Acknowledgement

I am greatly indebted to Dr. Mohan Kumar, Prof. Prabhakaran Nambiar (Head of Geology Dept. AWH Special College), Dr. Nisha (CUSAT), Dr. Biju Longinos (Kerala University), Mr. Jishnu, Dr. Praveen and Dr. Singanengam (Geological Society of India), Russel T. Sajeew and Volunteers of World Fossil Society for their encouragement and cooperation throughout my study.

## References

- Ana Parras et al. *Taphonomy and Sequence Stratigraphic Significance of Oyster-Dominated Concentrations from the San Julia 'N Formation, Oligocene of Patagonia, Argentina*, 48 A. Parras, S. Casad'io / Palaeogeography, Palaeoclimatology, Palaeoecology. 2005. 217; 47-66.
- Carriker, M.R., Palmer, R.E., and Prezant, R.S. *Functional Ultramorphology of the Dissoconch Valves of the Oyster Crassostrea Virginica*. Proceedings of the National Shellfisheries Association. 1980. 70; 139-183.
- Carter, J.G., and Clark, G.R., 1985: *Classification and Phylogenetic Significance of Molluscan Shell Microstructure*. In Broadhead T.W. (Ed.). Mollusks Notes for a Short Course. 50-63.
- Carter, J.G. *Evolutionary Significance of Shell Microstructure in the Palaeotaxadonta, Pteriomorpha and Isofilibranchia (Bivalvia; Mollusca)*. In Carter J.G. (Ed.). *Skeletal Biomineralization: Patterns, Processes and Evolutionary Trends*, 1990. 1; 135-412.
- D., Timothy, J., et al. *Variation of Recent and Fossil Crassostrea in Jamaica*. Paleontology. 1988. 31 (4) 1013-1028.
- E., Farinati et al. *Trace Fossils on Shelly Substrate. An Example from the Miocene of Patagonia, Argentina*. Acta Geologica Hispanica. 2002. 37 (1) 29-36.
- G.S., Bressan et al. *Taphonomic Analysis of Fossil Concentrations from La Manga Formation (Oxfordian), Neuquén Basin, Mendoza Province, Argentina*. Journal of Iberian Geology. 2010. 36 (1) 55-71.
- Geology and Mineral Resources of the States of India, Part VI –Tamil Nadu and Pondicherry*. Geological Survey of India. 2006.
- Gillikin, David Paul, Fjo De Ridder, Hans Ulens, Marc Elskens, Eddy Keppens, Willy Baeyens and Frank Dehairs. *Assessing the Reproducibility and Reliability of Estuarine Bivalve Shells (Saxidomus Giganteus) for Sea Surface Temperature Reconstruction: Implications for Paleoclimate Studies*. Palaeogeography, Palaeoclimatology, Palaeoecology. 2005. 228; 70-85.
- Halina Pugaczewska. *Jurassic Ostridae of Poland*. Acta Paleontologica Polonica. 1971. XVI.
- Kirby, M.X., and Jackson, J.B.C. *Extinction of a Fastgrowing Oyster and Changing Ocean Circulation in Pliocene Tropical America*. Geology. 2004. 32 (12) 1025-1028.
- Kirby, M.X. *Paleoecological Differences between Tertiary and Quaternary Crassostrea Oysters, as Revealed by Stable Isotope Sclerochronology*. Palaios. 2000. 15; 132-141.
- Kirby, M.X. *Differences in Growth Rate and Environment between Tertiary and Quaternary Crassostrea Oysters*. Paleobiology. 2001. 27 (1) 84-103.
- Mahadevan, S., and Nagappan Nayar, K. *Ecology of Oyster Beds*. Pub. In CMFRI Bull. 1987. 38; 7-13.
- McConnaughey, Ted. *13C and 18O Isotopic Disequilibrium in Biological Carbonates: II. In vitro Simulation of Kinetic Isotope Effects*. Geochimica et Cosmochimica Acta. 1989. 53; 163-171.

Melissa Southworth. *Oyster (Crassostrea Virginica, Gmelin 1791) Population Dynamics on Public Reefs in the Great Wicomico River, Virginia, USA*. Journal of Shellfish Research. 2010. 29 (2) 271-290.

K., Nagappan Nayar et al. *Oyster Culture-Status and Prospects*. Central Marine Fisheries Research institute, Bulletin. 1987. 38.

Ponder, Winston, F., and David, R., Lindberg, 2008: *Phylogeny and Evolution of the Mollusca*. Berkley, Los Angeles. University of California Press.

R.P., Kachhara, et al. *Lower Oligocene Bivalves of Ramanian Stage from Kachchh, Gujarat, India*. J. Earth Syst. Sci. 2012. 121 (2) 405-438.

Rao, K.V. *Edible Bivalves Mussels and Oysters*. In: *The Commercial Molluscs of India*. Bull. Cent. Mar. Fish. Res. Inst. 1974. 25; 4-39.

Riffin, T., Sajeev. *Occurrence of Arctostrea: Existence of high energy Paleoenvironment in Cauvery basin, India during Late Cretaceous*. International Journal of Scientific & Engineering Research. 2013. 4 (12) 1319-1328.

Surge, D.M., Lohmann, K.C., and Goodfriend, G.A. *Reconstructing Estuarine Conditions: Oyster Shells as Recorders of Environmental Change, Southwest Florida*. Estuarine, Coastal and Shelf Sciences. 2003. 57; 737-756.

Taylor, J., and Bushek, D. *Intertidal Oyster Reefs Can Persist and Function in a Temperate North American Atlantic estuary*. Marine Ecology - Progress Series. 2008. 361; 301-306.

# Interactions and Seismicity of Indian Tectonic Plate with its Neighboring Plates: An Overview

Venkata Dilip Kumar Pasupuleti and Pradeep Kumar Ramancharla

Earthquake Engineering Research Centre, IIT, Hyderabad, India

Correspondence should be addressed to Venkata Dilip Kumar Pasupuleti, dilipkumarpv@gmail.com

Publication Date: 8 September 2014

Article Link: <http://scientific.cloud-journals.com/index.php/IJAESE/article/view/Sci-202>



Copyright © 2014 Venkata Dilip Kumar Pasupuleti and Pradeep Kumar Ramancharla. This is an open access article distributed under the **Creative Commons Attribution License**, which permits unrestricted use, distribution, and reproduction in any medium, provided the original work is properly cited.

**Abstract** Understanding earthquakes and its prediction is most challenging tasks. Even though the earthquakes have been understood clearly, the prediction of earthquakes would take more time to come into reality. For this, collection of earthquake data and its interpretation plays a vital role. Its importance continues for few more decades in understanding the various aspects of earth structure and tectonic plate interactions. India, the second largest populous country of the world has experienced and is continuing to experience both inter and intra plate earthquakes, claiming life loss as well as damage to built environment. Apart from earthquakes, India has also experienced Tsunamis in both the directions; eastern tsunamis from Sumatra and western tsunamis from Makran. In this paper using past earthquake data, Indian plate interactions with its neighboring major (Eurasia, Africa & Australia) and minor plates (Arabia, Burmese & Sunda plate) have been understood. Upon clearly observing seven interactions, it is clear that interaction types, their lengths and thickness of plate play a great role in the occurrence of major to great earthquakes.

**Keywords** *Crustal Thickness; Earthquake Data; Plate Interaction Types; Interaction Lengths*

## 1. Introduction

Earthquakes accompany many changes in the earth from the smallest to the largest of the events. They are ideal for trying to understand dynamic patterns in the earth. As the most part earthquake phenomena is simple and discrete events which will objectively signal the stress vectors, motions, and shifts in the vast tectonic plates of the earth's crust. The patterns in earthquake activity directly provide an objective method to describe how plates are moving. Earthquakes can be classified based on their magnitude and focal depths.

Seismic stations of worldwide network records the various earthquakes occurring every day across the globe. These recorded earthquake data are analyzed with the help of computers. The data of geographical location and magnitude of all these detected earthquakes is used to plot the maps at the regional level. As a result, the details of present plate motion are always under observation. Figure 1

show the epicentral locations of earthquakes which have been recorded from 1900 to 2013, which also shows the plate tectonic boundaries on the globe. Figure 1 strongly suggests that the majority of these earthquakes are focused on the plate tectonic boundaries. Then, it becomes very important to develop a proper plate tectonic boundary model which prescribes interaction type and its behavior at the boundary.

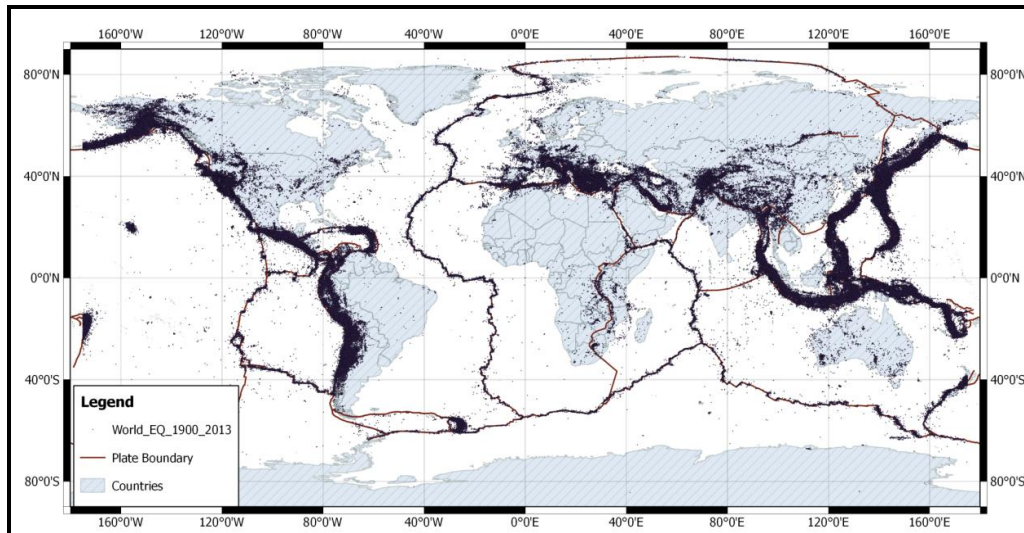


**Figure 1: World Earthquake Epicenters from 1900–2013**  
(Earthquake Data: NCEDC)

Many plate tectonic boundary models have been presented but there are no standard references that are generally accepted on these locations across globe (Peter, 2003). Minster and Jordan (1978); DeMets et al., (1990) (NUVEL-I); Zoback (1992) have published boundaries of large plate models as part of their world stress Map. Gordon (1995) has incorporated the distinction of plates from deforming zones. The Paleo-Oceanographic mapping project undertaken at the University of Texas has shaped a rough set of plate boundaries of large plates and mid-ocean spreading ridges. Muller et al., (1997) has published a map pertaining to the boundaries and also have gridded the oceanic lithosphere age with the help of digital models. An in-detail map of plate boundaries (working set) is maintained at a site by plate's project team, Institute of Geophysics (University of Texas) (Peter, 2003). A good number of studies have been conducted in the past four decades in order to study the fundamental changes in global tectonic process. Many new models have been introduced with the help of evolving data. This study focuses on Indian plate and its interactions with neighboring plates.

The plate tectonic boundary model (PB2002) by Peter Bird (2003) as shown in the Figure 2 is a revised version of the previous model PB1999 that was used in Bird et al., (2002). The digitized boundaries created by POMP have the leading basis for model PB2002. Which has a set of digitized boundaries created by POMP (Muller et al., 1997).

Peter Bird (2003) has described the whole global plates consisting of 14 large plates and 38 smaller plates equating to a total of 52 plates. In this, Arabia, Australia, Eurasia and India plates are considered to be larger plates and Sunda, Burma and Somalia are considered to be smaller plates. This study does not include reasons in differentiating larger or smaller plates, but it deals with their interaction with neighboring plates.

Peter Bird (2003) has divided plate tectonic interactions into seven classes viz Continental Convergent Boundary (CCB), Continental Transform Fault (CTF), Continental Rift Boundary (CRB), Oceanic Spreading Ridge (OSR), Oceanic Transform Fault (OTF), Oceanic Convergent Boundary

(OCB) and Subduction Zone (SZ) as represented in Figure 2 for whole global plates. Figure 2 show that Indian tectonic plate is undergoing all seven types of interactions.

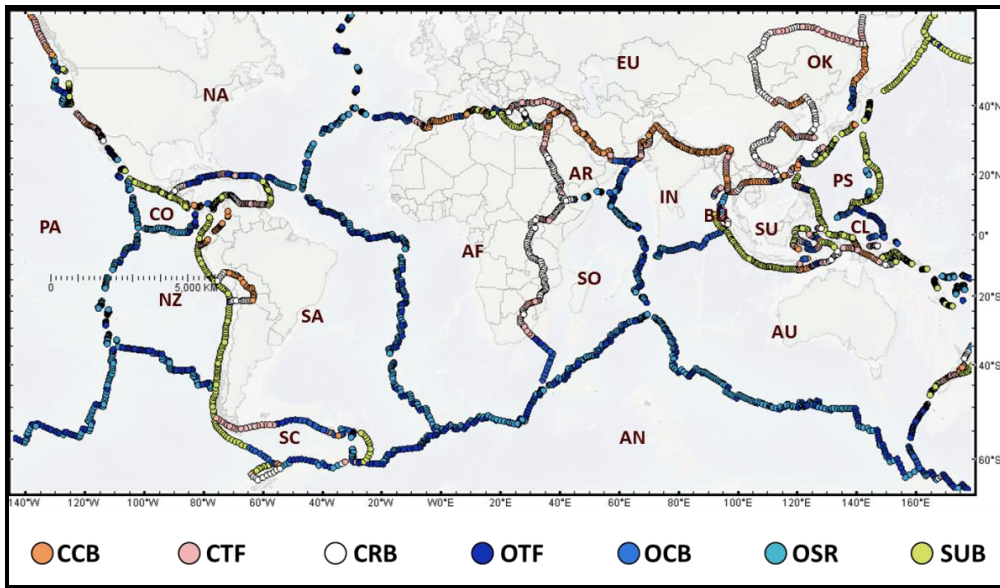


Figure 2: World Tectonic Plates with Interaction Types  
(Data: Peter Bird, 2003)

## 2. Great Earthquakes and Plate Junctions

Large earthquakes over a magnitude of eight are called “great earthquakes”. They have found to occur at an average gap of one and half years. Researchers believe that these great earthquakes occur in order to release stresses over a large area that are tectonic in nature. Figure 3 shows the epicentral locations of the great earthquakes occurred during 1900–2013.

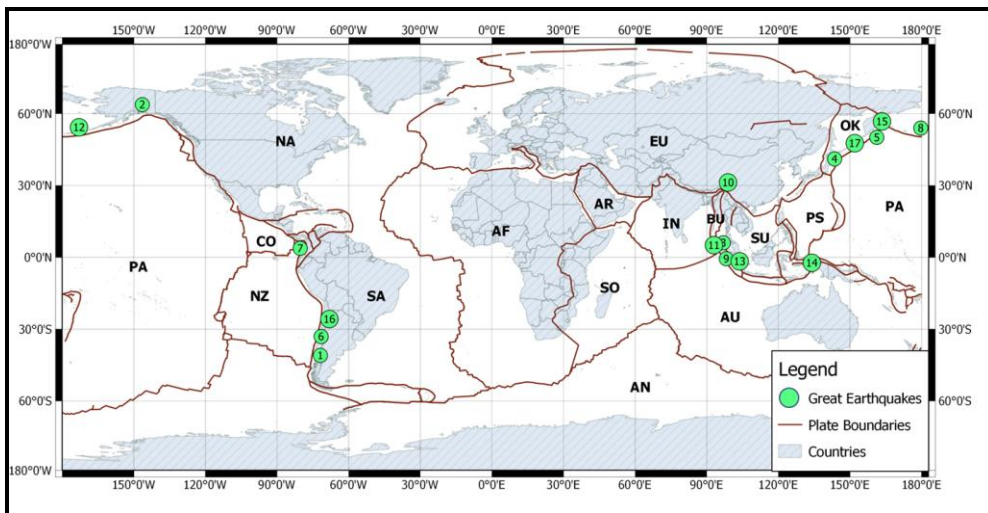


Figure 3: Epicentral Locations of Great Earthquakes of the World 1900–2013  
(Source: USGS)

**Table 1:** List of the 17 Largest Earthquakes in the World Since 1900, their Locations Close to Plate Junctions, and the Plates Associated with Each Earthquake. AN, Antarctica; AU, Australia; BU, Burma; CA, Caribbean; CO, Cocos; EU, Eurasia; IN, India; NA, North America; NZ, Nazca; OK: Okhotsk; PA, Pacific; PS, Philippine Sea; SA, South America; SU, Sunda  
(Source: USGS)

No.	Location	Date	M	Lat.	Long.	Reference	Associated Plates
1.	Chile	1960 05 22	9.5	-38.29	-73.05	Kanamori, 1977	NZ, SA, AN
2.	Prince William Sound, Alaska	1964 03 28	9.2	61.02	-147.65	Kanamori, 1977	PA, NA
3.	Off the West Coast of Northern Sumatra	2004 12 26	9.1	3.30	95.78	Park et al., 2005	IN, BU, AU, SU
4.	Near the East Coast of Honshu, Japan	2011 03 11	9.0	38.322	142.369	PDE	PA, PS, OK
5.	Kamchatka	1952 11 04	9.0	52.76	160.06	Kanamori, 1977	PA,NA,OK
6.	Offshore Maule, Chile	2010 02 27	8.8	-35.846	-72.719	PDE	NZ,SA,AN
7.	Off the Coast of Ecuador	1906 01 31	8.8	1.0	-81.5	Kanamori, 1977	NZ, SA, CO,CA
8.	Rat Islands, Alaska	1965 02 04	8.7	51.21	178.50	Kanamori, 1977	PA, NA
9.	Northern Sumatra, Indonesia	2005 03 28	8.6	2.08	97.01	PDE	IN, BU, AU, SU
10.	Assam - Tibet	1950 08 15	8.6	28.5	96.5	Kanamori, 1977	IN, EU, BU, SU
11.	Off the west coast of northern Sumatra	2012 04 11	8.6	2.311	93.063	PDE	IN, BU, AU, SU
12.	Andreanof Islands, Alaska	1957 03 09	8.6	51.56	-175.39	Johnson et al., 1994	PA, NA,
13.	Southern Sumatra, Indonesia	2007 09 12	8.5	-4.438	101.367	PDE	IN, BU, AU, SU
14.	Banda Sea, Indonesia	1938 02 01	8.5	-5.05	131.62	Okal and Reymond, 2003	AU, SU, PS, PA
15.	Kamchatka	1923 02 03	8.5	54.0	161.0	Kanamori, 1988	PA, NA, OK
16.	Chile-Argentina Border	1922 11 11	8.5	-28.55	-70.50	Kanamori, 1977	NZ,SA,AN
17.	Kuril Islands	1963 10 13	8.5	44.9	149.6	Kanamori, 1977	PA, PS, EU, OK

Table 1 provides the details of all the great earthquakes occurred in different locations (with respective to tectonic plates) of the world. Magnitudes of all these listed great earthquakes were in the range of 8.5 to 9.5. Except for 2, 8 and 12 on the western Aleutian trench, all other great earthquakes have occurred at the multiple-plate junctions. In the first sight, the 1964 Alaskan earthquake (refer to event 2) seems to be a case of two-plate interaction. However, when subduction zone in the western Aleutian trench in the north, and the right lateral strike-slip faulting environment along the San Andreas Fault in east are considered, then it does act like triple junction resulting in the stress to be built. In summary, it can be said that there is a strong correlation between plate junctions/inflexion points and epicentral locations of these earthquakes. Recently there have been few major observations about the correlation between great earthquakes, swarm activity (Kanamori, 1971), subduction process, oceanic plates (Benioff, 1954), focal depth and plate junctions.

Out of the 17 great earthquakes, five great earthquakes have occurred on or in the vicinity of Indian tectonic plates as mentioned in Table 1. Plate junctions which have been responsible for great earthquakes in and around Indian plate are mentioned in the Table 1. IN-BU-AU-SU & IN-BU-EU-SU are known as quadruple plate junctions leading to minor to great earthquakes.

Few major observations about great earthquakes; almost all the great earthquakes have occurred on or nearer to the plate boundaries; they have occurred nearer to the plate junctions (N.P., Rao, 2005); they have occurred at the zones of subduction (Larry Ruff and H., Kanamori, 1980); they have occurred where oceanic plate is subducting under continental plate (Luciana et al., 1988); and all the great earthquakes occurred are shallow in nature.

Indian tectonic plate interactions have led to five great earthquakes in the last 100 years and a few more are expected to occur in the near future at the Himalayan arc and the Burmese arc. A study of its interactions would lead to proper conclusions of great earthquakes and the intervals of their recurrence.

### 3. Indian Tectonic Setup

The Indian plate is bounded by zones of broadly distributed active deformation. The most widely distributed plate boundary in the world is actively deforming as continental India continues to collide with Eurasia. Beginning at the northern edge of India plate, along the Himalaya Range Front, active deformation extends through Tibet and into China, Mongolia, and as far north as Russia. Along the eastern flank the subduction of the Indian plate under the Burma plate in the Andaman-Nicobar Islands region. To the south the transition between the India plate and the Australian plate is uncertain as seismicity is dispersed over thousands of kilometers and shows no distinct trends that highlight an obviously distinct boundary. Along the western plate boundary, the Central Indian Ridge, the Carlsberg Ridge and Owen Fracture zone discretely separate Indian plate from the Somalian and Arabian plates through a series of spreading centers and transform faults.

Studies of global reconstructions phenomena have suggested that the Indian plate move at a rate of 54 mm/yr (0.054 m/yr) and hence leading to convergence with the Asian plate (DeMets et al., 1994). The interior of Indian tectonic plate have Himalayan mountain belt, Indo-Burmese range, peninsular shield, and Sindhu-Ganga-Brahmaputra alluvial plains.

#### 3.1. Indian Intraplate Deformation

The Indian shield region consists of various complex rift zones and several shear/thrust zones. Indian shield region is categorized as Stable Continental Region (SCR). However, Indian shield region has witnessed several earthquakes of magnitude six or more since 18<sup>th</sup> Century, some of which were disastrous (Bhatia et al., 1999). The spatial distributions of earthquakes of magnitude 6 and above are shown in the Figure 6 (c). This Intraplate seismicity exists across Central India that might be related to flexure of the plate as it is thrust below Tibet (Bilham et al., 2003).

The Narmada-Son Lineament (NSL) is one of the significant tectonic features of the Indian shield trending ENE-WSW apparently dividing the shield into two sectors, namely northern and southern sectors (Bhatia et al., 1999). This paleo-rift zone (Jain et al., 1995) exhibits high heat levels and strain rates estimated from seismicity that are larger than many stable continental regions (Rao, 2000). This suggests a potential concentration of intraplate deformation or kinematic separation of India into two distinct plates. Thinned and weakened lithosphere formed due to passive-margin normal faulting in the Cretaceous might also have led to the increased seismicity activity in the region (Biswas et al., 2007) and by heating from the plume head is the reason for the late Cretaceous Deccan flood basalts (Chandrasekhar et al., 2009). Ductile creeps occurring at depths from 10 km to 15 km leading to continental flexure, which is a major factor for intraplate tectonism. 285 earthquakes have occurred in the last forty years with varied magnitudes at different focal depths, of which 200 earthquakes have occurred majorly at the focal depths of range between 10 km to 15 km over Indian stable shield (Koyna, Killari and Bhuj earthquakes) (Khan, 2009).

The present day tectonics of the northeastern part of India is complicated because of the interaction between the active north-south convergence along the Himalaya (Seeber et al., 1981) and east-west convergence and folding within the Indoburman ranges deformation apparently evolved from subduction along a nearly east-west trending zone in Tertiary time to its present configuration (Mitchell, 1981). The Shillong plateau in the Northeast India exhibits considerable north-south shortening supported by the existence of large earthquakes such as the great ( $M_w$  8.1) Assam earthquake of 1897 (Bilham and England, 2001). In addition, detailed analysis of moderate earthquakes in the same region is also consistent with the north-south shortening (Angelier and Baruah, 2009). Exhumation rates deduced from low-temperature chronometric data suggest a convergence rate of 13 mm/yr (0.013 m/yr) across the plateau, since 9 Ma (Biswas et al., 2007). GPS

data in the Shillong Plateau region also show contraction with respect to stable India (Banerjee et al., 2008).

Seismic experiments conducted in southern Tibet suggest a crustal thickness of the order of 80 km (Hirn et al., 1984; Zhao et al., 1993; Mitra et al., 2005). For comparison, the crustal thickness of the Indian Shield is estimated at 40–44 km (Saul et al., 2000; Mitra et al., 2005). But from recent studies carried by Kumar et al., (2007) the given thickness of Indian plate is ranging from 80–100 km. In the same paper Kumar et al., (2007) has also mentioned that it is because of its lesser thickness Indian plate has actually moved at a velocity of 180 to 200 mm/yr (0.18 m/yr to 0.20 m/yr) before collision with Eurasian plate.

### 3.2. Indian Interplate Deformation

Figure 4 shows the tectonic plate boundaries of all the neighboring plates with Indian tectonic plate, whereas Figure 5 shows the type of interaction Indian tectonic plate having with its neighboring plates which are given in seven classes mentioned by Peter Bird (2003). These types of interactions experiencing by Indian plate are compared with the whole global plates. The values are mentioned in Table 2. But in detail, interaction types and their lengths in km are mentioned in Table 3.

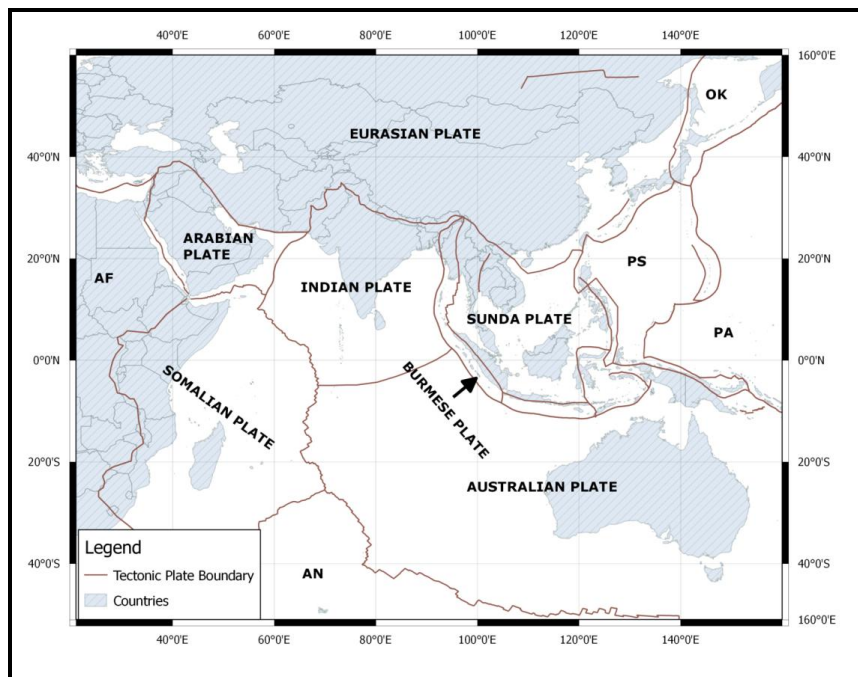


**Figure 4:** Indian Tectonic Plate with Its Neighbouring Plates

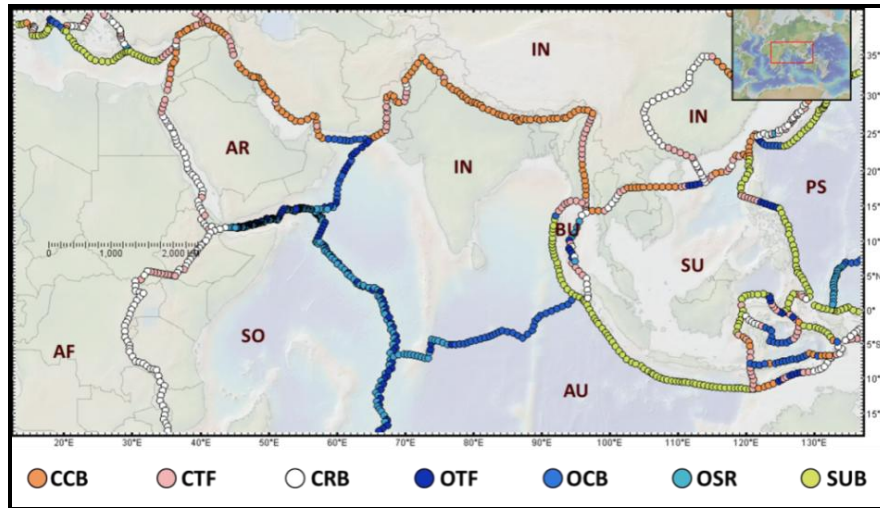


**Figure 5:** Indian Tectonic Plate with Its Neighboring Plates and Interaction Types  
(Data: Peter Bird, 2003)

**Table 2:** Interaction Type Length of Indian Plate and World Plate Lengths (CCB– Continental Convergent Boundary, CTF– Continental Transform Fault, CRB – Continental Rift Boundary, OSR – Oceanic Spreading Ridge, OTF– Oceanic Transform Fault, OCB – Oceanic Convergent Boundary, SUB – Subduction Zone)

Interaction Class	Total Length (km)	
	INDIA	WORLD
Continental Convergent Boundary (CCB)	4323.9	23003
Continental Transform Fault (CTF)	2086	26132
Continental Rift Boundary (CRB)	126	27472
Oceanic Spreading Ridge (OSR)	3827	67338
Oceanic Transform Fault (OTF)	2257	47783
Oceanic Convergent Boundary (OCB)	3076	17449
Subduction (SUB)	1417	51310

**Table 3:** Interaction Types and their Lengths in km of Indian Plate and its Neighboring Plates (IN – Indian Tectonic Plate, EU – Eurasian Plate, BU – Burmese Plate, AU – Australia Plate, SO – Somalia Plate)

Interaction Class	IN - EU	IN - BU	IN - AU	IN - SO	IN - AR	Total
<b>CCB</b>	<b>4323.9</b>	- NA -	- NA -	- NA -	- NA -	<b>4323.9</b>
<b>CTF</b>	<b>1586.7</b>	<b>499.4</b>	- NA -	- NA -	- NA -	<b>2086.1</b>
<b>CRB</b>	<b>126.5</b>	- NA -	- NA -	- NA -	- NA -	<b>126.5</b>
<b>OSR</b>	- NA -	- NA -	<b>1058.8</b>	<b>2486.8</b>	<b>281.5</b>	<b>3827.1</b>
<b>OTF</b>	- NA -	- NA -	<b>228.9</b>	<b>1218</b>	<b>810</b>	<b>2256.9</b>
<b>OCB</b>	- NA -	<b>88.8</b>	<b>2309.9</b>	<b>113.4</b>	<b>564.2</b>	<b>3076.3</b>
<b>SUB</b>	- NA -	<b>1416.6</b>	- NA -	- NA -	- NA -	<b>1416.6</b>

(NA – Not Applicable)

Indian plate along with its boundaries and neighboring plates is shown in Figure 6 that also shows the seismic activity from 1900 to 2013. Figure 6(a) gives the seismicity of different magnitudes. A close observation tells that larger magnitude earthquakes are more concentrated on the boundaries than the interior. Similarly Figure 6(b) shows the epicentral locations of all the earthquakes separated on the basis of their focal depths. Most of the earthquakes in the central region of Indian plate have focal depth less than 70 km which are shallow in nature. As we move from southern part to northern part and western part to eastern part, the focal depth is increasing, which also indicates that the plate thickness is increasing at the northern and southern boundaries. Figure 6(c) shows all the

earthquakes of magnitude more than 6. It can be said that major to great earthquakes are quite common on the boundaries and that the interior part of the Indian plate is seismically active. It is also observed that deep focus earthquakes are limited to Hindu Kush (100-300 km) and Burmese arc (90-150 km) (Mishra et al., 2012).

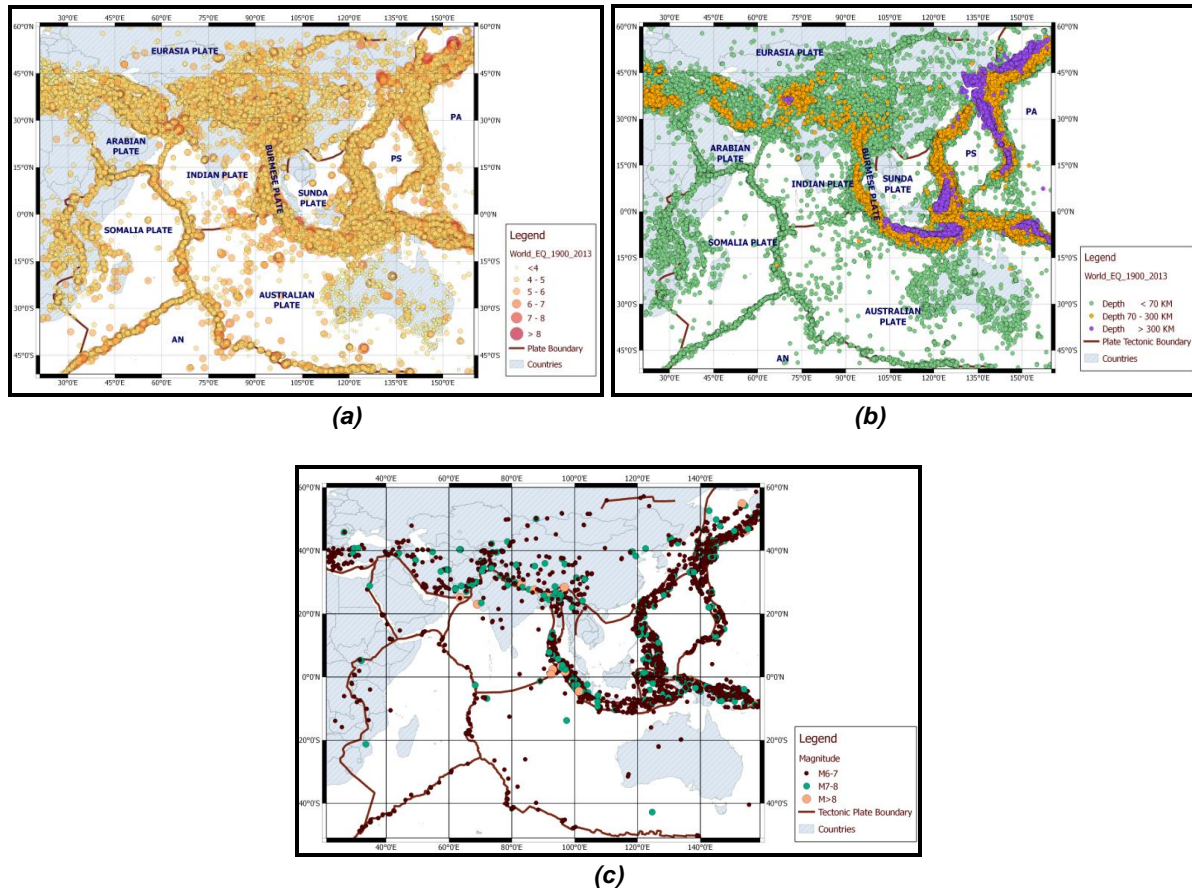


**Figure 6:** Epicenters in and around Indian Tectonic Plate (a) Figure Shows Epicenters with Different Magnitudes (b) Figure Shows Epicenters with Different Depths (c) Figure Shows Epicenters of Earthquakes Whose Magnitude is Equal or Greater than 6 (Earthquake Data: NCEDC)

In this study, we have divided the whole Indian tectonic plate interactions into six components; boundaries for each component are mentioned in Table 4, where minimum, maximum latitudes and longitudes are given. Figure 4 shows the complete tectonic plate boundaries of Indian and neighboring plates viz., Eurasian, Arabian, Somalian, Australian, Burmese and Sunda plates.

**Table 4:** Considered Areas for Our Study Detailing Its Location on the Globe

No.	Plate Interactions	Longitude		Latitude	
		Min	Max	Min	Max
1.	Indian – Neighboring Plates	21°0' E	160°0' E	51°0' S	60°0' N
2.	Indian – Eurasian Plate	46°0' E	112°0' E	5°0' N	44°0' N
3.	Indian – Australian Plate	60°0' E	174°0' E	63°0' S	35°0' N
4.	Indian – Arabian Plate	32°0' E	78°0' E	6°0' N	44°0' N
5.	Indian – Sunda Plate	72°0' E	135°0' E	12°0' S	36°0' N
6.	Indian – Burmese Plate	75°0' E	105°0' E	15°0' S	30°0' N
7.	Indian – Somalian Plate	22°0' E	86°0' E	52°0' S	20°0' N

## 4. Indian Tectonic Plate Boundary Interactions

### 4.1. Indian-Eurasian Plate

The Indian–Eurasian collision was brought about by the rifting of India from Africa and East Antarctica during the Mesozoic and by its migration northward as the intervening oceanic lithosphere was subducted beneath the Eurasian Plate. The two continents were once separated by the Tethys Sea, which was subducted beneath the southern margins of Eurasia. The Himalayan–Tibetan orogen was created mainly by the collision between Indian and Eurasian over the past 70–50 Myr (Yin & Harrison, 2000). Reconstruction plate motion of Indian plate relative to Eurasian plates has an abrupt decrease in the convergence rate from ~150 mm/yr (0.15m/yr) to 40-50 mm/yr (0.04-0.05 m/yr). Which might probably because of continuous collision (Molnar and Tapponnier, 1975). This movement into each other led to an indent of 3000 km into Eurasia, leading to generation of lateral escape and crustal thickening. This lateral escape and crustal thickening has led to the highest topographic features on earth (Molnar and Tapponnier, 1975). The present convergence rate is absorbed by crustal shortening across the Himalaya, estimated at  $19 \pm 2.5$  mm/yr based on geodetic measurements from central and eastern Nepal (Bettinelli et al., 2006). This convergence has been responsible for any large earthquake along the Himalayan arc in the past and could likely contribute to large earthquakes in the future (Bilham et al., 2001).

The Himalayas covering 20-38° N and 70-98° E is separated into three zones: (i) Central Himalayas (starting from 28-38° N latitude covering till 78-98° E longitude) (ii) Northeast Himalayas (starting from 20-28° N latitude covering till 88-98° E longitude) and (iii) Western Himalayas (starting from 30-38° N latitude covering till 70-78° E longitude) and forms a well-defined arc to the north of Indo-Gangetic plains and extends over a length of nearly 2500 km from west-northwest to east-northeast. Phenomena of tectonics and seismicity of Himalayas has been the area of interest for many researchers for the past few decades.

Continuous movement of Indian plates in North-northeastward led to stress accumulation and hence resulted in active thrusts and faults. These active thrusts and faults are the source for seismicity along the Himalayan arc in high levels (Gupta I.D., 2006). In the Hindu-Kush region the seismicity activity is focused at the depths of 220 km and hence, many large earthquakes have occurred in this region. Presence of vertical tensional axes in intermediate-depth events reflects the detachment of denser oceanic lithosphere from the active buoyant continental lithosphere (Luciana et al., 1988).

The entire Himalayan arc experiences thrust/fault systems. Major thrust/fault systems that span across the entire Himalayan arc from north to south are: the Indus Suture Thrust (IST), the Main Central Thrust (MCT), the Main Boundary Thrust (MBT) and the Himalayan Frontal Thrust (HFT), and the seismicity between the MCT and MBT are defined as the Main Himalayan Seismic Belt (MHSB). This belt has witnessed many large ( $M > 7.0$ ) and great earthquakes ( $M 8.0$  and above) (Kayal, 2001). The thrust zones in this region have become the prime areas for the earthquake events. The common crustal depths of these earthquake events were in the range of 20 km. Small earthquakes are very common and localized vertical movement is also evident in this region. Under thrusting of plates in this region is the major source for the seismicity activity. Seismic gaps (Figure 8) i.e. the regions of plate boundary which were not ruptured in the past century are predicted to be active locations for future great earthquakes. The major gaps defined are: Kashmir gap (west of 1905 Kangra earthquake), Central gap (region between the 1905 Kangra earthquake and 1934 Bihar earthquakes), Assam gap (region between the 1934 and 1950 Assam earthquake). The gap in the western most part called as location of complex earthquakes. In the past century, Himalaya belt has experienced various earthquakes of different magnitudes. Four great earthquakes of magnitude exceeding 8 and 10 earthquakes exceeding magnitude 7.5 have occurred in the same period (Bhatia et al., 1999).

Gupta I.D., (2006) stated that the Indo-Gangetic plains experience strains in areas in front of prodding subsurface ridges. These transverse features Himalaya does result in small to moderate magnitude earthquakes in Indo-gangetic plains at Himalayan foothill areas. Many more moderate to great earthquakes are expected to occur in the near future.

Several models are proposed by researchers in the explanation of the detachment surface along the Himalayas. Seeber and Armbruster (1981) provide the models to explain the rupture of the Himalayas at different parts i.e. lower, higher and Tethys Himalaya in terms of ‘detachment surface’. Ni and Barazangi (1984) have presented the geometry of seismotectonics of the Himalayan collision zone of the under thrusting Indian plate beneath Indo-Gangetic plains and Himalaya. The steady state tectonic model provided by Seeber and Armbruster (1981) states that MBT and MCT and other thrust are imbrication along the detachment surface merging at the depths with dipping northerly low angle. This steady state tectonic model is also supported by Ni and Barazangi (1984).

As a whole Indian plate and Eurasian plate are interacting in three classes: the largest being the continental convergent of approximate length 4323.9 km (orange dots) which includes complete Himalayan belt, continental transform of length 1586.7 km (pink dots) near north-western part and part of north-eastern which can be seen in the Figure 7(d), continental ridge of length 126.5 km (white dots) in the north western part, which is the least of all seven kinds of interactions.

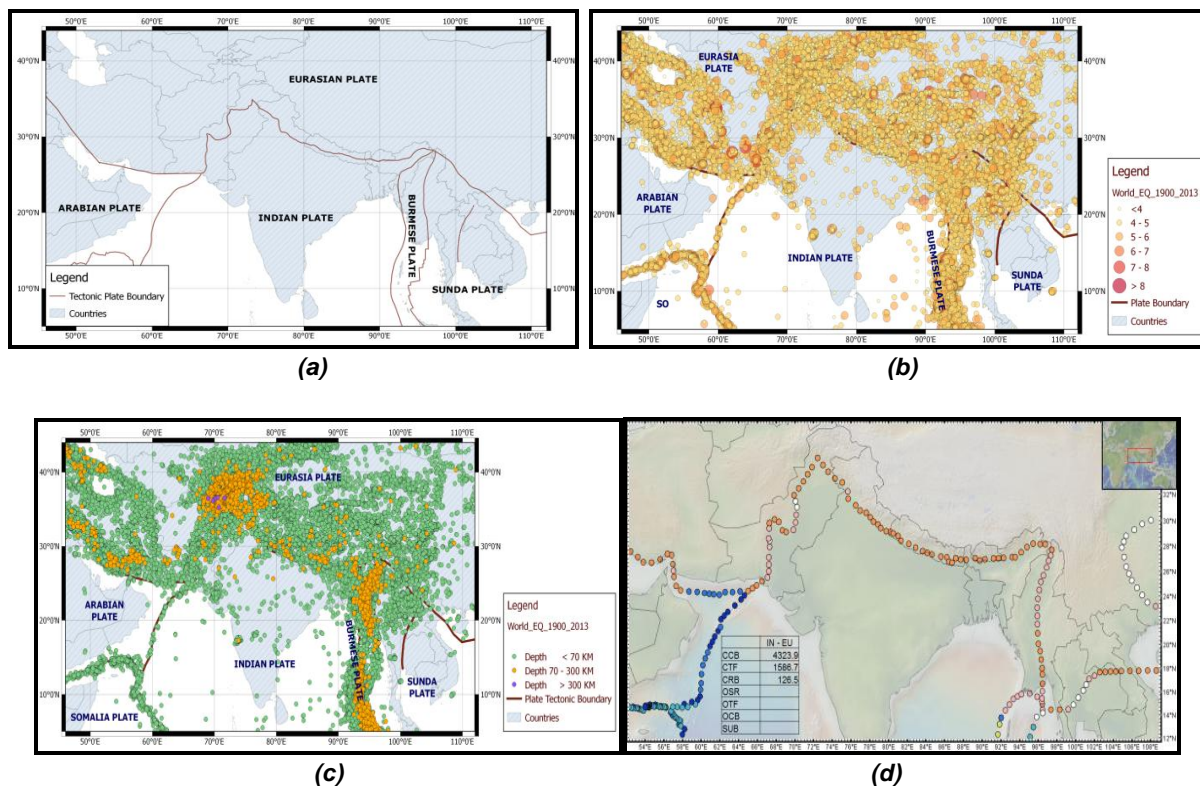


**Figure 7:** Interaction between Indian Tectonic Plate and Eurasian Plate; a) Tectonic Setup of India and Eurasia Plates; b) Figure Shows Epicenters with Different Magnitudes; c) Figure Shows Epicenters with Different Depths; d) Interaction Class Type (Earthquake Data: NCEDC)

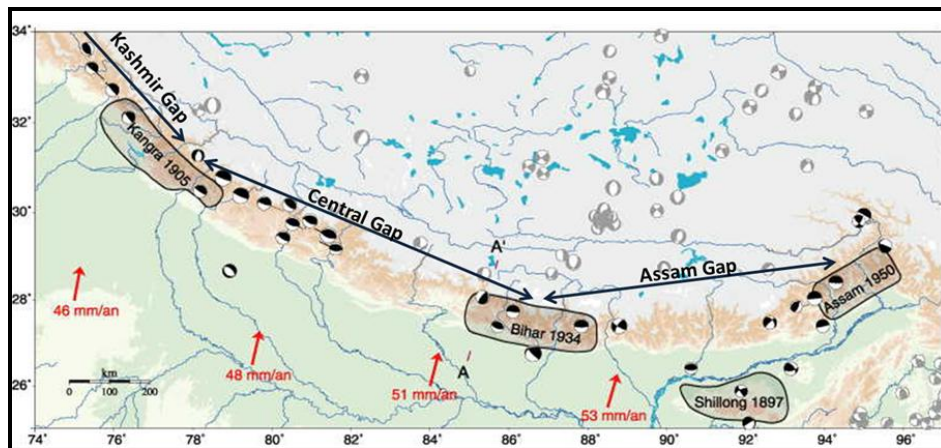


**Figure 8:** Map Shows Four Major Earthquakes and Seismic Gaps  
(Source: Avouac et al., 2001)

#### 4.2. Indian–Arabian Plate

The Indian-Arabian plate motion currently accommodated along the Owen Fracture Zone (OFZ) in the NW Indian Ocean (Fournier M., 2011). Large strike-slip plate boundaries form the OFZ like the San Andreas and are marked by a moderate seismicity (Fournier M, 2011). The OFZ connects with the Dalrymple Trough (Gordon and DeMets, 1989) which intersects the Makran subduction zone at the diffuse triple junction of the Indian, Arabian, and Eurasian plates. The southern extent of the OFZ terminates at the Indian, Arabian, and Somalian triple junction (Edwin, 2011).

It is found that the Arabian plate and the Indian plate move towards northwards at differential rates. The Arabian plate moves faster at a rate of 2 mm/yr to 4 mm/yr (0.002 m/yr to 0.004 m/yr) than the Indian plate as estimated by geodetic (Fournier et al., 2008b) and geological data (DeMets et al., 2010). The rotation of the Arabian with respect to Eurasian is calculated as a convergence along the Makran subduction zone at 23 mm/yr (0.023m/yr) (Reilinger et al., 2006).

The thickness of late Proterozoic Arabian shield varies across the regions. It has an average crustal thickness of 39 km. The crust thins to about 23 km along the Red Sea coast and to about 25 km along the margin of the Gulf of Aqaba. In the northern part, the crustal thickness ranges from 27-33 km and southeastern part of Arabian platform has a thickness ranging between 41-53 km (Al-Damegh et al., 2005).

As a whole Indian plate and Arabian plate are interacting in three classes viz oceanic spreading ridge of length 281.5 km (sky blue dots), oceanic transform of length 810 km (navy blue) and oceanic convergence of length 564 km (dark blue dots) as shown in the Figure 9 (d). Crustal thickness at the IN-AR boundary based on the past earthquake data would be less than 80 km as all the earthquakes occurred in the region are shallow (< 70 km) in nature. But, in the northern part of the Arabian plate which is colliding with the Eurasian plate, the crustal thickness is between 70 km and 300 km which can be seen in Figure 9(c).

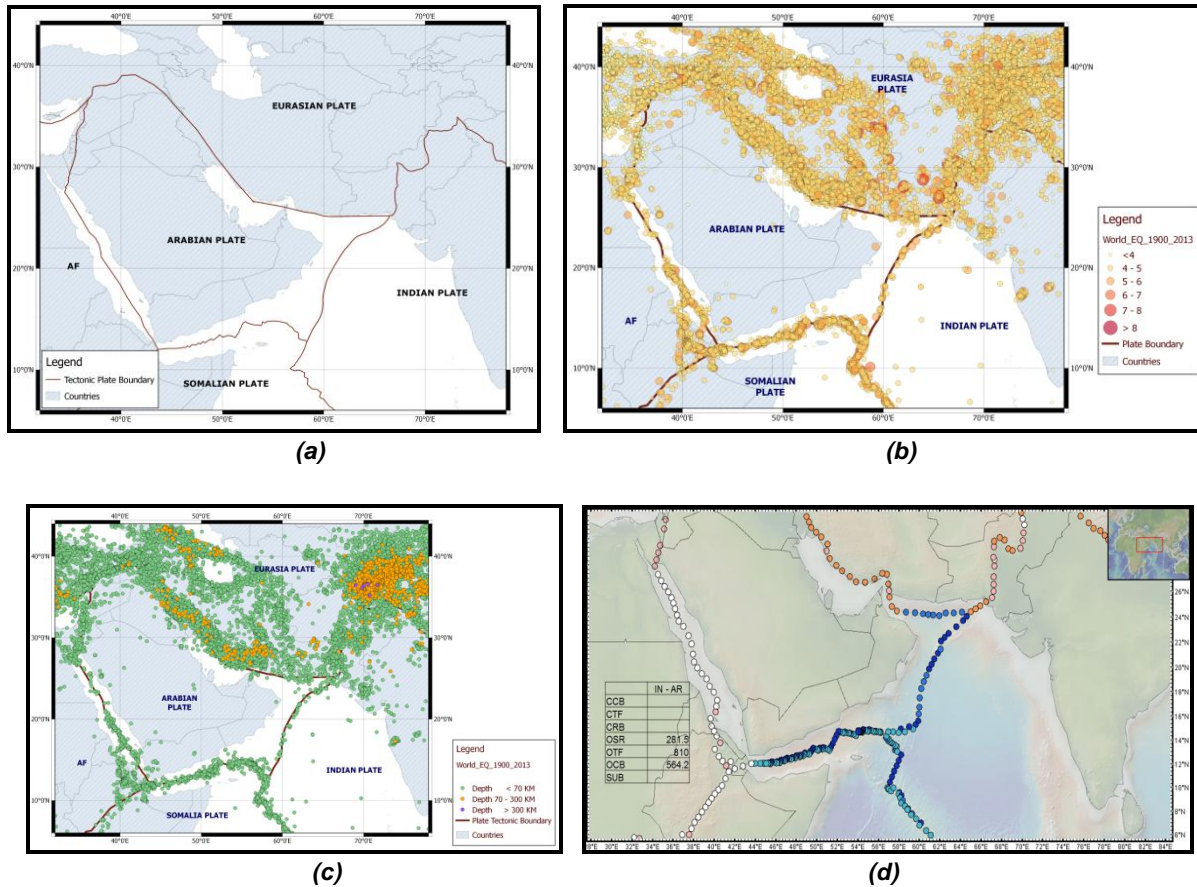


**Figure 9:** Interaction between Indian Tectonic Plate and Arabian Plate; a) Tectonic Setup of India and Arabian Plates; b) Figure Shows Epicenters with Different Magnitudes; c) Figure Shows Epicenters with Different Depths; d) Interaction Class Type (Earthquake Data: NCEDC)

### 4.3. Indian–Somalian Plate

The Indian plate is separated from Somalian plate along the mid-ocean ridge which is in the south of the Owen Fracture Zone. This boundary is completely submarine defined by the Carlsberg Ridge and the Central Indian Ridge (Edwin, 2011) highlighted by discrete seismicity. Arabian, Indian and Somalian plate meet at a junction called Aden-Owen-Carlsberg triple junction (Fournier et al., 2010). The motion between Indian and Somalia is important in understanding Indian plate path taken before and after collision with Eurasia (DeMets et al., 2005). At the same time, there has been no change in location for the past 20 Myr as indicated by India-Somalia rotation poles.

From the Figure 10(b), it can be inferred that there would be very less chance of occurrence of major earthquakes in this part of boundary. Except one earthquake remaining all of the earthquakes are of magnitude less than 7. And from Figure 10(c) the approximate crustal thickness at the India-Somalia boundary may lie between 100 and 200 km.

As a whole, the Indian plate and the Somalian plate are interacting in three classes viz oceanic spreading ridge of length 2486.8 km (sky blue dots), oceanic transform of length 1218 km (navy blue) and oceanic convergent of length 113.4 km (dark blue dots) as shown in the Figure 10(d).

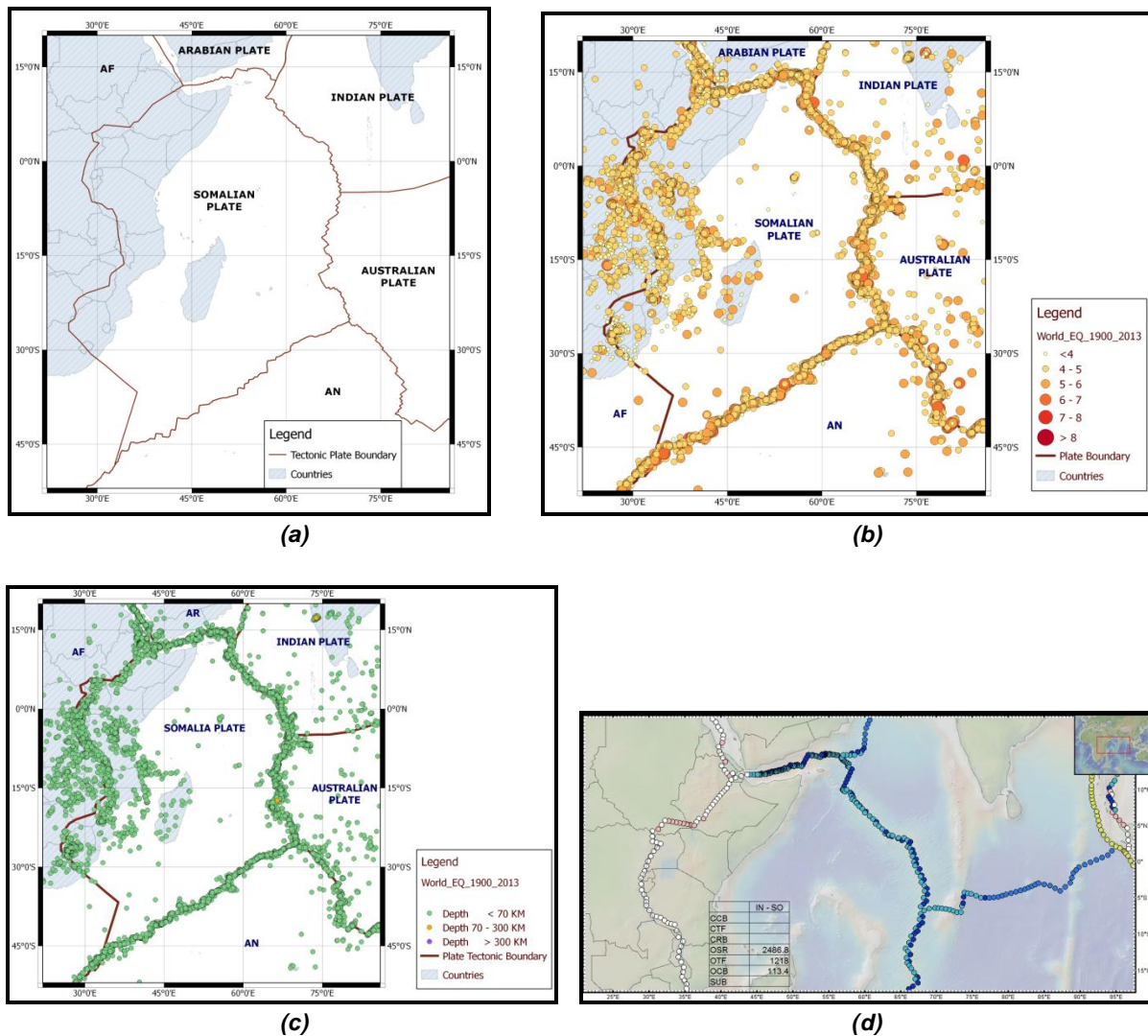


**Figure 10:** Interaction between Indian Tectonic Plate and Somalian Plate; a) Tectonic Setup of India and Somalian Plates; b) Figure Shows Epicenters with Different Magnitudes; c) Figure Shows Epicenters with Different Depths; d) Interaction Class Type (Earthquake Data: NCEDC)

#### 4.4. Indian–Australian Plate

In the early days of plate tectonics, India and Australia were viewed as forming a single rigid Indo-Australian plate divided from adjacent rigid plates by narrow boundaries (Wilson, 1965; Morgan, 1968). That is during the rifting of Gondawana, both plates formed on the northern side of spreading ridges that separated the northward-drifting continents from Antarctica (Norton and Sclater, 1979). However, the broad zones of seismicity surrounding and within the presumed single plate rapidly led to identification of diffuse plate boundaries (Stein, 2002). And in the central Indian Ocean, Indo-Australian plate is said to be broken into three smaller pieces separated by diffuse boundaries including Capricorn plate between India and Australia plates (Royer and Gordon, 1997, Helen Shen, 2012).

Compressional faults and folds have occurred in the Central Indian Basin south of India and west of the Ninetyeast ridge (NER) (Krishna et al., 2001). In contrast, deformation is mainly by strike-slip faulting in the Wharton Basin to the east of the NER (Deplus, 2001). In the middle of this deformed zone, the NER is a 4500 km volcanic ridge that displays active seismicity in some locations, but the

nature of deformation is unclear because geophysical data are sparse in the region (Sager et al., 2013). India-Capricorn plate boundary deformation is characterized by East West thrust faults that are spaced in the range of 5-10 km apart and 100-300 km long wavelength folds (Bull and Scrutton, 1992). This deformation does extend across the broad zone to the west side of the NER and began 14-18 Myr ago (Krishna et al., 2009).

Chamot Rooke (2007) states that the earthquakes have occurred in the diffused zone spread across the Central Indian Basin and Wharton basin from  $\sim 35^{\circ}$  S to  $\sim 7^{\circ}$  N. Very high seismic activity occurs in a band that stretches NE-SW from the Java Trench, across the northern NER, and continues into the Central Indian Basin, south of India. North east thrust faults related to subduction are the major events that are found near the Java trench. In the Central Indian Basin, mixed in earthquakes are observed dominantly by thrust, while other being strike-slip mechanisms are found near the equator (Sager et al., 2013).

The thinnest crust of 25 km occurs in Western Australia and the thickest crust of 61 km occurs in central Australia. The average crustal thickness in Australia is 38.8 km (Clitheroe et al., 2000). Australian plate experiences the subduction at 60 mm/yr (0.060 m/yr) at the western end and 76 mm/yr at the eastern end of the Sumatra coast. It is observed that the subduction rate decreases as one move from eastern end to the western end (Muller et al., 2008).

As a whole Indian plate and Australian plate are interacting in three classes viz oceanic spreading ridge of length 1058.8 km (sky blue dots), oceanic transform of length 228.9 km (navy blue) and oceanic convergence of length 2309.9 km (dark blue dots) that is eastern part of the interaction between AU-IN plates as shown in the Figure 11(d). Crustal thickness at the IN-AU boundary based on the previous earthquake data would be less than 80 km as all the earthquakes occurred in the region are shallow (< 70 km) in nature.

#### 4.5. Indian–Burmese Plate

The Burma-Andaman arc lies on the eastern margin of the Indian plate, along which an oblique convergence between the Indian and Burmese plates has been suggested (Fitch, 1972; Curray et al., 1979). The Burmese arc commences near eastern tip of Himalaya and extends for about 1100 km in north–south direction. The transition between the two arcs is marked by an aseismic zone (Chandra, 1984). The major tectonic features along the arc are the N-S trending Indo-Burman ranges in the north and the Andaman Nicobar ridge in the south. The Sumatran fault system in the southeast, the western Andaman fault and the Sagaing fault, further east, are the features supporting major right lateral movements in this region. The Sagaing fault separates the central low lands from the eastern high lands of Burma and seems to continue into the Andaman sea rift system which is characterized by sea floor spreading and transform faulting (Curray et al., 1979). The presence of the major right lateral strike-slip faults in the east, running parallel to both arcs, has been related to the oblique nature of convergence (Fitch, 1972; Maung, 1987). The development of the two arcs as distinct entities has been attributed by Maung (1987), to the northward drag of the Indo-Burman ranges and the Andaman-Nicobar ridge. According to Kundu and Gahalaut (2013) the Indo-Burmese arc is probably one of the least studied domains as far as plate motion, crustal deformation and earthquake occurrence processes that are concerned.

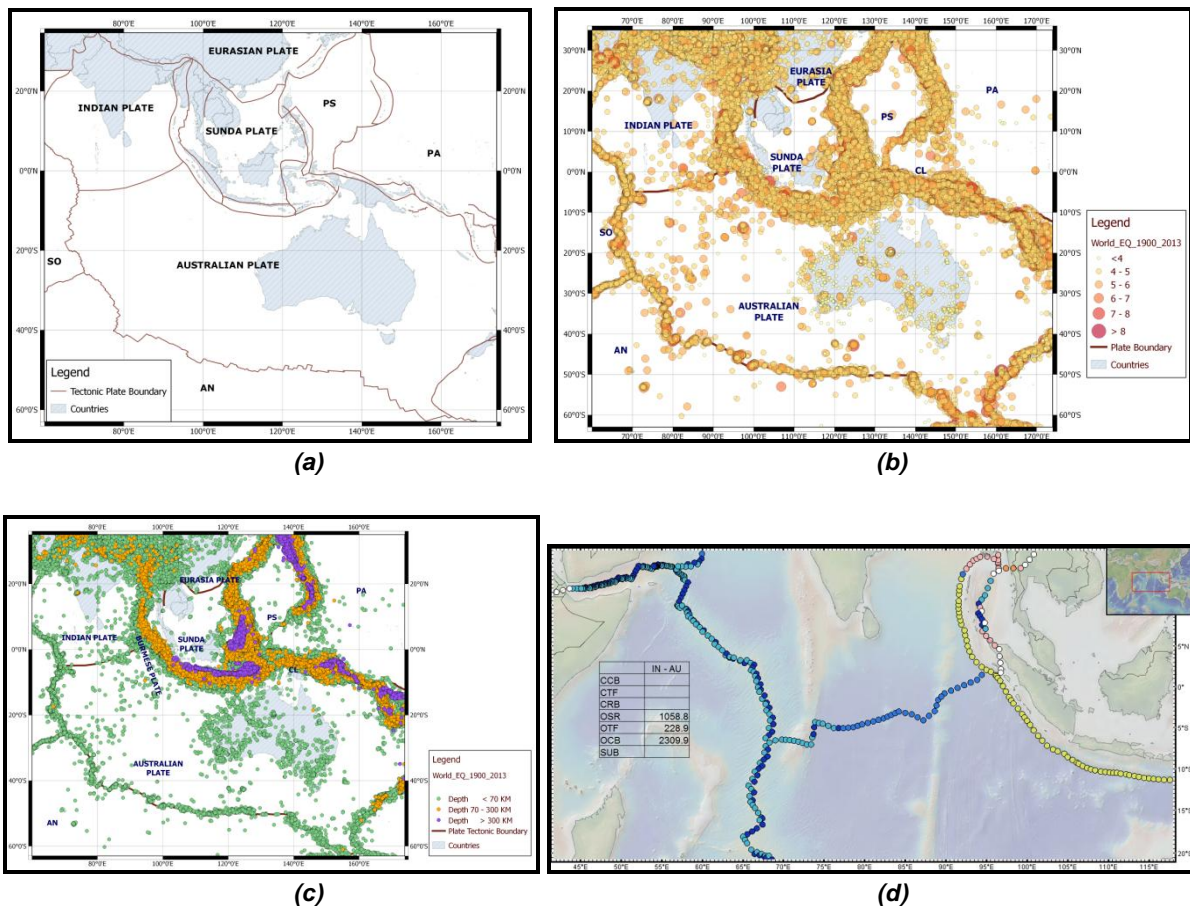


**Figure 11:** Interaction between Indian tectonic plate and Australian plate; a) Tectonic setup of India and Australian plates; b) Figure shows epicenters with different magnitudes; c) Figure shows epicenters with different depths; d) Interaction class type (Earthquake Data: NCEDC)

The collision pattern of Burmese and Indian plates led to the high seismicity in the Burmese arc. It is found to be decreasing from north to south of Burmese arc as due to migration of plates from north to south direction. The subduction process is said to be still continuing (Gupta I.D., 2006). Deep focus earthquakes at a depth of 200 km are observed to occur at approximately 250 km from Arakan Yoma ranges. Most of these earthquakes originated at Indo-Burmese zone, caused due to thrust fault mechanism. A few of them are due to strike-slip and normal faulting. Thrust faulting is seen to prevail at depths greater than about 70 km, while at shallower depths, strike-slip or normal faulting are occurring quite commonly (Verma, 1976; Rao, N.P., et al., 1999).

As a whole Indian plate and Burmese plate are interacting in three classes viz continental transform fault of length 499.4 km (pink dots), oceanic convergent of length 88.8 km (dark blue) and subduction of length 1416.6 km (green dots) as shown in the Figure 12(d). So we can say that December 26, 2004 great earthquake of magnitude 9.1 is a result of this subduction.

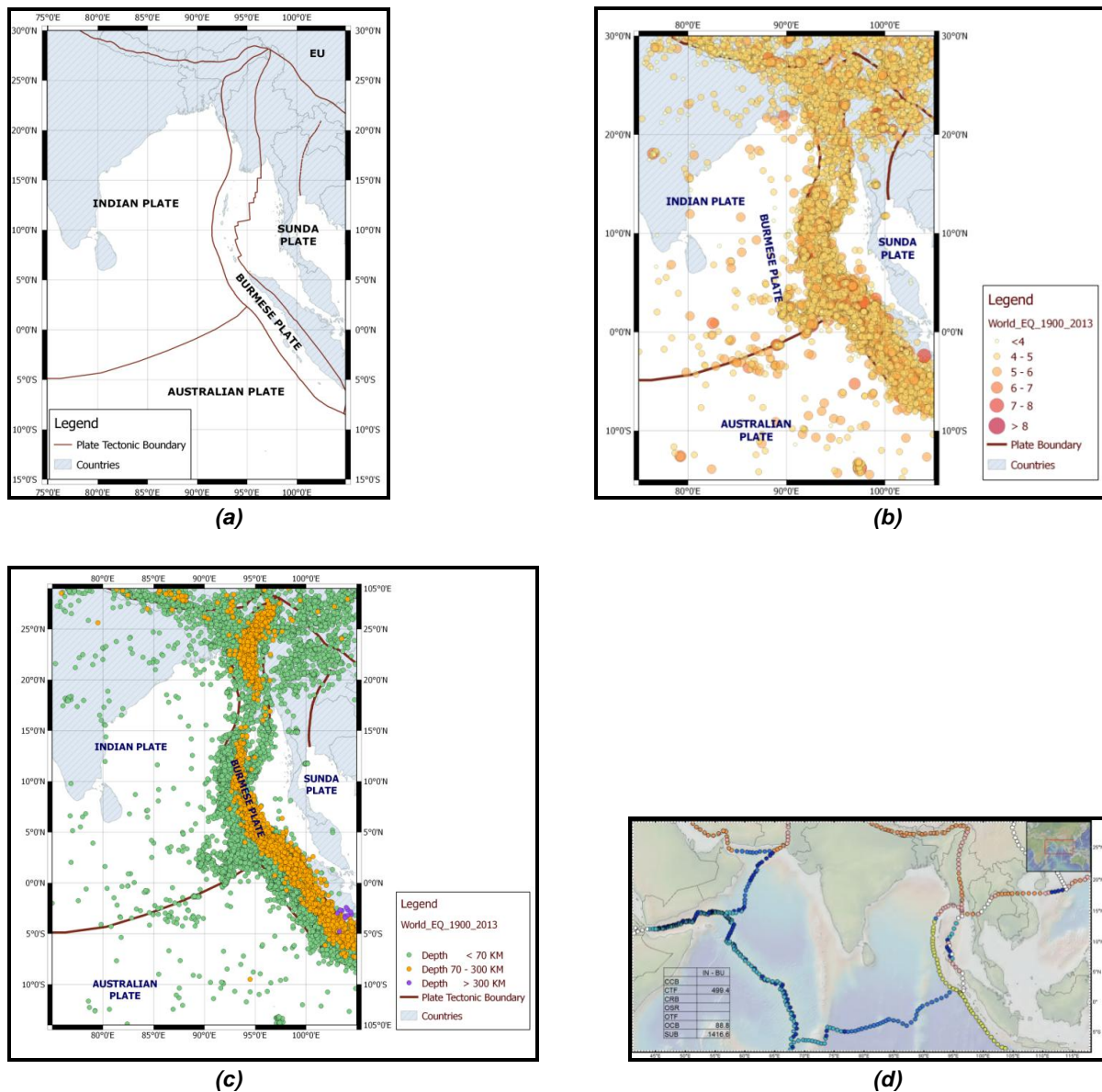


**Figure 12:** Interaction between Indian Tectonic Plate and Burmese Plate; a) Tectonic Setup of India and Burmese Plates; b) Figure Shows Epicenters with Different Magnitudes; c) Figure Shows Epicenters with Different Depths; d) Interaction Class Type (Earthquake Data: NCEDC)

#### 4.6. Indian-Sunda Plate

The interaction between the Indian plate and Sunda plate is most significant along the Sumatra-Andaman subduction zone, even though Indian plate does not interact with the Sunda plate directly as shown in the Figure 13(a), but its effect is observed in occurrences of earthquakes plotted in Figure 13(b) and Figure 13(c). When Indian-Sunda motion portioned along the mega thrust and the sub-parallel strike slip great Sumatra fault (McCaffrey et al., 2000). The Indian and Sunda land plates abut in Myanmar (Anne et al., 2006). The Sunda plate includes most of southeast Asia, the south China sea, the Malay Peninsula, most of Sumatra, Java, Borneo, and the intervening shallow seas. The very low rate of shallow earthquakes is evidence of its low anelastic strain rates. Sunda plate is separated from the Australia and Philippine Sea plates by subduction zones (Peter, 2003). Geodetic measurements show that the Sunda plate is currently moving eastward with respect to Eurasian plate

(Bock et al., 2003). With respect to Sunda, India moves around 35 mm/yr (0.035 m/yr) NNE (Anne et al., 2006).

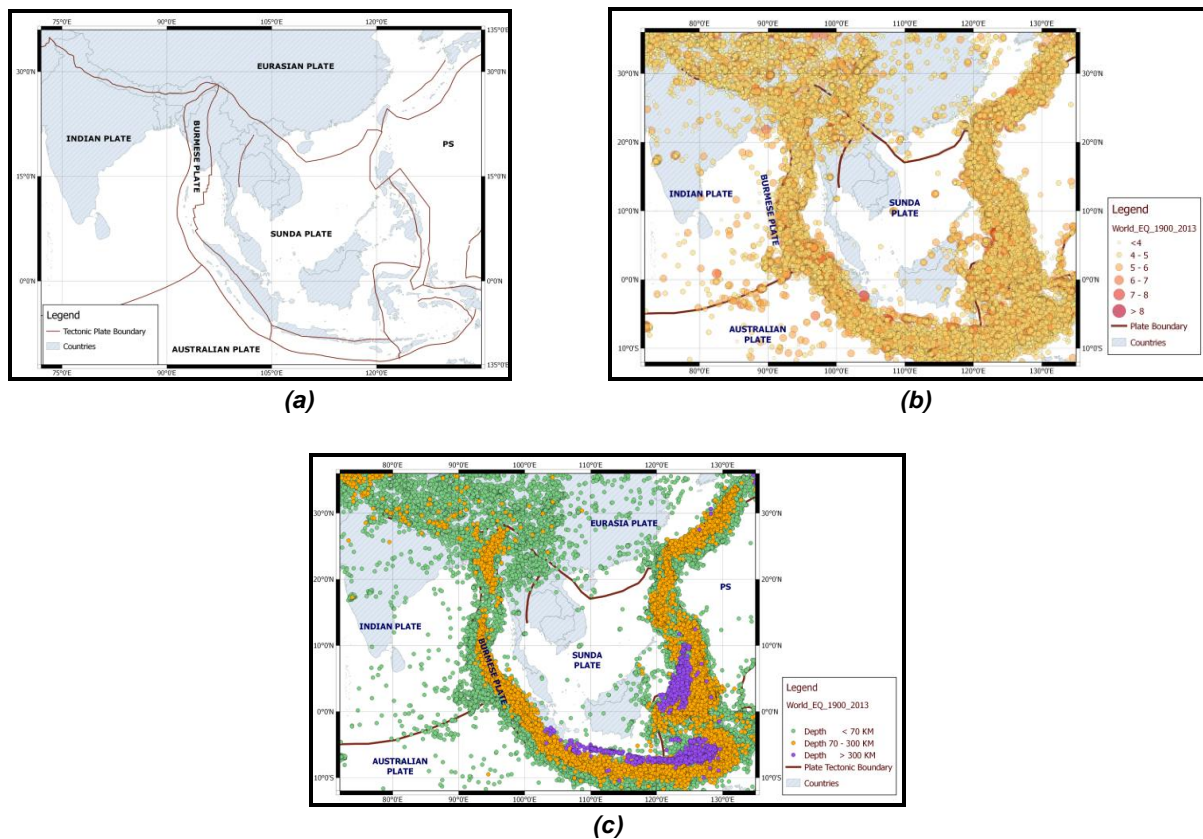


**Figure 13:** Interaction between Indian Tectonic Plate and Sunda Plate; a) Tectonic Setup of India and Sunda Plates; b) Figure Shows Epicenters with Different Magnitudes; c) Figure Shows Epicenters with Different Depths; (Earthquake Data: NCEDC)

## 5. Discussion

### 5.1. Indian Intra-Plate Deformation

As Indian plate is colliding in the northern part and subducting in the eastern part, its high impact is seen in the intraplate deformation which has been leading to minor to great earthquakes. Intraplate deformation in central India could also result from flexure of the Indian plate as it collides with Eurasian plate (Bilham et al., 2003). Once, Indian shield was considered to be a stable continental region. But now it has become seismically active. Given the observed seismicity along the Narmada Son, it is possible that Indian intraplate deformation is concentrated along this lineament. It also suggests that NSL divides Indian subcontinent in to two parts northern India and Southern India.

### 5.2. Indian Plate Boundary Interactions

The seismicity of the Himalaya arc tectonic belt is associated with the under thrusting of the Indian plate beneath the Eurasian plate (Molnar, 1979). Due to their continental interaction, the upper Indian crust was sheared off into a series of thrust sheets, which were crumpled and folded in the form of Himalaya (Gupta, 2006). Seeber and Armbruster (1981) have explained a tectonic model which postulates the existence of a gently dipping detachment thrust plane at depths ranging from about 20-40 km.

The Indo-Australian plate is unique among the earth's plates in its variety of first-order tectonic features, having a combination of active subduction zones, an extensive mid-ocean ridge system, significant areas of both continent-continent and continent island arc collision, and regions of intraplate oceanic-lithosphere deformation (Coblentz et al., 1998). Based on the observed seismicity the boundary between Australia and India is diffused. The formation of two triple plate junctions IN-AU-SO and IN-AU-BU could lead to future moderate to great earthquakes.

The Indian plate and Burmese plate interaction is the most active seismicity zone which has led to one of the greatest earthquake of the century (26<sup>th</sup> Dec., 2004, 9.1  $M_w$ ) apart from regular minor to major earthquakes. The focal depth variation of earthquakes is found to be between 7 km–300 km.

As compared to other interaction of Indian tectonic plate, interaction with Arabian plate and Somalian plate are not very high seismically active. Even though minor to major earthquakes are observed, they could also be probable reason for generating intraplate earthquakes. Still the reasons for Allah bund and Bhuj earthquake are being understood.

## 6. Conclusions

Past earthquake data have been very useful in understanding and modeling different plate tectonic models. Mainly three important points can be concluded or derived from the past earthquake data.

- i. Interaction types and their lengths
- ii. Approximate varying thickness of plate inner to boundaries from focal depths
- iii. Location of major to great earthquakes

As for the Indian tectonic plate is considered its interaction with neighboring plates have led to very large seismicity at the boundaries includes North-western, Northern, North-eastern, Eastern and Southern-eastern. With the current understanding if a three dimensional numerical model where all seven plates are interacting is modeled, it will probably give more insights about the locations of future major to great earthquakes. Understanding of this complete tectonic environment will improve as additional seismological and plate motion data accumulate. Stress models may provide further insight into the mechanics of the plate boundaries.

## References

Al-Damegh, K., Sandvol, E., and Barazangi, M. *Crustal Structure of the Arabian Plate: New Constraints from the Analysis of Teleseismic Receiver Functions*. Earth and Planetary, Science Letters. 2005. 231; 177-196.

Anne Socquet, Christophe Vigny, Nicolas Chamot-Rooke, Wim Simons, Claude Rangin and Boudewijn Ambrosius. *India and Sunda Plates Motion and Deformation along their Boundary in Myanmar Determined by GPS*. Journal of Geophysical Research. 2006. 111; B05406.

Avouac, J.P., Bollinger, L., Lavé J., Cattin, R., and M., Flouzat. *Le Cycle Sismique en Himalaya*. Comptes Rendus de l'Académie des Sciences - Series IIA. Earth and Planetary Science. 2001. 333 (9) 513-529.

Benioff, H. *Orogenesis and Deep Crustal Structure—Additional Evidence from Seismology*. Geological Society of America Bulletin. 1954. 65 (5) 385-400.

Bhaskar Kundu and V.K., Gahalaut. *Tectonic Geodesy Revealing Geodynamic Complexity of the Indo-Burmese Arc Region, North East India*. Current Science. 2013. 104 (7) 920-933.

Bird, P., Y.Y., Kagan, and D.D., Jackson. *Plate Tectonics and Earthquake Potential of Spreading Ridges and Oceanic Transform Faults, Plate Boundary Zones*. Geodynamic Series, American Geophysical Union. 2002. 30.

Bird, P. *An Updated Digital Model of Plate Boundaries*. *Geochemistry Geophysics Geosystems*. 2003. 4 (3) 10-27.

Clitheroe, G., Gudmundsson, O., and Kennett, B.L.N. *The Crustal Thickness of Australia*. *Journal of Geophysical Research*. 2000. 105 (B6) 13697-13713.

Coblentz, D., David, Shaohua Zhou and Richard, R., Hillis. *Topography, Boundary Forces, and the Indo-Australian Intraplate Stress Field*. *Journal of Geophysical Research*. 1998. 103 (B1) 919-931.

DeMets, C., Gordon R.G., Argus D.F., and Royer, J.Y. *Motion between the Indian, Capricorn and Somalian Plates since 20 Ma: Implications for the Timing and Magnitude of Distributed Lithospheric Deformation in the Equatorial Indian Ocean*. *Geophysical Journal International*. 2005. 161; 445-468.

DeMets, C., Gordon, R.G., Argus, D.F., and Stein, S. *Current Plate Motions*. *Geophysical Journal International*. 1990. 101; 425-478.

Gordon, R.G., 1995: *Global Earth Physics: A Handbook of Physical Constants*, Vol. 1. T.J. Ahrens (Ed.). American Geophysical Union, Washington, D.C. 66-87.

Gupta, I.D. *Delineation of Probable Seismic Sources in India and Neighbourhood by a Comprehensive Analysis of Seismotectonic Characteristics of the Region*. Elsevier, Soil Dynamics and Earthquake Engineering. 2006. 26; 766-790.

Helen Shen. *Unusual Indian Ocean Earthquakes Hint at Tectonic Breakup*. *Nature News and Comments*. 2012. 1-4.

Kanamori, H. *Great Earthquakes at Island Arcs and the Lithosphere*. *Tectonophysics*. 1971. 12; 187-198.

Khan, A.A. *Why Tectonically Stable Indian Shield Becomes Seismically Unstable*. *Journal of South Asia Disaster Studies*. 2009 2 (1) 129-138.

Larry Ruff and Hiroo Kanamori. *Seismicity and the Subduction Process*. *Physics of the Earth and Planetary Interiors*. 1980. 23; 240-252.

Luciana Astiz, Thorne Lay and Hiroo Kanamori. *Large Intermediate-Depth Earthquakes and the Subduction Process*. *Physics of the Earth and Planetary Interiors*. 1988. 53; 80-166.

Marc Fournier, Nicolas Chamot-Rooke, Mathieu Rodriguez, Philippe Huchon, Carole Petit, Marie-Odile Beslier and Sebastien Zaragosi. *Owen Fracture Zone: The Arabia-India Plate Boundary Unveiled*. *Earth and Planetary Science Letters*. 2011. 302; 247-252.

Marc Fournier, Nicolas Chamot-Rooke, Carole Petit, Philippe Huchon, Ali Al-Kathiri, Laurence Audin, Marie-Odile Beslier, Elia d'Acremont, Olivier Fabbri, Jean-Marc Fleury, Khaled Khanbari, Claude Lepvrier, Sylvie Leroy, Bertrand Maillot and Serge Merkouriev. *Arabia-Somalia Plate Kinematics, Evolution of the Aden-Owen-Carlsberg Triple Junction, and Opening of the Gulf of Aden*. *Journal of Geophysical Research*. 2010. 115.

- Minster, J.B., and T.H., Jordon. *Present-day Plate Motions*. J. Geophys. Res. 1978. 83; 8169-8184.
- Mishra, D.C. *Plate Tectonics–Historical Perspective and Seismicity of Indian Plate*. Journal of Geophysics. 2013. 36 (3) 125-133.
- Mueller, D., Roest W.R., Royer J.Y., Gahagan L.M., and Sclater J.G. *Digital Isochrones of the World's Ocean Floor*. J. Geophys. Res. 1997. 102; 3211-3214.
- Purnachandra, Rao N., and Hanmantha, Chary A. *What caused the Great Sumatran Earthquakes of 26 December 2004 and 28 March 2005*. Current Science. 2005. 89 (3) 449-452.
- Sager, W.W., Bull, J.M., and Krishna, K.S. *Active faulting on the Ninetyeast Ridge and Its Relation to Deformation of the Indo-Australian Plate*. J. Geophys. Res (B: Solid Earth). 2013. 118; 4648-4668.
- Satish C., Bhatia, Ravi M., Kumar and Harsh K., Gupta. *A Probabilistic Seismic Hazard Map of India and Adjoining Regions*. Annali Di Geofisica. 1999. 42 (6) 1153-1164.
- Seeber, L., and Armbruster, J.G., 1981: *Great Detachment Earthquakes along the Himalayan Arc and Long Term Forecasting*. Earthquake Prediction: An International Review. Simpson, David W., and Richards, Paul G. (Eds.). American Geophysical Union, Washington, DC. 259-277.
- Seth Stein, Giovanni F., Sella and Emile A., Okal. 2002: The January 26, 2001 Bhuj Earthquake and the Diffuse Western Boundary of the Indian Plate. Plate Boundary Zones, Geodynamic Series 30, American Geophysical Union. 243-254.
- Wiens, D.A., Stein, S. Demets, C., Gordon, R.G., and Stein, C. *Plate Tectonic Models for Indian Ocean "Intraplate" Deformation*. Tectonophysics. 1986. 132 (1-3) 37-48.
- Zoback, M.L. *First and Second-Order Patterns of Stress in the Lithosphere: The World Stress Map Project*. Journal of Geophysical Research. 1992. 97; 11703-11728.

# Illustration and Taxonomy of Late Neogene Deep Sea Agglutinated Benthic Foraminifera from the Exmouth Plateau in the Eastern Indian Ocean

Virendra Bahadur Singh<sup>1</sup>, Ajai Kumar Rai<sup>2</sup> and Uday Bhan<sup>3</sup>

<sup>1</sup>Department of Petroleum Engineering, Graphic Era University, Dehradun, Uttarakhand, India

<sup>2</sup>Department of Earth and Planetary Sciences, Nehru Science Centre Building, Faculty of Science, University of Allahabad, Allahabad, Uttar Pradesh, India

<sup>3</sup>Department of Petroleum Engineering & Earth Sciences, University of Petroleum and Energy Studies, Dehradun, Uttarakhand, India

Correspondence should be addressed to Virendra Bahadur Singh, to.virendra@gmail.com

Publication Date: 25 September 2014

Article Link: <http://scientific.cloud-journals.com/index.php/IJAESE/article/view/Sci-213>



Copyright © 2014 Virendra Bahadur Singh, Ajai Kumar Rai and Uday Bhan. This is an open access article distributed under the **Creative Commons Attribution License**, which permits unrestricted use, distribution, and reproduction in any medium, provided the original work is properly cited.

**Abstract** Agglutinated benthic foraminifera were investigated from two ODP Sites 762B and 763A located on the Exmouth Plateau off north west Australia in the eastern Indian Ocean over an interval of Late Miocene to Late Pleistocene. Sixteen species of agglutinated benthic foraminifera are recorded from 152 samples from these sites. The foraminifera are generally well preserved. All the recorded taxa described and illustrated herein belong to ten genera and five families.

**Keywords** *Benthic Foraminifera; Late Neogene; Taxonomy; Agglutinated; Eastern Indian Ocean; Paleoecology*

## 1. Introduction

Benthic foraminifera is one of the most abundant and diverse group of organisms which may form more than fifty percent of eukaryotic biomass in the deep sea (Gooday et al., 1992). They have probably the longest and most complete fossil record of any member of the deep sea benthos (Douglas and Woodruff, 1981). Studies show that many species have long stratigraphic ranges and cosmopolitan occurrences (e.g. Berggren, 1976; Boltovosky, 1978b; Tjalsma and Lohman 1983; Kaiho, 1998). Taxonomy play a significant role in the understanding of ecologic and biostratigraphic importance of benthic foraminifera. Ambiguous taxonomic identifications in many studies have resulted in inconsistent ecologic interpretations while using the same taxon or taxa in different regions. Thus a reliable taxonomy assists in comparing paleontologic data and offers a more reliable understanding of the paleoecological history of different regions. The present study will improve our understanding of the Eastern Indian Ocean agglutinated benthic foraminifera, their bathymetry, and water mass relation.

## 2. Study Area

The present work is based on agglutinated benthic foraminifera from the two ODP sites (Table 1) 762B (Lat.  $19^{\circ}53.24'$  S, Long.  $112^{\circ}15.24'$  E Water depth 1360 m) and 763A (Lat.  $20^{\circ}35.20'$  S, Long.  $112^{\circ}12.50'$  E Water depth 1368 m) drilled on the Exmouth Plateau in the Eastern Indian Ocean (Figure 1) during Leg 122 of D/V Glomar Challenger. Exmouth Plateau is bounded on the north by Argo abyssal plain, Gascoyne and Cuvier abyssal plain stretch westward from the Exmouth Plateau and western Australian margin. All these abyssal plains were formed by two separate rifting and sea-floor spreading events, as they contain correlatable seafloor spreading magnetic anomalies and basement seismic reflection pattern suggestive of oceanic crust (Powell, 1978; Veevers and Cotterill, 1978; Veevers, 1984) off north west coast of Australian margin creating first Argo then the Gascoyne and Cuvier abyssal plain (Powell, 1978). The Exmouth Plateau is a rifted and subsided fragment of continental crust which is above the calcium carbonate compensation depth making it an ideal site for deposition of fossiliferous calcareous sedimentary sequences. The core samples at both the sites are 10 cm<sup>3</sup> plugs of sediment consisting mainly of foraminifera rich nanofossil ooze. Both the sites have almost continuous and well-preserved Late Neogene sections.

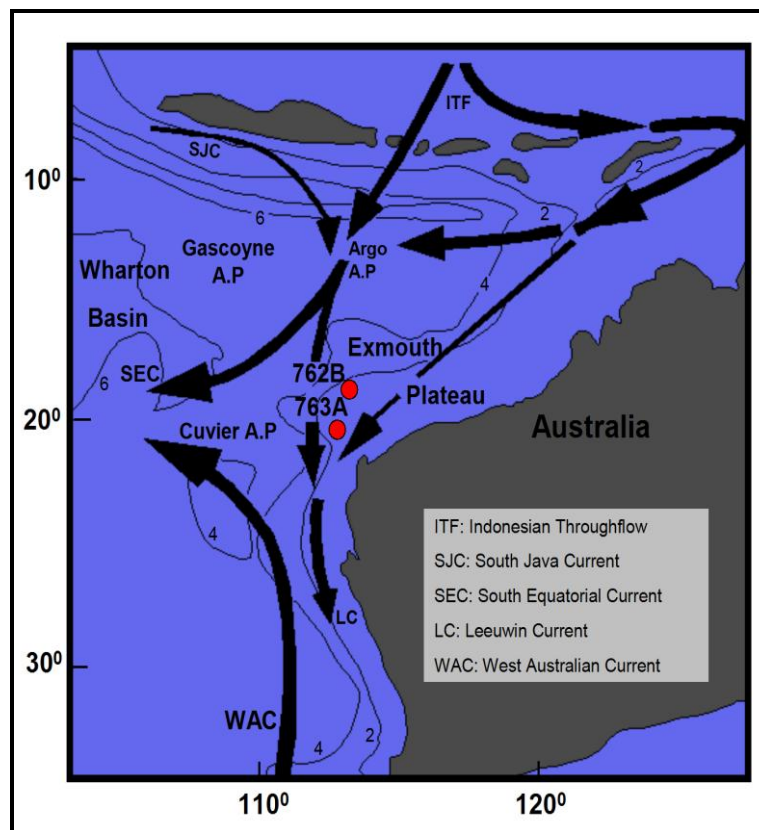


**Figure 1:** Oceanographic Setting and Locations of ODP site 762B and 763A in the Southeast Indian Ocean; Depth Contours are in Kilometers

## 3. Materials and Methods

Approximately 10cm<sup>3</sup> of each core sample was soaked in dilute (<5%) hydrogen peroxide solution and water (1:3 ratio) until clays had fully disaggregated. It was then gently washed over a 63 µm and 149 µm Tyler Sieves. Though the H<sub>2</sub>O<sub>2</sub> is aggressive to carbonates, the concentration is too low (< 2%) to affect the test of benthic foraminifera. After drying a microsplitter was used to separate a representative portion of the >149 µm fraction estimated to contain about 300 specimens of benthic foraminifera. All the benthic foraminiferal specimens from the splitted samples >149 µm size fraction

were picked and mounted on microfaunal assemblage slides for identification. These slides are kept in the Micropaleontology Laboratory of Department of Earth and Planetary Sciences, Allahabad University, Allahabad, India. The >149 µm fraction was selected because it gives the most climatic information in the shortest time (Imbrie and Kipp, 1971) and is the size fraction adopted by many paleoclimatic studies especially those in the Indian Ocean (e.g. Corliss 1979a; Gupta and Srinivasan, 1992a, b; Wells et al., 1994; Nomura, 1995; Rai and Srinivasan, 2000 and others). All the mounted benthic foraminiferal individuals were then identified, counted and recorded as the percentage of the total assemblage.

**Table 1:** Location of Sites, Their Depth and Number of Samples

Leg	Site	Latitude	Longitude	Depth (m)	Name of Samples
122	762B	19°53.24' S	112° 15.24' E	1360 m	76
122	763A	20°35.20' S	112° 12.50' E	1368 m	80

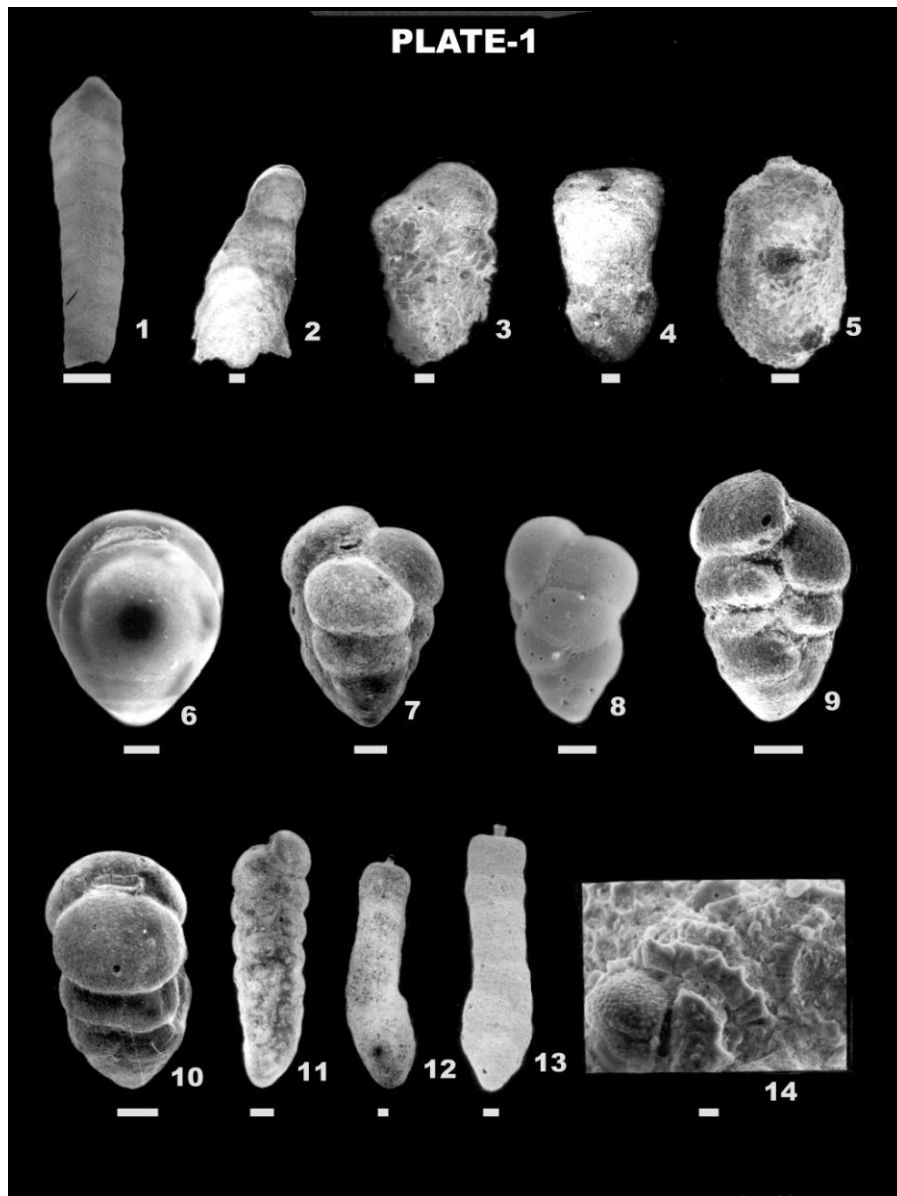
#### 4. Systematics

We presented systematic taxonomy for all the agglutinated species recorded at the sites 762B and 763A. For determinations at the generic level, we largely followed the taxonomy established by Loeblich and Tapan (1987), but taxonomic studies by Barker (1960), Bolotoskoy (1978a), Srinivasan and Sharma (1980), Hermelin (1989), Bornmalm (1997) have also been considered. Identifications of foraminiferal species were made using Barker (1960), Boltovskoy (1978a), Srinivasan and Sharma (1980), Hermelin (1989) and Bornmalm (1997). The generic nomenclature follows Loeblich and Tapan (1964, 1987)

Order : FORAMINIFERIDA Eichwald, 1830  
 Suborder : TEXTULARIINA Delage and Herouard, 1896  
 Superfamily: SPIROPECTAMMINACEA Cushman, 1927  
 Family : SPIROPECTAMMINIDAE Cushman, 1927  
 Subfamily : SPIROPECTAMMININAE Cushman, 1927  
 Genus : *Bolivinopsis* Yakovlev, 1891  
 Type Species: *Bolivinopsis capitata* Yakovlev, 1891

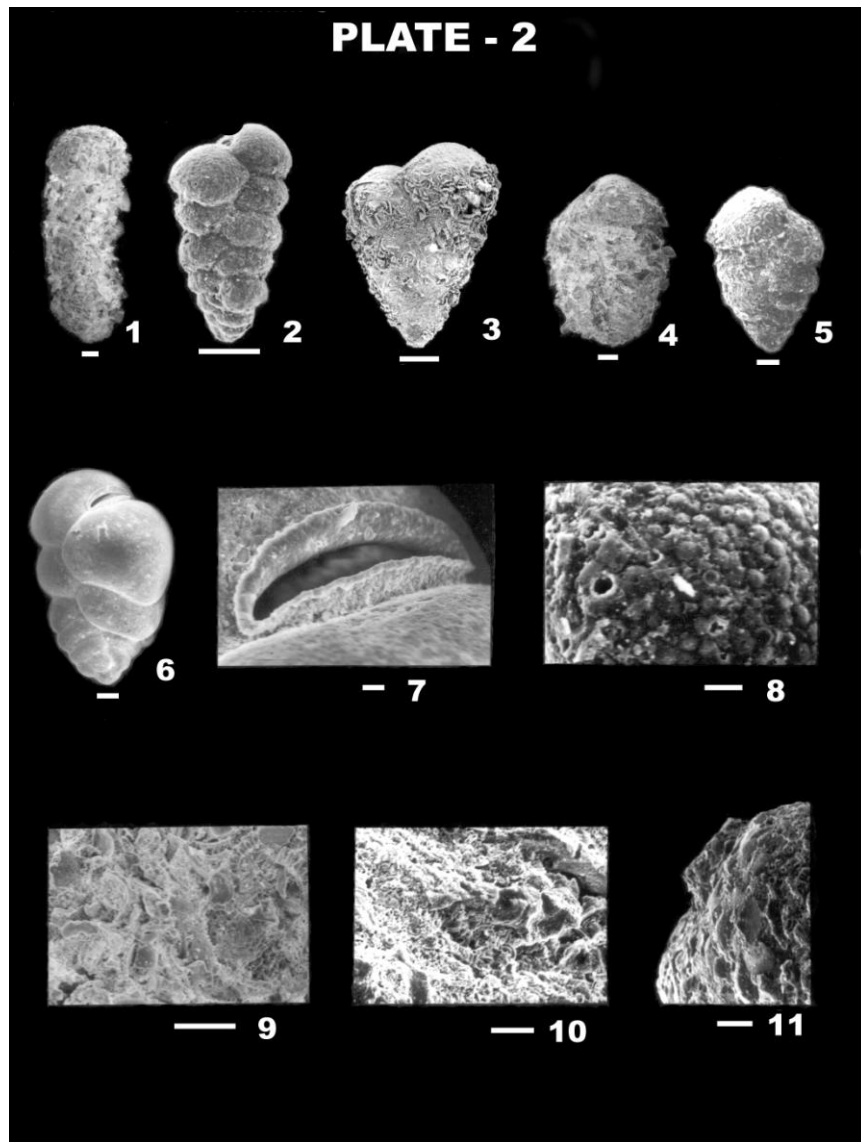
*Bolivinopsis praelonga* (Schwager, 1866)

Plate 1, Figure 1



**Plate 1:** (Scale bar 100 $\mu$ m for Figures 1-13, 10 $\mu$ m for Figure 14)

Figure 1: *Bolivinopsis praelonga* (Schwager) side view; Figure 2: *Vulvulina nicobarica* (Schwager) side view; Figures 3-4: *Gaudryina solida* Schwager, 3 side view, 4 apertural views, and 14 enlarged view of Figure 3 showing apertural area. Surface covered with broken fragments of foraminiferal test; Figure 5: *Ruakituria magdalidiforme* (Schwager) side view; Figure 6: *Dorothia brevis* Cushman and Stainforth side view; Figure 7: *Eggerella bradyi* (Cushman) top view; Figure 8: *Karriella baccata* (Schwager) side view; Figure 9-10: *Karriella bradyi* (Cushman) side view, 10 apertural view; Figure 11: *Karriella subrotundata* (Schwager) side view; Figure 12-13: *Martinottiella communis* (d'Orbigny) side view



**Plate 2:** (Scale bar 100 $\mu$ m for Figures 1-6, 9, 10 $\mu$ m for Figures 7-8, 10-11)

Figures 1, 9. *Martinottiella scabra* (Cushman), 1 Side View, 9 enlarged view of Figure 1 showing apertural area. Surface Covered with Broken fragments of foraminiferal test; Figures 2, 8. *Textularia agglutinans* d'Orbigny, 2 side view, 8 enlarged view of Figure 2 showing surface covered with Nanoforam; Figure 3. *Textularia halkyardi* Lalicker side view; Figures 4, 10. *Textularia lythostrotta* (Schwager), 4 side view, 10 enlarged view of Figure 4; Figures 5, 11. *Siphotextularia rolshauseni* Phleger and Parker, 5 side view, 11 enlarged view of Figure 5; Figures 6-7 *Siphotextularia solita* (Schwager), 6 side view, 7 enlarge view of Figure 6

- 1866 *Textularia praelonga* Schwager: p. 252, pl. 7, Figures 104  
 1930 *Textularia praelonga*; Mc Donald, p. 70, pl. 1, Figure 104  
 1941a *Spiroplectoides praelonga*; Le Roy, p. 31, pl. 3, Figures 95-96  
 1978a *Bolivinopsis cubensis*; Boltovskoy, p. 154, pl. 1, Figures 30-32  
 1980 *Bolivinopsis praelonga*; Srinivasan and Sharma, p. 12, pl. 4, Figure 1  
 1985 *Bolivinopsis praelonga*; Boersma, p. 988, pl. 3, Figures 3-4  
 2004 *Bolivinopsis praelonga*; Rai and Singh, Jour. Geol. Soc. of India, v. 63, p. 418

## Remarks

The specimen found in this work is closely similar to *Bolivinopsis cubensis* reported by Boltovskoy, 1978a from the Late Cenozoic deep sea sequences of the northern Indian Ocean.

## Bathymetry and Paleoecology

*Bolivinopsis praelonga* was recorded from lower bathyal (1253m) to lower abyssal (3010m) in the Indian Ocean (Boltovskoy, 1978a; Rai and Singh, 2004). Nomura (1991) also reported this species from lower bathyal depth (1074m) from the Broken Ridge in the eastern Indian Ocean. This species has also been recorded from lower bathyal depths in the Tasman Sea and Chatham Rise (Boersma, 1986). *B. praelonga* lives as deep infaunal and having higher  $\delta^{13}\text{C}$  than epifaunal species because *B. praelonga* construct a test which is granular in appearance and the microstructure of the shell material may influence the isotopic values of the test (Rathburn et al., 1996).

## Distribution at Sites 762B and 763A

*B. praelonga* shows rare and sporadic occurrences during Late Miocene to Early Pliocene at both the sites 762B and 763A.

Subfamily : VULVULININAE Saidova, 1981  
Genus : *Vulvulina* d'Orbigny, 1826  
Type species : *Vulvulina capreolus* Cushman, 1928

*Vulvulina nicobarica* (Schwager), 1866

Plate 1, Figure 2

- 1866 *Bigenerina nicobarica* Schwager; p. 196, pl. 4, Figures. 7a-c. (Labelled in the plate caption as *B. nicobarensis*)  
1927 *Vulvulina spinosa*; Cushman, p. 111, pl. 23, Figure 1  
1930 *Bigenerina nicobarensis*; Mc Donald, p. 68, pl. 1, Figure 7  
1934 *Vulvulina nicobarica*; Cushman, p. 105, pl. 10, Figures 6a-b  
1978a *Vulvulina spinosa*; Boltovskoy, p. 173, pl. VIII, Figures 41  
1980 *Vulvulina nicobarica*: Srinivasan and Sharma, p. 12, pl. 2, Figures 5-7  
1995 *Vulvulina spinosa*; Nomura, pl. 3, Figures 19a, b  
2004 *Vulvulina nicobarica*; Rai and Singh, Jour. Geol. Soc. of India, v. 63, p. 420 (list)

## Remarks

*Vulvulina spinosa* Cushman recorded by Boltovskoy (1978a), Nomura (1991) from Indian Ocean are closely resembles with the *Vulvulina nicobarica* recorded in the present work.

## Bathymetry and Paleoecology

*V. nicobarica* has been recorded from 1253 to 2237m depths at Ninetyeast Ridge (Boltovskoy, 1978a; Nomura, 1991), 1074m at the Broken Ridge (Nomura, 1991) in the Indian Ocean. Gupta (1994) reported *V. nicobarica* from 832m depth in the Red Sea and 4300 to 4600m water depth from Pacific Ocean (Thomas, 1985).

**Distribution at Sites 762B and 763A**

*Vulvulina nicobarica* occurs rarely and sporadically during Late Miocene to Late Pliocene at both the sites 762B and 763A.

Superfamily : VERNEUILINACEA Cushman, 1911  
 Family : VERNEUILINIDAE Cushman, 1911  
 Subfamily : VERNEUILININAE Cushman, 1911  
 Genus : *Gaudryina* d'Orbigny 1839  
 Type species : *Gaudryina rugosa* Cushman, 1911

*Gaudryina solida* Schwager, 1866

Plate 1, Figures 3-4, 14

1866 *Gaudryina solida* Schwager; p. 119, pl. 4, Figures 11a-c  
 1930 *Gaudryina solida*; Mc Donald, p. 68, pl. 1, Figures 11a-c  
 1937 *Gaudryina solida*; Cushman, p. 59, pl. 9, Figures 6-7  
 1941b *Gaudryina solida*; Le Roy, p. 69, pl. 2, Figures 6,7  
 1964 *Gaudryina solida*; Le Roy, p. 18, pl. 1, Figures 28, 29  
 1978a *Gaudryina trinitatensis*; Boltovskoy, p. 160, pl. 4, Figures 10, 11  
 1980 *Gaudryina solida*; Srinivasan and Sharma, p. 15, pl. 2, Figures 1-3  
 2004 *Gaudryina solida*; Rai and Singh, Jour. Geol. Soc. of India, v. 63, p. 419 (list)

**Remarks**

*G. solida* has distinct agglutinated test which is composed of calcareous particles and broken foraminiferal tests (Pl. 1, Figure 14) cemented together. Comparison of *G. solida* with the forms recorded as *Gaudryina trinitatensis* Nuttall from the Late Cenozoic deep sea sections of the northern Indian Ocean (Boltovskoy, 1978a) reveals that both these forms are identical. Therefore *G. trinitatensis* has been included in the synonymy.

**Bathymetry and Paleoecology**

*G. solida* has been reported from lower bathyal depth (1253 m) at Ninetyeast Ridge in the Indian Ocean (Boltovskoy, 1978a). Boersma (1985) recorded this species from Ontong-Java Plateau at 2207 m and Tasman Sea at 1068 to 2131m depths.

**Distribution at Sites 762B and 763A**

*Gaudryina solida* shows common occurrence during Late Miocene to Late Pleistocene at both the sites 762B and 763A.

Superfamily : ATAXOPHRAGMIACEA Schwager, 1877  
 Family : GLOBOTEXTULARIIDAE Cushman, 1927  
 Subfamily : LIEBUSELLINAE Saidova, 1981  
 Genus : *Ruakituria* Kennett, 1967  
 Type species : *Ruakituria pseudorobusta* Kennett, 1967

*Ruakituria magdalidiforme* (Schwager, 1866)

Plate 1, Figure 5

1866 *Ataxophragmium magdalidiforme* Schwager; p. 193, pl. 4, Figures 1a-c

- 1918 *Bulimina magdalidiforme*; Sidebottom, p. 124, pl. 3, Figures 12-15  
 1930 *Ataxophragmium magdalidiforme*; Mc Donald, p. 68, pl. 1, Figures 1a-c  
 1937 *Textulariella magdalidiformis*; Cushman, p. 66, pl. 7, Figures 9, 10  
 1980 *Ruakituria magdalidiforme*; Srinivasan and Sharma, p. 20, pl. 1, Figures 1-10, 15, 23  
 2004 *Ruakituria magdalidiforme*; Rai and Singh, Jour. Geol. Soc. of India, v. 63, p. 420 (list)

### Remarks

*R. magdalidiforme* has a characteristic elongated comma-shaped aperture. Srinivasan and Sharma (1980) considered *R. magdalidiforme* and *R. laceratum* as microspheric and megalospheric forms respectively. The microspheric forms are distinctly larger and subcylindrical with broad, rounded initial end than the megalospheric forms.

### Distribution at Sites 762B and 763A

*R. magdalidiforme* occurs very rarely during Late Pliocene to Middle Pleistocene at site 762B.

- Superfamily : TEXTULARIACEA Ehrenberg, 1838  
 Family : EGGERELLIDAE Cushman, 1937  
 Subfamily : DOROTHIINAE Balakhmatova, 1972  
 Genus : *Dorothia* Plummer, 1931  
 Type species : *Gaudryina bulletta* Carsey, 1926

### *Dorothia brevis* Cushman and Stainforth, 1945

Plate 1, Figure 6

- 1945 *Dorothia brevis* Cushman and Stainforth; p. 18, pl. 2, Figure 5  
 1978a *Dorothia brevis*; Boltovskoy, p. 158, pl. 3, Figure 31  
 1985 *Dorothia brevis*; Kurihara and Kennett, pl. 1, Figure 10  
 2004 *Dorothia brevis*; Rai and Singh, Jour. Geol. Soc. of India, v. 63, p. 418 (list)

### Remarks

*Dorothia brevis* is characterized by initial polyserial stage followed by abruptly expanding biserial stage.

### Bathymetry and Paleoecology

This species has a very wide depth range (~1200 m to 4,500 m) in the Indian Ocean (Boltovskoy, 1978a; Nomura, 1991; Gupta, 1994).

### Distribution at Sites 762B and 763A

*D. brevis* shows rare and sporadic occurrences during Late Miocene to Late Pleistocene at both the sites 762B and 763A.

- Subfamily : EGGERELLINAE Cushman, 1937  
 Genus : *Eggerella* Cushman, 1935  
 Type species : *Verneuilina bradyi* Cushman, 1911

*Eggerella bradyi* (Cushman, 1911)

Plate 1, Figure 7

- 1911 *Verneuilina bradyi* Cushman: p. 54, Figure 87  
 1937 *Eggerella bradyi*; Cushman, p. 52, pl. 15, Figures 19a-b  
 1953 *Eggerella bradyi*; Phleger, Parker and Pierson, p. 27, pl. 5, Figures 8-9  
 1960 *Eggerella bradyi*; Barker, p. 96, pl. 47, Figures 4-7  
 1978a *Eggerella bradyi*; Boltovskoy, p. 158, pl. III, Figure 33  
 1985 *Eggerella bradyi*; Mead, p. 225-226, pl. 1, Figures 1a-b  
 1989 *Eggerella bradyi*; Hermelin, p. 32, pl. 2, Figures 1-2  
 1991 *Eggerella bradyi*; Nomura, p. 55, pl. 1, Figures 12a-b  
 1992 *Eggerella bradyi*; Mackensen, p. 668, pl. 1, Figures 1-2  
 1994 *Eggerella bradyi*; Gupta, p. 362, pl. 1, Figure 2  
 1997 *Eggerella bradyi*; Bornmalm, p. 23, Figures 13E-F  
 2005 *Eggerella bradyi*; Hess and Kuhnt, Mar. Micropal., v. 54, text Figure 5a

### Remarks

The test of *Eggerella bradyi* is finely agglutinated which is composed of calcareous particles cemented together. *E. bradyi* shows considerable variation in its height: width ratio. Both, highly conical and more cylindrical forms of this species are recorded in the present work.

### Bathymetry and Paleoecology

*E. bradyi* has wide geographic distribution and it has been reported from the all bathyal and abyssal depths of the world's oceans. Mead (1985) recorded a regular increase in the relative abundance of this species with depth between 1493 m to 3122 m in the southeast Atlantic. Nomura (1991) reported *E. bradyi* from lower bathyal depths at the Broken Ridge and Ninetyeast Ridge in the Indian Ocean. Gupta (1994) found *E. bradyi* from lower bathyal (1623 m) to lower abyssal (5082 m) depths in the Indian Ocean. In the southeast India Ocean *E. bradyi* is reported between 2500 and 4500 m depths (Corliss, 1979a). This species shows highest relative abundance during interglacial episodes (Schnitker, 1984). Peterson (1984) found a close association of this species with the Indian Deep Water (IDW). *E. bradyi* has very high abundance in deeper water especially below 3500 m in the South China Sea (Jian and Wang, 1997). In the Somali basin *E. bradyi* found to associated with degraded organic matter (Gupta, 1997).

### Distribution at Sites 762B and 763A

*E. bradyi* occurs commonly and almost continuously throughout the studied section from Late Miocene to Late Pleistocene at both the sites 762B and 763A.

Genus : *Karriella* Cushman, 1933  
 Type species : *Gaudryina siphonella* Reuss, 1851

*Karriella baccata* (Schwager, 1866)

Plate 1, Figure 8

- 1866 *Gaudryina baccata* Schwager; p. 200, pl. 4, Figures 12a-b  
 1884 *Gaudryina baccata*; Brady, p. 379, pl. 46, Figures 8-11 (in part)  
 1930 *Gaudryina baccata*; Mc Donald, p. 68, pl. 1, Figures 12a-b  
 1937 *Karriella baccata*; Cushman, p. 133, pl. 15, Figures 20, 22-24 (not Figure 21)  
 1980 *Karriella baccata*; Srinivasan and Sharma, p. 17, pl. 2, Figures 12, 19  
 1994 *Karriella baccata*; Gupta, p. 364, pl. 1, Figures 3

## Remarks

The test of *K. baccata* shows considerable variation in its twisting along the axis. According to Srinivasan (in Srinivasan and Sharma, 1980), the forms referred to *baccata* by Brady (1884) from the southwest Ireland are identical to Schwager's species.

## Bathymetry and Paleoecology

*K. baccata* is comparatively a deep water species (Brady, 1884). Gupta (1994) reported this species in a wide depth range from lower bathyal (1623 m) to lower abyssal (4054 m) depths in the Indian Ocean. *K. baccata* has been also recorded by Boersma (1985) from the Ontong-Java Plateau (2207 m), Tasman Sea (1299 m) and Chatham Rise (1209 m).

## Distribution at Sites 762B and 763A

*K. baccata* is a very rare species which occurs during Late Miocene to Late Pliocene at site 762B and Late Miocene to Middle Pleistocene at site 763A.

*Karreriella bradyi* (Cushman, 1911)

Plate 1, Figures 9-10

- 1911 *Gaudryina bradyi* Cushman; p. 67, text-Figure 107
- 1937 *Karreriella bradyi*; Cushman, p. 135, pl. 16, Figures 6-11
- 1945 *Karreriella bradyi*; Cushman and Todd, p. 8, pl. 1, Figure 20
- 1949 *Karreriella bradyi*; Bermudez, Cushman Lab. Foram. Res., Spec. Publ., no. 24, p. 89 pl. 5, Figures 11-16
- 1960 *Karreriella bradyi*; Barker, p. 94, pl 46, Figures 1- 4
- 1978a *Karreriella bradyi*; Boltovskoy, p. 162, pl. IV, Figures 28, 29
- 1979 *Karreriella bradyi*; Corliss, p. 5, pl. 1, Figures 5-6
- 1985 *Karreriella bradyi*; Hermelin and Scott, p. 212, pl. 1, Figure 8
- 1989 *Karreriella bradyi*; Hermelin, p. 33.
- 1991 *Karreriella bradyi*; Nomura, p. 55, pl. 1, Figures 13a-c
- 1992 *Karreriella bradyi*; Mackensen, p. 668, pl. 1, Figures 11-12
- 1995 *Karreriella bradyi*; Nomura, pl. 2, Figure. 40, pl. 3, Figures 11a-b, 12a-b
- 1997 *Karreriella bradyi*; Bornmalm, p. 24, Figure 13 G

## Remarks

*Karreriella bradyi* has finely agglutinated test which is composed of calcareous particles cemented together. The specimens encountered in the present work are identical to the forms described as *K. bradyi* from northern Indian Ocean (Boltovskoy, 1978a) and eastern Indian Ocean (Nomura, 1991).

## Bathymetry and Paleoecology

*K. bradyi* is an almost cosmopolitan species with a wide depth range from lower neritic zone to abyssal zone (Brady, 1884; Pflum and Frerichs, 1976). Miao and Thunell (1993) recorded *K. bradyi* midway between the lysocline (3,200 m) and CCD (3,800 m) in the South China Sea.

## Distribution at Sites 762B and 763A

*K. bradyi* frequently occurs throughout the studied section from Late Miocene to Late Pleistocene at both the sites 762B and 763A.

*Karreriella subrotundata* (Schwager), 1866  
Plate 1, Figure 11

- 1866 *Gaudryina subrotundata* Schwager; p. 198, pt. 4, Figures 9a-c  
1930 *Gaudryina subrotundata*: Mc Donald, p. 68, pl. 1, Figures 9a-c  
1937 *Dorothia* (?) *subrotundata*; Cushman, p. 94, pl. 10, Figure 15  
1980 *Karreriella subrotundata*; Srinivasan and Sharma, p. 17, pl. 2, Figures 11, 18

### Remarks

*K. subrotundata* differs from *K. bradyi* in possessing rounded aperture on slender neck. The specimens of present investigation are found to be identical to the forms figured and described as *K. subrotundata* by Boltovskoy, (1978a) from northern Indian Ocean and Srinivasan and Sharma (1980) from Andman Nicobar Island.

### Bathymetry and Paleoecology

The characteristic elongate and tapered test of *K. subrotundata* broadly reveals an infaunal microhabitat preference (Gooday, 1994).

### Distribution at Sites 762B and 763A

*K. subrotundata* occurs sporadically during Late Miocene to Late Pliocene at site 762B and Late Miocene to Middle Pleistocene at site 763A.

### Distribution at Sites 762B and 763A

Late Miocene to Middle Pleistocene.

- Genus : *Martinottiella* Cushman, 1933  
Type species : *Clavulina communis* d'Orbigny, 1826

*Martinottiella communis* (d'Orbigny, 1826)  
Plate 1, Figures 12-13

- 1826 *Clavulina communis* d'Orbigny: p. 196, pl. 12, Figures 1, 2  
1884 *Clavulina communis*; Brady, p. 394-395, pl. 48, Figures 1-13  
1937b *Martinottiella communis*; Cushman, p. 148, pl. 17, Figures 4-9  
1960 *Martinottiella communis*; Barker, p. 98, pl. 48 Figures 3, 4, 6-8  
1980 *Martinottiella communis*; Ingel, Jr. et al. p. 140, pl. 4, Figures 14, 15  
1986 *Martinottiella communis*; Belanger and Berggren, p. 331, pl. 1, Figures 3, 4  
1989 *Martinottiella communis*; Hermelin, p. 34, pl. 2, Figures 5-6  
1997 *Martinottiella communis*; Bornmalm, p. 25, pl. 1, Figure 13H  
2005 *Martinottiella communis*; Murgese and Deckker, Mar. Microp., v. 56, p. 46 (list)

### Remark

In the present work encountered species shows aperture a small round opening on a neck at the centre of the ultimate chamber.

### Bathymetry and Paleoecology

Gupta (1994) reported *M. communis* from the upper abyssal depth (2262 m) at Ninetyeast Ridge in the Indian Ocean. Thompson (1980) found this species from 3300 m to 6000 m in the Japan Trench area. Boersma (1985) recorded *M. communis* from lower bathyal depths (1068-1391 m) in the Tasman Sea and Chatham Rise. This species has also been recorded at lower bathyal depth in the eastern South Atlantic Ocean (Schmiel et al., 1997). Hayward et al (2001, 2003) reported this species from shallower depth (300m) in the New Zealand Sea.

### Distribution at Sites 762B and 763A

*M. communis* occurs almost continuously from Late Miocene to Late Pleistocene at both the sites 762B and 763A.

*Martinottiella scabra* (Cushman, 1936)  
Plate 2, Figures 1, 9

- 1936 *Pseudoclavulina scabra* Cushman: p. 20, pl. 3, Figure 11  
1978a *Martinottiella scabra*; Boltovskoy, Marine Geology, vol. 26, p. 162, pl. IV, Figures 34, 35  
2004 *Martinottiella scabra*; Rai and Singh, Jour. Geol. Soc. of India, v. 63, p. 420 (list)

### Remarks

This species is characterized by coarsely agglutinated test, comprising mainly of broken foraminiferal tests (Pl. 2, Figure 9). Examined specimens are identical to those figured by Boltovskoy (1978a) as *Martinottiella scabra* from the northern Indian Ocean deep sea cores.

### Bathymetry and Paleoecology

This species occurs in a wide depth range (1074m to 3010m) in the Indian Ocean. (Boltovskoy, 1978a; Nomura, 1991).

### Distribution at Sites 762B and 763A

*M. scabra* shows rare and sporadic occurrences during Late Miocene to Late Pliocene at both the sites 762B and 763A.

- Family : TEXTULARIIDAE Ehrenberg, 1838  
Subfamily : TEXTULARIINAE Ehrenberg, 1838  
Genus : *Textularia* DeFrance, 1824  
Type species : *Textularia sagittula*, DeFrance, 1824

*Textularia agglutinans* d'Orbigny, 1839  
Plate 2, Figures 2, 8

- 1839 *Textularia agglutinans* d'Orbigny: p. 144, pl. 1, Figures 17, 18  
1884 *Textularia agglutinans*; Brady, p. 363, pl. 43, Figures 1-3  
1960 *Textularia agglutinans*; Barker, p. 88, pl. 43 Figures 1-3  
1985 *Textularia agglutinans*; Boersma, pl. 10, Figures 3-4  
2005 *Textularia agglutinans*; Murgese and Deckker, Maine Micropaleontology, v. 56, p. 46 (list)

**Remarks**

Specimens are similar to form recorded and figured as *Textularia agglutinans* by Gupta (1994).

**Bathymetry and Paleoecology**

Gupta (1994) reported *T. agglutinans* from upper middle bathyal (832m) to lower bathyal (1795m) depths in the Red Sea and from lower bathyal (3030m) to abyssal (5082m) depths in the Indian Ocean. This species has also been reported by Jian et al. (1999) at 1556 m depth in the South China Sea. Boersma (1985) reported this species from lower bathyal depths in the Coral Sea, Tasman Sea and Chatham Rise. Murgese and Deckker (2005) also reported this species in the eastern Indian Ocean from lower bathyal depth.

**Distribution at Sites 762B and 763A**

This species shows very rare and sporadic occurrence during Pliocene at site 762B and Late Miocene to Late Pleistocene at site 763A.

*Textularia halkyardi* Lalicker, 1935

Plate 2, Figure 3

1935 *Textularia halkyardi* Lalicker: p. 45, pl. 7, Figure 5.

1978a *Textularia halkyardi*; Boltovskoy, p. 170, pl. VII, Figures 47-48

2004 *Textularia halkyardi*; Rai and Singh, Jour. Geol. Soc. of India, v. 63 p. 420 (list)

**Remarks**

Specimens of *T. halkyardi* recorded in the present work are identical to those figured as *T. halkyardi* by Boltovskoy (1978a) from the northern Indian Ocean.

**Bathymetry and Paleoecology**

*T. halkyardi* has been recorded from lower bathyal depths (1200m to 2000m) at the Ninetyeast Ridge in the Indian Ocean Boltovskoy (1978a). Nomura (1991) also reported this species from lower bathyal (1074 m) depth at the Broken Ridge, eastern Indian Ocean.

**Distribution at Sites 762B and 763A**

This species shows infrequent and low occurrences during Late Miocene to Middle Pleistocene at both the sites 762B and 763A.

*Textularia lythostrota* (Schwager, 1866)

Plate 2, Figures 4, 10

1866 *Placanium lythostrotum* Schwager; p. 194, pl. 4, Figures 4a-c

1930 *Placanium lythostrotum*; Mc Donald, p. 68, pl. 1, Figures 4a-c

1934 *Textularia* cf. *lythostrotum*; Cushman, p. 105, pl. 10, Figures 3

1940 *Textularia lythostrotum*; Coryell and Rivero, p. 324, pl. 41, Figures 3

1964 *Textularia lythostrota*; Le Roy p. 17, pl. 16, Figure 1b

1980 *Textularia lythostrota*; Srinivasan and Sharma, p. 13, pl. 1, Figures 19-21

1985 *Textularia lythostrota*; Boersma, p. 990, pl. 3, Figures 8-9

- 1994 *Textularia lythostrota*; Gupta, p. 366, pl. 1, Figures 4, 15  
 2005 *Textularia lythostrota*; Murgese and Deckker, Mar. Micropal., v. 56, p. 46 (list)

### Remarks

This species has characteristic pentagonal shape and coarsely agglutinated test which is composed of fragments of foraminiferal test (Pl. 2, Figure 10).

### Bathymetry and Paleoecology

Gupta (1994) recorded *T. lythostrota* from lower bathyal (1623-1764m) and abyssal (5082m) depths in the Indian Ocean. This species has also been reported from lower bathyal (1299m) to upper abyssal (2131m) depths in the Tasman Sea (Boersma, 1985).

### Distribution at Sites 762B and 763A

*T. lythostrota* is characterized by common and frequent occurrences during Late Miocene to Late Pleistocene at both the sites 762B and 763A.

- Subfamily : SIPHOTEXTULARIINAE Loeblich and Tappan, 1985  
 Genus : *Siphotextularia* Finlay, 1939  
 Type species : *Siphotextularia wairoana* Finlay, 1939

*Siphotextularia rolshauseni* Phleger and Parker, 1951  
 Plate 2, Figures 5, 11

- 1951 *Siphotextularia rolshauseni* Phleger and Parker: p. 4, pl. 1, Figures 23, 24  
 1953 *Siphotextularia rolshauseni*; Phleger, Parker and Pierson, p. 26, pl. 5, Figure 7  
 1971 *Siphotextularia rolshauseni*; Schnitker, p. 210, pl. 1, Figures 15a-b  
 1978a *Siphotextularia rolshauseni*; Boltovskoy, p. 169, pl. VII, Figure 10  
 1981 *Siphotextularia rolshauseni*; Cole, p. 36, pl. 5, Figure 7  
 1986 *Siphotextularia rolshauseni*; Kurihara and Kennett, pl. 1: 3  
 1999 *Siphotextularia rolshauseni*; Kuhnt, Hess and Jian, p. 141 pl. 2 Figure 1  
 2001 *Siphotextularia rolshauseni*; Hayward, Carter, Grenfell and Hayward, J., New Zealand Journal of Geology and Geophysics, v. 44, Figures 14H-I  
 2003 *Siphotextularia rolshauseni*; Hayward, Grenfell, Sabaa and Hayward, J., New Zealand Journal of Geology and Geophysics, v. 46, Figure 4A  
 2004 *Siphotextularia rolshauseni*; Rai and Singh, Jour. Geol. Soc. of India, v. 63, p. 420 (list)

### Remarks

This species is characterized by distinctly agglutinated test and rounded aperture produced on a tubular neck (Pl. 2, Figure 11).

### Bathymetry and Paleoecology

Boltovskoy (1978a) recorded this species from lower bathyal (1253m) to lower abyssal (3010m) depths at the Ninetyeast Ridge in the northern India Ocean. Corliss (1979a) reported this species from 2500 to 4600m in the southeast Indian Ocean. Jian et al., (1999) found this species at 1556m depth in the South China Sea. *S. rolshauseni* has a bathymetric range from the lower middle bathyal to abyssal depths in the Gulf of Mexico (Pflum and Frerichs, 1976). *S. rolshauseni* is a characteristic

indicator species for low organic carbon flux rates during the Last Glacial Maximum (LGM) in the Norwegian Greenland Sea (Nees and Struck, 1994).

#### Distribution at Sites 762B and 763A

This species has been frequently recorded from Late Miocene to Late Pleistocene section at sites 762B and 763A.

*Siphotextularia solita* (Schwager, 1866)

Plate 2, Figures 6, 7

1866 *Placanium solitum* Schwager: p. 195, pl. 4, Figures 6a-c

1930 *Placanium solitum*; p. 68, pl. 1, Figures 6a

1934 *Textularia solita*; Cushman, p. 104, pl. 10, Figures 2a-b

1980 *Siphotextularia solita*; Srinivasan and Sharma, p. 14, pl. 2, Figures 9, 10, 15

#### Remarks

The encountered specimens are identical to the form reported and figured as *Siphotextularia solita* by Srinivasan and Sharma (1980).

#### Bathymetry and Paleoecology

Gupta (1994) reported this species from lower bathyal (1623m) to lower abyssal (3633m) depths in the Indian Ocean. *S. solita* has also been recorded from lower bathyal depths (1000-2000m) in the Coral Sea, Tasman Sea and Chatham Rise (Boersma, 1985).

#### Distribution at Sites 762B and 763A

This species has been frequently recorded during Late Miocene to Late Pleistocene section at both the sites 762B and 763A.

### 5. Conclusion

Deep-sea sediments of the Exmouth Plateau in the Eastern Indian Ocean are represented by well preserved agglutinated benthic foraminifera. The depth range of the most of the recorded agglutinated benthic foraminifera suggests lower bathyal to abyssal deep sea environments.

### Acknowledgements

We thank ODP for providing samples. We also thank Dr. Devesh K. Sinha for their help in SEM. This work was supported by grants of Council of Scientific and Industrial Research, Government of India [No. 24(0231/96/EMR-II)].

### References

Barker, R.W. *Taxonomic Notes on the Species Figured by H.B. Brady in His Report on the Foraminifera Dredged by H.M.S. Challenger During the Years 1873-1876*. Society of Economic Paleontologists and Mineralogists Special Publication. 1960. 9; 1-238.

Berggren, W.A., Benson, R.H., Haq, B.U., Riedel, W.R. Sanfilippo, A., Schrader, H.J., and Tjalsma, R.C. *The El Cuervo Section (Andalusia Spain). Micropaleontologic Anatomy of an Early Late Miocene Lower Bathyal Deposit*. Marine Micropaleontology. 1976. 1; 195-241.

- Boersma, A., 1985: *Biostratigraphy and Biogeography of Tertiary Bathyal Benthic Foraminifers: Tasman Sea, Coral Sea and on the Chatham Rise (Deep Sea Drilling Project, Leg 90)*. In: Initial Reports of the Deep Sea Drilling Project. Kennett, J.P., von der Borch, C.C., et al. (Eds.). 90; 961-1036.
- Boltovskoy, E. *Late Cenozoic Benthonic Foraminifera of the Ninetyeast Ridge (Indian Ocean)*. Marine Geology. 1978a. 26; 139-175.
- Boltovskoy, E., and Wright, R., 1976: *Recent Foraminifera*. Junk, The Hague. 515.
- Boltovskoy, E. *Studio biostratigraphico y paleontologico (foraminiferos bentonicos) del Cenozoico superior al este de las Islas Malvinas (DSDP, Crucero 36, Sitios 327 y 329) mus. Argentino Cienc Nat. Rev. Geo. 1978b. 8 (2) 19-70.*
- Bornmalm, L. *Taxonomy and Paleocology of Late Neogenr Benthic Foraminifera from the Caribbean Sea and Eastern Equatorial Pacific Ocean*. Fossil and Strata. 1997. 96.
- Brady, H.B. *Report on the Foraminifera Dredged by HMS Challenger, During the Years 1873-1876. Report of Scientific Results of the Exploration Voyage of HMS Challenger*. Zoology. 1884. 9; 1-814.
- Corliss, B.H. *Taxonomy of Recent Deep-Sea Benthonic foraminifera from the Southeast Indian Ocean*. Micropaleontology. 1979. 25; 1-19.
- Douglas, R.G., and Woodruff, F., 1981: *Deep-sea Benthic Foraminifera*. In: The Oceanic Lithosphere in the Sea. Emiliani, C. (Ed.). Wiley, New York, N.Y. 1233-1327.
- Gooday, A.J. *The Biology of Deep-Sea Foraminifera: A Review of Some Advances and Their Applications in Paleoceanography*. Palaios. 1994. 9; 14-31.
- Gooday, A.J., Levin, L.A., Linke, P., and Heeger, T., 1992: *The Role of Benthic Foraminifera in Deep Sea Food Webs and Carbon Cycling*. In: Deep Sea Food Chains and the Global Carbon Cycle. Rowe, G.T. and Pariente, V. (Eds). Kluwer, Dordrecht. 63-91.
- Gupta, A.K., and Srinivasan, M.S. *Uvigerina Proboscidea Abundances and Paleoceanography of the Northern Indian Ocean DSDP Site 214 during the Late Neogene*. Marine Micropaleontology. 1992. 19; 355-367.
- Gupta, A.K., and Srinivasan M.S. *Quaternary Bottom Water Circulation and Benthic Foraminiferal Changes in the Northern Indian Ocean*. Indian Journal of Geology. 1990b. 16; 351-367.
- Gupta, A.K. *Taxonomy and Bathymetric Distribution of Holocene Deep-Sea Benthic Foraminifera in the Indian Ocean and the Red Sea*. Micropaleontology. 1994. 40 (4) 351-367.
- Hayward, B.W., Carter, R., Grenfell, H.R. and Hayward, J.J. *Depth Distribution of Recent Deep-Sea Benthic Foraminifera East of New Zealand, and their Potential for Improving Paleobathymetric Assessments of Neogene Microfaunas*. N.Z. J. Geol. Geophys. 2001. 44; 555-587.
- Hayward, B.W., Grenfell, H.R., Sabaa, A., and Hayward, J.J. *Recent Deep-Sea Benthic Foraminifera from Offshore Taranaki, New Zealand*. N.Z. J. Geol. Geophys. 2003. 46; 489-518.

- Hermelin, J.O.R. *Pliocene Benthic Foraminifera from the Ontong-Java Plateau (Western Equatorial Pacific Ocean)*. Faunal Response to the Changing Paleoenvironment. Cushman Foundation for Foraminiferal Research, Special Publication. 1989. 26; 3-143.
- Imbrie, J., and Kipp, N., 1971: *A New Micropaleontological Method for Quantitative Paleoclimatology: Application to a Late Pleistocene Caribbean core*. In: The Late Cenozoic Glacial Ages. Turekian, K.K. (Ed.). Yale University Press. 71-181.
- Jian, Z., Wang, L., Kienast, M., Sarnthein, M., Kuhnt, W., Lin, H. and Wang, P. *Benthic Foraminiferal Paleoceanography of the South China Sea over the Last 40,000 Years*. Marine Geology. 1999. 156; 159-186.
- Jian, Z., and Wang, L. *Late Quaternary Benthic Foraminifera and Deep-Water Paleoceanography in the South China Sea*. Marine Micropaleontology. 1997. 32; 127-154.
- Jian, Z., Wang, L., Kienast, M., Sarnthein, M., Kuhnt, W. and Wang, P. *Benthic Foraminiferal Paleoceanography of the South China Sea over the Last 40,000 years*. Marine Geology. 1999. 156; 159-186.
- Kaiho, K. *Global Climatic Forcing of Deep-Sea Benthic Foraminiferal Test Size during the Past*. Geology. 1998. 26; 491-494.
- Loeblich, A.R.JR., and Tappan, H., 1964: *Sarcodina, Chiefly "Thecamoebians" and Foraminifera*. Treatise on Invertebrate Paleontology, Protista 2, Part C. In: R.C. Moore (Ed.) Kansas University Press, USA. 900.
- Loeblich, A.R.JR. and Tappan, H., 1987: *Foraminiferal Genera and Their Classification*. Van Nostrand Reinhold Company, New York. 970.
- Mead, G.A. *Recent Benthic Foraminifera in the Polar Front Region of the Southwest Atlantic*. Micropaleontology. 1985. 3; 211-248.
- Miao, Q., and Thunell, R. *Recent Deep-Sea Benthic Foraminiferal Distributions in the South China and Sulu Seas*. Marine Micropaleontology. 1993. 22; 1-32.
- Miao, Q., and Thunell, R.C. *Recent Deep-Sea Benthic Foraminiferal Distributions in the South China and Sulu Seas*. Marine Micropaleontology. 1993. 22; 1-32.
- Murgese, S.D., and Deckker, P.D. *The Distribution of Deep-Sea Benthic Foraminifera in Core Tops from the Eastern Indian Ocean*. Marine Micropaleontology. 2005. 56; 25-49.
- Nees, S., and Struck, U. *The Biostratigraphic and Paleoceanographic Significance of Siphotextularia Rolshauseni Phleger and Parker in Greenland Sea Sediments*. Journal of Foraminiferal Research. 1994. 244; 233-240.
- Nomura, R. *Oligocene to Pleistocene benthic foraminifer assemblages at sites 754 and 756, eastern Indian Ocean*. Proc. Ocean Drilling Program, Sci. Results. 1991. 121; 31-76.
- Nomura, R. *Paleogene to Neogene Deep-Sea Paleoceanography in the Eastern Indian Ocean: Benthic Foraminifera from ODP Sites 747, 757 and 758*. Micropaleontology. 1995. 41 (3) 251-290.

- Peterson, L.C. *Recent Abyssal Benthic Foraminiferal Biofacies of the Eastern Equatorial Indian Ocean*. Marine Micropaleontology. 1984. 8; 479-519.
- Pflum, C.E., and Frerichs, W.E. *Gulf of Mexico Deep-Water Foraminifera*. Cushman Foundation for Foraminiferal Research, Special Publication. 1976. 14; 1-125.
- Powell, T.G. *An Assessment of Hydrocarbon Source Rock Potential of the Canadian Arctic Island*. Geological Survey of Canada. 1978. 78-12.
- Rai, A.K., and Singh, V.B. *Late Neogene Deep Sea Benthic Foraminiferal Biostratigraphy of ODP Site 762B and 763A (Exmouth Plateau), Eastern Indian Ocean*. Journal of Geological Society of India. 2004. 63; 415-429.
- Rai, A.K., and Srinivasan, M.S. *Deep Sea Benthic Foraminiferal Response to the Pliocene Palaeoenvironments of the Northern Indian Ocean*. Geobios. 2000. 33 (3) 301-308.
- Rathburn, A.E., Corliss, B.H., Tappa, K.D., and Lohmann, K.C. *Comparisons of the Ecology and Stable Isotopic Compositions of Living (Stained) Benthic Foraminifera from the Sulu Sea and South China Sea*. Deep Sea Research I. 1996. 43; 1617-1646.
- Schmiedl, G., Mackensen, A., and MULLER, P.J. *Recent Benthic Foraminifera from the Eastern South Atlantic Ocean: Dependence on Food Supply and Water Masses*. Marine Micropaleontology. 1997. 32; 249-287.
- Srinivasan, M.S., and Sharma, V., 1980: *Schwager's Car Nicobar Foraminifera in the Reports of the Novora Expedition-A Revision*. Today and Tomorrow's Printers and Publishers, New Delhi. 83.
- Thomas, E. *Late Eocene to Recent Deep-Sea Benthic Foraminifera from the Central Equatorial Pacific Ocean*. Init. Rep. DSDP. 1985. 94; 997-1031.
- Tjalsma, R.C., and Lohman, G.P. *Paleocene-Eocene Bathyal and Abyssal Benthic Foraminifera from the Atlantic Ocean*. Micropaleontology Special Publication. 1983. 4 (I-iii) 1-90.
- Veevers, J., and Cotterill, D. *Western Margin of Australia: Evolution of a Rifted Arch System*. Geological Society of America Bulletin. 1978. 337-355.
- Veevers, J.M., 1984: *Morphotectonics of the Divergent or Rifted Margins, in Phanerozoic Earth*. History of Australia, Clarendon, Oxford. 168-210.
- Wells, P., Wells, G., Cali, J., and Chivas, A. *Response of Deep-Sea Benthic Foraminifera to Late Quaternary Climate Changes, Southeast Indian Ocean, Offshore Western Australia*. Marine Micropaleontology. 1994. 23; 185-229.

# Landslide Sensitivity Assessment of Existing Twin Tunnels: A Case Study of National Highway-76 between Udaipur - Pindwara, Rajasthan, India

Bhardwaj Govind Singh<sup>1</sup>, Mehta Mayank<sup>1</sup>, Md Yeasin Ahmed<sup>2</sup> and Robert Evans<sup>2</sup>

<sup>1</sup>Department of Mining Engineering, CTAE, MPUAT, Udaipur, Rajasthan, India

<sup>2</sup>School of Engineering, Department of Civil and Construction Engineering, Centre for Sustainable Infrastructure, Swinburne University of Technology, Australia

Correspondence should be addressed to G.S. Bhardwaj, bhardwaj\_gs@rediffmail.com

Publication Date: 20 November 2014

Article Link: <http://scientific.cloud-journals.com/index.php/IJAESE/article/view/Sci-253>



Copyright © 2014 Bhardwaj Govind Singh, Mehta Mayank, Md Yeasin Ahmed and Robert Evans. This is an open access article distributed under the **Creative Commons Attribution License**, which permits unrestricted use, distribution, and reproduction in any medium, provided the original work is properly cited.

**Abstract** Highways motorway tunnel failure is a major problem in rocky mountainous regions. Modes of failures are in various ways includes failures of cut hills close proximity to the tunnel crown, along the longer axis, internal part of the tunnel and collapse of the civil construction structure. To ensure their continued safe operation as well as appropriate repair and improvement works, a wide range of investigations has been carried out to confirm the conditions of tunnels and establish the causes and extent of deterioration and damage. The geometry of the slope surface, material profile & their spatial distribution, material properties viz. geo-mechanical, structural, phreatic surface, and local climatic conditions are the primary causes. The earthquake force, distributed load and vehicle induced forces acting upon the tunnel area aggravates the failure. Tunnel stability status analysis and data interpretation from the tunnel area helps in predictive assessment of probable modes of failure. Looking to the frequency of failures in the cut hills of adjoining part of the tunnels and traffic blockade, a study has been carried out on twin tunnels of national highway number 76 between Udaipur-Pindwara, Rajasthan India. The twin tunnel road passage is part of the folded Aravalli mountain chain.

**Keywords** *Aravalli Mountain; Factor of Safety; Failure Surfaces; Four-Lane Road*

## 1. Introduction

Tunnels are essential part of highways development & strengthening in hilly area, which leads to economic growth, connects people, provides speedy and safe travel. It reduces the gradient of the road, and to preserve the visual line of the hills and provide crossing points for wildlife ([en.wikipedia.org/wiki/Engelberg\\_Tunnel](http://en.wikipedia.org/wiki/Engelberg_Tunnel)). National Highway number 76 from Udaipur to Pindwara (Longitude 72° 43' (E) & latitude 24° 35' (N) and 73° 3' (E) latitude 24° 47' (N) longitude) envisages 4-lanning of the existing single roads (Figure 1). The 4-lanning improvement work extends to all

components of the road namely, pavements, bridges, drains, structures within right-of-way, improvement of the road geometry and construction of twin tunnels. The road passes through hilly areas, reserve dense mixed forest, steep slopes and nearly flat stony scrubland. The ground elevation varies from 212 metres above mean sea level (MSL) at Amirgarh to 907 metres above MSL at Jaswantgarh. Annual average rainfall at these locations ranges from 1020 mm to 596 mm (at Udaipur) average maximum temperature varies from 37.8°C to 41.2°C with the average minimum being between 3.4°C and 9.3°C. The 35 km road passage between Jaswantgarh to Bekaria is prone to landslides and rock fall. Due to landslides and rock-fall several times the twin tunnel have been blocked/closed temporarily for clearing of the fallen soil, debris and boulders. It became inconveniences in vehicular movement through the tunnels and causes fatal accidents repeatedly. The twin motor way tunnels 1 and 2 have been studied in details to assess the sensitivity of failure.

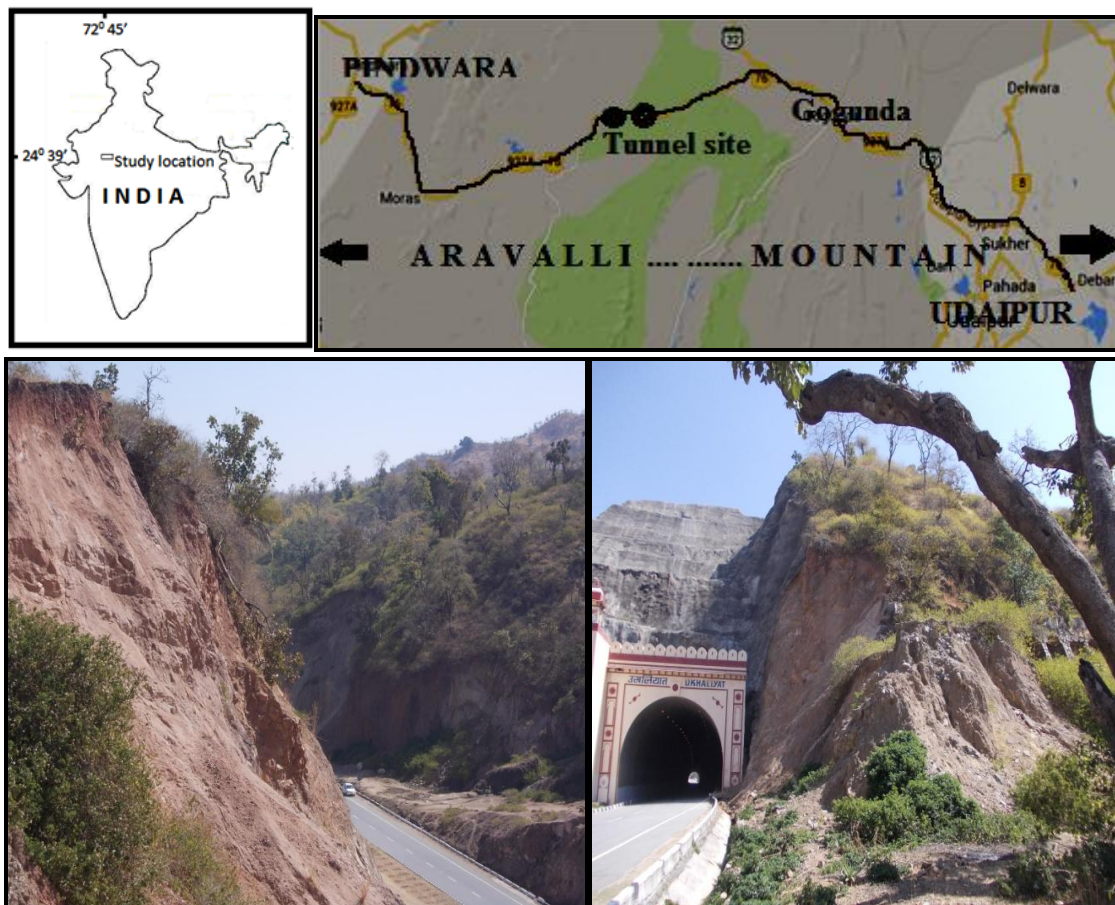


**Figure 1:** Showing Location of Tunnel and Photographs Envisaging the Seriousness of the Problem

Effective risk management requires in the case of twin tunnels area landslide & assessment of inherently uncertain events and circumstances, typically addressing how likely the uncertainty is to occur, and what the effect would be if it happened. The credibility and value of the risk process is enhanced if data are collected with care and using proper tools to assess (David A. Hillson et al., 2004). The estimation of the long-term probability occurrence of landslides based on the derived distribution technique, where the statistical behavior of the rainfall process and material property and slope parameters considered for establishing relation with Factor of Safety (Estefania Munoz et al., 2012). Robin G. McInnes et al., 2002 published their findings on ground instability problems and stressed upon the importance of implementation of management strategies and integrating the research in to strategic planning. Numerous slopes are affected by small movements related to the progressive failure of rock slopes induced by weathering and water pressure in the structural planars. Prevention and mitigation of landslide hazards requires establishing (O.J. Lateltin, 2002). Importance

of such studies has been realized by the facts that the number and extent of roads will expand dramatically this century. Globally, at least 25 million kilometres of new roads are anticipated by 2050; a 60% increase in the total length of roads over that in 2010. Nine-tenths of all road construction is expected to occur in developing nations (Stephen G. et al., 2014). Roads can promote social and economic development and at the same time, they also open a Pandora's Box of environmental problems (William F. Laurance et al., 2014).

## 2. Materials and Method

### 2.1. About the Twin Tunnels

Within a span of five kilometers, the tunnels are excavated in the hills which comprises structurally complex geological formations comprises soil, phyllite and quartzites of highly weathered, Jointed and Folded nature (Figure 2). The particulars of twin tunnels are given in Table 1.

*Table 1: Particulars of the Tunnels*

Name of the Twin Tunnel/ Milestone Location Udaipur- Pindwara Road Passage NH27 India	Length (m)	Dia. (m)	Rock Mass in Which it is Constructed	Technical Details
Tunnel-1 (Ukhliyat) Km60.690-Km61.060	370	9.83	Fair to poor	Thin Soil layer as uppermost hill rock mass material, phyllite below the soil and quartzite as intercalations within phyllite and soil. Intense weathered
Tunnel-2 (Khokharianal) Km65.510-Km65.710	200	9.83	Fair to poor	Thick Soil profile as uppermost material, phyllite below the soil and quartzite as intercalations within phyllite and soil. Intense weathered

It is constructed in phase: E-W corridor package 1, Unidirectional travel tunnel, Year of construction: April 2005; Services by SNC Lavalin, Canada International Inc. & Sheladia Associates India Pvt Ltd, Ahmedabad, India.

### 2.2. Description of Twin Tunnels Area

The upper hill load height is 85 meters maximum. The engineering design is proper but at some places its modifications are desired. The hill cuts on either side of the tunnel entry-exit are not treated in proper way, road cut hills on either side are sliding on the road. The phreatic surface is above the floor of the tunnels & piezometric surface is erratic, at some of the points it is 1 to 2 meters higher than the natural ground levels. The reason could be joints planes i.e. joint spacing is 0.10 to 2.8 meters, closely spaced and persistence is 12 to 15 meters maximum. Watery conditions of tunnels in tunnel-1 are more serious as compared to tunnel-2. This factor is added to the failure (Figure 2).

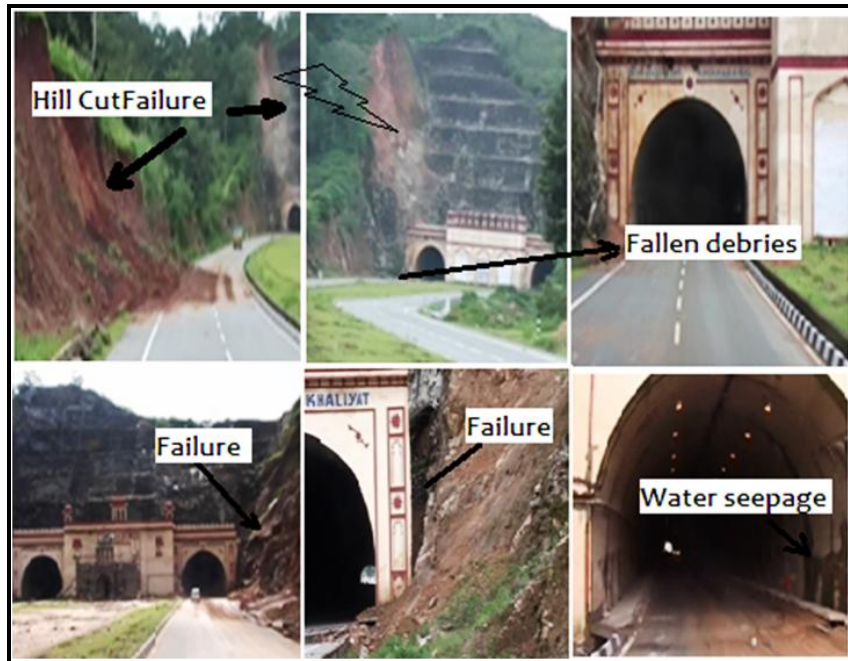


**Figure 2:** Photographs Showing Sensitive Tunnel Side Failures

The location of tunnels is shown in digital elevation model, part of the Aravalli Mountain traversing by the four lane road, generated with GIS software (Figure 3).

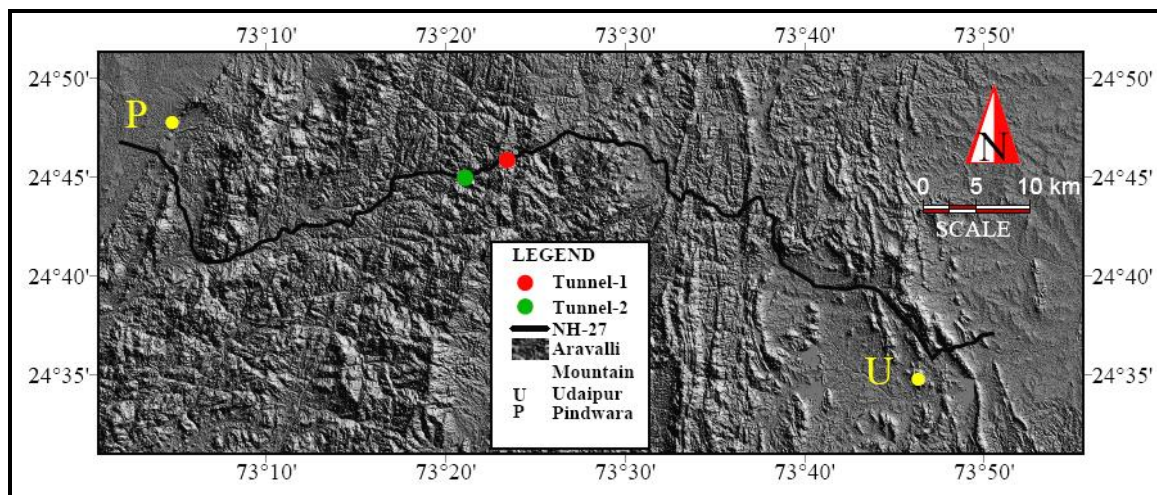


**Figure 3:** DEM of Aravalli Mountain Showing Tunnels

### 2.3. Material Properties of the Tunnel Area

Mainly three types of material constituting the tunnel area hill i.e. soil, phyllites and quartzite. The cohesion, phi and unit weight properties of the material ranges from 90-240, 27-36 and 18-21 respectively. The values obtained by the laboratory testing, further matched with the software data file available with the Manual of Galena Slope stability software version 4.0 (Table 2).

**Table 2:** Material and Water Properties (3 Materials: Mohr-Coulomb Isotropic)

Material Type/ Properties	Cohesion	Phi	Unit Weight	Ru
Soil	0.00	36.0	18	1.10
Phyllite	240.00	36.0	21	1.10
Quartzite	90.00	27.0	20	1.10
Unit weight of water: 9.810				

#### 2.4. External Forces

In this case the external forces acting are identified on the basis of site investigations, toll plaza data collected and literature review. The distributed load, vehicular movement noise induced transmitted force and earthquake forces are the active external forces and used for the analysis as input parameter. These particulars of the forces are tabulated in Table 3.

**Table 3:** External Forces Acting on Tunnels

Tunnel Number	Vehicular Forces Type			
	Noise level range (24 hourly)	Frequency of maximum noise level exposure (24 hourly)	Vibrations Range in pseudo-static coefficient (24 hourly)	Frequency of maximum vibration level exposure (24 hourly)
Tunnel-1	64 to 90dB	500	0.02-0.08	500
Tunnel-2	64 to 88dB	500	0.03-0.09	500

#### 4. Landslide and Rock Fall Models of the Tunnel Hills

Roadside hill cut slopes are unsafe; these cuts were developed due to cutting of hills in the Aravalli Mountainous region. The preliminary geological, geotechnical and stability analysis carried out using Galena software shows that most of the slopes are having factor of safety less than one. The stress concentration pattern obtained by finite elemental analysis shows that in the toe area of the cut is indicative of its criticalness from failure aspect (Bhardwaj G.S. et al., 2011, 2012). Rockfall is a major problem in high hill slopes and rocky mountainous regions and construction of highways at these rockfall prone areas often require stable slopes. The causes of Rockfall are presence of discontinuities, high angle cut slopes, heavy rainfall, and unplanned slope geometry etc. Slope geometry is one of the most triggering parameters for rockfall, when there are variations in slope angle along the profile of slope (M. Ahmad et al., 2013). Reliable estimates of slope stability are essential for safe design and planning of road cut hill slopes which accommodate a number of tourist destinations around the world. The failure of cut slopes along these hills puts human life in grave danger and it is also disastrous for the economy (Kainthola et al., 2012). Assessment of the stability concerns of the adjoining part and twin tunnels has been carried out. For software analysis the spatial distribution of the rock mass as a geological material, slope surface geometry, and phreatic surface are given by the X-Y coordinates of the tunnel face analyzed (Table 4).

The computer generated tunnel crown face depicting all details are given in the Figure 4. The tunnel failure sensitivity has been modeled by considering magnitude of the forces applied & their direction in which, acting on the tunnels. The details of acting forces are given in the Table 5 and particulars of generated failure surfaces criticalness in Table 6.

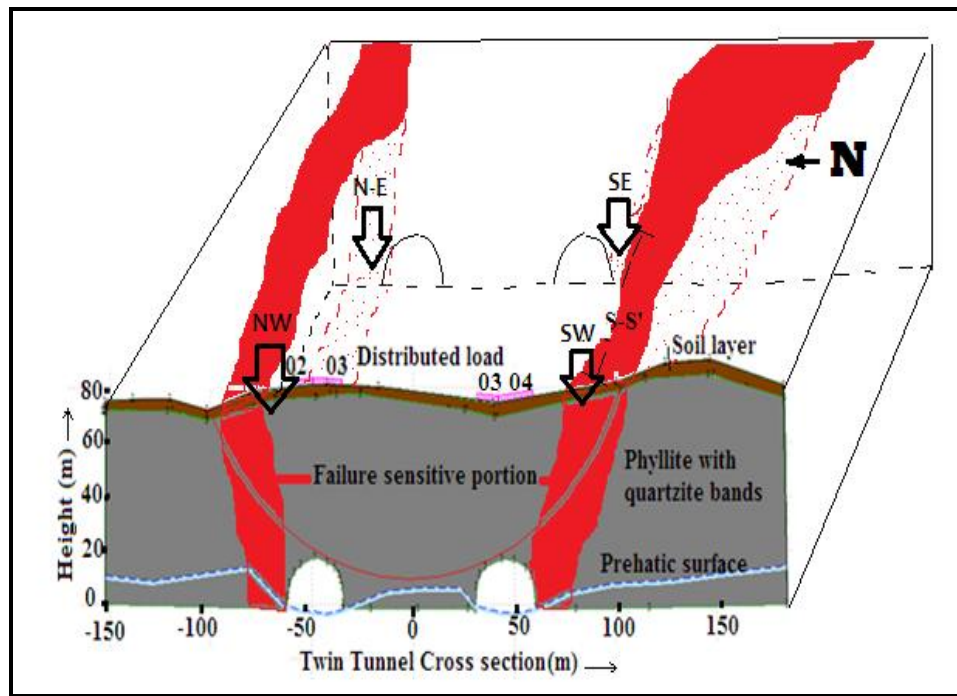


Figure 4: Showing Twin Tunnel Ukhliyat, NH76 Gogunda-Pindwara, Western India

Table 4: Material (10 Profiles), Slope Surface (01) and Phreatic Surface Profiles (01)

Profile	Material position/ Type	Material Distribution Coordinates (X,Y)
Profile:1 (3 Points)	Material beneath: 1-Soil	(-9.41, 94.21); (106.24,93.68) (106.24, 93.68)
Profile:2 (18 points)	Material within: 2 – Phyllite	(89.97, 0.12) (0.12,0.10) (2.77, 8.22) (5.95, 16.87) (8.42, 24.29) (11.25, 34.70) (5.13, 46.01) (17.96, 52.01) (21.13, 60.66) (24.31, 69.67) (29.43, 79.73) (32.96, 82.56) (44.09, 84.67) (56.10, 85.91) (65.45, 86.26) (75.52, 87.68) (89.47, 89.97) (89.97, 0.12)
Profile:3 (11 points)	Material within: 3 – Quartzite	(21.42, 53.20) (23.08, 59.51) (23.91, 62.34) (24.91 66.49) (26.23, 71.64) (27.90, 76.80) (29.39, 79.95) (30.39, 80.29) (25.40,60.68) (23.08, 54.86) (21.42, 53.20)
Profile: 4 (9 points)	Material within: 3 – Quartzite	(11.94, 25.61) (13.44, 34.09) (15.43, 39.74) (16.26, 45.22) (17.93, 45.89) (16.76, 37.91) (15.27, 33.42) (14.44, 29.10) (11.94, 25.61).
Profile: 5 (10 points)	Material within: 3 – Quartzite	(31.72, 64.83) (32.72, 70.65) (33.55, 74.30) (34.71,79.95) (36.21, 83.11) (40.86, 83.94) (39.53, 78.62) (34.88, 69.48) (33.05, 66.33) (31.72, 64.83)
Profile: 6 (23 points)	Material within: 3 – Quartzite	(21.25, 31.10) (24.07 , 36.42) (26.23, 41.57) (28.56, 47.72) (30.06, 55.86) (32.55, 60.84) (34.71, 65.50) (37.04, 67.32) (38.37, 66.99) (38.53, 64.67) (37.53, 61.84) (35.87, 58.35) (34.21, 53.53) (32.38, 50.71) (30.06, 47.05) (29.56, 43.06) (28.23, 40.07) (26.73, 36.91) (25.07, 34.59) (23.91, 32.59); (23.08, 31.43) (22.75, 30.93) (21.25, 31.10)
Profile: 7 (24 points)	Material within: 3 – Quartzite	(1.81, 0.19) (4.80, 6.01) (6.63, 11.16) (10.28, 18.14) (14.60, 25.28) (16.93, 32.10) (18.42, 37.58) (21.91, 45.72) (23.41, 50.37) (25.40, 51.21) (26.07, 50.54) (26.07, 48.71) (24.41, 45.72) (23.08, 39.91) (20.75, 37.08) (20.25, 33.42) (18.92, 31.10) (17.76, 28.44) (16.76, 26.11) (15.77, 24.45) (12.44,19.13) (7.79, 10.99) (5.13, 4.34) (1.81,0.19)
Profile: 8 (11 points)	Material within: 1 – Soil	(18.42, 47.38) (19.42, 51.70) (20.42, 55.69) (21.75, 59.85) (22.75, 63.17) (24.41, 67.82) (25.40,68.49) (23.74, 61.51) (21.58, 53.53) (20.42, 49.21) (18.42, 47.38)

Profile: 9 (11 points)	Material within: 1 – Soil	(18.42, 39.74) (19.92, 44.39) (22.41, 52.04) (24.91,59.18) (27.73,68.99) (30.06, 79.95) (32.05, 81.78) (28.39,65.66) (25.07, 56.52) (20.75, 43.89) (18.42, 39.74)
Profile: 10 (17 points)	Material within: 1 – Soil	(26.73, 48.55) (28.23, 54.20) (29.39, 60.35) (31.39, 63.34) (34.54, 67.66) (36.54, 72.14) (38.86,77.29) (40.69, 83.61) (43.52, 84.61) (39.86,75.47) (36.70, 70.15) (35.54, 67.32) (34.21, 64.83) (32.55,60.35) (30.39, 57.19) (29.23,52.53) (26.73, 48.55)
Slope surface Profile (16 points)	Comprised of Soil, phyllite and quartzite	(0.12, 0.10) (2.77, 8.22) (5.95, 16.87) (8.42, 24.29) (11.25, 34.70) (15.13, 46.01) (17.96, 52.01) (21.13, 60.66) (24.31, 69.67) (29.43, 79.73) (32.96, 82.56) (44.09, 84.67) (56.10, 85.91) (65.45, 86.26) (75.52 , 87.68) (89.47, 89.97)
Phreatic surface profile (15 points)	Water level surface	(3.75, -0.08) (8.58, 2.25) (16.40, 5.58) (25.05, 6.91) (33.86, 7.08) (49.17, 8.24) (57.98, 7.58) (65.47, 7.08) (71.29, 9.41) (75.95, 9.57) (82.10, 9.74) (85.60, 9.24) (88.09, 8.08) (89.76, 7.91) (90.09, 7.91)

**Table 5:** Showing Details of Various Forces Acting on Tunnel-1

Induced Forces on the Soil & Rock Mass	Distributed Load (2-Loads)				Pseudo-static Earthquake Coefficient	External Force (Vehicle Movement Induced)		
	X-Left	Pressure	X-Right	Pressure		Value	X-Pos'n	Angle
1	29.56	2.0	32.05	3.0	0.150	2.0	10.12	335.0
2	40.53	3.0	43.02	4.0	0.150	5.0	33.71	270.0

**Table 6:** Showing Parameters of Failure Surface for Critical Search Defined by: XL, XR, R

Particulars	XC	YC		
Circle Centre(C)	-135.82	142.80		
Circle radius (R)	189.00			
Intersections value assigned	XL	YL	XR	YR
	6.45	18.37	44.02	84.66
Generated Failure surface (X,Y Coordinates)	(6.45, 18.37) (9.08, 21.44) (11.63, 24.56) (14.13, 27.74) (16.55, 30.97) (18.90, 34.25) (21.19, 37.58) (23.40, 40.96) (25.54, 44.38) (27.61, 47.85) (29.60, 51.36) (31.51, 54.92) (33.35, 58.51) (35.11, 62.15) (36.80, 65.81) (38.40, 69.52) (39.93,73.26) (41.37, 77.03) (42.74, 80.83) (44.02, 84.66)			
Variable restraints	Parameter descriptor and value assigned			
	XL	XR	R	
Range of variation	7.00	11.00	9.00	
Trial positions within ranges	9	9	9	

In order to overcome difficulties of tunnel failure, field observation of the deformation behavior seems to be most promising. The stability of tunnels is assessed by comparing the derived strains with critical failure strains of the soil or rock (Sakurai S. et al., 1983). According to Sotirios V., 2007, a fundamental element of the observational method in geotechnical engineering practice is the utilization of a carefully laid out performance monitoring system which provides rapid insight of critical behavioral trends of the work. He has considered general geology and preliminary rock formation data of twin tunnel project of 450 meter long, named as Heshang highway tunnel located in South China (Sotirios V., 2007). Similarly way the numerical analyses of the tunnels have been done and their results are shown in computer generated images (Figure 5).

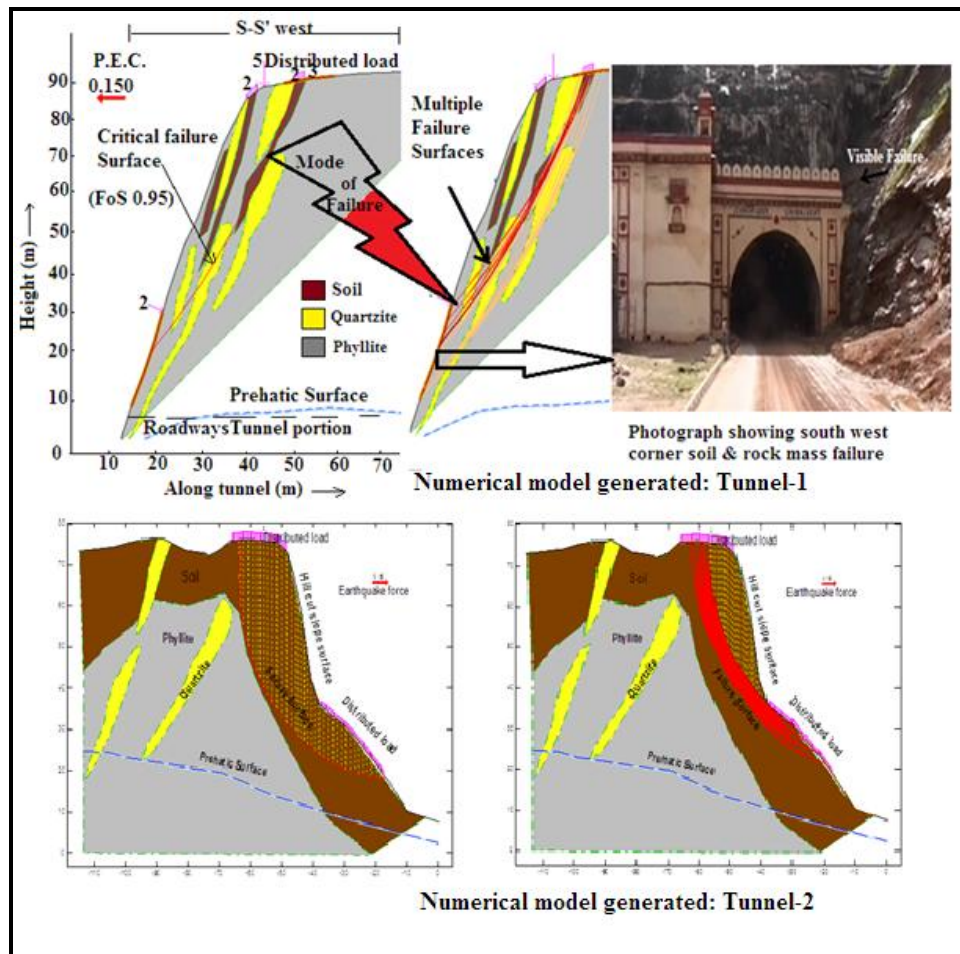


Figure 5: Showing Numerical Analysis Modeled Failure Sensitive Tunnel Faces

## 6. Conclusions and Recommendations, Measures Suggested

Rock-mass of tunnel hills categorized as fair to poor due to variation in material along X, Y and Z axis. External forces acting upon the hill rock material to weaken and resulting failures. The phreatic water surface is above the tunnel floor, which is fluctuating seasonal and related to rainfall precipitation. This causes watery conditions in tunnels. Computer generated model showing the failure sensitive portion by critical search of failure surfaces and factor of safety less than one. The present study identifies several failure planes at the twin tunnel side and entry -exist portion is more sensitive. A regular monitoring is needed for maintaining the safety of the tunnel structure and transport through the passage. Preventive maintenances' works may be undertaken well in advance.

Further works related to the site specific preventive measures like growing species, apply geo-textile, side design modification, lowering phreatic surface, prevention of rain water percolation in the sensitive rock mass, modus operandi about entry-exit side clearance, may be planned and undertaken in nature-friendly way.

## Acknowledgements

Sincere acknowledgements are due to Department of Science and Technology, Rajasthan to provide financial assistance for research work. We are thankful to Director Research, Dean and Comptroller M.P.U.A.T., Udaipur for providing necessary assistance time to time.

## References

Wikipedia®. Wikimedia Foundation, Inc. Webpage Last Modified on 5 August 2014.  
en.wikipedia.org/wiki/Engelberg\_Tunnel.

Feasibility Study and DPR for Rehabilitation and Upgrading to 4/6 lanes NH-14 km 246/800 to Km 340/000 & NH-76 Km 0/000 to Km 110/000 Palanpur to Udaipur; East-West Corridor, Package No. 1, Final Detailed Project Report Volume I Main Report, Government of India National Highways, Authority of India Ministry of Road Transport & Highways.

Sakurai, S. and Takeuchi, K. *Back Analysis of Measured Displacement of Tunnels*. Rock Mechanics and Rock Engineering. 1983. 16; 173-180.

Sotirios Vardakos, 2007: *Back-analysis Methods for Optimal Tunnel Design*. Submitted Dissertation, Virginia Polytechnic Institute and State University, In: Civil and Environmental Engineering, January 24, 2007 Blacksburg, Virginia.

[http://scholar.lib.vt.edu/theses/available/etd-02052007-104922/unrestricted/PHD\\_Dissertation\\_Vardakos\\_ver\\_2.pdf](http://scholar.lib.vt.edu/theses/available/etd-02052007-104922/unrestricted/PHD_Dissertation_Vardakos_ver_2.pdf) accessed on 27.2.2013

David, A., Hillson and David, T., Hulett, 2004: *Assessing Risk Probability: Alternative Approaches*. Originally Published as a Part of 2004 PMI Global Congress Proceedings– Prague, Czech, 2004. David Hillson & David Hulett. 1-7.

Estefania Munoz, Andres Ochoa and Hernan Martinez, 2012: *NH31B-1608: Landslide Probability Assessment by the Derived Distributions Technique*. <http://fallmeeting.agu.org/2012/eposters/eposter/nh31b-1608/> acceded on 28.2.2013.

Robin G. McInnes and Jenny Jakeways, 2002: *Instability Planning and Management: Seeking Sustainable Solutions to Ground Movement Problems*. Proceeding of the International Conference Organised by the Centre for the Coastal Environment, Isle of Wight Council. 20-23rd May 2002. Ventnor, Isle of Wight, UK.

Lateltin, O.J. *Landslides, Landuse Planning and Risk Management: Switzerland as a Case Study*. *Instability Planning and Management: Seeking Sustainable Solutions to Ground Movement Problems*. Proceeding of the International Conference Organised by the Centre for the Coastal Environment, Isle of Wight Council, and Held in Ventnor, Isle of Wight, UK on 20-23rd May 2002. 89-96.

Ahmad, M., Umrao, R.K., Ansari, M.K., Rajesh Singh and Singh, T.N. *Assessment of Rockfall Hazard along the Road Cut Slopes of State Highway-72, Maharashtra, India*. *Geomaterials*. 2013. 3; 15-23.

Kainthola, P., Singh, Wasnik, A.B., and Singh, T.N. *Distinct Element Modelling of Mahabaleshwar Road Cut Hill Slope*. *Geomaterials*. 2012. 2 (4) 105-113.

Bhardwaj, G.S. and Salvi, B.L. *Geo-Technical and FE Analysis of Road Side Rock Cut Slopes: A Case Study*. *Journal of Environ Tech & Construction Engg*. 2012. 01 (01) 31-38.

Bhardwaj, G.S., Salvi, B.L., Mayank Mehta and Sourabh Gaur. *Utility of Sensor Networking at Highways in Hilly Area*. *Journal of Environmental Science, Computer Science and Engineering & Technology*. 2012. 1 (2) 132-140.

Bhardwaj, G.S. and Salvi, B.L., 2011: *Slope Stability Aspects: A Case Study of the Road Side Hill Cuts NH-8, Between Udaipur-Ahmedabad, Rajasthan, India*. Proc. International Conference on Environmental Technology & Construction Engineering for Sustainable Development ICETCESD. Sylhet, Bangladesh, 10-12 March. 240.

Stephen, G. Perz. *Sustainable Development: The Promise and Perils of Roads*. Nature. 2014. 513; 178-179.

William, F. Laurance, Gopaldasamy Reuben Clements, Sean Sloan, Christine S. O'Connell, Nathan D. Mueller, Miriam Goosem, Oscar Venter, David P. Edwards, Ben Phalan, Andrew Balmford, Rodney Van Der Ree and Irene Burgues Arrea. *A Global Strategy for Road Building*. Nature. 2014. 513; 229-232.

## GIS and Spatial Evaluation of Groundwater Quality for Drinking and Irrigation Purposes in Thalaivasal Block, Southern India

Anbazhagan S.<sup>1</sup>, Muthumaniraja C.K.<sup>2</sup>, Jothibas A.<sup>1</sup> Chinnamuthu M.<sup>1</sup>, and Rajendran M.<sup>3</sup>

<sup>1</sup>Centre for Geoinformatics and Planetary Studies, Department of Geology, Periyar University, Salem, India

<sup>2</sup>Groundwater Division, Erode, Tamil Nadu, India

<sup>3</sup>Groundwater Division, Salem, Tamil Nadu, India

Correspondence should be addressed to S. Anbazhagan, anbu02@gmail.com

Publication Date: 17 December 2014

Article Link: <http://scientific.cloud-journals.com/index.php/IJAESE/article/view/Sci-238>



Copyright © 2014 Anbazhagan S., Muthumaniraja C.K., Jothibas A., Chinnamuthu M., and Rajendran M. This is an open access article distributed under the **Creative Commons Attribution License**, which permits unrestricted use, distribution, and reproduction in any medium, provided the original work is properly cited.

**Abstract** The knowledge of groundwater quality is useful in effective management of water resource in a basin. The present study was carried out to evaluate the groundwater quality for domestic and irrigation purposes in Thalaivasal block. The study area Thalaivasal block is located in Salem district, a typical hard rock terrain in the State of Tamil Nadu. The block is already categorized under 'dark area' by the State Groundwater Department. Groundwater quality data were collected for 54 locations from State Surface and Groundwater Resource Organization to understand hydro-geochemical characteristics of the groundwater in the block. The major elements and various hydro-geochemical parameters such as total hardness, TDS, salinity, SAR and Na% were studied to understand the groundwater quality. The Piper trilinear and Gibbs diagrams were plotted to know the dominance of groundwater chemistry and type. The results have shown that the majority of the groundwater samples fall in category I (Ca-Mg-Cl-SO<sub>4</sub>) and IV (Ca-Mg-HCO<sub>3</sub>) with normal earth alkaline water. The GIS spatial integration of various quality parameters indicates that about 40% of the area is not suitable for drinking and irrigation practices either in terms of undesirable or doubtful category. The final GIS output provided drinking water quality mapping with desirable, permissible, permissible water with hardness and unsuitable category. Similarly, irrigation water quality map was generated with excellent, good, doubtful and unsuitable category in the block.

**Keywords** Groundwater Quality; Spatial Integration; Gibbs Diagram; India

### 1. Introduction

Water, the precious resource available on the earth is contaminated either by rock water interaction or anthropogenic activities. In the last few decades, there has been a tremendous increase in demand for fresh water due to exploration of population, accelerated pace of industrialization and urban expansion. The demand for groundwater in a region requires detail assessment of availability and quality. Groundwater quality assessment is one of the important parameters in any groundwater resource evaluation study, particularly for domestic and irrigation purposes. The naturally occurring

rock water interaction, application of fertilizers, unsanitary conditions and improper waste disposal are the main sources which contaminate the groundwater.

Several studies are carried out to assess the geochemical characteristics of groundwater (Sujatha and Reddy, 2003; Laluraj et al., 2005; Subramani et al., 2005; Jeevanandam et al., 2006; Janardhana Raju et al., 2009; Ahmad and Qadir, 2011; Alexakis, 2011; Aghazadeh and Mogaddam, 2010; Ravikumar and Somashekar, 2012). Many studies are conducted to assess the suitability of groundwater for drinking and agriculture purposes (Aravindan, 2003; Aksoy and Scheytt, 2007; Rakad et al., 2009; Asadi et al., 2007; Dar et al., 2011; David et al., 2011). Such detailed studies provided geochemical evolution of groundwater (Garrels, 1967; Paces, 1973; Sarin et al., 1989; Gupta and Subramanian, 1998; Ravikumar and Somashekar, 2012). Groundwater quality variation of shallow aquifers are influenced by surface water irrigation in the commend areas (Nandakumar and Murthy, 1997; Chourasia and Tellarn, 1992). Groundwater quality for drinking purpose is concerned; the desirable limit of major elements and their derivatives such as hardness, TDS and salinity are important (Dar et al., 2010). Statistical methods are adopted to characterize the surface and groundwater quality, classification and selection of artificial recharge sites (Tellam, 1996; Saleh et al., 1999; Mohan et al., 2000; Aravindan and Manivel, 2003; Lambrakis et al., 2004; Pejman et al., 2009; Emmanuel et al., 2009; Ravikumar and Somashekar, 2012; Anbazhagan and Ramasamy, 2006). In the recent years, GIS technology is more useful for data integration and represent spatial distribution of groundwater quality for drinking and irrigation purposes (Anbazhagan and Nair, 2004; Anbazhagan et al., 2006; Sanjay Kumar and Goyal, 2010; Aravindan et al., 2010). There is an inadequacy in groundwater resource for irrigation use in Thalaivasal block. The increased demand for water for various sections like domestic use, agriculture practices and industrial growth such as sugar industry, sago industry, hatchery and painting units have raised serious problem. The irrigation practices in the block are gradually changing and agricultural lands are being converted into fallow land for commercial settlement. The objective of the present study is to assess the groundwater quality in Thalaivasal block and to delineate suitable groundwater zones for drinking and irrigation purposes.

## 2. Study Area

The study area Thalaivasal block is located in Salem district, in the southern part of India. Based on extensive groundwater development, the block is categorized as one of the 'dark block' in the state of Tamil Nadu. It means that the groundwater development reaches >70% of available resources (CGWB, 2009). The block is bounded by Kalrayan hills in the north, Chinna Salem block in the east, Veppanthattai block in the south, Gangavalli and Attur blocks (Salem district) in the west (Figure 1). It is lying in between 78°39'00" to 78°50'40" Eastern longitudes and 11°23'00" to 11°42'00" Northern latitudes. The total area of block is 400 sq. km and bifurcated into 41 panchayat villages. Thalaivasal block is known for aggressive agricultural practices, such as tapioca and sugarcane cultivation. Semi-arid climate prevails in the block. The annual average rainfall in the block is 700mm, which is lower than the state average rainfall (980mm). The block is mostly covered by pediments and pediplain with extensive coverage of black soil. In the present situation, agricultural practices are mostly re-oriented based on the availability of groundwater resource in the block. Gneisses are the major rock types covered in the northern and southern part of the block. In total, about 300 sq. km area (70%) covered by gneissic rocks comprises of granitoid gneiss, granitic gneiss, biotite gneiss and hornblende biotite gneiss. The charnockitic groups of rocks are occupied in the central part of the block for about 100 sq. km area. The general trend of the formations is NE to SW direction. The gneissic rocks are mostly foliated and weathered when compared to charnockites. The joints and fracture controlled lineaments are mostly weathered condition and support for groundwater accumulation and exploration. At present, both dug wells and bore wells in the block are catering groundwater supply to the drinking and irrigation. Vasishta nadhi and Sweta nadhi are the two major rivers in the block. These rivers are mostly contaminated by urban drainage and waste water from industry (Figure 2).

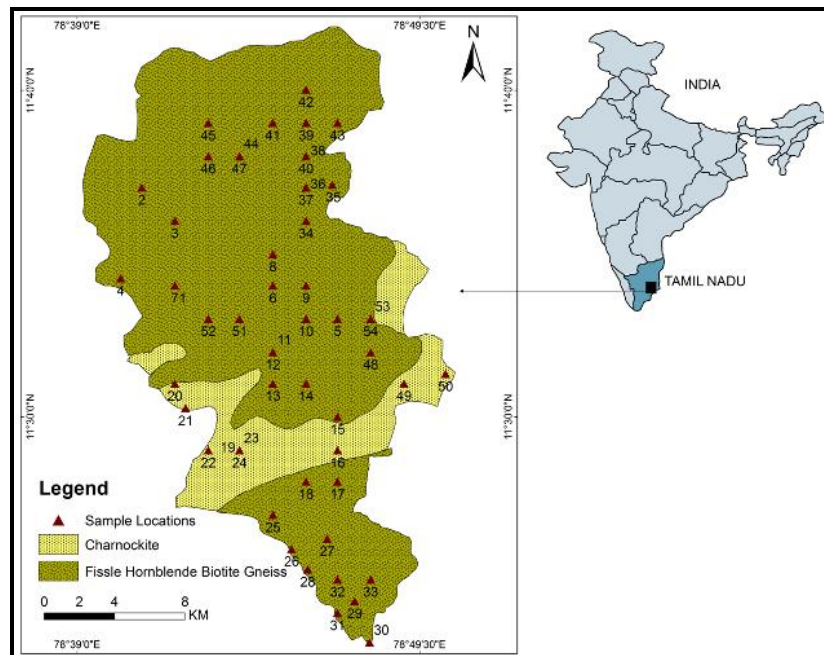


**Figure 1:** The Study Area Thalaivasal Block Located in the Southern Part of India in the State of Tamil Nadu; The Map Show the Rock Types and Groundwater Sample Locations



**Figure 2:** Vasishta Nadhi (a) and Sweta Nadhi (b) are the Two Main Rivers in Thalaivasal Block, Contaminated by Urban Sewage and Industrial Waste Water. The Surface Water is Mostly Stagnated and Contaminating Near by Aquifer

### 3. Methodology

Groundwater quality data were collected from the State Groundwater Department for 54 locations in Thalaivasal block (Figure 1). The groundwater quality for drinking purpose was assessed in terms of physical and chemical parameters based on Bureau of Indian Standards (BIS, 1991) (Table 1). The major elements such as calcium, sodium, potassium, magnesium, chloride, bicarbonate, nitrate and sulphate were considered for drinking water quality assessment. In addition, the Total Dissolved Solids (TDS), Total Hardness (TH) in the groundwater samples were estimated. For irrigation water quality assessment, salinity, Na% and sodium adsorption ratio (SAR) were considered. In order to assess the parameter which influence the groundwater chemistry and type of groundwater the Piper trilinear and Gibbs diagrams were plotted. GIS is an effective tool to deal spatial information, develop input data for water quality spatial mapping (Burrough, 1986). In the present study, ArcGIS 9.3

software is used for spatial integration and quality mapping. Based on drinking water quality standards, the spatial distributions of major elements, Total hardness and TDS in the groundwater were integrated with the help of Inverse Distance Weightage (IDW) module available in GIS software. Similarly, irrigation quality mapping was done through integration of EC, Na% and SAR. The output maps have shown that the various groundwater quality zones for drinking and irrigation purposes.

## 4. Results and Discussion

### 4.1. Drinking Water Quality Assessment

Calcium is one of the most abundant elements in the groundwater. In Thalaivasal block, 'Ca' concentration in groundwater ranges from 30mg/l to 330mg/l. The 'Ca' concentration in groundwater less than 75mg/l is desirable for domestic consumption, in between 75 to 200mg/l is permissible limit and considered as moderate quality for drinking and exceeds 200 mg/l is not suitable for drinking, considered as poor quality. In Thalaivasal block, about 30% of area covered by desirable limit of 'Ca', suitable for domestic purposes, 65% of zone under permissible limit and 5% in the block exceeds the permissible quality. The high 'Ca' concentration deposit encrustation in water supply structure and create adverse effect on domestic use.

**Table 1:** Physical and Chemical Parameters of Groundwater Samples in the Thalaivasal Block Show Statistical Summary, BIS and WHO Standards and the Percentage of Area Covered Under Desirable, Permissible and Undesirable Quality of Water

Parameters (Unit)	Range	Mean	Mode	Median	Sd	Who Standard (1997) Desirable-Permissible Limit	Bis Standard (1991) Desirable-Permissible Limit	% of Desirable	% of Permissible	% of Undesirable
pH (mg/l)	7.3-8.2	8	8	8	0	7-9.2	6.5-8.5	--	100	--
EC (µs/cm)	690-5710	1755	1435	1611	831	--	--	--	--	--
TDS (mg/l)	362-3288	941	874	862	484	500-1500	500-2000	10	80	10
TH (mg/l)	150-1200	570	400	570	210	100-500	300-600	--	35	65
Ca (mg/l)	30-330	95	72	86	49	75-200	75-200	37	47	16
Mg (mg/l)	5-170	81	88	84	37	30-150	30-100	9	86	5
Na (mg/l)	7-762	142	55	95	141	50-200	--	25	55	20
K (mg/l)	0-11.32	1	1	1	2	10-12	--	98	2	--
HCO <sub>3</sub> (mg/l)	214-769	455	409	430	127	300-600	--	9	80	11
Cl (mg/l)	35-1354	276	340	220	211	250-600	250-1000	55	41	4
SO <sub>4</sub> (mg/l)	6-402	81	12	48	89	200-600	200-400	98	2	--
NO <sub>3</sub> (mg/l)	3-124	34	27	29	22	50-100	45-100	78	20	2

The excess concentration of magnesium (>100mg/l) is also causes encrustation in water supply structure and considered as adverse quality for drinking. Magnesium with less than 30mg/l in groundwater is considered as suitable water for drinking; such desirable quality zone represents 30% area in the block. The permissible limit of 'Mg' considered up to 100mg/l, such moderate quality zones (within 30-100mg/l) are found in the central part of the study area; represent about 60% aerial coverage. The undesirable quality of water (>100mg/l) occupied about 10% of the area in the block.

Potassium is an essential element for human being, animals and growth of plants. It derived in food chain mainly from vegetation and soil. The main sources of potassium in groundwater include rain water, weathering of potash silicate minerals particularly clayey bearing host rocks, fertilizers and surface water irrigation. European Economic Committee (ECC) has provided the guideline limit of potassium at 10mg/l for drinking water. Most of the groundwater samples in the block have permissible limit of potassium.

Primary source of bicarbonate ions in groundwater is the dissolved  $\text{CO}_2$  in rain water when enters into the soil, dissolves more carbon-dioxide. Decay of organic matter and  $\text{SO}_4$  reducing bacteria may also release  $\text{CO}_2$  for dissolution. Water charged with  $\text{CO}_2$  dissolve carbonate minerals and when it passes through soil and rocks to give bicarbonates. Concentration of bicarbonate in the groundwater ranges from 214mg/l to 769mg/l. Desirable limits are found in the north and central part of the block (9%) with concentration of <300mg/l. About 80% of the block covered under permissible limit and 11% of the area exceeds the permissible limit and not suitable for drinking. The high concentration of bicarbonate may be due to leaching of mineral substances in the soil during infiltration of water from sewage (Mittal and Verma, 1997).

The concentration of nitrate in groundwater contributed by atmosphere, legumes, plant debris, animal excretion and fertilizer added to the crops. Normally, the nitrate concentration in groundwater is less than 10mg/l (Todd, 1955; Karanth, 1989). The high concentration of nitrate in groundwater gives bitter taste and in some cases, more than 45 mg/l reported to cause methemoglobinemia in infants. In Thalaivasal block, nitrate concentration in groundwater ranges from 4 to 71 mg/l. In terms of nitrate, the block restricted only 10% of the area have desirable quality of groundwater for drinking (10%). About 80% of groundwater samples show permissible limit of nitrate (>10mg/l to <45mg/l) in the groundwater. Nearly 10% of groundwater samples in the block have nitrate concentration with more than 45mg/l.

In general, the concentration of chloride ion in groundwater is fairly low, usually less than 100mg/l, unless the water is brackish or saline. Chloride added to the subsurface via industrial discharges, sewage, animal waste and road salting. Chloride is one of the major elements decides quality of water for drinking purposes. Chloride with more than desirable limit (>250mg/l) affect the taste and palatability, increase the corrosion. The groundwater zone with less than 250mg/l 'Cl' content considered as suitable (desirable) for drinking. Permissible groundwater quality represents 250 to 600mg/l of 'Cl'. Poor zone represents the 'Cl' concentration with more than 600mg/l. In Thalaivasal block, the concentration of chloride in groundwater is ranges from 35-1354mg/l. About 40% of the area under desirable quality, 50% of the areas fall in permissible limit and remaining 10% of the area not suitable for drinking water quality. High chloride concentration is found in the western part of the study area.

The concentration of sulphate in groundwater with <200mg/l is classified as desirable groundwater quality for drinking. Presents of sulphate with more than 200mg/l may likely to cause gastrointestinal irritation. In the study area, sulphate in groundwater ranges from 6 to 402 mg/l. However, in most part of the block fall well within the desirable limit (80%).

Groundwater hardness is one of the important parameters determining the suitability of groundwater for domestic and industrial purposes. It is primarily control by the amount of calcium and magnesium, and to a lesser extent, iron in the water. These ions react with soap to form precipitation and with certain anions present in the water to form scale. Groundwater hardness has no known adverse effect; however, it causes more consumption of detergents at the time of cleaning and some evidence indicates its role in heart decease (Schroeder, 1960). Groundwater hardness is measured by adding up the concentration of calcium, magnesium and converting the value to an equivalent concentration of calcium carbonate in mg/l of water. Based on hardness value, groundwater can be classified as soft (0-75mg/l), moderately hard (75-150mg/l), hard (150-300mg/l) and very hard (>300mg/l) (Sawyer and McCarty, 1967). The suitable range of hardness for drinking water quality is 80 to 100 mg/l; the moderately suitable quality fall in the range of 100 to 300mg/l. Groundwater hardness with >300 mg/l is considered as poor quality and >600mg/l is normally unacceptable for domestic purposes. The spatial distributions of the groundwater hardness in the study area vary from 280 to 1300 mg/l. In Thalaivasal block, only 10% of the area covered under desirable quality zone, about 70% fall in permissible limit and remaining 20% zone under undesirable quality zone.

Total Dissolved Solids (TDS) is the concentration of total weight of dissolved solids, which express the degree of salinity in a medium. TDS in groundwater contributed by various sources such as rock-water interaction, sewage, urban runoff and industrial waste (Joseph, 2001; Swarna Latha, 2008). The high TDS concentration in the groundwater decreases the quality and affects the taste of water. As per BIS (1991), the desirable limit of TDS in groundwater is 500mg/l and >500mg/l, may cause gastro-intestinal irritation. TDS content from 500mg/l to 1000mg/l is groundwater in permissible limit for drinking water quality and beyond which (>1000mg/l) the water is not suitable for drinking purposes. The distribution of TDS in groundwater in the study area ranges from 413 to 3288mg/l. Very high concentration of TDS observed at Thittacheri, where groundwater is contaminated by sewage waste and surface water infiltration. The dense residential area located in the north (Thittacheri) and southern (Kattukottai) part of the block, associated with high TDS content. Desirable quality of water with low TDS content restricted with a small area (10%); about 80% of the area covered by permissible quality zone and remaining 10% of area exceeds the permissible limit of TDS where groundwater is not suitable for drinking.

#### 4.2. Irrigation Water Quality Assessment

The excessive amounts of dissolved ions in groundwater affect crops and agricultural soil both in terms of physical and chemical characteristics, thus reducing the productivity. Presences of dissolved ions lower the osmotic presence in the plant cells, this preventing water from reaching the branches and leaves. The quality and suitability of groundwater for irrigation purposes is determined by salinity hazard, sodium percent and sodium absorption ratio (SAR).

The total concentration of soluble salts in groundwater can be expressed as specific conductance (EC) or salinity hazard. Based on electrical conductivity, the groundwater samples are expressed as excellent quality to brain water with extremely high EC concentration (Table 2). Based on EC value in the Thalaivasal block, groundwater classified into four classes from excellent to poor quality of water for irrigation (Table 3). Salinity hazard primarily determine the quality of water for irrigation. An elevated salt content in the groundwater leads to the formation of saline soil and it affects salt intake capacity of plants through their roots. High salinity water cannot be used, in place of restricted drainage; excess salinity diminishes the osmotic activity of plants, capacity of absorption of water and nutrients from the soil (Wilcox, 1955; Saleh et al., 1999). The EC value in the block ranges from 690 $\mu$ s/cm to 5710 $\mu$ s/cm. Richard (1954) classified the irrigation water into four groups based on salinity hazard (EC values). In Thalaivasal block, majority of the groundwater samples fall in fair to poor salinity category.

**Table 2:** Classification of Groundwater Samples Based on EC

Electrical Conductivity $\mu$ s/cm	Water Salinity	No. of Samples (Thalaivasal Block)	% of Samples (Thalaivasal Block)
0-250	Low (excellent quality)	Nil	Nil
251-750	Medium (Good quality)	01	2
751-2250	High (Permissible quality)	45	83
2251-6000	Very high	08	15
6001-10000	Extensively high	--	--
10001-20000	Brines moderately conc.	--	--
20001-50000	Brines highly conc.	--	--
50001-100000	Brines extremely high conc.	--	--
>100000	Brines extremely high conc.	--	--

**Table 3:** Salinity and Alkalinity Hazard Classification of Groundwater for Irrigation

Water Class	Salinity Hazard			Alkali Hazard		
	EC	No. of Samples	Percentage	SAR	No. of Samples	Percentage
Excellent	<250	--	--	<10	25	45
Good	250-750	2	4	10-18	12	22
Fair (medium)	750-2250	44	81	18-20	1	2
Poor (bad)	>2250	8	15	>20	17	31

Sodium concentration in groundwater has an important role in determination of irrigation water quality. Through the process of Base Exchange, sodium replaces calcium in the soil and which reduces the permeability of soil. The sodium in irrigation water is usually represented as percent sodium and it can be determined as follows (Doneen, 1962).

$$\text{Sodium percent} = \frac{(\text{Na} + \text{K})100}{\text{Ca} + \text{Mg} + \text{Na} + \text{K}}, \quad (1)$$

Where, the quantities of Ca, Mg, Na and K are expressed in milligram per liter (epm).

The sodium percentage in groundwater samples of Thalaivasal block ranges from 4% to 80 % and classified into five categories from excellent to doubtful quality water (Table 4). About 22% of groundwater samples fall in doubtful groundwater quality for irrigation.

**Table 4:** Groundwater Quality for Irrigation Based on Sodium Percentage

% Na	Quality of water	No. of samples	% of samples
<20	Excellent	12	22
20-40	Good	16	29
40-60	Permissible	15	27
60-80	Doubtful	11	22
>80	Unsuitable	Nil	Nil

The Sodium Absorption Ratio (SAR) indicates the effect of relative cation concentration on sodium accumulation in the soil. It expressed the reaction with the soil and to know reduction in its permeability. SAR is a more reliable method than sodium percentage to assess the quality impact on irrigation. Therefore, SAR is considered as a better yardstick to measure of Na (alkali) hazard in irrigation water. It directly related to the adsorption of sodium by soil and valuable criterion for determining the suitability of groundwater for irrigation. SAR is calculated using following formula:

$$\text{SAR} = \frac{\text{Na}^+}{\sqrt{\text{Ca}^{2+} + \text{Mg}^{2+}/2}}, \quad (2)$$

Where, all ionic concentrations are expressed as milliequivalents per liter (meq/l).

The SAR in block varies from 0.74 to 59.5. Majority (67%) of groundwater samples in Thalaivasal block is suitable (good to excellent) for irrigation practices. In the eastern and southern part of the block (about 33%), SAR has shown poor to fair category.

### 4.3. Groundwater Facies

#### A. Trilinear Diagram

In order to understand the hydrogeochemical facies of the study area, the value of major oxides in groundwater samples were plotted and compared through Piper (1994) trilinear diagram. The diagram consists of two lower triangles show the percentage distribution of the major cations ( $Mg^{++}$ ,  $Ca^{++}$ , and  $Na^+$  plus  $K^+$ ) and the major anions ( $Cl$ ,  $SO_4$  and  $CO_3$  plus  $HCO_3$ ) and a diamond-shaped part above that summarizes the dominant cations and anions to indicate the water type. The water types are designated according to the area in which they occur on the diagram segments. The trilinear diagram is useful in highlight the chemical relationship among groundwater samples in more specific terms. The cation distribution indicates that the groundwater samples range in composition from sodium/potassium to predominantly mixed cations. Small percentages of the groundwater samples have Ca-Mg cation type. In the anion triangle, bicarbonate/chloride water type predominant and small fraction of mixed anion-type of water (Figure 3). Further, the groundwater can be classified into following category based on the combined points located in diamond shaped field. In Thalaivasal block, majority of the groundwater samples fall in I ( $Ca^{2+}$ - $Mg^{2+}$ - $Cl$ - $SO_4$ ) type and IV ( $Ca^{2+}$ - $Mg^{2+}$ - $HCO_3$ ) type normal earth alkaline water with prevailing bicarbonate and chloride water type.

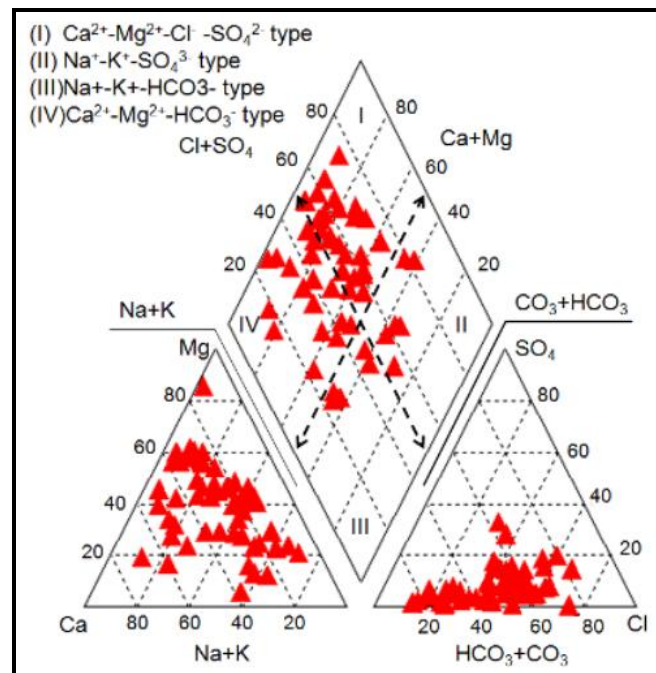
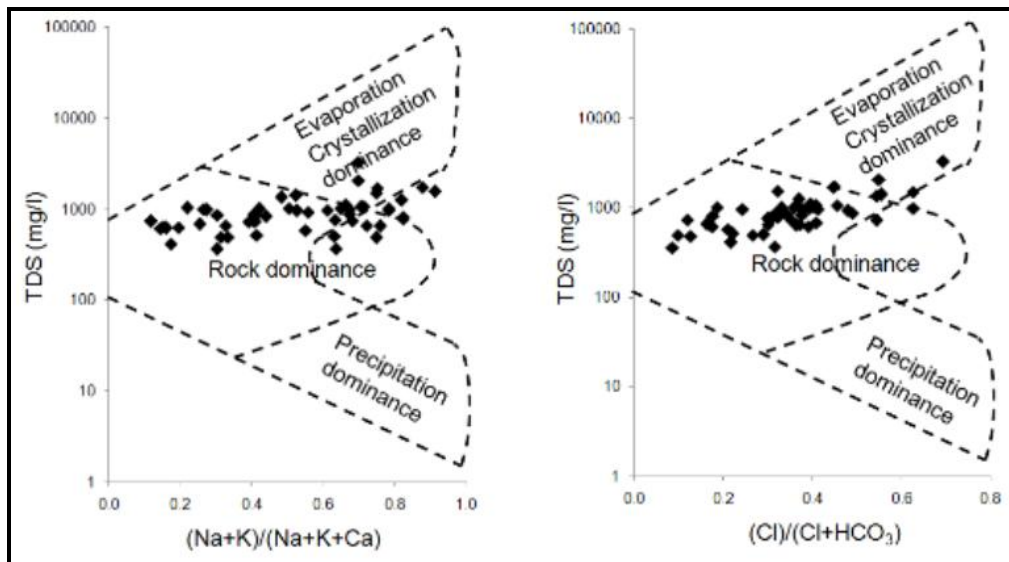


Figure 3: Piper Trilinear Diagram for Groundwater Samples in Thalaivasal Block

#### B. Gibbs Diagram

In Gibbs (1970) diagram the ratio of dominant anions and cations were plotted against the value of TDS. This diagram is useful to know the groundwater chemistry and relationship of the components of water from their respective aquifers like chemistry of rock types, chemistry of precipitated water and rate of evaporation. In this case, Gibbs variation diagrams were plotted as ratio I for cations i.e.  $[(Na+K)/(Na+K+Ca)]$ , and ratio II for anions  $(Cl)/(Cl+HCO_3)$  against values of TDS (Figure 4). From these plots, it is inferred that majority of the groundwater samples are fall in rock dominance area, indicate the source of mineral constituents in water is mainly from the dissolution of rocks.



**Figure 4:** Gibbs Variation Diagrams Plotted TDS against (a)  $[(Na + K) / (Na+K+Ca)]$  and (b)  $[Cl/(Cl +HCO_3)]$

#### 4.4. GIS Spatial Integration and Quality Evaluation

In GIS spatial integration, nine parameters including seven major elements (Ca, Mg, Na,  $HCO_3$ , Cl,  $NO_3$  and  $SO_4$ ), total hardness and TDS in the groundwater samples were considered for drinking water quality mapping in the block. Among major elements, the concentration of potassium in the groundwater is mostly within the desirable limit. The groundwater samples in the block were divided into desirable, permissible and undesirable quality of water for drinking based on the concentration of major elements, total hardness and TDS. The groundwater with desirable quality is suitable for drinking. Permissible condition represents the moderate quality of groundwater and it can be utilized in absence of desirable quality of water. Presence of elements beyond permissible limit represents undesirable quality of water, which is not suitable for drinking. Thematic maps for above mentioned nine parameters were generated by interpolating point data using IDW module in GIS. Such thematic maps have shown desirable, permissible and undesirable quality zones with respect to individual parameter. All nine thematic maps were spatially integrated through 'intersect overlay' module in GIS. The output map has shown combination of nine parameters into 90 polygons. This map was again reclassified into 4 quality zones as desirable, permissible, permissible water with hardness and unsuitable category based on controlling quality parameters (Figure 5). The analysis shows that in most of the locations, the concentration of sulphate and nitrate are well within the desirable limit. However, in significant area, groundwater hardness exceeds the permissible limit (28%). The desirable quality zone covered only 12% in the block; the major parts of the area covered by permissible quality (44%) and about 16% of the area have unsuitable groundwater quality for drinking.

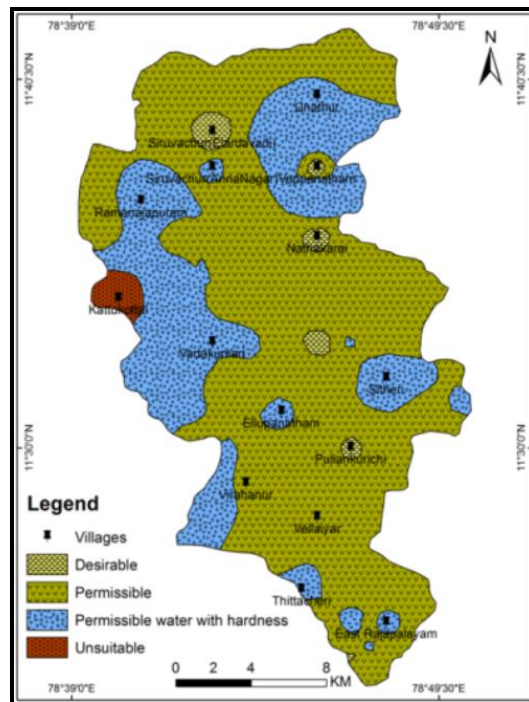


**Figure 5:** Spatially Integrated Groundwater Quality Mapping for Drinking Water in Thalaivasal Block

For irrigation water quality mapping, salinity hazard, Na% and SAR were considered and spatially integrated through GIS. The spatial integration of such quality parameters provides 21 polygons in different combinations. Based on the range of values in each parameter, the groundwater samples were classified into different quality zones. In the final output, the groundwater in the block is clustered into excellent, good, doubtful and unsuitable quality of water respectively covered in 36%, 24%, 21% and 19% (Figure 6).

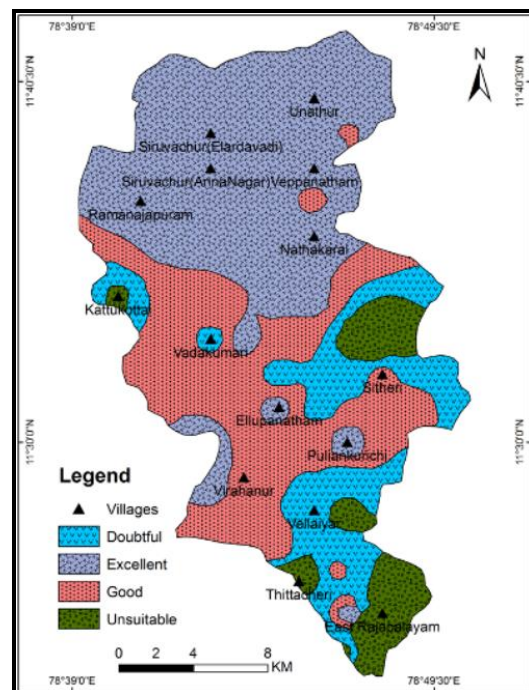


**Figure 6:** Thalaivasal Block Categorized under Various Groundwater Quality Zone for Irrigation through GIS Spatial Integration of Salinity, Na% and SAR

## 5. Conclusion

Groundwater quality assessment for drinking and irrigation was carried out in the Thalaivasal block using GIS spatial integration. The results have shown that very limited areas have suitable quality of water (12% desirable) for drinking. Though the major part of the area covered by permissible limit (44%), which can be considered as moderately suitable quality for drinking. The high concentration of calcium and magnesium results increase of groundwater hardness in the block, which accounts for 28% of the area. The source of calcium may be due to sewage and industrial waste water. The remaining 16% of the area is not suitable for drinking. From the Gibbs diagram, it is inferred that the main source for groundwater contamination is rock water interaction. In addition, the infiltration of urban drainage and industrial sewage are also adding contamination to the groundwater. As per as irrigation water quality is concerned, about 60% of the area suitable for agricultural practices, where the groundwater quality is excellent to good. The remaining 40% of the area covered by doubtful to unsuitable quality of water for irrigation. The shortage of groundwater source, quality problem and failure of monsoons prevents continuous agricultural practices in the block. It is necessary to adapt alternative cropping pattern and aquifer management practices in the block. The GIS spatial outputs useful for planners for understand groundwater quality standards for drinking and irrigation in the block.

## Acknowledgement

The authors thank State Groundwater Department, Tamil Nadu for providing groundwater quality data. The comments and suggestions of anonymous reviewer help to improve the article standard.

## References

- Ahmad, Z., and Qadir, A. *Source Evaluation of Physicochemically Contaminated Groundwater of Dera Ismail Khan Area, Pakistan*. Environmental Monitoring Assessment. 2011. 175; 9-21.
- Aghazadeh, N., and Mogaddam, A.A. *Assessment of Groundwater Quality and its Suitability for Drinking and Agricultural uses in the Oshnavieh Area, Northwest of Iran*. Journal of Environmental Protection. 2010. 1; 30-40.
- Aksoy, A.O., and Scheytt, T. *Assessment of Groundwater Pollution around Torbali, Izmir, Turkey*. Environmental Geology. 2007. 53; 19-25.
- Alexakis, D. *Assessment of Water Quality in the Mesolonghi–Etoliko and Neochorio Region (West Greece) Using Hydrochemical and Statistical Analysis Methods*. Environmental Monitoring and Assessment. 2011.
- Anbazhagan, S., and Nair, A.M. *Geographic Information System and Groundwater Quality Mapping in Panvel Basin, Maharashtra, India*. Journal of Environmental Geology. 2004. 45; 753-761.
- Anbazhagan, S., and Ramasamy, S.M. *Evaluation of Areas for Artificial Groundwater Recharge in Ayyar Basin, Tamil Nadu, India Through Statistical Terrain Analysis*. Journal of Geological Society of India. 2006. 67; 59-68.
- Aravindan, S., Shankar, K., Poovalinga, Ganesh B., and Dharani Rajan, K. *Groundwater Geochemical Mapping of in the Hard Rock Area of Gadilam River Basin, Using GIS Technique, Tamil Nadu*. Indian Journal of Applied Geochemistry. 2010. 12 (2) 209-216.

Aravindan, S., and Manivel, M. *Hydrogeomorphological Mapping in the Hard Rock Region of Gadilam River Basin, Villupuram District, Tamil Nadu*. Indian Journal of Geomorphology. 2003. 8; 111-116.

Asadi, S.S., Vuppala, P., and Reddy, M.A. *Remote Sensing and GIS Techniques for Evaluation of Groundwater Quality in Municipal Corporation of Hyderabad (Zone-V), India*. International Journal of Environmental Research and Public Health. 2007. 4 (1) 45-52.

BIS. *Drinking Water Specifications*. Bureau of Indian Standards, IS: 10500 (Revised 2003), 1-5.

Burrough, P.A., and McDonnell, R.A., 1998: *Creating Continuous Surfaces from Point Data*. In: Principles of Geographic Information Systems; Burrough P.A., Goodchild M.F., McDonnell R.A., Switzer P., Worboys M. (Eds.). Oxford, UK: Oxford University Press.

CGWB. Central Ground Water Board Report. 2009. 24.

Chourasia, L.P., and Tellam, J.H. *Determination of the Effect of Surface Water Irrigation on the Groundwater Chemistry of a Hardrock Terrain in Central India*. Hydrological Sciences Journal. 1992. 37 (4) 313-328.

Dar, A.I., Mithas A. Dar, and Sankar, K. *Nitrate Contamination in Groundwater of Sopore Town and Its Environs, Kashmir, India*. Arabian Journal Geosciences. 2010. 3; 267-272.

Dar, I.A., Sankar, K., Shafi, T., and Dar, M.A. *Investigation of Groundwater Quality in Hardrock Terrain Using Geoinformation System*. Environmental Monitoring Assessment. 2011. 176 (1-4) 575-595.

Doneen, L.D. *The Influence of Crop and Soil on Percolating Water*. Proc. 1961 Biennial Conference on Groundwater Recharge. 1962. 156-163.

Emmanuel, E., Pierre, M.G., and Perrodin, Y. *Groundwater Contamination by Microbiological and Chemical Substances Released from Hospital Wastewater: Health Risk Assessment for Drinking Water Consumers*. Environment International. 2009. 35; 718-726.

Garrels, R.M., 1967: *Genesis of Some Groundwaters from Igneous Rocks*. In: Researches in Geochemistry; Abelson P.H. (Ed.). New York: Wiley. 405.

Gupta L.P., and Subramanian V. *Geochemical Factors Controlling the Chemical Nature of Water and Sediments in the Gomti River, India*. Environmental Geology. 1998. 30; 1-21.

Janardhana Raju, N., Prahlad Ram and Sangita Dey. *Groundwater Quality in the Lower Varuna River Basin, Varanasi District, Uttar Pradesh*. Journal Geological Society of India. 2009. 73; 178-192.

Jeevanandam, M., Kannan, R., Srinivasalu, S., and Rammohan, V. *Hydrogeochemistry and Groundwater Quality Assessment of Lower Part of the Ponnaiyar River Basin, Cuddalore District, South India*. Environmental Monitoring and Assessment. 2006. 132; 263-274.

Joseph, K., 2001: *An Integrated Approach for Management of Total Dissolved Solids in Reactive Dyeing Effluents*. International Conference on Industrial Pollution and Control Technologies, Hyderabad.

Karant, K.R., 1989: *Groundwater Assessment, Development and Management*. New Delhi: Tata McGraw-Hill. 154.

- Laluraj, C.M., Gopinath, G., and Dineshkumar, P.K. *Groundwater Chemistry of Shallow Aquifers in the Coastal Zones of Cochin*. Industrial Applied Ecology and Environmental Research. 2005. 3 (1) 133-139.
- Lambrakis, N., Antonakos, A., and Panagopoulos, G. *The Use of Multicomponent Statistical Analysis in Hydrogeological Environmental Research*. Water Research. 2004. 38; 1862-1872.
- Mohan, R., Singh, A.K., Tripathi, J.K., and Chowdhary, G.C. *Hydrochemistry and Quality Assessment of Groundwater in Naini Industrial Area, Allahabad District, Uttar Pradesh*. Journal of Geological Society of India. 2000. 55; 77-89.
- Nandakumar, P., and Murthy, D.S.S., 1997: *Irrigation Related Groundwater Quality Variations in Shallow Basaltic Aquifer in Ghataprabha Irrigation Project Command Area, Karnataka, India– a Statistical Evolution*. International Conference on Management of Drinking Water Resources. December 3-5, Chennai, India. 223-238.
- Paces, T. *Steady State Kinetics and Equilibrium between Groundwater and Granite Rock*. Geochim Cosmochim Acta. 1973. 37; 2641-2663.
- Pejman, A.H., Nabi Bidhendi, G.R., Karbassi, A.R., Mehrdadi, N., and Esmaeil Bidhendi, M. *Evaluation of Spatial and Seasonal Variations in Surface Water Quality using Multivariate Statistical Techniques*. Journal of Environmental Science and Technology. 2009. 6 (3) 467-476.
- Ravikumar, P., and Somashekar, R.K. *Assessment and Modelling of Groundwater Quality Data and Evaluation of their Corrosiveness and Scaling Potential Using Environmetric Methods in Bangalore South Taluk, Karnataka State, India*. Water Resources. 2012. 39 (4) 446-473.
- Rakad, T., Abdallah, A., and Kasem, S. *Water Quality Evaluation of the Groundwater Resources in Amran Basin, Yemen*. Current World Environment. 2009. 4 (1) 1-7.
- Richard, L.A., 1954: *Diagnoses and Improvement of Saline and Alkali Soils*. Agriculture Hand Book 60: USDA, USA.
- Saleh, A., Al Ruwaih, F., and Shehata, M. *Hydrogeochemical Processes Operating within the Main Aquifers of Kuwait*. Journal of Arid Environments. 1999. 42; 195-209.
- Sarin, M.M., Krishnaswami, S., Killi, K., Somayajulu, B.L.K., and Moore, W.S. *Major ion Chemistry of the Ganga-Brahmaputra River Basin System: Weathering Processes and Fluxes to the Bay of Bengal*. Geochim Cosmochim Acta. 1989. 53; 997-1009.
- Sanjay Kumar and Goyal. *GIS Based Spatial Distribution Mapping and Suitability Evaluation of Groundwater Quality for Domestic and Agricultural Purpose in Kaithal District, Haryana State, India*. Environmental Earth Sciences. 2010.
- Sawyer, C.N., and McCarty, P.L., 1967: *Chemistry for Sanitary Engineers*. 2nd Ed. New York: McGraw–Hill.
- Schroeder, H.A. *Relations between Hardness of Water and Death Rates from Certain Chronic and Degenerative Diseases in the United States*. Journal of Crohn's Disease. 1960. 12; 586-59.

Subramani, T., Elango, L., and Damodarasamy, S.R. *Groundwater Quality and its Suitability for Drinking and Agricultural Use in Chittar River Basin, Tamil Nadu, India*. Environmental Geology. 2005. 47; 1099-1110.

Sujatha, D., and Reddy, B.R. *Quality Characterization of Groundwater in the South-Eastern Part of the Ranga Reddy District, Andhra Pradesh, India*. Environmental Geology. 2003. 44; 579-586.

Suvedha, M., Gurugnanam, B., Suganya, M., and Vasudevan, S. *Multivariate Statistical Analysis of Geochemical Data of Groundwater in Veeranam Catchment Area, Tamil Nadu*. Journal of Geological Society of India. 2009. 74; 573-578.

Swarna Latha, P., 2008: *Studies on Spatial and Temporal Changes of Land Use and Land Cover, Groundwater Quality and Shoreline of Greater Visakhapatnam Municipal Corporation, Andhra Pradesh, India Using Remote Sensing and GIS Techniques*. Ph.D. Thesis, Andhra University, Visakhapatnam.

Tellam, J.H. *Interpreting the Borehole Water Chemistry of the Permo-Triassic Sandstone Aquifer of the Liverpool Area, IJK*. Geological Journal. 1996. 31; 61-87.

Todd, G.K., 1955: *Groundwater Flow in Relation to the Flooding Stream*. Proceedings of the American Society Civil Engineers. 81; 628-1, 628-21.

Wilcox, L.V., 1955: *Classification and Use of Irrigation Water*. US Department of Agri., Circ, Washington, DC.

WHO. *Guidelines for Drinking Water Quality in Health Criteria and Other Supporting Information*. 1984. 2; 336.

## Experimental Studies on Silicate as the Limiting Nutrient in Altering Phytoplankton Community Structure

Shanthi R.<sup>1</sup>, A. Vinoth Gowtham<sup>1</sup>, L. Senthilnathan<sup>1</sup>, D. Poornima<sup>1</sup>, R.K. Sarangi<sup>2</sup>, and T. Thangaradjou<sup>1</sup>

<sup>1</sup>Centre of Advanced Study in Marine Biology, Faculty of Marine Sciences, Annamalai University, Tamilnadu, India

<sup>2</sup>Marine Biology Division, Marine, Earth and Planetary Sciences Group, Space Application Centre (ISRO) Ahmedabad, Gujarat, India

Correspondence should be addressed to T. Thangaradjou, umaradjou@yahoo.com

Publication Date: 2 December 2014

Article Link: <http://scientific.cloud-journals.com/index.php/IJAESE/article/view/Sci-248>



Copyright © 2014 Shanthi R., A. Vinoth Gowtham, L. Senthilnathan, D. Poornima, R.K. Sarangi, and T. Thangaradjou. This is an open access article distributed under the **Creative Commons Attribution License**, which permits unrestricted use, distribution, and reproduction in any medium, provided the original work is properly cited.

**Abstract** In the present study, nutrient enrichment experiments were carried out to understand the role and importance of silicate in the phytoplankton blooming. Water temperature (26.6 – 29.8°C), salinity (33 - 37‰), pH (8.01 – 8.64), and DO (4.26 – 6.38mg l<sup>-1</sup>) not showed significant variation and not play important role in the phytoplankton growth. At the first day of the experiment, nutrient concentrations (NO<sub>3</sub> - 9.44μM, NO<sub>2</sub> – 1.51μM, PO<sub>4</sub> – 24.40μM and SiO<sub>3</sub> – 45.60μM) were at its maximum concentration in enrichment tanks and it gradually decreased (PO<sub>4</sub> – 14.19μM and SiO<sub>3</sub> – 6.11μM) at the end of experiment period, suggested uptake of nutrients by the experimental microalgal species. The pronounced maximum chlorophyll concentration (8.90μg l<sup>-1</sup>) in tank5 corresponding with addition of highest concentration of silicate (25μM), clearly pointed out that silicate addition has influenced the diatom dominated microalgal growth evidenced by the increased chlorophyll concentration. Increased utilization of SiO<sub>3</sub> supported by PO<sub>4</sub> indicates the nutrient preference by the diatom. The regression trend recorded in the present study could be used as the positive signal in mapping silicate using remote sensing techniques. The regression analysis between silicate and chlorophyll showed significant correlation coefficient (R<sup>2</sup> = 0.609) and increased phytoplankton growth rate (0.277 d<sup>-1</sup>) at tank 5 when compared to control substantially proved the uptake of silicate by phytoplankton community dominated by diatoms.

**Keywords** *Chlorophyll; Diatoms; Nitrate; Phosphate; Si:N; Si:P*

### 1. Introduction

In the estuarine ecosystem, the biomass and productivity of phytoplankton in different size ranges are important factors regulating the productivity of higher tropical-level organisms. The pelagic algal communities make important contributions to the smooth functioning of aquatic ecosystem. Since the earliest days of phytoplankton ecology, nutrients have been invoked as one of the variables

controlling phytoplankton community structure and biomass (Whipple and Jackson 1899). The nutrient rich freshwater pulsed into estuaries alters turbidity, water temperature, salinity, and nutrient concentrations and ratios at irregular intervals, creating a highly dynamic habitat (Day *et al.* 1982, Lane *et al.* 1999).

Dissolved nutrient concentrations are used to infer the status of nutrient limitation. Where the nutritional requirement is concerned, phytoplankton takes elements in relatively fixed proportion for growth if no nutrient is limiting. Nitrogen (N), phosphorus (P), and silicon (Si) dissolved in seawater are essential elements for phytoplankton growth and their supply in the ocean. Besides N and P, phytoplankton growth can also be limited by silica and trace element (Harrison *et al.*, 1987) more important by the presence of N or Si determine the microalgal dominance either dinoflagellates dominant or diatom dominant.

Silicon (Si) is an important requirement for diatom growth and its availability in the coastal ocean primarily depends on freshwater runoff (Falkowski *et al.* 1998). Silicon in sea water may be present in the suspension, in particles of clay or sand, as a constituent of diatoms, etc., or in solution in the form of silicate, usually estimated by the colorimetric method. Diatom production can be limited by the availability of dissolved silicate (DSi), and DSi depletion relative to their major nutrients have been observed to select for non-siliceous flora (Conley and Malone, 1992).

Silicate ( $\text{Si}(\text{OH})_4$ ), through phytoplankton processes its link to diatom structure and metabolism, may control important regions of the ocean, e.g. in coastal upwelling (Dugdale, 1972, 1983, 1985; Dugdale and Goering, 1970; Dugdale *et al.*, 1981) and Antarctic seas (e.g. Sakshaug *et al.*, 1991). Diatoms have an absolute requirement for silicon (Lewin, 1962), without which valves are not formed, and the cell cycle is not completed (Brzezinski *et al.*, 1990; Brzezinski, 1992). Silico flagellates share this requirement for silicon, but they do not grow rapidly or form large blooms.

In recent years, nutrient uptake kinetics has been considered to be important in this respect. Maximal uptake and growth rates were considered to be the important parameters determining the outcome of species competition at higher nutrient concentrations. A common technique for determining nutrient limitation in phytoplankton is the nutrient enrichment bioassay (Hecky and Kilham, 1988). This type of bioassay involves placing water samples in containers supplied with one or a number of nutrients (such as ammonium, nitrate, phosphate, silicate and trace metals), and measuring the phytoplankton growth over time (Fisher *et al.*, 1999). If growth is rapid and exponential in a sample containing a particular nutrient, but is very poor in samples not containing that nutrient, then it is considered that the nutrient is limiting phytoplankton growth in the system.

Experimental additions of the inorganic nutrients to seawater samples suggest that several elements play limiting roles, including N, P, Si and Fe (Martin *et al.*, 1991; Downing, 1997). Silicate is found to be an important nutrient for diatom growth in both marine and fresh waters. Hence, the present study was carried out to assess the significant role of silicate in the phytoplankton growth by conducting an enrichment experiment.

## 2. Materials and Methods

Enrichment experiments were done to determine the nutrient limitation status of phytoplankton. The experiment was commenced for 8 days with six 100L open culture tanks containing 50 litres of filtered sea water each and kept in natural environmental condition. The seawater in all tanks was agitated constantly with aerator. The natural phytoplankton community, dominated by diatoms, was collected during high tide using phytoplankton net (No. 30) made of bolting silk (mesh aperture size:  $48\mu\text{m}$ ) and 50 ml of the phytoplankton concentrate was added into each tank. Natural sea water without any addition of silicate was maintained as the control tank. The initial nutrient concentrations of

experimental seawater are shown in Table 1. In order to trigger the phytoplankton bloom ammonium sulphate, super phosphate and urea in the ratio 10:2:2 was added in all the tanks. Culture tanks containing natural phytoplankton community were subjected to different concentrations of silicate ( $\text{NaSiF}_6$ ) (5, 10, 15, 20, 25  $\mu\text{M}$ ) in order to obtain a situation which concentration of silicate enhance phytoplankton biomass in tanks. Seawater was sampled every 24h to analyze dissolved oxygen, pH, salinity, nutrients and chlorophyll *a* along with natural water temperature of each tanks. The same experiment was again repeated twice for the justification of tank experiment results with the changing environmental conditions. This is essentially required as the enrichment experiment was carried out in outdoor conditions.

**Table 1:** Background Value of Experimental Seawater in the Tanks

Experiment	$\text{NO}_2$ ( $\mu\text{M}$ )	$\text{NO}_3$ ( $\mu\text{M}$ )	$\text{PO}_4$ ( $\mu\text{M}$ )	$\text{SiO}_3$ ( $\mu\text{M}$ )	Chlorophyll <i>a</i> ( $\mu\text{g l}^{-1}$ )
1.	0.56	4.58	0.03	22.53	1.41
2.	0.50	5.03	0.04	21.57	1.39
3.	0.52	4.98	0.03	22.14	1.45

Surface water temperature was measured using digital multi-stem thermometer of  $0.1^\circ\text{C}$  accuracy. Salinity was measured using a hand held refractometer (Atago hand refractometer, Japan) and the pH was measured using a pH meter (Cyberscan pH 1100) with the accuracy of  $\pm 0.01$ . Dissolved oxygen was estimated by following the modified Winkler's method (Strickland and Parsons, 1972). Water samples were collected by using plastic container and filtered immediately using a millipore filtering system through a  $0.45\mu\text{m}$  GF/C filter paper and dissolved micronutrients such as nitrite, nitrate, reactive silicate and inorganic phosphate were estimated by following standard methods described by Strickland and Parsons (1972) and measurements were made by using a PC based double beam Spectrophotometer (Shimadzu UV-2450).

Phytoplankton biomass in all the cultures was obtained as chlorophyll fluorescence. Chlorophyll *a* concentration was determined by a pre-calibrated fluorometer (Turner Designs, Trilogy) after extraction with 90% acetone (UNESCO, 1994). The growth rate (*R*) of phytoplankton in each tank was estimated on a daily basis, employing the equation  $R = \ln(\text{Chl}_t/\text{Chl}_0)/t$ , where  $\text{Chl}_t$  is concentration of chlorophyll after the time *t* (day), and  $\text{Chl}_0$  is the initial chlorophyll concentration (Reynold, 1984). Measurements were done up to 7 days to obtain the growth rate of phytoplankton with respect to silicate concentration.

### 3. Results

During the enrichment experiment, the observed water temperature (Figure 1) was varied between  $26.6$  and  $29.8^\circ\text{C}$  in all the tanks with the maximum temperature on 5<sup>th</sup> day of the experiment, while the salinity in all the tanks were increased from the 1<sup>st</sup> day onwards from 33‰ to 37‰ at the end of the experiment (Figure 2). The pH values were not dramatically changed in all tanks and it ranged between 8.01 and 8.64 with the minimum on the 1<sup>st</sup> day of the experiment in tank 2 and maximum on the 6<sup>th</sup> day in tank 5 (Figure 3). The dissolved oxygen (DO) concentrations were found to be low ( $4.26\text{ mg l}^{-1}$ ) at the 1<sup>st</sup> day of the experiment and it was increased with increased chlorophyll concentration and the maximum DO concentration ( $6.38\text{ mg l}^{-1}$ ) was observed in the tank 5 on 7<sup>th</sup> day of the experiment which was coincided with the highest chlorophyll concentration (Figure 4).

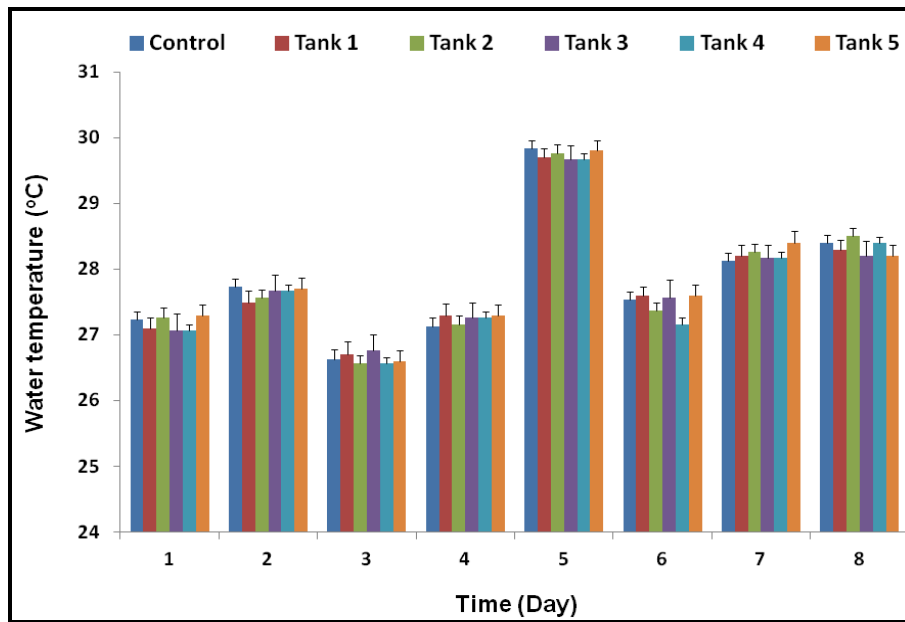


**Figure 1:** Variation of Water Temperature Recorded during the Experiment Period in Different Tanks

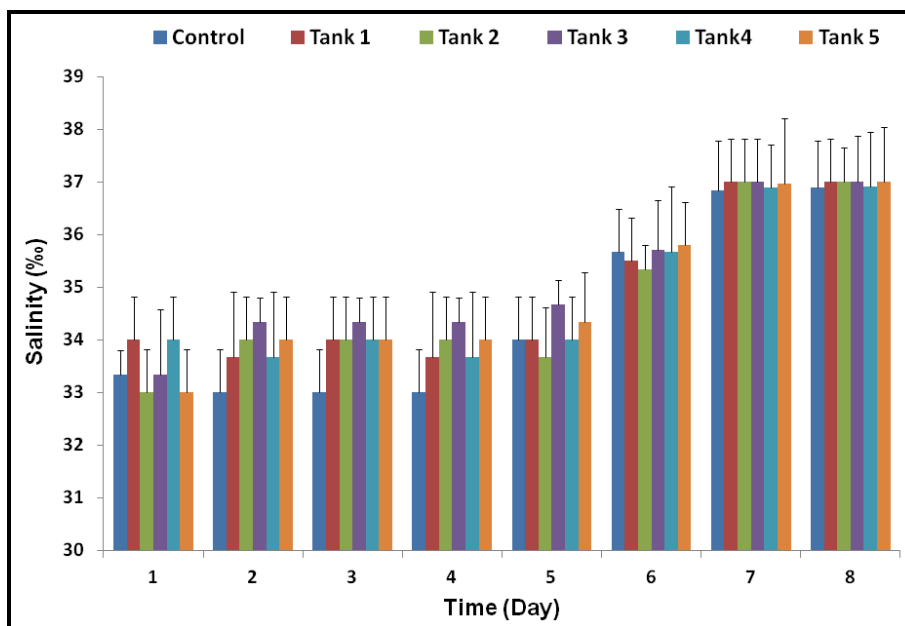


**Figure 2:** Variation of Salinity Recorded during the Experiment Period in Different Tanks

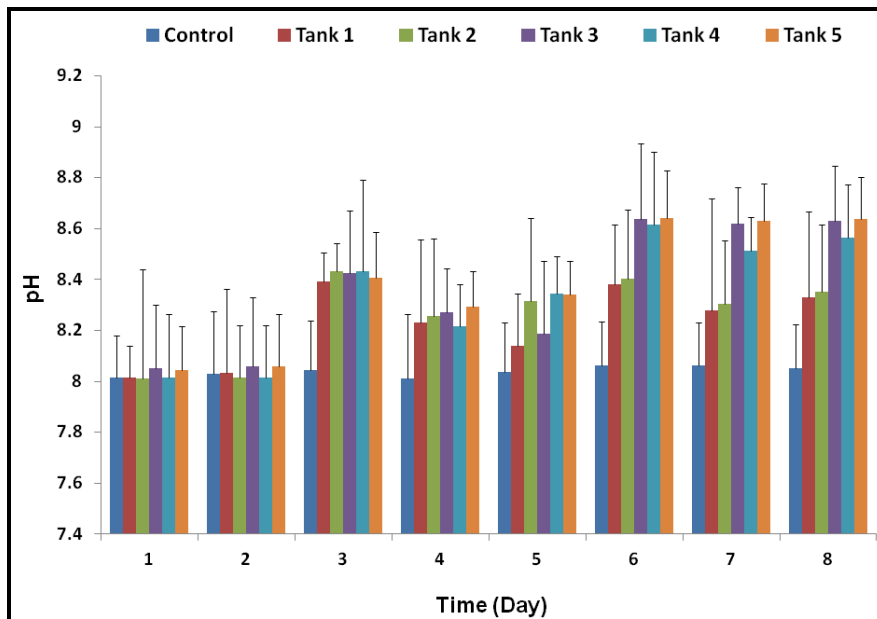


**Figure 3:** Variation of pH Recorded during Experiment Period in Different Tanks

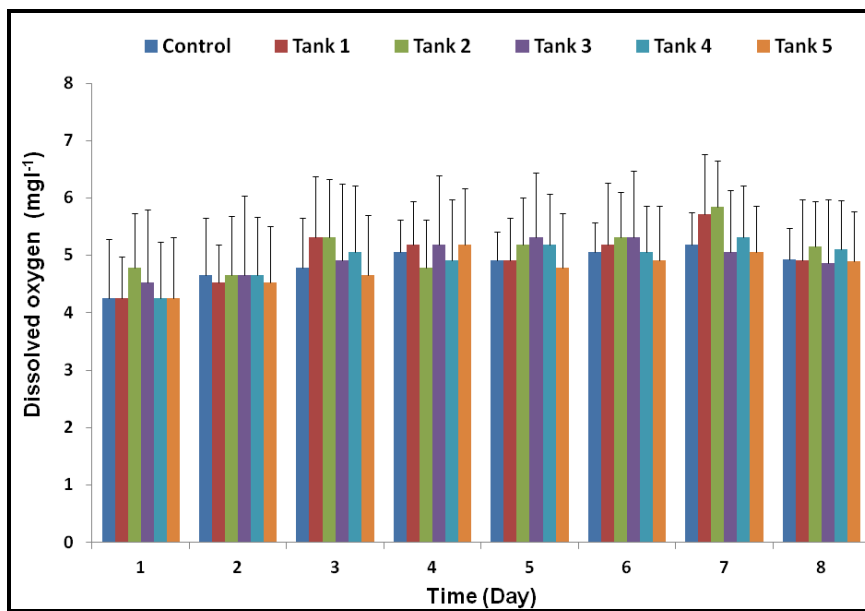


**Figure 4:** Variation of Dissolved Oxygen Recorded during Experiment Period in Different Tanks

The observed nutrients and chlorophyll concentrations during the enrichment experiment was shown in Figures 5-9. At the first day of the experiment all the tanks recorded with high nutrient ( $\text{NO}_3 - 9.44\mu\text{M}$ ,  $\text{NO}_2 - 1.51 \mu\text{M}$ ,  $\text{PO}_4 - 24.40 \mu\text{M}$ ,  $\text{SiO}_3 - 45.60 \mu\text{M}$ ) and low chlorophyll ( $1.17 \mu\text{g l}^{-1}$ ) concentrations, after that the chlorophyll concentration started to increase with decreasing nutrients in all the tanks and it registered the maximum chlorophyll concentration ( $8.90 \mu\text{g l}^{-1}$ ) at the end of the day 7<sup>th</sup> day with the lowest nutrient concentrations ( $\text{NO}_3 - 4.5 \mu\text{M}$ ,  $\text{NO}_2 - 0.56 \mu\text{M}$ ,  $\text{PO}_4 - 14.19 \mu\text{M}$ ,  $\text{SiO}_3 - 6.11 \mu\text{M}$ ). Followed by this, the chlorophyll concentration has been declined on the 8<sup>th</sup> day.

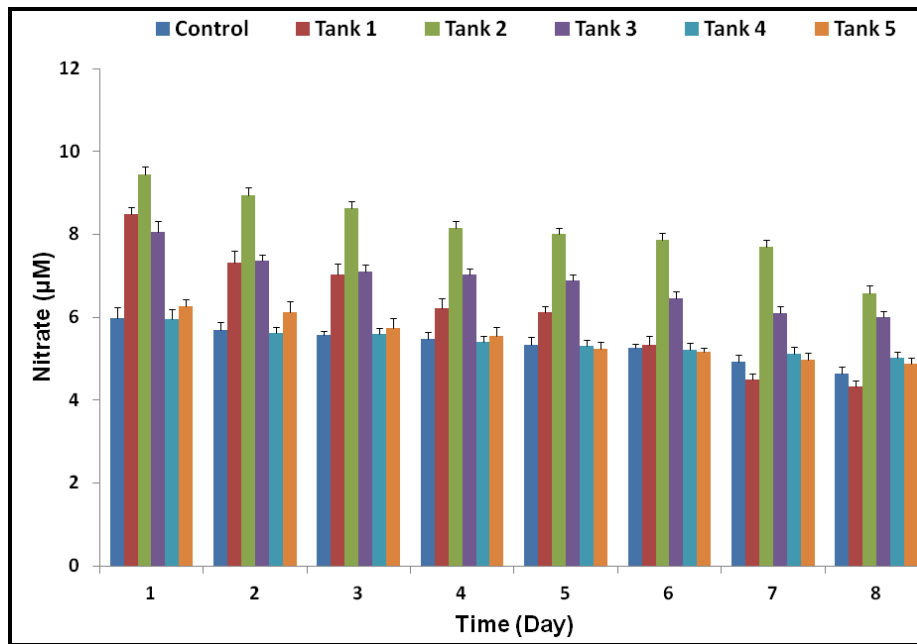


Figure 5: Variation of Nitrate (NO<sub>3</sub>) Concentration Recorded During Experiment Period in Different Tanks

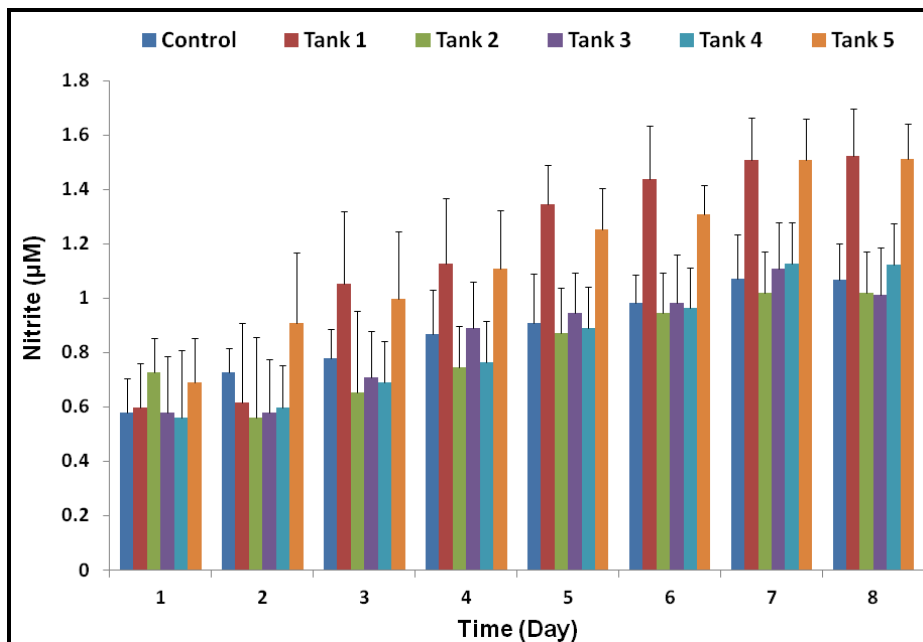
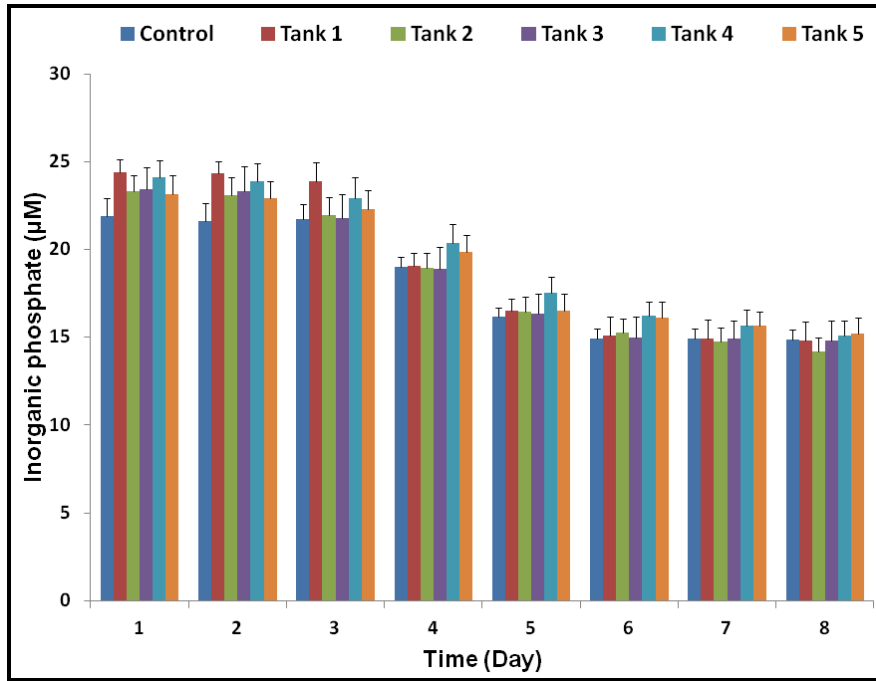
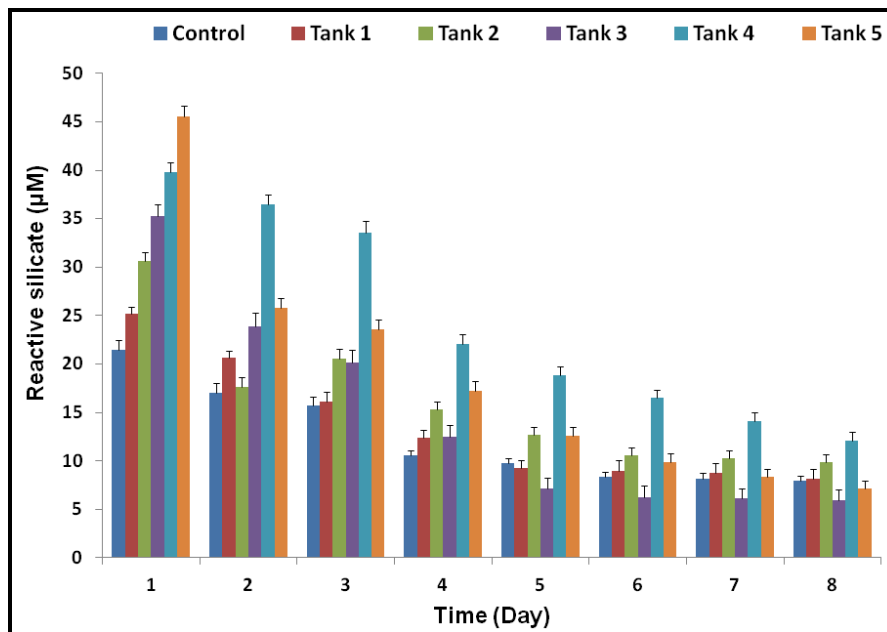


Figure 6: Variation of Nitrite (NO<sub>2</sub>) Concentration Recorded During Experiment Period in Different Tanks



**Figure 7:** Variation of Inorganic Phosphate ( $PO_4$ ) Concentration Recorded during Experiment Period in Different Tanks



**Figure 8:** Variation of Reactive Silicate ( $SiO_3$ ) Concentration Recorded During the Experiment Period in Different Tanks

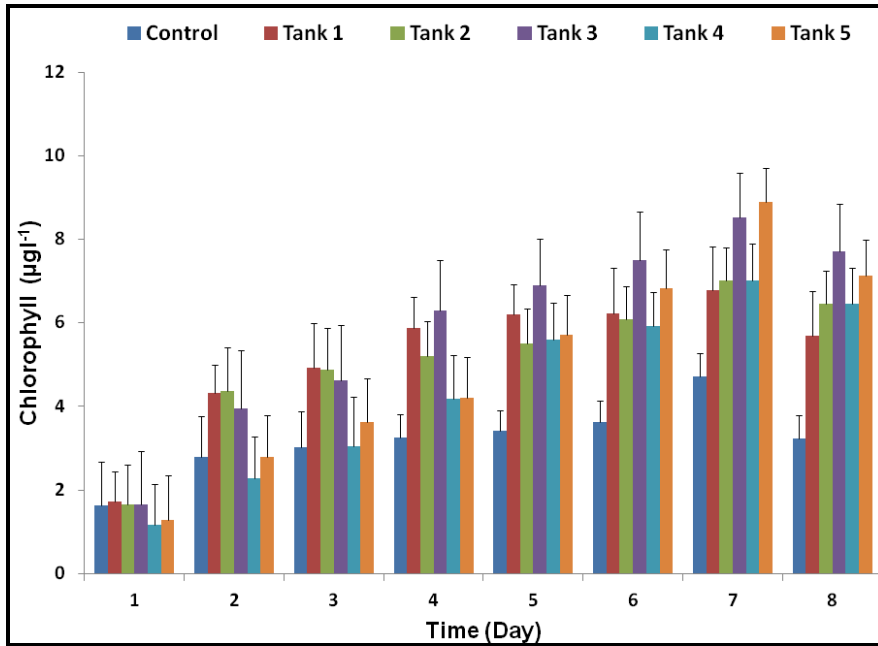


Figure 9: Variation of Chlorophyll Concentration Recorded During the Experiment in Different Tanks

During the experiment the Si:N and Si:P ratio registered the maximum (6.554, 1.971) in the tank 1 and tank 5 respectively with the minimum Si:N ratio (0.845) on 6<sup>th</sup> day and Si:P ratio (0.409) on the 7<sup>th</sup> day in tank 3 (Figures 10 & 11). The growth rates for phytoplankton as inferred from the chlorophyll a concentration in the experiment are shown in Figure 12. Significant increase in chlorophyll a concentration recorded in tank 5 supplemented with 25 µM silicate and it also shown the higher growth rate ( $0.277d^{-1}$ ) than control on 7<sup>th</sup> day of experiment. Almost all experimental tanks recorded higher growth rate than the control indicating silicate as limiting nutrient in controlling phytoplankton especially diatoms. Small changes in chlorophyll a concentration was observed in other four tanks with silicate additions of 5, 10, 15, 20 µM respectively. The regression analysis between silicate and chlorophyll measurements showed the significant correlation ( $R^2 = 0.609$ ) and inverse relationship between both parameters in all the tanks throughout the experiment period (Figure 13).

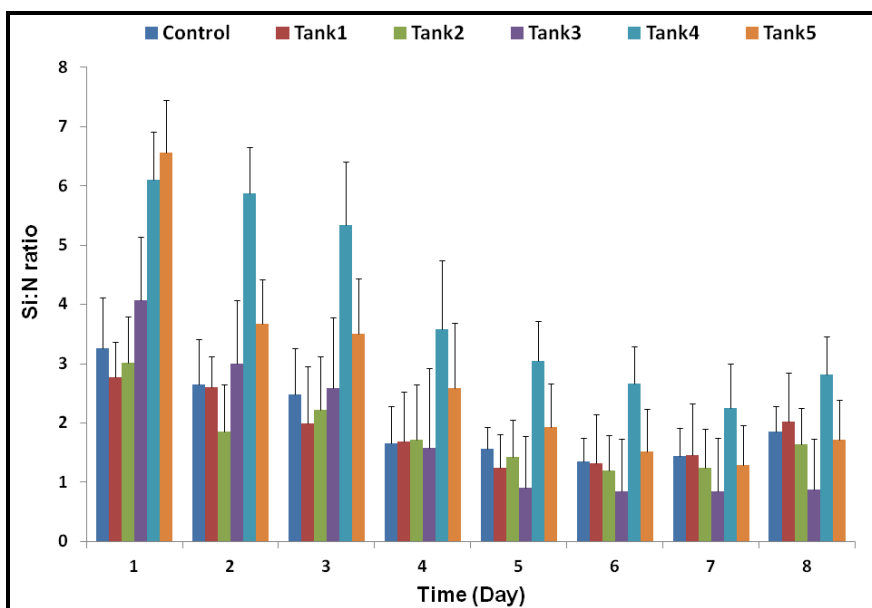


Figure 10: Variation of Si: N Ratio Recorded During the Experiment in Different Tanks

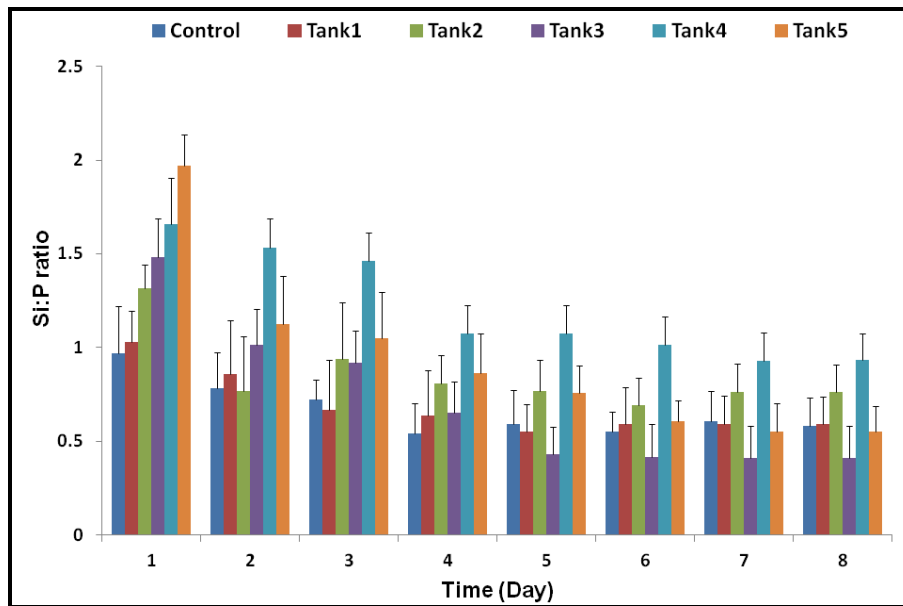


Figure 11: Variation of Si:P Ratio Recorded During the Experiment in Different Tanks

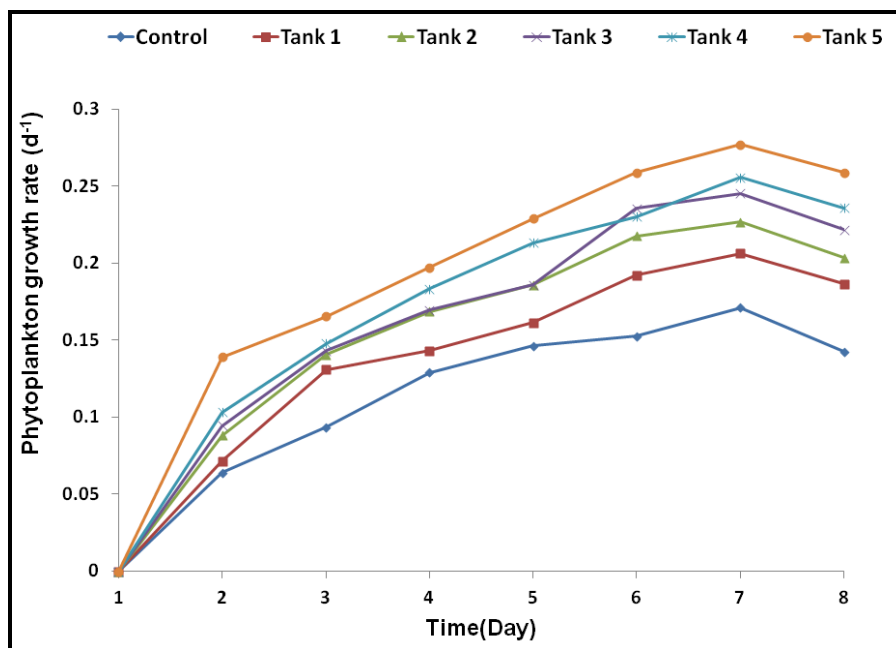
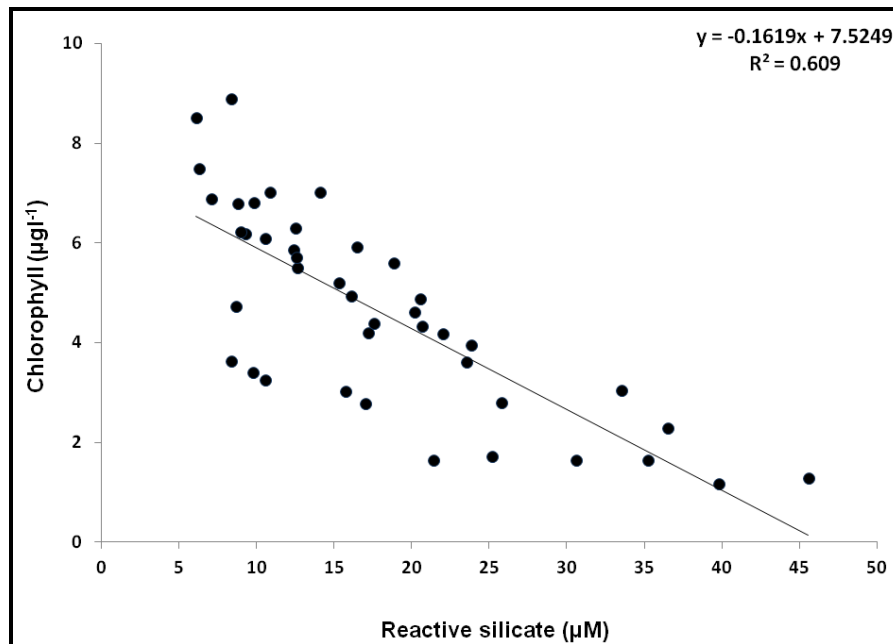


Figure 12: Trends of Phytoplankton Growth Rate in Experimental Tanks



**Figure 13:** Regression Plot of Reactive Silicate ( $\text{SiO}_3$ ) and Chlorophyll

Thus from the above results, it was confirmed that the addition of nutrients promote the phytoplankton growth, while addition of the highest silicate concentrations enhanced the phytoplankton growth further when compared to other nutrients during the experiment. This confirmed that the silicate act as one of the limiting nutrient for the phytoplankton production especially when diatoms dominating the phytoplankton community structure.

#### 4. Discussion

Nutrients limitation of phytoplankton has been reported extensively in different seas. Among those nutrients, nitrogen and phosphorus play particularly important role in limiting biological productivity (Gruber, 2004). Phytoplankton growth can also be limited by silica and trace elements (Harrison *et al.*, 1987; Martin *et al.*, 1991; Ditullio *et al.*, 1993). Previously, nutrient enrichment experiments carried out in different parts of the world indicates the role of specific nutrients in promoting the phytoplankton abundance. Nitrate addition was strongly promoted phytoplankton bloom, which was also proved by the nutrient enrichment experiments of the northwestern Indian ocean (Takeda *et al.*, 1995); adding nitrate and phosphate separately or together in the central Indian ocean (Tang *et al.*, 2009) *in-situ* nutrient enrichment experiment in the Bohai and Yellow sea by adding nitrate, phosphate and silicate (Zou *et al.*, 2001) etc.

During experimental period, temperature not showed any significant variation between the tanks as all the tanks were exposed to open sunlight. Previous studies (Eppley, 1972; Goldman *et al.*, 1974; Yoder, 1979) have proved that temperature plays an important role in the growth of diatoms. However, the community sensitivity to temperature may be far smaller than the species sensitivity because of the adaptation of different organisms to a specific temperature range (Sarmiento and Gruber, 2006). From this experiment results, it is evident that temperature does not play any important role on the growth of phytoplankton as a community.

The salinity values were increased from the first day up to the end of the experiment which might be due to the evaporation of the surface water with increase in temperature (Govindasamy *et al.*, 2000; Gowda *et al.*, 2001; Rajasegar, 2003) and not compensated with any additional water supply. In the present study, the pH not showed significant variation (8.01 to 8.64) and well within the optimal pH

range (6.5 to 8.2) for sustainable aquatic life (Murdoch *et al.*, 2001; Adeyemo *et al.*, 2008) especially for the phytoplankton growth. The DO level varied between  $4.26 \text{ mg l}^{-1}$  (1<sup>st</sup> day) and  $6.38 \text{ mg l}^{-1}$  (7<sup>th</sup> day). DO is the measure of photosynthetic activity of phytoplankton biomass (Satpathy *et al.*, 2009), this is clearly evident from the significant positive relationship obtained for DO with phytoplankton biomass. Even in the present study a gradual increase of DO with increase of chlorophyll was noted when the experiment progresses.

In the aquatic environment ambient Si:N concentration ratios have been used (Howarth, 1988; Levasseur and Therriault, 1987) to identify silicate or nitrate as the limiting nutrient. Since the Si:N:P ratio of the diatoms is calculated as 16:16:1 (Brzezinski, 1985). Silicate through its link to diatom structure and metabolism may control phytoplankton processes in important regions of the ocean (Dugdale, 1972; Dugdale and Goering, 1970; Dugdale *et al.*, 1981).

Nutrient enrichment increased phytoplankton biomass indicating nutrient limitation. Most probably this nutrient limitation in an environment has been studied by using the nutrient ratios such as N:P, N:Si, and Si:P. Si:N ratios were  $>1$  during experiment suggesting silicate enriched nutrient regime in the water column (Paul *et al.*, 2008) and it indicated silicate as a primary limiting nutrient than nitrate while adding the higher concentrations of silicate in the tanks (Kudela and Dugdale, 2000). While, Si:P ratios were found to be low ( $<1$ ) and it could be attributed to the higher phosphate concentrations available in the water than the silicate.

Silicate depletion along with the nitrate excess in the seawater could be an indication of diatom dominance (Goffart *et al.*, 2000; Goeyens *et al.*, 2000). Such a diatom dominated system has the potential for the possible silicate limitation. Moreover, indirect evidence of the link between phytoplankton community structure and carbon exportation is given by nitrate and silicate signatures (Goeyens *et al.*, 1991; Lancelot, 1993). The high abundance of diatoms could be attributed to the high Si:N ratio or low Si:P ratio such realms are reported to support diatom dominated systems (Bethoux *et al.*, 2002).

Variation in concentrations of nutrients during the experimental period showed the significant utilization of nutrients by phytoplankton for their survival. At the first day of the experiment all the nutrients registered their uniform concentrations in all the tanks with minimum chlorophyll concentration. The highest chlorophyll concentration was observed in tank 5 at the end of the experiment with very low silicate concentration than other tanks, suggesting that rapid uptake of silicate by the phytoplankton and it is also confirmed by the regression analysis between silicate and chlorophyll with good correlation coefficient ( $R^2 = 0.609$ ) which showed inverse relationship with significant decrease of silicate with increase in chlorophyll. On the other hand the utilization of nitrate and phosphate was found to be lower than silicate and varied marginally throughout the experiment period which indicates a preference of silicate by the diatoms clearly.

Several studies support that silicate can potentially limit phytoplankton growth (Conely and Malone, 1992; Egge and Aksnes, 1992; Smith and Hitchcock, 1994; Justic *et al.*, 1995; Kudela and Dugdale, 2000). The phytoplankton growth rate also found to be high in the tank 5 whereas control tank showed the very less growth rate than the other tanks, suggesting that addition of silicate at various concentrations in tanks could enhance the phytoplankton population with respect to their nutrient ratios. Tomasky *et al.* (1999) found evidence of such increased phytoplankton biomass in response to nutrient additions in experimental enclosures.

## 5. Conclusion

The present experiment on nutrient enrichment with addition of silicate confirmed the influence of silicate on the phytoplankton growth especially diatoms and composition in the excess of other nutrients such as nitrate and phosphate. Despite nitrogen and phosphorous, our experimental results clearly confirmed the uptake of silicate by phytoplankton and suggested that silicate plays a decisive role in diatom growth and act as a limiting nutrient in the diatom dominated waters. Silicate is extensively used to determine the phytoplankton community structure of the aquatic environment. The regression values can further be tested in natural conditions to establish chlorophyll and silicate ratio so as to develop algorithms for silicate estimation using remote sensing techniques.

## Acknowledgement

The authors are thankful to the authorities of Annamalai University for their support and encouragement during the course of study.

## References

- Adeyemo, O.K., Adedokun, O.A., Yusuf, R.K., and Adeleye, E.A. *Seasonal Changes in Physico-Chemical Parameters and Nutrient Load of River Sediment in Ibadan City, Nigeria*. Global Nest Journal. 2008. 10 (3) 326-336.
- Bethoux, O., Nel, A., Lapeyrie, J., Gand, G., and Galtier, J., *Raphogla rubra* gen. *The Oldest Representative of the Clade of Modern Ensifera (Orthoptera; Tettigoniidea, Gryllidea)*. European Journal of Entomology. 2002. 99; 111-116.
- Brzezinski, M.A. *The Si:C:N Ratio of Marine Diatoms; Inter Specific Variability and the Effect of Some Environmental Variables*. Journal of Phycology. 1985. 21; 347-357.
- Brzezinski, M.A. *Cell-Cycle Effects on the Kinetics of Silicic Acid Uptake and Resource Competition among Diatoms*. Journal of Plankton Research. 1992. 14; 1511-1536.
- Brzezinski, M.A., Olson, R.J., and Chisholm, S.W. *Silicon Availability and Cell Cycle Progression in Marine Diatoms*. Marine Ecological Progress Series. 1990. 67; 83-96.
- Conley, D.J., and Malone, T.C. *Annual Cycle of Dissolved Silicate in Chesapeake Bay; Implications for the Production and Fate of Phytoplankton Biomass*. Marine Ecological Progress Series. 1992. 81; 121-128.
- Day, J.W., Hopkinson, J.R., and Conner, C.S., 1982: *An Analysis of Environmental Factors Regulating Community Metabolism and Fisheries Production in a Louisiana Estuary*. In: Estuarine Comparisons; Kennedy, V.S. (Ed.). New York: Academic Press. 121-136.
- Ditullio, G.R., Hutchins, A.D., and Bruland, W.K. *Interaction of Iron and Major Nutrients Controls Phytoplankton Growth and Species Composition in the Tropical North Pacific Ocean*. Limnology and Oceanography. 1993. 38 (3) 495-508.
- Downing, M., 1997: *Facilitating Market Development*. Energy Crops Forum. Fall. 2.
- Dugdale, R.C, Jones, B.H., MacIsaac, J.J., and Goering, J.J. *Adaptation of Nutrient Assimilation*. In: Physiological Bases of Phytoplankton Ecology; T. Platt (Ed.). Canadian Bulletin of Fisheries and Agricultural Sciences. 1981. 210; 234-250.

- Dugdale, R.C., and Goering, J.J. *Nutrient Limitation and the Path of Nitrogen in Peru Current Production Scientific Results of the South East Pacific Expedition*. Anton Bruun Report. 1970. 5; 5.3-5.8.
- Dugdale, R.C. *Chemical Oceanography and Primary Productivity in Upwelling Regions*. Geoforum. 1972. 11; 47-61.
- Dugdale, R.C., Wilkerson, F.P., and Minas, H.J. *The Role of a Silicate Pump in Driving New Production*. Deep Sea Research. 1995. 42; 697-719.
- Dugdale, R.C., 1983: *Effects of Source Nutrient Concentrations and Nutrient Regeneration on Production of Organic Matter in Coastal Upwelling Centers*. In: *Coastal Upwelling*. Plenum Press. 175-182.
- Dugdale, R.C. *The Effects of Varying Concentration on Biological Production in Upwelling Regions*. CALCOF, Report. 1985. 26; 93-96.
- Egge, J.K., and Aksnes, D.L. *Silicate as Regulation Nutrient in Phytoplankton Competition*. Marine Ecological Progress Series. 1992. 83; 281-289.
- Eppley, R.W. *Temperature and Phytoplankton Growth in the Sea*. Fisheries Bulletin. 1972. 70; 1063-1085.
- Falkowski, P.G., Barber, R.T., and Smetacek, V. *Biogeochemical Controls and Feedbacks on Ocean Primary Production*. Science. 1998. 281; 200-206.
- Fisher, T.R., Gustafson, A.B., Sellner, K., Lacouture, R., Haas, L.W., Wetzel, R.L., Magnien, R., Everitt, D., Michaels, B., Karrh, R. *Spatial and Temporal Variation of Resource Limitation in Chesapeake Bay*. Marine Biology. 1999. 133; 763-778.
- Goeyens, L., Sorensson, F., Treguer, P., Morvan, J., Panouse, M., and Dehairs, F. *Spatiotemporal Variability of Inorganic Nitrogen Stocks and Uptake Fluxes in the Scotia Weddell Confluence area during November and December*. Marine Ecological Progress Series. 1991. 77; 7-19.
- Goeyens, L., Elskens, M., Catalano, G., Lipizer, M., Hecq, J.H., and Goffart, A. *Nutrient Depletions in the Ross Sea and Their Relation with Pigment Stocks*. Journal of Marine Systems. 2000. 27; 195-208.
- Goffart, A., Catalano, G. and Hecq, J.H. *Factors Controlling the Distribution of Diatoms and Phaeocystis in the Ross Sea*. Journal of Marine Systems. 2000. 27; 161-175.
- Goldman, J.C., Oswald, W.J., and Jenkins, D. *The Kinetics of Inorganic Carbon Limited Algal Growth*. Journal of Water Pollution Control Federation. 1974. 46; 554-571.
- Govindasamy, C., Kannan, L., and Azariah, J. *Seasonal Variation in Physico-Chemical Properties and Primary Production in the Coastal Water Biotopes of Coromandel Coast, India*. Journal of Environmental Biology. 2000. 21; 1-7.
- Gowda, G., Gupta, T.R.C., Rajesh, K.M., Gowda, H., Lingadhal C., and Ramesh, A.M. *Seasonal Distribution of Phytoplankton in Nethravathi Estuary, Mangalore*. Journal of Marine Biological Association of India. 2001. 43; 31-40.

- Gruber, N., 2004: *The Dynamics of the Marine Nitrogen Cycle and Its Influence on Atmospheric CO<sub>2</sub>*. In: *The Ocean Carbon Cycle and Climate*; Follows, M., and Oguz, T., (Eds.). NATO ASI Series, Dordrecht: Kluwer Academic. 97-148.
- Harrison, W.G., Platt, T., and Lewis, M.R. *F-Ratio and Its Relationship to Ambient Nitrate Concentration in Coastal Waters*. *Journal of Plankton Research*. 1987. 9; 235-245.
- Hecky, R.E., and Kilham, P. *Nutrient Limitation of Phytoplankton in Freshwater and Marine Environments: A Review of Recent Evidence on the Effects of Enrichment*. *Limnology and Oceanography*. 1988. 33 (4) 196-822.
- Howarth, R.W. *Nutrient Limitation of Net Primary Production in Marine Ecosystems*. *Annual Review of Ecological Systems*. 1988. 19; 89-110.
- Justic, D., Rabalais, N.N., Turner, R.E., and Dortch, Q. *Changes in Nutrient Structure of River Dominated Coastal Waters; Stoichiometric Nutrient Balance and its Consequences*. *Estuarine Coastal and Shelf Sciences*. 1995. 40; 339-356.
- Kudela, R.M., and Dugdale, R.C. *Regulation of Phytoplankton New Production as Determined by Enclosure Experiments with Nutrient Additions in Monterey Bay, California*. *Deep-Sea Research*. 2000. 2 (47) 1023-1053.
- Lancelot, C. *The Mucilage Phenomenon in the Continental Coastal Waters of the North Sea*. *Science of Total Environment*. 1993. 165; 83-112.
- Lane, M.E., Kirshen, P.H., and Vogel, R.M. *Indicators of the Impacts of Global Climate Change on U.S. Water Resources*. *Journal of Water Research PL-ASCE*. 1999. 125 (4) 194-204.
- Levasseur, M.E., and Therriault, J.C. *Phytoplankton Biomass and Nutrient Dynamics in a Tidally Induced Upwelling; The Role of the N; Si, Ratio*. *Marine Ecological Progress Series*. 1987. 39; 87-97.
- Martin, J.H., Gordon, R.M., and Fitzwater, E.S. *The Case for Iron Limitation*. *Limnology and Oceanography*. 1991. 36 (8) 1793-1802.
- Murdoch T., Cheo, M., and O'Laughlin, K., 2001; *Streamkeeper's Field Guide; Watershed Inventory and Stream Monitoring Methods*. Adopt-A-Stream Foundation, Everett, WA. 297.
- Rajasegar, M. *Physico-Chemical Characteristics of the Vellar Estuary in Relation to Shrimp Farming*. *Journal of Environmental Biology*. 2003. 24; 95-101.
- Reynolds, C.S., 1984: *The Ecology of Freshwater Phytoplankton*. Cambridge: Cambridge University Press. 384.
- Sakshaug, E., Slagstad, D., and Holm-hansen, O. *Factors Controlling the Development of Phytoplankton Blooms in the Antarctic Ocean – A Mathematical Model*. *Marine Chemistry*. 1991. 35; 259-271.
- Sarmiento, J.L., and Gruber, N. *Ocean Biogeochemical Dynamics, Princeton*. *Nature*. 2006. 441; 964-967.

- Satpathy, K.K., Gouri Sahu, Mohanty, A.K., Prasad, M.V.R., and Panigrahy, R.C. *Phytoplankton Community Structure and Its Variability During Southwest to Northeast Monsoon Transition in the Coastal Waters of Kalpakkam, East Coast of India*. International Journal of Oceans and Oceanography. 2009. 3 (1) 43-74.
- Smith, G.I., and Hitchcock, R. *Nutrient Enrichments and Phytoplankton Growth in the Surface Waters of the Louisiana Bight*. Estuaries. 1994. 17 (4) 740-753.
- Strickland, J.D., and Parsons, T.R. *A Manual of Seawater Analysis*. Fisheries Research Board of Canada. 1972. 167; 310.
- Takeda, S., Kamarani, A., and Kawanobe, K. *Effects of Nitrogen and Iron Enrichments on Phytoplankton Communities*. Marine Chemistry. 1995. 50; 229-241.
- Tang, S., Jiang, L., and Wu, Z.J. *Adding Nitrate and Phosphate Separately or Together in the Central Indian Ocean; A Nutrient Enrichment Experiment*. Ocean Science Discussions. 2009. 6; 2649-2666.
- Tomasky, G., Barak, J., Valiela, L., Behr, P., Soucy, L., and Foreman, K. *Nutrient Limitation of Phytoplankton Growth in Waquoit Bay, Massachusetts, USA; A Nutrient Enrichment Study*. Aquatic Ecology. 1999. 33; 47-55.
- UNESCO. *Protocols for the Joint Global Ocean Flux Study (JGOFS) Core Measurements*. In: IOC Manuals and Guides. UNESCO Paris. 1994. 29; 97-100.
- Whipple, G.C., and Jackson, D.D. *Asterionella- Its Biology, Its Chemistry, and Its Effect on Water Supplies*. Journal of New England Water Works Association. 1899. 4; 1-25.
- Yoder, J. *Effect of Temperature on Light-Limited Growth and Chemical Composition of Skeletonema Costatum (Bacillariophyceae)*. Journal of Phycology. 1979. 15; 362-370.
- Zou, L., Zhang, J., Pan W.X., and Pengzhan, Y. *In Situ Nutrient Enrichment Experiment in the Bohai Yellow Sea*. Journal of Plankton Research. 2001. 23 (10) 1111-1119.

## Nutrient Enrichment Experiment to Establish Relationship between Chlorophyll and Phosphate

D. Poornima<sup>1</sup>, K. Thennarasu<sup>1</sup>, R. Ranith<sup>1</sup>, R. Shanthi<sup>1</sup>, R.K. Sarangi<sup>2</sup>, and T. Thangaradjou<sup>1</sup>

<sup>1</sup>Centre of Advanced Study in Marine Biology, Faculty of Marine Sciences, Annamalai University, Parangipettai, Tamilnadu, India

<sup>2</sup>Marine Biology Division, Marine, Earth and Planetary Sciences Group, Space Application Centre (ISRO), Ahmedabad, Gujarat, India

Correspondence should be addressed to T. Thangaradjou, umaradjou@yahoo.com

Publication Date: 1 December 2014

Article Link: <http://scientific.cloud-journals.com/index.php/IJAESE/article/view/Sci-252>



Copyright © 2014 D. Poornima, K. Thennarasu, R. Ranith, R. Shanthi, R.K. Sarangi, and T. Thangaradjou. This is an open access article distributed under the **Creative Commons Attribution License**, which permits unrestricted use, distribution, and reproduction in any medium, provided the original work is properly cited.

**Abstract** *In-situ* nutrient enrichment experiment was conducted to know the relationship between chlorophyll and phosphate so as to assess the significant role of phosphate in the phytoplankton growth. During the experiment period temperature (27.9-33.7°C), salinity (31-35 ‰) and pH (7.74-8.07) values were not shown dramatic changes as the experimental studies are conducted for the short period only. DO was found to show an oscillating trend (2.77-6.68 mg l<sup>-1</sup>) with phytoplankton population variations. Nutrient concentrations (NO<sub>3</sub>:1.05-12.63 μM, NO<sub>2</sub>:0.29-1.67 μM, PO<sub>4</sub>: 0.07-28.32 μM and SiO<sub>3</sub>:4.19-23.89 μM) showed maximum concentration at the first and second day of the experiment in enrichment tanks and it gradually decreased (PO<sub>4</sub> and SiO<sub>3</sub>) on last day of the experiment period. The pronounced maximum chlorophyll concentration in tank 5 on 5<sup>th</sup> day corresponding with addition of highest concentration of phosphorus, clearly pointed out that phosphorus addition had influenced the plankton growth. Increased utilization of PO<sub>4</sub> and support of SiO<sub>3</sub> indicates diatoms prefer silicate and phosphate for growth than the nitrates. Nitrate enrichment in the tank in later part of the experiment indicates nitrogen cycling processes. Increased phytoplankton uptake and growth rate at tank 5 when compared to control, substantially proved the uptake of phosphate by phytoplankton under culture system.

**Keywords** *Chlorophyll; Nitrate; N:P Ratio; Phosphate; Reactive Silicate*

### 1. Introduction

Phytoplankton are the most important primary producers of the aquatic environment and contributes up to 50% of the global primary production. Phytoplankton growth in estuaries and coastal seas is dependent on a number of parameter, especially nutrient availability, light penetration and intensity and mixing with in the water column. Nutrient availability is frequently referred as key factor regulating phytoplankton growth, biomass and species composition (Roelke *et al.*, 1999). Historically, nitrogen and phosphorus (Schindler, 1977; Wyne and Berman, 1980; Birch *et al.*, 1981; Lean and Pick, 1981)

are believed to be the nutrients most commonly limiting phytoplankton production in marine and fresh water ecosystems (Hecky and Kilham, 1988; Elser *et al.*, 1990; Dodds *et al.*, 1993).

Phosphorus plays a crucial role in energy transformation during algal photosynthesis. It is vital to algal metabolic processing including the synthesis of nucleotides, phospholipids and sugar phosphates (Wetzel, 1983). The diatom had reached its limits of growth with the available P. The P-enriched aquatic system utilized atmospheric nitrogen (N) and carbon (C) for algal production and this resulted in significant increase in ecosystem primary production. Phosphorus addition triggers undesirable cyanobacterial blooms unless N is added, however, addition of C or N in the absence of P enrichment the effects are minor (Schindler, 1974). According to Liebig's law of the minimum single nutrient should limit algal growth at any given time.

A common technique for determining nutrient limitation in phytoplankton is the nutrient enrichment bioassay (Hecky and Kilham, 1998) by measuring the phytoplankton growth in a sample containing a particular nutrient of interest and by keeping all other parameters constant. The effect of altered nutrient regimes on phytoplankton biomass can be quantified by measuring the community growth response to a controlled nutrient environment over short time intervals (Paerl, 1982). In this regard, short term (1 week) nutrient manipulation bioassays provide a management tool for addressing the issue of immediate phytoplankton response to enhanced nutrient concentrations (Conley, 2000; Conely *et al.*, 2009; Pearl, 2009). The present study was carried out to assess the significant role of phosphate in the phytoplankton growth for future remote sensing applications.

## 2. Materials and Methods

An enrichment experiment was carried out to determine the nutrient limitation status of phytoplankton. The experiment was commenced for 10 days with six 100 L open culture tanks containing 50 litres of filtered sea water each and kept in natural environmental condition. The seawater in all tanks was agitated with aerator. The natural phytoplankton concentrate dominated by diatoms (50 ml) was inoculated in all the tanks. The initial nutrient concentrations of experimental seawater are recorded (Table 1) and phytoplankton bloom was triggered with the addition of ammonium sulphate and urea in the ratio 10:2. Super phosphate ( $\text{NaH}_2\text{PO}_4$ ) (5, 10, 15, 20 and 25  $\mu\text{M}$ ) was added at different concentrations in order to obtain a situation which concentration of phosphate enhance phytoplankton biomass in tanks. Water samples at every 24 h was analysed for DO, pH, salinity, nutrients and chlorophyll *a* and temperature was measured. The same experiment was repeated two times for confirmation of the accuracy.

**Table 1:** Background Value of Experimental Seawater in the Tanks

Experiment	$\text{NO}_2$ ( $\mu\text{M}$ )	$\text{NO}_3$ ( $\mu\text{M}$ )	$\text{PO}_4$ ( $\mu\text{M}$ )	$\text{SiO}_3$ ( $\mu\text{M}$ )	Chl <i>a</i> ( $\mu\text{g l}^{-1}$ )
1	0.48	5.46	0.12	23.24	1.34
2	0.39	5.28	0.18	22.34	2.01
3	0.51	4.98	0.16	23.02	1.02

Surface water temperature was measured using digital multi-stem thermometer of 0.1°C accuracy. Salinity was estimated using a hand held refractometer (Atago hand refractometer, Japan) and the pH was measured using a pH meter (Cyberscan pH 1100) with the accuracy of  $\pm 0.05$ . Dissolved oxygen was estimated by following the modified Winkler's method (Strickland and Parsons, 1972). Filtered water samples (0.45 $\mu\text{m}$  GF/C filter paper) were used to analyse dissolved micronutrients such as nitrite, nitrate, reactive silicate and inorganic phosphate by following the methods described by Strickland and Parsons (1972) and measurements were made by using a PC based double beam spectrophotometer (Shimadzu UV-2450).

Chlorophyll *a* concentration determined by a pre-calibrated fluorometer (Turner Designs, Trilogy) after extraction with 90% acetone (UNESCO, 1994). The growth rate (*R*) of phytoplankton in each tank was estimated on a daily basis (Reynolds, 1984). Phosphate uptake was determined by measuring the disappearance of nutrients from tank each day. The uptake was calculated as follows:

$$V = C_i - C_t / t,$$

Where *V* is the daily uptake rate ( $\mu\text{M}$ ),  $C_i$  and  $C_t$  are the initial and final nutrient concentration respectively and *t* is the time period of uptake ( $\text{d}^{-1}$ ) (Domingues *et al.*, 2010). All the experiments were conducted for three times so as to have a check on change in environmental variables as the study was carried out in outdoor system.

### 3. Results

During the experiment, water temperature varied between 27.9 and 33.7°C in all the experimental tanks and registered maximum temperature on 7<sup>th</sup> day and minimum on 1<sup>st</sup> day of the experiment (Figure 1). Salinity values not showed drastic changes (31 to 35 ‰), and the maximum salinity recorded at last 3 days and minimum was recorded on 1<sup>st</sup> and 2<sup>nd</sup> day of the experiment in all tanks (Figure 2). pH values were not shown dramatic changes throughout the experiment period and it ranged between 7.74 (3<sup>rd</sup> days Tanks-2) and 8.07 (10<sup>th</sup> day tank-5) (Figure 3). Dissolved oxygen concentration varied between 2.77 and 6.68  $\text{mg l}^{-1}$ , the maximum DO content was observed in tank 3 on 6<sup>th</sup> day and minimum was observed in tank 3 on 10<sup>th</sup> day of the experiment (Figure 4).

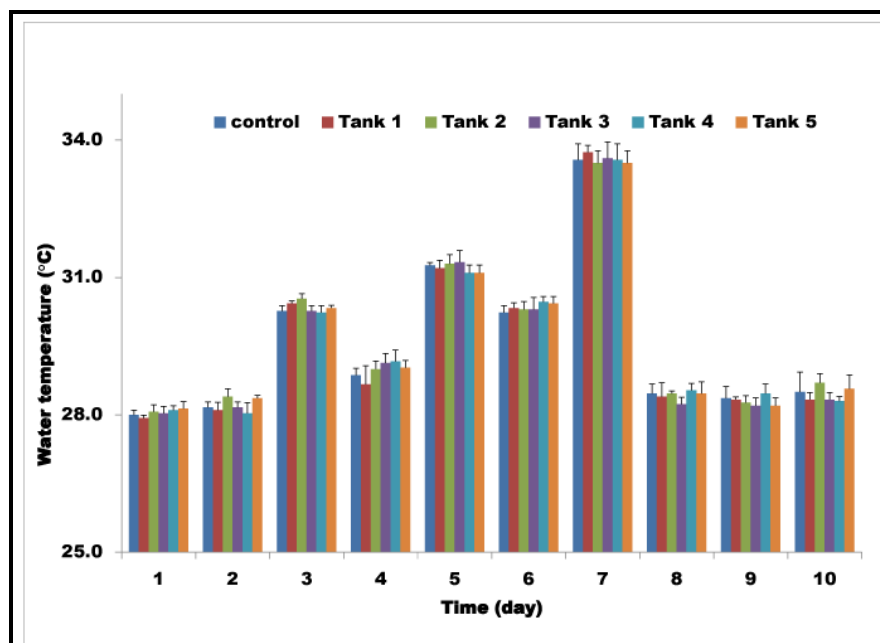


Figure 1: Variation of Water Temperature Recorded During the Experiment Period in Different Tanks

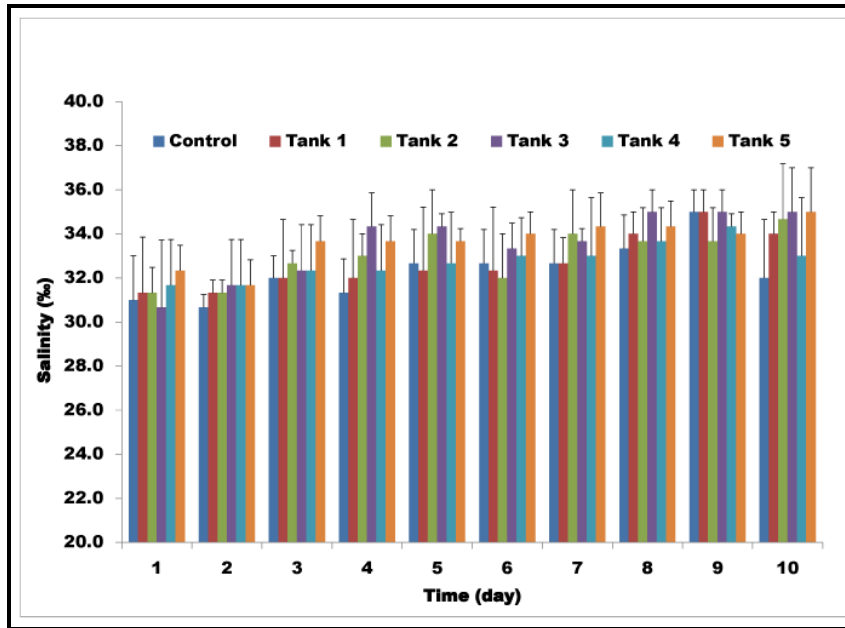


Figure 2: Variation of Salinity Recorded During the Experiment Period in Different Tanks

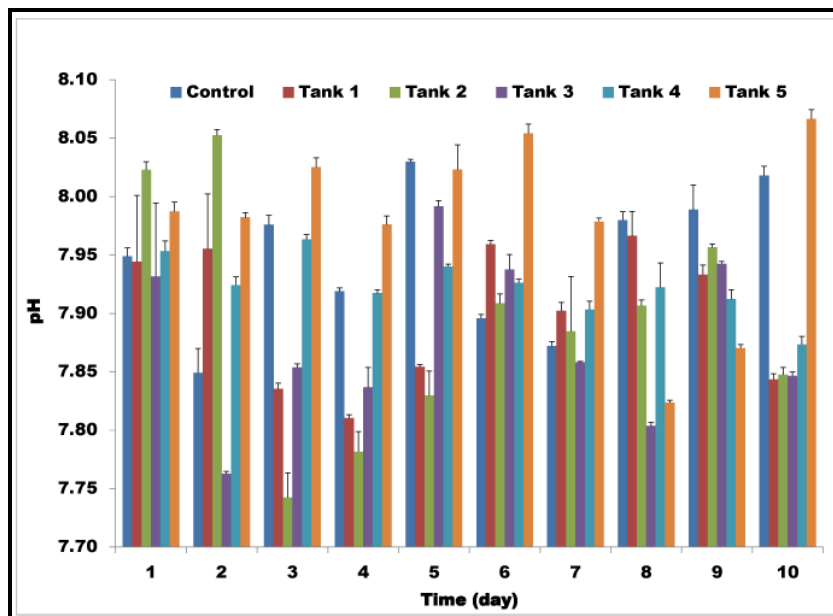


Figure 3: Variation of pH Recorded During the Experiment Period in Different Tanks

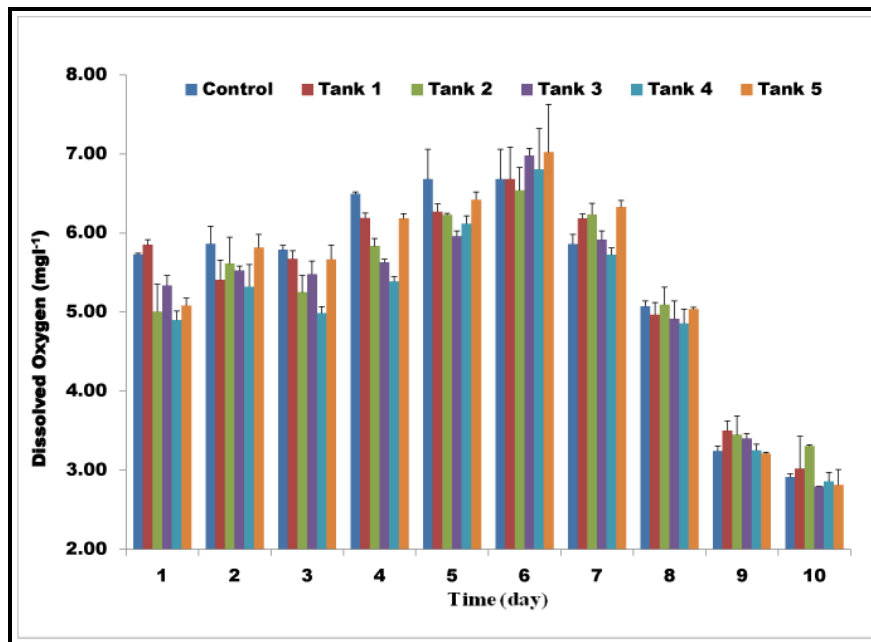


Figure 4: Variation of DO Recorded During the Experiment Period in Different Tanks

The inorganic nutrient concentrations were varied between the experimental tanks based on the nutrient addition with respect to culture period. The highest nitrate concentration (12.63  $\mu\text{M}$ ) was recorded in tank-5 on 1<sup>st</sup> day and lowest (1.05  $\mu\text{M}$ ) nitrate content was registered in tank-1 on 4<sup>th</sup> day (Figure 5). Nitrite concentration varied between 0.29  $\mu\text{M}$  in tank-5 on 6<sup>th</sup> day and 1.67  $\mu\text{M}$  in tank-2 on 1<sup>st</sup> day (Figure 7). Highest inorganic phosphate values (28.32  $\mu\text{M}$ ) were registered at tank-5 on 1<sup>st</sup> day of experiment and the minimum 0.79  $\mu\text{M}$  was recorded in tank-1 on 10<sup>th</sup> day. All the tanks have shown their higher phosphate concentration on the 1<sup>st</sup> day and lowest concentration on last day of the experiment (Figure 7).

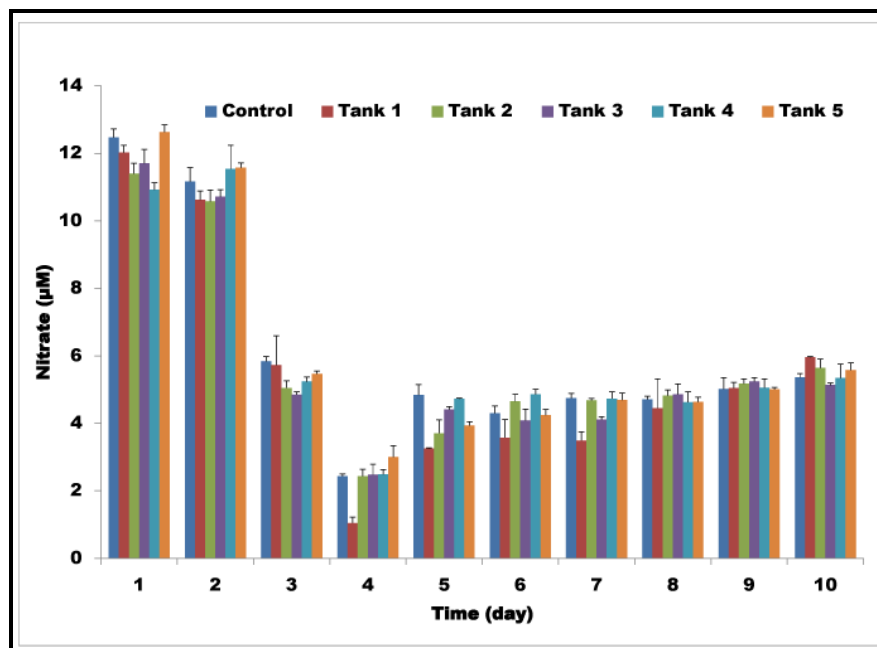
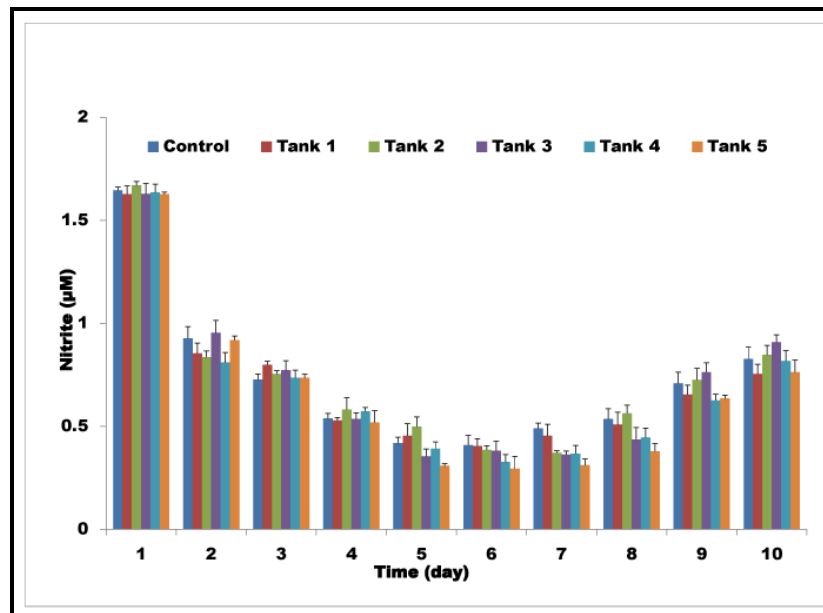
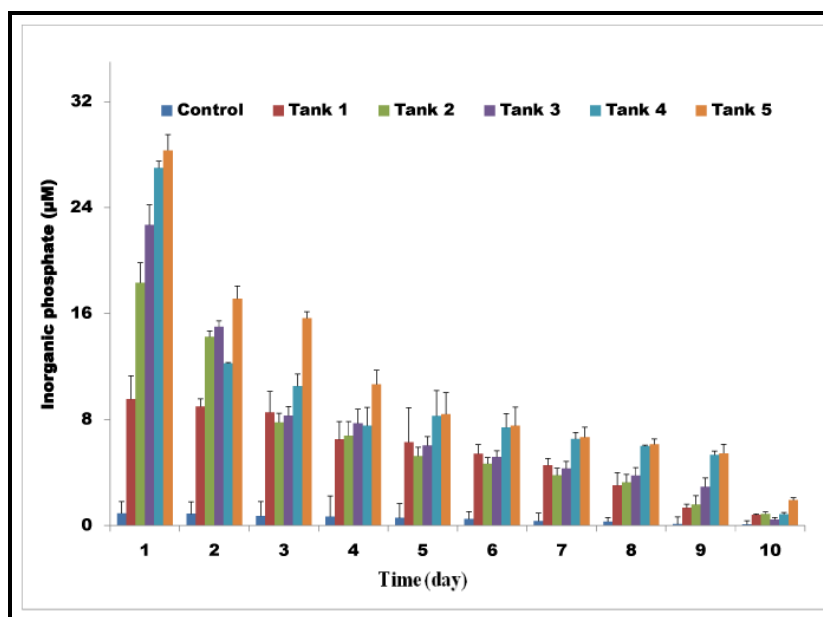


Figure 5: Variation of Nitrate ( $\text{NO}_3$ ) Concentration Recorded During the Experiment Period in Different Tanks



**Figure 6:** Variation of Nitrite ( $\text{NO}_2$ ) Concentration Recorded During the Experiment Period in Different Tanks



**Figure 7:** Variation of Inorganic Phosphate ( $\text{PO}_4$ ) Concentration Recorded During the Experiment Period in Different Tanks

The silicate concentrations in the tanks were ranged from 4.19 to 23.89  $\mu\text{M}$ . The minimum silicate concentration was registered on 10<sup>th</sup> day and the maximum concentration was observed on 1<sup>st</sup> day in tank-3 (Figure 8). Chlorophyll a concentration varied between 1.5 and 10.77  $\mu\text{g l}^{-1}$  with the highest and lowest value in tank-5 on 5<sup>th</sup> and 1<sup>st</sup> day respectively (Figure 9). The N:P was found to be low (<1) up to 9<sup>th</sup> day of the experiment and it became higher (>1) on 10<sup>th</sup> day only (Figure 10). While, Si:P ratio shows higher values >1 from 7<sup>th</sup> day to end of the experiment and lower values (<1) were observed up to 7<sup>th</sup> day of the experiment (Figure 11).

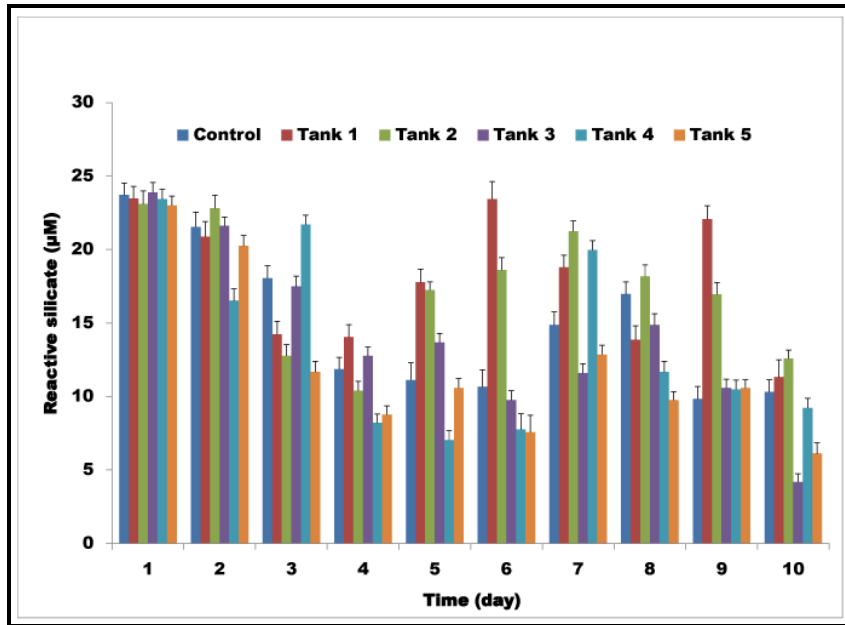


**Figure 8:** Variation of Reactive Silicate ( $\text{SiO}_3$ ) Concentration Recorded During the Experiment Period in Different Tanks

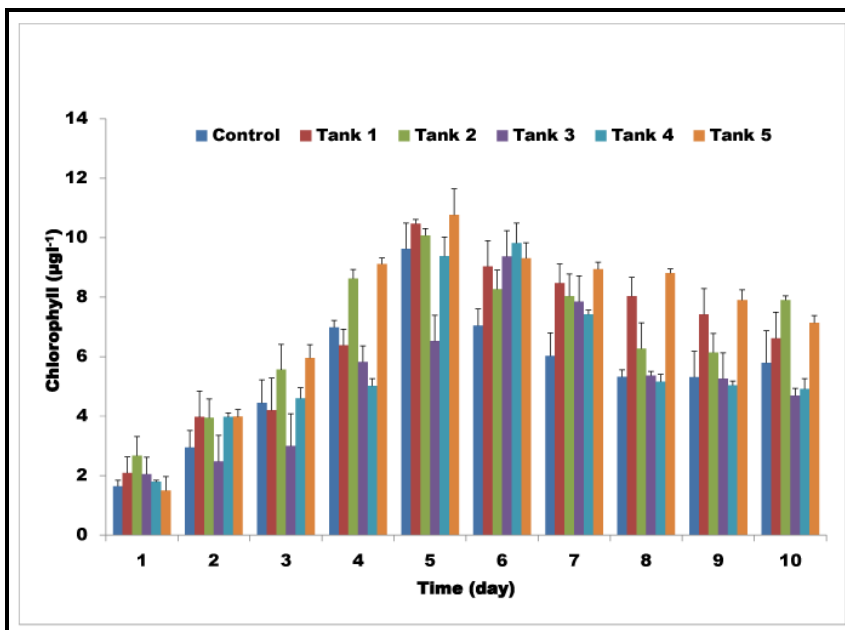


**Figure 9:** Variation of Chlorophyll Concentration Recorded During the Experiment Period in Different Tanks

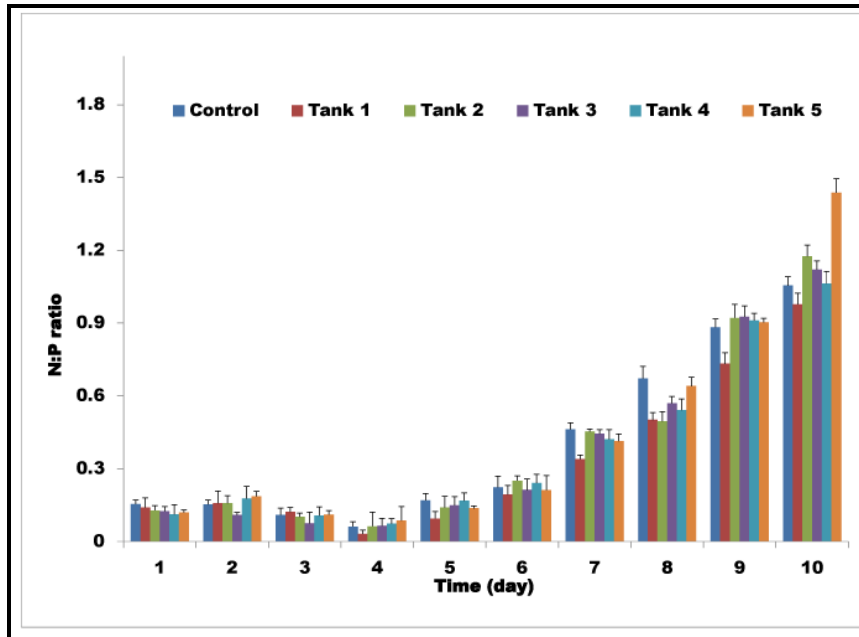


Figure 10: Variation of N:P Ratio During Experiment in Six Tanks

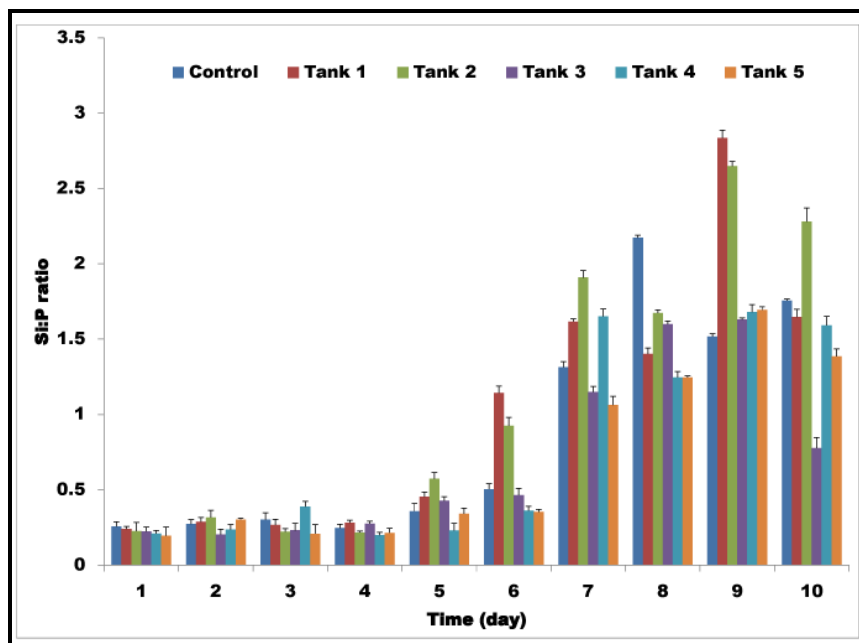


Figure 11: Variation of Si:P Ratio Recorded During the Experiment Period in Different Tanks

Significant phosphate consumption occurred in all tanks during the experiment, with no significant phosphate consumption in the control were observed in (Figure 12). The phosphate uptake rate was ranged between  $6.728 \text{ d}^{-1}$  and  $36.8365 \text{ d}^{-1}$  and it was found to be high on 2<sup>nd</sup> day of the experiment in tank-5.

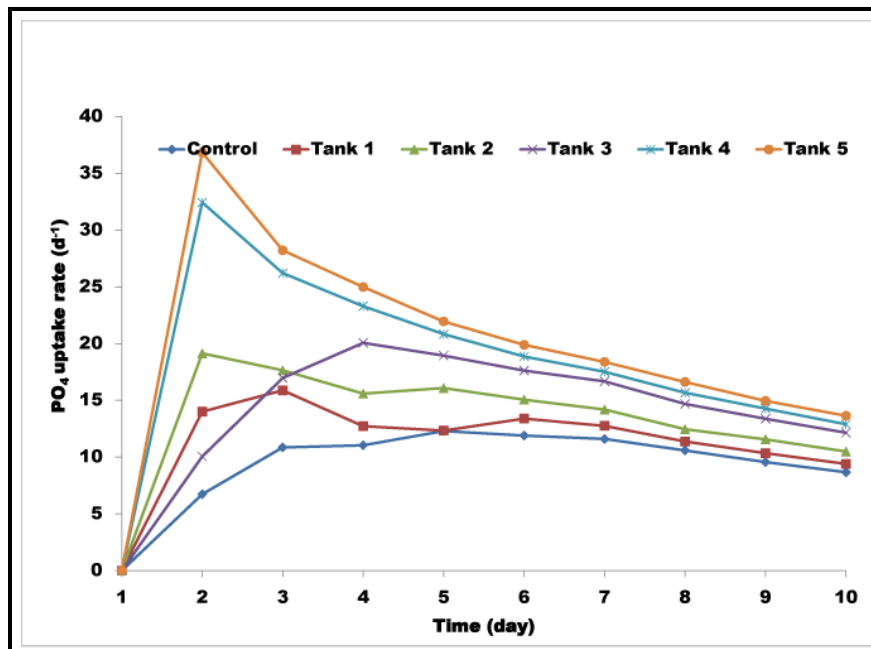


Figure 12: Trends of Phosphate Uptake Rate (R) Recorded During the Experiment Period in Different Tanks

The highest growth rate ( $0.451 \text{ d}^{-1}$ ) of the phytoplankton also observed on 2<sup>nd</sup> day of the experiment in tank-5 and other tanks were also shown their highest growth rate on 3<sup>rd</sup> day (Figure 13). While the lowest growth rate ( $0.083 \text{ d}^{-1}$ ) was observed in tank-3 on 10<sup>th</sup> day of experiment. The pronounced increase in phytoplankton growth rate was significantly coincide with the maximum uptake of phosphate, suggest that phosphorus uptake enhanced the phytoplankton growth in enrichment tanks and confirmed that it serve as one of the limiting nutrient in phytoplankton production.

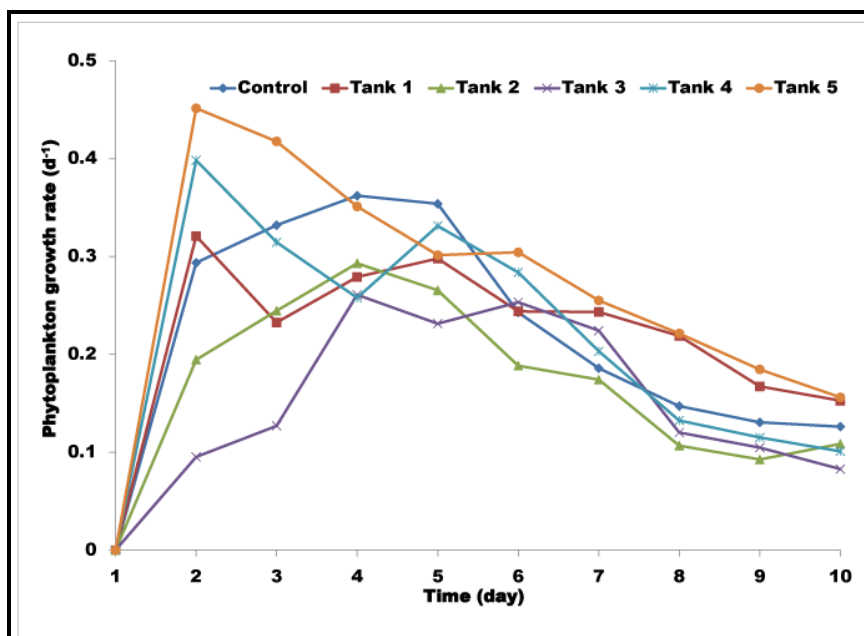


Figure 13: Trends of Phytoplankton Growth Rate (R) Recorded During the Experiment Period in Different Tanks

#### 4. Discussion

Understanding the role of essential nutrients to the phytoplankton growth is crucial for the successful control of eutrophication in coastal areas. The limiting nutrients can be detected by using different methods, e.g. by inorganic nitrogen to phosphorous ratios (Neill, 2005), enrichment experiments (Ryther and Dunston, 1971; Graneli, 1987) or measuring intracellular concentrations of nutrients (Hecky and Kilham, 1988). Despite providing significant information on the effects of nutrient availability on phytoplankton growth and community structure, nutrient enrichments do not constitute a straightforward methodology when it comes to interpreting and extrapolating results to natural systems.

However nutrient limitation of phytoplankton has been reported extensively in different seas. Among those nutrients, nitrogen and phosphorus play an important role in limiting biological productivity (Gruber, 2004). Nitrate addition was strongly promoted phytoplankton bloom, which was also proved by the nutrient enrichment experiment in the northwestern Indian Ocean (Takeda *et al.*, 1995) nitrate and phosphate in central Indian Ocean (Tang *et al.*, 2009) and nitrate, phosphate and silicate (Zou *et al.*, 2001) in Yellow sea.

As the experiment was carried out at a common place, this physical environment was kept as common for all the experimental tanks and not registered any drastic variation. Salinity increased from the first day up to the end of the experiment which might be due to the evaporation of the water with increase in temperature in the culture tanks and there is no water compensation was made for this purpose. In the present study, the pH not showed significant variation (7.74 - 8.07) and was well within the optimal pH range (6.5 to 8.2) for sustainable aquatic life (Adeyemo *et al.*, 2008) and it favors the phytoplankton growth. Generally, a fluctuation in pH value is attributed to factors like removal of CO<sub>2</sub> by photosynthesis through bicarbonate degradation, low primary productivity, reduction of salinity and temperature and decomposition of organic materials (Rajasegar, 2003) among others.

The DO level varied between 2.77 mg l<sup>-1</sup> (10<sup>th</sup> day) and 6.68 mg l<sup>-1</sup> (6<sup>th</sup> day). The decreased DO content at the end of the experiment could be attributed to decrease in oxygen release, increased respiration of higher population and increase in salinity and temperature reducing the oxygen dissolution. The increased DO content is coincided with the increased phytoplankton biomass up to 6<sup>th</sup> day of the experiment after that phytoplankton biomass was started to decrease with decrease in DO content. DO is the measure of photosynthetic activity of phytoplankton biomass and after reaching saturation in growth competition for nutrients space and utilization of DO by the cells itself during night hours led to the reduction in DO after 6<sup>th</sup> day.

Rapid uptake of nutrients (NO<sub>3</sub>, NO<sub>2</sub> and SiO<sub>3</sub>) were observed beyond 2<sup>nd</sup> day of the experiment in all the tanks with increase in phytoplankton biomass which is inferred from chlorophyll a concentration and it started to increase with decrease in chlorophyll concentration on 7<sup>th</sup> day onwards up to the end of the experiment. It clearly showed that addition of nitrogen and phosphorus greatly stimulated algal growth as measured by chlorophyll a production. Zaret *et al.* (1981) reported an increase in chlorophyll concentrations after 48 hour of incubation in the presence of added nitrogen and phosphorous. This increase is an excellent augment with the results of our experiment.

Nutrient concentrations in enrichment tanks will tend to decrease over time as result of cellular uptake. Therefore, a certain nutrient that was not limiting at the beginning of the experiment may become limiting after a few days of incubation. If a nutrient is not limiting at the time of beginning of the experiment, nutrient consumption in enriched tanks after nutrient addition will not be different from consumption in the controls (Domingues *et al.*, 2011). Ault *et al.* (2000) argued that increases in

growth rate in response to nutrient enrichment over the course of an experiment do not necessarily mean that phytoplankton growth was nutrient limited.

The inorganic phosphate (IP) concentration in all the experimental tanks were found to be higher at the first day of the experiment and started to decrease on 2<sup>nd</sup> day with enhanced phytoplankton growth, suggested the uptake of phosphate by the phytoplankton. This is also confirmed with the increasing uptake rate of phosphorous on 2<sup>nd</sup> day of experiment along with pronounced increase in phytoplankton growth rate. But the phytoplankton growth rate and nutrient uptake rate was started to decrease at the end of the experiment due to the decay of phytoplankton cells after its proliferation. Increased levels of phosphorous led to a massive proliferation in phytoplankton, indicating phosphorous initially as the limiting nutrient in the tanks (Higgins *et al.*, 2006). The relationship between phytoplankton biomass and phosphorous availability in marine systems has been examined by several researchers (Riley, 1965; Smith, 1984; Downing, 1997; Guildford and Hecky, 2000 and Hoyer *et al.*, 2002). However, a strong correlation between instantaneous measurement of chlorophyll *a* and dissolved inorganic phosphorous was reported 30 years ago by Ketchum (1969).

Phytoplankton growth responded significantly to nutrient enrichment in most tanks. However, increased nutrient consumption rates without simultaneous increase in phytoplankton net growth were also observed on several occasions. Considering the specific phytoplankton groups, diatoms were the main component of phytoplankton biomass.

The N:P and Si:P ratios were found to be low (<1) up to the 9<sup>th</sup> day of the experiment after that it become higher (>1) at the end of the experiment. For most marine coastal waters and inland seas nitrogen is thought to be the most limiting nutrient for phytoplankton production (Ryther and Dunstan, 1971, Howarth, 1988, Graneli *et al.*, 1990). However, a few cases have been reported where phosphorous limits production (Berland *et al.*, 1980, Smith, 1984), and phosphorous has been suggested to be limiting in marine coastal waters only when large nutrient loads with high N:P ratios reach coastal waters (Howarth, 1988). Rapid phytoplankton growth in tanks depleted nitrogen supplies and declined N:P ratio. However, nutrient (NO<sub>3</sub>) enrichment in culture tanks was noted at the end of the experiments indicating liberation of nitrogen through ammonia liberated by the culture organisms. Axler *et al.* (1994) determined that N:P ratio >1 indicated phosphorus limitation, while nitrogen limitation was associated with ratios <1. Thus, in the present study phosphorous limitation is evident in the end of the experiment and nitrogen limits the phytoplankton growth at the initial stages of experiment.

Overall, the net growth of phytoplankton in enrichment tanks seemed to be phosphorous limited at the end of the experiment. Increased phosphate net consumption rates in all phosphate enriched tanks were associated to significant increase in community biomass (from 1.5 to 10.77µg l<sup>-1</sup>).

Phosphorus is an essential nutrient utilized by all organisms for energy transport and growth, yet little is known about the role of phosphorus plays in the production and distribution of plankton in the world's ocean.

## 5. Conclusion

To conclude the present study, it was found that the phosphate plays vital role in the phytoplankton production at higher nutrient concentrations and it extensively used to determine the phytoplankton community structure of the aquatic environment. Hence, establishing a clear relationship between the target nutrients and chlorophyll would help assess the nutrients at spatial scale using satellite datasets.

## Acknowledgement

The authors are thankful to the authorities of Annamalai University for their support and encouragement for the study.

## References

- Adeyemo, O.K., Adedokun, O.A., Yusuf, R.K., and Adeleye, E.A. *Seasonal Changes in Physico-Chemical Parameters and Nutrient Load of River Sediments in Ibadan City, Nigeria*. Global NEST Journal. 2008. 10 (3) 326-336.
- Ault, T., Velzeboer, R., and Zammit, R. *Influence of Nutrient Availability on Phytoplankton Growth and Community Structure in the Port Adelaide River, Australia: Bioassay Assessment of Potential Nutrient Limitation*. Hydrobiology. 2000. 429; 89-1.
- Axler, R.R., Rose, C., and Tikkanen, C.A. *Phytoplankton Nutrient Deficiency as Related to Atmospheric Nitrogen Deposition in Northern Minnesota Acid-Sensitive Lakes*. Aquatic Science. 1994. 51; 1281-1296.
- Berland, B.R., Bonin, D.J., Maestrini, S.Y. *Azote ou phosphore? Considerations sur le 'paradoxe nutritionnel' de la mer mediterrane*. Oceanologica Acta. 1980. 3; 135-142.
- Birch, P.B., Gordon, D.M., and McComb, A.J. *Nitrogen and Phosphorus Nutrition of Cladophora in the Peel-Harvey Estuarine System, Western Australia*. Botanica Marina. 1981. 24; 381-387.
- Conley, D.J. *Biogeochemical Nutrient Cycles and Nutrient Management Strategies*. Hydrobiology. 2000. 410; 87-96.
- Conley, D.J., Paerl, H.W., Howarth, R.W., Boesch, D.F., Seitzinger, S.P., Havens, K.E., Lancelo, C., and Likens, G.E. *Controlling Eutrophication: Nitrogen and Phosphorus*. Science. 2009. 323; 1014-1015.
- Dodds, W.K., Strausss, E.A., and Lehmann, R. *Nutrient Dilution and Removal Bioassays to Estimate Phytoplankton Response to Nutrient Control*. Archieve of Hydrobiology. 1993. 128; 467-481.
- Domingues, R., Tania, B., Anselmo, P., Barbosa, B., Sommer, U., and Helena Galvao, M. *Nutrient Limitation of Phytoplankton Growth in the Freshwater Tidal Zone of a Turbid, Mediterranean Estuary*. Estuarine Coastal and Shelf Sciences. 2011. 91; 282-297.
- Domingues, R.B., Anselmo, B. Barbosa, U. Sommer and M. Helena Galvao. *Nutrient Limitation of Phytoplankton Growth in the Freshwater Tidal Zone of a Turbid, Mediterranean Estuary*. East Coast of Shelf Science. 2010.
- Downing, J.A. *Marine Nitrogen: Phosphorus Stoichiometry and the Global N:P Cycle*. Biogeochemistry. 1997. 37; 237-252.
- Elser, J.J., Marzolf, E.R., and Goldman, C.R. *Phosphorus and Nitrogen Limitation of Phytoplankton Growth in Freshwaters of North America: A Review and Critique of Experimental Enrichments*. Canadian Journal of Fisheries and Aquatic Science. 1990. 47; 1468-1477.
- Graneli, E. *Nutrient Limitation of Phytoplankton in a Brackish Water Bay Highly Influenced by River Discharge*. Estuarine Coastal and Shelf Sciences. 1987. 25; 555-565.

- Graneli, E., Wallstrom, K., Larsson, U., Graneli, W. and Elmgren, R. *Nutrient Limitation of Primary Production in the Baltic Sea Area*. *Ambio*. 1990. 19 (3) 142-151.
- Guildford, S.J., and Hecky, R.E. *Total Nitrogen. Total Phosphorus and Nutrient Limitation in Lakes and Oceans: Is there a Common Relationship?* *Limnology and Oceanography*. 2000. 45; 1213-1223.
- Hecky, R.E., and Kilham, P. *Nutrient Limitation of Phytoplankton in Freshwater and Marine Environments: A Review of Recent Evidence on the Effects of Enrichment*. *Limnology and Oceanography*. 1988. 33; 796-822.
- Higgins, T., Colleran, E., and Raine, R. *Transition from P- To N- Limited Phytoplankton Growth in an Artificial Lake on the Flooded Cutaway Peatland in Ireland*. *Applied Vegetation Science*. 2006. 9; 223-230.
- Howarth, R.W. *Nutrient Limitation of Net Primary Production in Marine Ecosystems*. *Annual Review of Ecology and Systematics*. 1988. 19; 89-110.
- Hoyer, M.V., Frazer, T.K., Notestein, S.K., and Canfield, D.E. *Nutrient, Chlorophyll and Water Clarity Relationship in Florida' Nearshore Coastal Waters with Comparisons to Freshwater Lakes*. *Canadian Journal of Fisheries and Aquatic Science*. 2002. 59; 1024-1031.
- Ketchum, B.H. *Relation between Circulation and Planktonic Populations in Estuaries*. *Ecology*. 1969. 35; 191-200.
- Lean, D.R.S., and Pick, F.R. *Photosynthetic Response of Lake Plankton to Nutrient Enrichment: A Test for Nutrient Limitation*. *Limnology and Oceanography*. 1981. 26; 1001-1019.
- Neill, M. *A Method to Determination Which Nutrients is limiting for Plant Growth in Estuarine Water at Any Salinity*. *Pollution Bulletin*. 2005. 50; 945-955.
- Paerl H.W. *Factors Limiting Productivity of Freshwater Ecosystem*. *Advanced Microbiology and Ecology*. 1982. 46; 75-110.
- Paerl, H.W. *Controlling Eutrophication along the Freshwater Marine Continuum: Dual Nutrient (N and P) Reductions are Essential*. *Estuaries and Coasts*. 2009. 32; 593-601.
- Rajasegar, M. *Physico-Chemical Characteristics of the Vellar Estuary in Relation to Shrimp Farming*. *Journal of Environmental Biology*. 2003. 24; 95-101.
- Reynolds, C.S., 1984: *The Ecology of Freshwater Phytoplankton*. Cambridge: Cambridge University Press.
- Riley, G.A. *A Mathematical Model of Regional Variations in Plankton*. *Limnology and Oceanography*. 1965. 10; 202-215.
- Roelke, D.L., Eldridge, P.M., and Cifuentes, L.A. *A Model of Phytoplankton Competition for Limiting and Nonlimiting Nutrients: Implications for Development of Estuarine and Nearshore Management Schemes*. *Estuaries*. 1999. 22; 92-104.
- Ryther, J.H., and Dunstan, W.M. *Nitrogen, Phosphorus, and Eutrophication in the Coastal, Marine environment*. *Science*. 1971. 171; 1008-1013.

- Schindler, D.W. *Eutrophication and Recovery in Experimental Lakes: Implications for Lake Management*. Science. 1974. 184; 897-899.
- Schindler, D.W. *Evolution of Phosphorus Limitation in Lakes*. Science. 1977. 195; 260-262.
- Schindler, D.W. *Whole-Lake Eutrophication Experiment with Phosphorus, Nitrogen and Carbon*. Verhandlungen International Verein Limnology. 1975. 19; 3221-3231.
- Smith, S.V. *Phosphorus versus Nitrogen Limitation in the Marine Environment*. Limnology and Oceanography. 1984. 29 (6) 1149-1160.
- Takeda, S., Kamarani, A., and Kawanobe, K. *Effects of Nitrogen and Iron Enrichments on Phytoplankton Communities*. Marine Chemistry. 1995. 50; 229-241.
- UNESCO. *Protocols for the Joint Global Ocean Flux Study (JGOFS) Core Measurements*, IOC Manuals and Guides, UNESCO Paris. 1994. 29; 97-100.
- Strickland, J.D. and Parsons, T.R. *A Manual of Seawater Analysis*. Fisheries Research Board Canada. 1972. 167; 310.
- Wetzel, R., 1983: *Limnology*. 2nd Edition. Philadelphia: Saunders College Publishing.
- Wyne, D., and Berman, T. *Hot Water Extractable Phosphorus - An Indicator of Nutritional Status of *Peridinium Cinctum* (Dinophyceae) from Lake Kinneret (Israel)*. Biology. 1980. 16; 40-44.
- Zaret, T.M., Devol, A.H., and Dos Santos, A. *Nutrient Addition Experiments in Lago Jacaretinga, Central Amazon Basin, Brazil*. Verhandlungen International Limnology. 1981. 21; 721-724.
- Zou, L., Zhang, J., Pan, W.X., and Pengzhan, Y. *In-Situ Nutrient Enrichment India*. Journal of Zoological Society of India. 2001. 13; 180-181.